Cooperative Fault Estimation and Accommodation in Formation Flight of Unmanned Vehicles

Seyyedmohsen Azizi

A Thesis
in
The Department
of
Electrical and Computer Engineering

Presented in Partial Fulfillment of the Requirements
for the Degree of Doctoral of Philosophy at
Concordia University
Montréal, Québec, Canada

December 2010

CONCORDIA UNIVERSITY

SCHOOL OF GRADUATE STUDIES

This is to certify that the thesis prepared

By: Seyyedmohsen Azizi

Entitled: Cooperative Fault Estimation and Accommodation in Formation Flight of Unmanned Vehicles

and submitted in partial fulfillment of the requirements for the degree of

DOCTOR OF PHILOSOPHY (Electrical & Computer Engineering)

complies with the regulations of the University and meets the accepted standards with respect to originality and quality.

Signed by the final examining committee:

_____ Chair
Dr. A. Hanna

_____ External Examiner
Dr. M.J. Zuo

_____ External to Program
Dr. Z. Tian

_____ Examiner
Dr. S. Hashtrudi Zad

_____ Examiner
Dr. M.R. Soleymani

_____ Thesis Supervisor
Dr. K. Khorasani

Approved by _____
Dr. M. Kahrizi, Graduate Program Director

December 13, 2010

_____
Dr. Robin A.L. Drew, Dean
Faculty of Engineering & Computer Science

ABSTRACT

Cooperative Fault Estimation and Accommodation in Formation Flight of Unmanned Vehicles

Seyyedmohsen Azizi, Ph.D.
Concordia University, 2010

Formation flying is a new concept that is envisaged for a cluster of networked unmanned vehicles, such as unmanned aerial vehicles, unmanned ground vehicles, unmanned underwater vehicles, and satellites and that has generated a number of challenging problems that calls for development of novel technologies. Specifically, due to the stringent precision control requirements that are imposed on the position and the attitude of vehicles (e.g., satellites in autonomous space missions), an important area of research is that of fault diagnosis, identification, and recovery (FDIR). Considerable research has been devoted to FDIR in mostly conventional single entity unmanned or manned systems with far less practical considerations given to the non-trivial problem of fault recovery in a network of unmanned systems. The main objective of this thesis is to investigate the problem of cooperative fault estimation and accommodation in formation flight of networked unmanned vehicles by developing a multi-level hierarchical methodology to generalize the FDIR capabilities of existing technologies to networked formation systems. In this framework, to perform fault estimation and recovery tasks three levels are proposed and identified, namely a low-level (LL), a formation-level (FL), and a high-level (HL). The specific contributions of this thesis in each of these levels are as follows.

The LL is at the subsystem or component (vehicle) level, and generally conventional quantitative model-based or computationally intelligent-based methods can be applied to design the low-level fault estimation (LLFE) and low-level fault recovery (LLFR) modules. In this thesis for the LLFE a systematic approach based on theories from directed graphs (digraphs) and structural observability is proposed to design the structure of distributed estimation filters that are termed as sub-observers (SOs). Results from robust H_∞ linear filtering and Kalman filtering (KF) domains are subsequently employed to design distributed sub-observers. An approach based on decentralized fixed mode, acyclic digraphs, and Lyapunov functions is developed to investigate and study the stability properties of the overall estimation problem. Based on the fault severity estimates, robust H_∞ recovery controllers are designed at the LLFR module.

At the FL, the formation-level fault estimation (FLFE) module estimates fault severities by maintaining cooperation (that consists of communication and data fusion) among the distributed SOs. This cooperation is achieved by implementing a (HL-driven) communication topology and a local solution to the distributed optimization problem, which aims at fusing the data from the SOs locally and feeding the updated data back to SOs for adjustments to the estimation approach. The formation-level fault recovery (FLFR) module then accounts for the performance degradations of the faulty vehicle by using a (HL-driven) formation structure reconfiguration that imposes certain criteria and constraints on the input signals of other healthy vehicles. These criteria include enforcing the healthy vehicles to expend more control effort/energy to compensate for the performance degradation of the faulty vehicle, or imposing a constraint on the desired input vectors to satisfy error specifications of the overall formation mission.

The HL module is a supervisor that observes the behavior of the formation and makes decisions regarding the distributed SOs reconfiguration and formation structure reconfiguration for the FLFE and FLFR modules, respectively. For the FLFE module the role of the HL supervisor is specified by developing a graph theoretic framework. The supervisor limits the effects of local uncertainties/unreliabilities on the estimation performance of the FLFE module by determining the desired (optimal) path of the corresponding digraphs that yields the appropriate communication topology among the distributed sub-observers. For the FLFR module the HL supervisor evaluates the performance of the entire formation by collecting information from the performance monitoring module and comparing them with the error specifications of the formation mission. In case that the supervisor detects any performance degradations, it activates the FLFR module.

In this thesis, by integrating the above three levels (that are, LL, FL, and HL), a cooperative fault estimation and accommodation framework is proposed to compensate for the performance degradations of a formation flight of unmanned vehicles subjected to local failures. This integrative and cooperative approach improves and enhances the capabilities of the existing techniques by configuring the estimation and the formation system and by determining the necessary and essential information exchanges among the vehicles.

Dedicated to
my mom Forough, my late dad Hossein,
and my wife Niloofar, with love and gratitude.

ACKNOWLEDGEMENTS

I would like to convey my sincere gratitude and deep appreciation to my supervisor Dr. K. Khorasani for his enthusiasm, encouragement, and sound advice throughout my PhD study. I have been motivated and inspired by his priceless support, dedication, and guidance at every stage of my thesis.

I would like to extend my gratitude to my thesis committee members, Dr. M. J. Zuo, Dr. Z. Tian, Dr. M. R. Soleymani, and Dr. S. Hashtrudi Zad, and to my comprehensive exam and seminar committee members, Dr. B. W. Gordon and Dr. W. Hamouda. I sincerely appreciate the time and support they offered me throughout this work.

I am thankful to all my friends and colleagues for providing a warm and friendly environment for me to live and learn. I am especially grateful to Davood Yazdani, Mani Tousi, Nathalia Parra, Ganesh Koraginjala, Rasul Mohammadi, Nader Meskin, Amitabh Barua, Elham Semsar, and Amin Mannani with whom I have shared wonderful moments.

I am particularly indebted to my parents Forough and Hossein and my sisters Masoumeh and Mahsa for all of their never-ending love and support.

Finally, I would like to thank my adorable wife Niloofar for all her love, patience, support, and encouragement.

TABLE OF CONTENTS

LIST OF TABLES

LIST OF FIGURES

LIST OF ABBREVIATIONS AND SYMBOLS

List of Abbreviations

AMF	Absolute Measurement Formation
AOCS	Attitude and Orbital Control Systems
CSSO	Constrained State Sub-Observer
CSSOFF	Constrained State Sub-Observer with Fusion Feedback
DES	Discrete-Event System
DFM	Decentralized Fixed Mode
DOF	Degrees Of Freedom
DS	Deep Space
E	Estimation (Digraph)
EKF	Extended Kalman Filtering
FDI	Fault Detection and Isolation
FDIR	Fault Detection, Isolation, and Recovery
FF	Fusion Feedback
FFC	Formation Flying Control
FFI	Formation Flying Interferometer
FL	Formation Level
FLFE	Formation Level Fault Estimation
FLFR	Formation Level Fault Recovery
HL	High Level
HOF	Hard Over Failure
ILO	Iterative Learning Observer
KF	Kalman Filter
LL	Low Level
LIP	Lock In Place
LISA	Laser Interferometer Space Antenna
LLFE	Low Level Fault Estimation
LLFR	Low Level Fault Recovery
LMI	Linear Matrix Inequality
LOE	Loss Of Effectiveness
LQR	Linear Quadratic Regulator
LTI	Linear Time-Invariant
L/F	Leader/Follower
MIMO	Multiple-Input Multiple Output

MMST	Multiple-Model Switching and Tuning
NN	Neural Network
PCA	Principal Component Analysis
PHA	Probabilistic Hybrid Automata
PLA	Partial Least Squares
PM	Performance Monitoring
POE	Planetary Orbital Environment
QTA	Qualitative Trend Analysis
RMF	Relative Measurement Formation
SD	State Dependency
SN	Supporting Neighbor
SO	Sub-Observer
SOD	Sub-observer Dependency
SODE	Sub-observer Dependency Estimation
TPF	Terrestrial Planet Finder
UAV	Unmanned Aerial Vehicle
UGV	Unmanned Ground Vehicle
UKF	Unscented Kalman Filtering
UUV	Unmanned Underwater Vehicle
UV	Unmanned Vehicle
VS	Virtual Structure
WAMF	Weighted Absolute Measurement Formation
WE	Weighted Estimation
WSODE	Weighted Sub-observer Dependency Estimation

List of Symbols

A	State transition matrix
A_S	Satellite cross-section area exposed to solar radiation force
$A_{x,y}$	xy-axes state transition matrix
B_i	Actuator matrix of vehicle $\#i$
B_{x_i}	x-axis actuation matrix of vehicle $\#i$
b_{x_i}	x-axis actuator gain of vehicle $\#i$
B_{x_i,y_i}	xy-axes actuation matrix of vehicle $\#i$
$\bar{B}$	Nominal actuator matrix of a vehicle
$\hat{B}_i$	Estimate of actuator matrix of vehicle $\#i$
$\hat{b}_{x_i}$	Estimate of x-axis actuator gain of vehicle $\#i$

$\bar{b}_{x_i}$	Nominal x-axis actuator gain of vehicle $\#i$
$COND^{(i)}$	Condition of sub-observer $SO^{(i)}$
$COST^{(i)}$	Cost of sub-observer $SO^{(i)}$
$COST_C^{(i)}$	Communication cost of sub-observer $SO^{(i)}$
$COST_E^{(i)}$	Estimation cost of sub-observer $SO^{(i)}$
$COST_R^{(i)}$	Recovery cost of sub-observer $SO^{(i)}$
C_C	Communication cost coefficient
C_E	Estimation cost coefficient
C_F	Rotation center in the formation-level fault recovery
C_L	Rotation center in the low-level fault recovery
C_R	Recovery cost coefficient
C_S	Solar radiation coefficient
$D^{(i)}$	Domain of sub-observer $SO^{(i)}$
E_{AMF}	Edge set of absolute measurement formation digraph
E_E	Edge set of estimation digraph
e_{ij}	Edge of a digraph
E_P	Edge set of a path P in a digraph
E_{RMF}	Edge set of relative measurement formation digraph
e_s	Error specification
E_{SD}	Edge set of state dependency digraph
E_{SOD}	Edge set of sub-observer dependency digraph
E_t^N	Total error norm
E_{x_i}	x-axis cumulative control effort of vehicle $\#i$
$E_{x_{ij}}$	x-axis tracking error between vehicles $\#i$ and $\#j$
$\mathscr{E}\{.\}$	Expected value of a random variable
f_i	Actuator fault matrix of vehicle $\#i$
F_S	Solar radiation force
$\hat{f}_i$	Estimate of actuator fault matrix of vehicle $\#i$
G_{AMF}	Absolute measurement formation digraph
G_E	Estimation digraph
G_{RMF}	Relative measurement formation digraph
G_{SD}	State dependency digraph
G_{SOD}	Sub-observer dependency digraph
$I^{(i)}$	Input set of sub-observer $\#i$
I_S	Solar radiation intensity
K_i	Feedback matrix of vehicle $\#i$
$K^{(i)}$	Gain of sub-observer $SO^{(i)}$
L_i	Distance of vehicle $\#i$ from rotation center

ℓ	Fusion feedback parameter
m_i	Total mass of vehicle $\#i$
N	Total number of vehicles
n	Total number of states
$\mathscr{N}(\{i\})$	Neighbor set of vehicle $\#i$ or sub-observer $SO^{(i)}$
$\mathscr{N}^s(\{i\})$	s-order neighbor set of vehicle $\#i$
$\mathscr{N}^{[1,\infty]}(\{i\})$	Full-order neighbor set of vehicle $\#i$
$\mathscr{N}^+(\{i\})$	Inclusive neighbor set of vehicle $\#i$
$\mathscr{N}^{+[1,\infty]}(\{i\})$	Inclusive full-order neighbor set of vehicle $\#i$
$\mathscr{N}_k(\{i\})$	x_k-corresponding nearest neighbor set of sub-observer $SO^{(i)}$
$O^{(i)}$	Output set of sub-observer $SO^{(i)}$
P	A path in a digraph
$R^{(i)}$	Range of sub-observer $SO^{(i)}$
$\mathscr{R}(i)$	Recovery status operator
Set_I^{so}	Initial set of sub-observers
Set_R^{so}	Reconfigured set of sub-observers
$SO^{(i)}$	Sub-observer $\#i$
U_d	Overall desired input vector
U_i	Input vector of vehicle $\#i$
U_i^d	Desired input vector of vehicle $\#i$
U_i^r	Reference input vector of vehicle $\#i$
U_s	Overall stabilizing control vector
U_{x_i}	x-axis input vector of vehicle $\#i$
u_{x_i}	x-axis input parameter of vehicle $\#i$
$u_{x_i}^d$	Desired x-axis input parameter of vehicle $\#i$
U_{x_i,y_i}	xy-axes input vector of vehicle $\#i$
V_{AMF}	Absolute measurement formation digraph
V_E	Vertex set of estimation digraph
v_i	Vertex $\#i$ of a digraph
V_L	Speed of light
V_P	Vertex set of a path P in a digraph
V_{RMF}	Vertex set of relative measurement formation digraph
V_{SD}	Vertex set of state dependency digraph
v_{sink}	Sink vertex of a digraph
V_{SOD}	Vertex set of sub-observer dependency digraph
v_{source}	Source vertex of a digraph
$V_{x_{ij}}$	Sensor noise of the measurement x_{ij}
$v_{x_{ij}}$	x-axis relative velocity between vehicles $\#i$ and $\#j$

$\hat{v}_{x_{ij}}^{(k)}$	Estimate of state $v_{x_{ij}}$ by sub-observer $SO^{(k)}$
W_{x_i}	x-axis disturbance of vehicle $\#i$
$\bar{W}_{x_i}$	x-axis dynamics unreliability/uncertainty of vehicle $\#i$
X	Overall state vector of the system
X_i	State vector of vehicle $\#i$
X_i^d	Desired state vector of vehicle $\#i$
X_i^r	Reference state vector of vehicle $\#i$
x_{ij}	x-axis relative position between vehicles $\#i$ and $\#j$
X_{x_i}	x-axes state vector of vehicle $\#i$
$X_{x_{ij}}$	x-axis relative state vector between vehicles $\#i$ and $\#j$
X_{x_i,y_i}	xy-axes state vector of vehicle $\#i$
$\hat{x}_{ij}^{(k)}$	Estimate of state x_{ij} by sub-observer $SO^{(k)}$
Y_i	Output vector of vehicle $\#i$
y_{v_i}	Measurement of v_i
Y_{x_i}	Measurement vector of x-axis state of vehicle $\#i$
y_{x_i}	Measurement of x_i
$Y_{x_{ij}}$	Measurement vector of x-axis relative state between vehicles $\#i$ and $\#j$
Y_{x_i,y_i}	Measurement vector of xy-axes states of vehicle $\#i$
α_i	Parameter of centralized feedback
α_{ij}	Parameter of decentralized feedback
β_{ij}^k	Decentralized feedback gain
Ω	Adjacency matrix of a digraph
ω	Rotation maneuver frequency
ω_{ij}	Element ji of adjacency matrix
ϕ_i	Desired trajectory phase of vehicle $\#i$
π_i	Actuator fault matrix of vehicle $\#i$
π_{x_i}	x-axis actuator fault parameter of vehicle $\#i$
τ	Time delay (constant)
$\hat{\pi}_i^{(k)}$	Estimte of fault parameter π_i by sub-observer $SO^{(k)}$
$\hat{\pi}_{x_i}^{(k)}$	Estimte of fault parameter π_{x_i} by sub-observer $SO^{(k)}$

Chapter 1

Introduction

Formation flying is a new concept that is proposed for a cluster of vehicles that has posed a number of challenging problems all calling for development of novel technologies. Due to the strict high-precision control requirements necessary in formation flying missions, the problem of fault diagnosis, identification, and recovery (FDIR) has become critically significant in this field of study. The autonomy requirement of these missions makes the FDIR problem even more critical and significant.

1.1 Motivation and Applications

Since the concept of precision formation flying control (FFC) was introduced in the literature [6], [7], the importance of FDIR for these systems has been recognized [8], [9], [10]. Considerable research has already been devoted to fault diagnosis in vehicle systems [11], [12], [13], [14], [15]. However, majority of these works have been developed on a single-vehicle mission, with far less practical considerations given to the nontrivial problem of fault recovery [16], [17], [18], [19]. Considering the complexities that are involved with these costly formation flying missions, there is an important area of research regarding the FDIR in FFC of multiple vehicle missions.

Distribution of a dynamical system among a large fleet of formation vehicles, which are possibly positioned at distant relative positions, imposes many complexities and computational/communicational constraints on the control and FDIR of the formation system at different levels including component, subsystem, system, vehicle, formation, and high-level supervisor. Therefore, formation flying requires a multi-level hierarchical fault diagnosis system, where all levels are in communication with one another. The cooperation and information exchanges among different levels of the multi-level diagnosis system would then necessitate and introduce new issues and research problems. There is no standard or conventional methodology that completely describes cooperation and information

exchanges among different system levels for achieving the most reliable and efficient fault diagnosis under various possible scenarios. This is an open area of research where defining different possible fault scenarios in the formation and the corresponding cooperative algorithms among the multiple levels of the diagnosis system need to be investigated.

In a satellite formation flying framework, multiple small satellites cooperate to accomplish the objective of one larger and more expensive one. Developing multiple smaller satellites has many benefits over a single satellite including simpler design, faster build time, higher reliability and redundancy, higher resolution, and the ability to view scientific payload targets from multiple angles or at multiple times. These characteristics make them ideal for many applications including astronomy, communications, meteorology, and environmental studies.

Depending on the application, there are two types of satellite formations, namely trailing and cluster. Trailing formations are formed by multiple satellites orbiting on the same path. They are displaced from each other at a specific distance to produce either varied viewing angles of one target or to view a target at different times. Trailing satellites are especially suited for meteorological and environmental applications such as viewing the progress of a fire, cloud formations, and making 3D views of hurricanes. Notable trailing pairs are Landsat 7 with EO-1 [20], and CALIPSO with CloudSat [21].

Cluster formations are formed by satellites in a dense (relatively tightly spaced) arrangement. These arrangements are best suited for distributed sensing and sparse antenna arrays for gravitational mapping, high resolution interferometry, and making maps of the Earth. In all these applications, separate instruments on a large number of low cost spacecraft are fused to replace for an expensive huge single platform. The examples of cluster formation flying missions are Terrestrial Planet Finder (TPF) [1] (Figure 1.1), Infra-Red Space Interferometer "Darwin" (IRSI/Darwin) [2] (Figure 1.2), and Laser Interferometer Space Antenna (LISA) [2] (Figure 1.3). The TPF mission tries to find and characterize Earth-like planets orbiting other stars. The objective of this mission is to resolve a planet that is a million to a billion times weaker in contrast compared to its parent star at attitude separations on the order of milliarcseconds. The Darwin mission is aimed at detection of other Earth-like planets as well as interferometric imaging of astrophysical objects. LISA is a NASA/ESA common collaborative project. The objective of this formation mission is to detect and observe gravitational waves, in the frequency range of 10^{-4} to 10^{-1} Hz, from massive black holes.

Formation flying is also applicable to a cluster of networked unmanned vehicles, such as unmanned aerial vehicles (UAVs), unmanned ground vehicles (UGVs), and unmanned underwater vehicles (UUVs). In these domains, formation flying promises several practical applications, such as reconnaissance [22], surveillance [23], communication relaying [24], and search and rescue [25]. Some of these tasks may be dangerous and will not

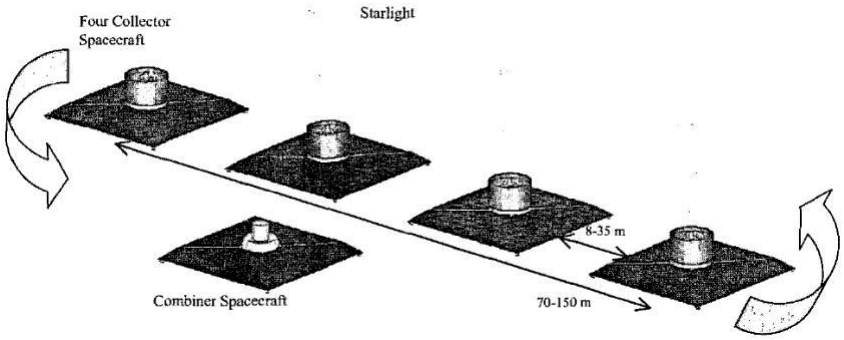

Figure 1.1: A formation flying interferometer (FFI) schematic [1].

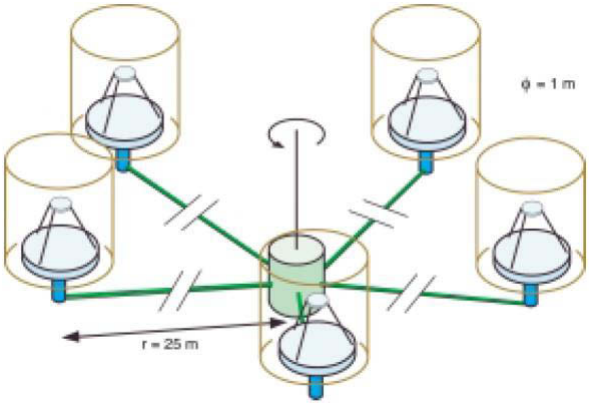

Figure 1.2: Schematic of the six-telescope formation in Darwin [2].

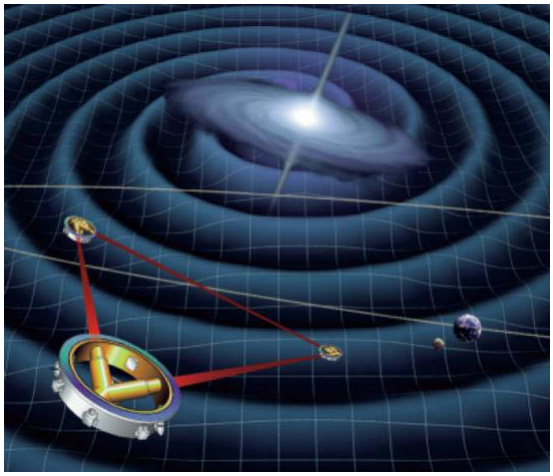

Figure 1.3: Artist's concept of gravitational waves emitted by a binary system, with the three-spacecraft LISA configuration and the Earth-Moon system [2].

be recommended for human pilots, thus making them ideal for autonomous unmanned vehicles.

In the subsequent sections, the most relevant existing results in the literature in the areas of formation flying and FDIR are reviewed. First, some reported results of unmanned vehicle formation and formation flying satellites are provided. An overview of the FDIR is then presented, and finally, the most relevant FDIR algorithms are reviewed.

1.2 Literature Review

In this section, relevant literature review regarding multi-vehicle formation systems is presented. The focus is concentrated on the formation flying satellites, since this type of formation is investigated and studied in the simulation section of this thesis as an application area. Moreover, fault detection, isolation, and recovery (FDIR) approaches in the literature are reviewed that include quantitative model-based, qualitative model-based, history-based, and fault recovery and estimation methods.

1.2.1 Unmanned Vehicle Formation

Formation flying is defined as a set of more than one vehicle whose dynamic states are coupled through a common control law [6]. In formation flying, at least one vehicle must track a desired state relative to another one, and the tracking control law must depend on the state of this other vehicle. However, in constellation missions there exists no such coupling among the vehicles. In this sense, GPS satellites are categorized as a constellation, and not as a formation.

The problem of cooperative control in unmanned vehicle systems is studied in [26] and [27]. Different control techniques have been applied to the unmanned aerial vehicles including neural networks [28], adaptive LQ control [29], nonlinear model predictive control [30], and backstepping design including input saturations [31].

In [32], a novel framework for the leader-follower formation control is developed for the control of multiple quadrotor unmanned aerial vehicles (UAVs) based on spherical coordinates. A neural network (NN) control law for the dynamical system is introduced to learn the complete dynamics of the UAV, and stability of the entire formation is demonstrated by using Lyapunov theory. In [33], a control system is designed for the formation flight of multiple UAV helicopters based on the leader-follower structure. Moreover, a collision avoidance scheme based on some predefined alert zones and protected zones is employed to avoid possible collisions of UAV helicopters in the actual formation flight test. In [34], a behavior-based decentralized approach is proposed for unmanned aerial vehicle (UAV) formation flight. The behavior-based approach is considered to promptly react

to various situations because its control input is decided based on the relative weight of each agent's desired behavior. In [35], synchronized position tracking controller is incorporated in formation flight control of multiple flying wings. It is shown that the performance and effectiveness of the formation controller are improved by using the virtual structure approach to maintain formation geometry.

In [36], a fuel efficient control scheme is proposed for aircraft formation flight based on energy equations, which aims at minimizing the fuel difference of the aircraft. In [37], vision-based UAV formation flight methods are discussed, and critical section-formation guidance, moving object extraction, and object tracking are studied in detail. An unscented Kalman filtering (UKF) technique is applied to the problem of object tracking in order to improve the often-used extended Kalman filtering (EKF) technique. In [38], longitudinal and lateral fuzzy controllers are designed to solve the multi-UAV formation control problem. Q-Learning method, which is a type of reinforcement learning, is used to tune the corresponding parameters in the output membership functions of a fuzzy controller. Also, different conditions including coordinative turning, tense-loose shape changing, shape sequence changing and collision avoiding scenarios are simulated with the formation control methodology, which is comprised of centralized decision and decentralized control solutions.

In [23], motion and formation control of a team of three unmanned aerial vehicles (UAVs) are considered for a particular surveillance task, in which a decentralized control scheme is designed and analyzed based on a non-hierarchical sensing/control structure. In [39], uninhabited aerial vehicles (UAVs) are tasked with locating a group of active emitters based on two different approaches. The first approach is a simple heuristic that assigns the closest three UAVs to the highest priority emitter. The performance of the algorithm is improved by using the second approach, in which a cost is assigned for each UAV team and emitter combination based on the current angular separation of the UAVs around an emitter, and by how much each UAV team can perfect its geometry in a given time period. In [40], a two-stage optimal coalition formation algorithm is proposed that assigns appropriate numbers of UAVs satisfying the desired requirements for carrying out munitions in support of battlefield operations.

In [41], navigation problems of unmanned air vehicles (UAVs) flying in a formation in a free and an obstacle-laden environment are investigated, and a model predictive control-based tracking controller is used to track the references that are generated in order to handle practical vehicle constraints. In [22], the problem of close target reconnaissance by a formation of three unmanned aerial vehicles (UAVs) is considered. The overall close target reconnaissance involves subtasks of avoiding obstacles or no-fly-zones, avoiding inter-agent collisions, reaching a close vicinity of a specified target position, and forming an equilateral triangular formation around the target. A decentralized control scheme

is developed for this overall task considering unidirectional sensing/control architecture. In [42], the problem of formation flight is considered for a set of unmanned air vehicles (UAV) in a possible obstacle laden environment. A novel decentralized control design procedure is developed which guarantees collision and obstacle avoidance. The control design is based on a modified virtual leader-follower structure and a simple consensus protocol.

1.2.2 Formation Flying Satellites

Based on the considered modeling complexities, satellite formation flying missions are categorized into two main classes: *Deep Space (DS)* and *Planetary Orbital Environment (POE)* [6]. In POE, the spacecraft are affected by orbital dynamics as well as environmental disturbances, while in DS the absolute and relative spacecraft dynamics can be represented by double integrators. Due to limited availability of resources in DS missions, the problems of optimal formation rotation and path planning are of high significance. The optimality in DS is mainly in the sense of fuel consumption, which has been investigated in [43], [44], [45], [46]. In these methods, fuel-balancing in formation rotation and path planning is achieved through formation reconfiguration. A reconfiguration is defined as a reassignment of spacecraft positions in a formation.

A satellite orbiting the Earth is influenced by many perturbing forces, torques and disturbances. Gravitational perturbation (J_2) [47], [48] and gravitational torque [49] highly affect satellites in lower altitudes due to the non-symmetric and non-homogenous characteristic of the Earth. The atmospheric drag [47], [49] is a dominating force at low altitudes whereas for high altitude orbits it may be ignored. Other major perturbing factors could be listed as solar radiation [50] and solar wind [47], the magnetic field of the Earth, and the gravitational force of the Moon and the Sun [51], [52]. These perturbing factors are compared and illustrated in Figure 1.4 [3]. In [53], dimensional analysis is used to estimate the magnitudes of various disturbances. In [54] and [55], the effects of gravity perturbation are analyzed and considered to control the satellite formation. In [56] the effects of sensor noise on the formation flying control are investigated. The entire formation path planning problem could be modeled by a multi-objective optimization problem, where feasible solutions should satisfy the trade-offs between multiple goals such as fuel consumption and maneuver time [57], [58].

In [7] five basic formation architectures are defined: *Multiple-Input Multiple-Output (MIMO)*, *Leader/Follower (L/F)*, *Virtual Structure (VS)*, *Cyclic*, and *Behavioral*. In the MIMO architecture, the formation is modeled by a multiple-input multiple-output plant. Using this dynamic model of the entire formation, all the methods and theories of modern control can be applied to formation control, detection and estimation problems. The most

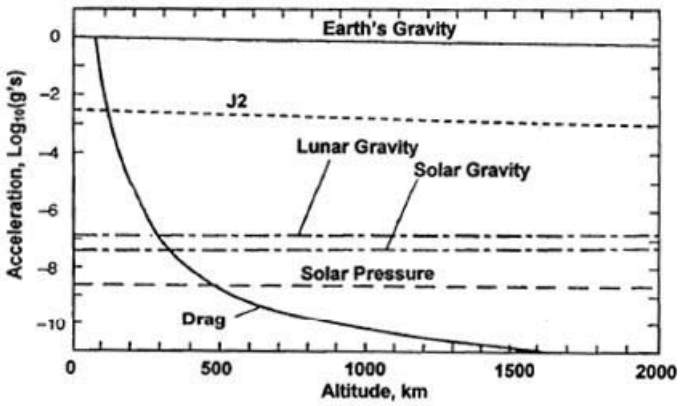

Figure 1.4: The influence of the disturbing forces at different altitudes [3].

studied FFC architecture in the literature is L/F structure. In this architecture, a hierarchical structure is used for designing the spacecraft controllers. In the VS architecture, the overall formation is modeled by a virtual rigid body that the spacecraft are the rigid parts of it. The Cyclic architecture is similar to L/F in the sense that it is considered as the interconnection of individual spacecraft controllers. However, Cyclic differs from L/F in the sense that the controller connections are not hierarchical. In a Behavioral architecture, there exists a combination of several behaviors, for which individual controllers are designed. Therefore, in such architectures the individual controllers achieve different and possibly competing behaviors.

The MIMO architecture requires access to the entire formation state for the controller to be optimal. Therefore, it requires the highest amount of information exchange. The stringent communication requirements negatively affects robustness of MIMO algorithms to local failures such as communication delay and faults. In the L/F architecture, both of these concerns, namely information requirements and robustness, are addressed at the expense of global optimality. In L/F architecture, each spacecraft requires the local information about the states of its leader, and so the formation control and coordination are simplified and reduced to individual tracking problems. However, the drawback of L/F architecture is that it does not guarantee a globally optimal formation controller due to the framework of locally optimal individual controllers. The Cyclic architecture improves the L/F architecture by making non-hierarchical connections between individual spacecraft controllers, which require more communication effort. In the sense of optimality and communication requirements, the Cyclic architecture lies between the MIMO and L/F architectures.

Formation Coordination/Feedback Architecture: Generally, there are four types of formation control problems, namely (a) unconstrained initialization, (b) initialization with collision avoidance, (c) unconstrained translation and rotation, and (d) constrained translation and rotation [4], [5], [59]. The problem of coordinating multiple spacecraft in formation flying is addressed in [4], [59]. This architecture is shown in Figure 1.5-(a). In this figure, the system S_i represents the i^{th} spacecraft. The vectors u_i and y_i are the input and output measurement vectors of the i^{th} spacecraft, respectively. The local controller for the i^{th} spacecraft is denoted by the block K_i. The input and output of K_i are the coordination variables ξ and the performance variable z_i, respectively. The block F is the formation control and represents the primary coordination mechanism in the system. The inputs of F are the performance variables z_i of each spacecraft and the output y_G of the supervisor. The outputs of F are the coordination variable ξ to the local controllers and the performance vector z_F to the supervisor. The supervisor G is a discrete-event system (DES) that derives the input y_G to the formation control F by using the performance vector z_F from F. This coordination/feedback architecture provides a convenient and rigorous framework to apply and compare various centralized and decentralized control approaches for different formation flying architectures.

In Figure 1.5-(b), a decentralized scheme for spacecraft formation control via the virtual structure approach is proposed [5]. In this figure, the disturbance input vector w_i represents external forces and torques to the i^{th} spacecraft S_i. The blocks $F^{(k)}$ and $K_i^{(j)}$ represent the k^{th} formation control and the j^{th} local controller for the i^{th} spacecraft, respectively. It is assumed that different control strategies are required for different operational modes. Therefore, the supervisor determines which formation control $F^{(k)}$ and local spacecraft control $K_i^{(j)}$ is required for a certain formation maneuver.

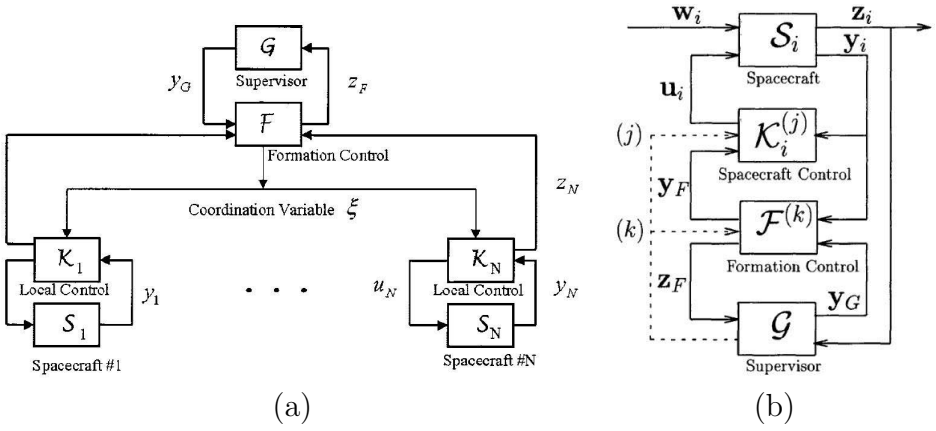

Figure 1.5: Coordination/feedback architecture with (a) centralized [4] and (b) decentralized scheme [5].

1.2.3 Fault Detection, Isolation, and Recovery (FDIR)

In a process, the term "fault" is defined as a deviation of a variable or parameter from its normal range. There are three general types of faults that may occur in a process, namely parameter changes, structural (system/controller) changes, and sensor and actuator faults. Fault detection, isolation and estimation is an important area of research that can enable fault prognostic systems to prevent total failure through early detection and diagnosis. The desirable characteristics of a fault diagnostics system are [8]: quick detection and diagnosis, isolability, robustness, novelty identifiability, classification error estimate, adaptability, explanation facility, modeling requirements, storage and computational requirements, and multiple fault identifiability. The fault diagnosis methods are classified into two general classes of model-based and history-based approaches, each of which can be categorized into qualitative and quantitative methods. In the following, these methods will be explained and discussed in detail.

Quantitative Model-Based Methods: The quantitative model-based approaches are mostly based on general state-space models and input-output representations of a process. Most of these approaches require system linearity. Therefore, in case of a nonlinear system, the system is linearized around an operating point. Moreover, the faults could be modeled as either additive or multiplicative terms. The most frequently used FDI approaches include diagnostic observers, parity relations, Kalman filters and parameter estimation [8], [60]. All model-based FDI methods require two steps. In the first step, residuals are generated to illustrate any inconsistencies between the actual and the nominal (healthy) system, and in the second step, a decision rule is implemented to interpret and diagnose the source of the inconsistent residuals.

In [13] general diagnostic observer methods are discussed for linear systems. Also, some earlier works based on diagnostic observers can be found in [61]. In [62], [11], [14] the fundamental problem of robust fault detection is investigated and the effects of faults are decoupled from each other and from the effects of modeling errors to achieve the desired robustness properties. In [12], the problem of fault diagnosis by using nonlinear observer-based approaches is investigated. The experimental results indicate that the robustness issue becomes more important as the system model complexity increases. In this regard, robustness is always an important problem that requires analytical and experimental verifications. In [63] and [64], a geometric approach is used to design observers for actuator fault detection and isolation in satellite translational and attitude dynamics, respectively. In [18], a hybrid fault diagnosis and recovery is proposed for a team of unmanned vehicles, and the proposed hybrid method offers a better fault detection as compared to the previous model-based detection methods.

Another approach that can be used to design nonlinear observers for state estimation is based on Kalman filters [14], [65]. In this approach, the observer gain matrix, which is the linearized gain matrix around an operating point, is time-variant. These filters work well in estimating faults that are slowly varying. But in case of jump failures, the performance of Kalman filters degrade considerably. For nonlinear systems, the standard Kalman filter is modified to the form of extended Kalman filter (EKF). In [66], suboptimal EKFs are developed to enhance the trade-offs between computational load and diagnosis accuracy. In [67] EKF is used in the application of fault detection in aircraft control systems, and in [68] a bank of Kalman filters is used for fault diagnosis of reaction wheels in satellites.

Parity equation approach is another quantitative model-based approach for fault diagnosis. This method is based on checking the parity (consistency) of the system models with the known inputs and measured sensor outputs. One can obtain parity equations by rearranging or transforming the input-output models, such that the resulting algebraic equations indicate an explicit relation between the input and output time-sequence data vectors. In most applications these equations are rather easy to generate from on-line process data [69], [70]. One important aspect of fault diagnosis is fault isolation, which requires feasible generation of residual vectors that are orthogonal for different faults. Therefore, in parity equations the model structure is rearranged such that desired fault isolability is achieved.

Qualitative Model-Based Methods: In some applications, the accurate mathematical model of a system may not be available, and therefore it is not effective to apply quantitative model-based methods. In such cases although a mathematical model cannot be accurately derived, qualitative behavior models can be developed quite efficiently for the purpose of qualitative model-based fault diagnosis. These methods include diagraph based causal models, fault trees, qualitative physics, and abstraction hierarchy [9]. In [71] a fault-tree approach is proposed to strengthen existing efficient fault-detection mechanisms in satellite reaction wheel, with an additional ability to classify different types of faults to effectively determine potential failure causes in a subsystem. In [72] multiple fault detection with a signed digraph based fault diagnosis is proposed. In [73] a fault detection method based on fault trees is used in a risk assessment and reliability analysis. In all these methods, a qualitative model of the system is developed using the incomplete and uncertain knowledge of the behavior of the system. The qualitative model is consequently analyzed using the qualitative model-based methods to make partial conclusions.

Besides the advantages of qualitative model-based methods, these methods have a major drawback that involves the generation of spurious solutions. Considerable research has been conducted on the qualitative model-based methods to reduce the number of

spurious solutions [9]. This drawback is due to the fact that there exists no qualitative behavior model that can completely and explicitly represent a system. Therefore, the performance of these diagnosis methods is considerably affected by any new condition that is not defined in the knowledge base.

History-Based Methods: In some applications, the model of the system may not be available; instead the history of the input-output data of the system is stored and is available for diagnosis purposes. In contrast to the model-based approaches, process history-based methods are best candidates for applications with history-based data and lack of model-based information [74], [75], [76]. One method to code the historical data to use in a history-based diagnosis system is that of "feature extraction" [10]. Feature extraction can be categorized into two classes of qualitative and quantitative processes. Qualitative feature extraction includes expert systems and qualitative trend analysis (QTA), and quantitative feature extraction includes statistical methods (principal component analysis (PCA), partial least squares (PLS), and statistical classifiers) and neural networks. One major deficiency of history-based methods is that they highly rely on the consistency of historical data, and therefore the performance of history-based diagnosis systems is fragile when encountering new process and environmental data.

Generally, none of the diagnosis methods above can completely satisfy all the desirable characteristics of an ideal diagnostic system. For example, causal digraph is a powerful tool in explaining the faults but weak in isolating multiple faults. Furthermore, quantitative model-based approaches are very efficient in fault isolation. The conclusion is that an efficient integration of various diagnosis methods can indeed result in an optimal hybrid diagnosis system that can overcome the deficiencies and drawbacks of a given single method.

Fault Recovery Methods: There are two general methods to design a fault-tolerant control system: passive and active. In active control, the control system is redesigned online when a fault is diagnosed and its severity is estimated. Such an active fault tolerant control system consists of fault detection, fault severity estimation, and control reconfiguration. In passive control, the control system is designed such that its performance is robust to probable faults and failures with certain bounded severities. Typical techniques are adaptive control and robust control [16], [77], [78].

Considerable research has already been devoted to fault diagnosis and recovery for the satellite's attitude and orbital control systems (AOCS). In [19] a model-based fault recovery is presented for the attitude control subsystems of a satellite using magnetic torquers. It is shown that the analytical redundancy of magnetic torquers can be utilized to recover the possible fault in any of them. In [79], [80] statistical local approach is

specifically designed for diagnosis and identification of faults with very small magnitudes. The approaches in [81], [82], [83] are based on the sliding mode observer, and the design of an observer in [81] boils down to solving LMIs. In [84], [85], the authors have designed an iterative learning observer (ILO), which uses a learning mechanism instead of using integrators that are commonly used in classical adaptive observers. The ILO overcomes the difficulty in identifying time-varying thruster faults by adaptive observers. In [16], [86] an adaptive Kalman filtering algorithm is developed to estimate the reduction of control effectiveness in a closed-loop setting. The state estimates are fed back to achieve the steady-state regulation, while the control effectiveness estimate is used for the on-line tuning of the control law.

In [77], by solving a Lyapunov equation a robust state-space observer is proposed to simultaneously estimate descriptor system states, actuator faults, their finite time derivatives, and attenuate input disturbances in any desired accuracy. Moreover, a fault-tolerant control scheme is worked out by using the estimates of the descriptor states and faults, and the linear matrix inequality (LMI) technique. In [87], a fault is assumed to belong to a finite set of parameters (modes), and a sliding mode controller is designed for accommodation of each mode in a hierarchical framework. In [88], a fuzzy adaptive sliding mode control is implemented for fault accommodation. In [89] the authors proposed robust fault diagnosis methods by using Lyapunov redesign method. In [78] adaptive control is applied to systems with actuator uncertainty and failure. In [90] an adaptive observer/estimator bank is used to detect and identify faults, and a controller bank is designed to constitute the structure of the multiple-model switching and tuning (MMST) controller.

Estimation Methods: Estimation techniques have been extensively investigated in the literature for various applications ranging from tracking and navigation [91] to fault diagnosis and recovery [17], [92]. Due to the distributed nature of many multi-agent systems, such as formation flying vehicles, decentralized filtering techniques are of most interest to the estimation area. In [93] and [94], decentralized estimation algorithms are surveyed and applied to the state estimation of formation flying satellites. The simulation results show that decentralized reduced-order filters result in near optimal estimates while balancing the constraints on communication and computation among the satellites. Moreover, a hierarchical architecture is presented to embed the decentralized estimators while scaling the problem to very large fleets. In [95], [96], the state estimation is performed based on parallel operation of full-order observers with local measurements. A necessary condition on communication topology is developed to guarantee stability of simultaneous parallel estimators and controllers.

Most efforts on distribution of Kalman filters are based on full-order observers [97],

[98], which are not ideally communication-wise efficient. In [99], [100] and recently in [101], [102], [103] the efforts have been made to distribute the Kalman filtering technique among the vehicles in a fleet. In [101], [102], [103] the overall system model is divided into several subsystems according to the physical considerations of the system. A local Kalman filter is designed for state estimation in each subsystem. Among the local Kalman filters, the common observations are fused using bipartite fusion graphs and consensus averaging algorithms. The performance is shown to be acceptable, as compared to a centralized Kalman filter, while the method offers less communicational complexity. In [104] cascaded Kalman filters are proposed for estimation of multiple biases for applications to ground vehicles.

Another distributed estimation method among local filters is based on consensus filters. The consensus problems in coordination of multi-agent systems are surveyed in [105]. The results cover both the cases of time-varying and time-invariant information exchange topologies. In [106], [107], distribution of Kalman filter is performed in a consensus framework for the special case of static systems. Besides, it is pointed out that the case of dynamic systems is an open topic of research. In [108], [109], [110], the case of distributed Kalman filtering for dynamic systems is tackled using micro-Kalman filters, and the resulting estimates are fused using a consensus scheme. It is shown that the consensus error would be within a finite error bound whose radius depends on the variation rate of the measured states.

In [111] and [112], the authors proposed a centralized scheme for the fault tolerant estimation in the general case of nonlinear systems. However, the problem of distributed fault tolerant estimation cannot be solved by employing their approach. In the distributed fault tolerant estimation, the overall model is distributed among multiple local agents and the system information is cooperatively provided by the local agents and is partially available to the local agents due to the communication constraints among them. Furthermore, in [111] and [112], the proposed method is based on the "differential algebra" theory [113], in which multiple derivatives of the output sensor and input signals are required. However, the sensor noise has a negative impact on the performance of multiple differential operators that is a drawback of the differential algebra theory [114].

It should be noted that none of the methods in the literature properly address the process fault in the form of parameter drift. A *drift* is a comparatively long-term change in a parameter of a system or equipment. Hence, parameter drifts make the estimation, recovery and accommodation procedures rather challenging. The time-dependent parameter drifts can be handled through on-line and on-board parameter estimation techniques. Hence, accurate quantitative models of the system are required for the purpose of parameter drift estimation. Different parameter estimation methods are surveyed in [15]. These methods require accurate dynamic models of the process and are computationally very

intensive for large processes. One way of reducing the computational load is to implement parameter estimation techniques for reduced order models, which require robustness consideration and analysis. In [115], a robust H_∞ estimator is used for fault diagnosis in a satellite, and hence the estimation performance is robust to uncertainties and disturbances. In [17], fault detection, isolation and recovery (FDIR) is performed for nonlinear satellite models by using a parameter estimation approach.

1.3 Our Proposed Methodology

Various methods have been proposed in the literature for the problem of fault diagnosis, identification, and recovery (FDIR) for a single unmanned vehicle. However, none of these methods have properly introduced and investigated the concept of cooperative fault estimation and accommodation in formation flight of unmanned vehicles. Formation flight of unmanned vehicle missions require an autonomous cooperative fault diagnosis, identification and recovery (FDIR) scheme among the various levels ranging from the low-level (LL) to the formation-level (FL) and high-level (HL). In this thesis, the problem of fault estimation and accommodation in formation flight of unmanned vehicles is investigated based on a multi-level hierarchical and cooperative scheme, which improves and enhances the capabilities of existing fault estimation and accommodation technologies in the domain of formation flight of unmanned vehicles. Three levels are proposed and identified in this framework, namely a low-level (LL), a formation-level (FL), and a high-level (HL) fault estimation and accommodation.

Our proposed framework for a cooperative FDIR system is shown in Figure 1.6. In this figure, the bus lines represent the general possible information exchanges among different modules of the formation. The solid and dashed lines represent internal and inter-level information exchanges, respectively, that are of main concern in this research. The scenario investigated for this framework deals with cooperative fault estimation and recovery, in which two levels, namely the LL and FL are considered.

The LL module corresponds to the vehicle level including all the components (actuators, sensors, power supply, etc.), and generally conventional quantitative model-based methods can be applied to design the estimation and recovery modules in the LL module. Conventional filtering methods are used to estimate the severity of a fault, and conventional linear controllers are designed based on the new set of parameter estimates. If the fault is not properly estimated in the LL module, the faulty vehicle is *partially recovered*. The high-level (HL) module includes a supervisor that receives information from the performance monitoring (PM) module, which observes the behaviors of all the vehicles in the formation. If the HL module detects any degradation in the performance of the partially LL-recovered vehicles, then the HL module forwards the recovery task to the FL module.

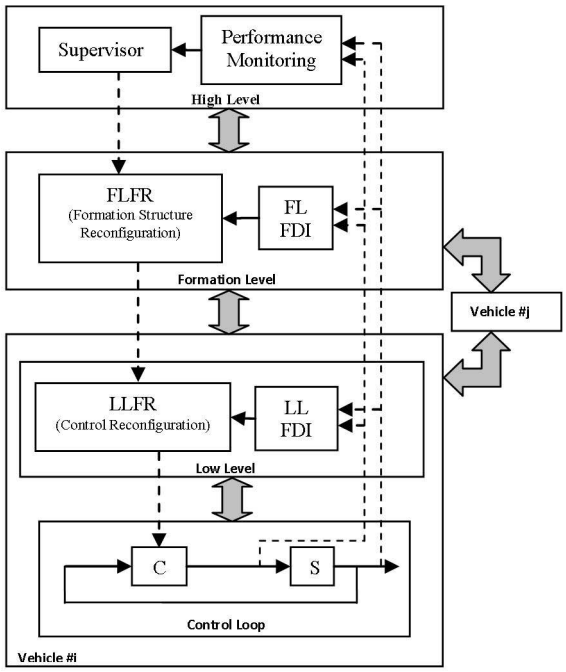

Figure 1.6: The multi-layer hierarchical cooperative FDIR system for a network of unmanned vehicles.

At the FL module, all the vehicles are considered as one integrated unit, so that their interactions are taken into account. The above overall and formation-level interacting units can be employed to estimate and accommodate probable faults in the vehicles more effectively. The formation-level fault estimation (FLFE) module estimates the fault severities cooperatively by utilizing distributed estimation filters, namely sub-observers (SOs), whose cooperation and data fusion are maintained by a HL supervisor. The formation-level fault recovery (FLFR) module accounts for the performance degradations of a partially low-level recovered vehicle at the cost of HL-driven formation structure reconfiguration that imposes certain criteria on the input signals of other healthy vehicles.

The HL module is a "supervisor" that observes the performance and behavior of the formation and makes decisions on the tasks of distributed sub-observer reconfiguration and formation structure reconfiguration, respectively, for the FLFE and FLFR modules. The autonomous FDIR requires cooperation among different levels of this multi-level and hierarchical scheme, while maintaining a minimum amount of information exchange among the vehicles, to handle different scenarios associated with faulty situations.

In the switching estimation/control framework, the dwell time is defined as a positive time constant that guarantees stability of the system provided that the consecutive switching times between controllers and estimators are larger than the dwell time [116]. Analysis of the switching limitations of the dwell time is beyond the scope of this thesis,

and therefore for sake of simplicity we assume that this condition is implicitly satisfied before any switching among estimators as well as control reconfigurations takes place.

1.4 Thesis Contributions

In this thesis, a multi-level hierarchical scheme is proposed to improve and enhance the fault detection, isolation and recovery (FDIR) capabilities of existing technologies in formation flight of unmanned vehicles. The contributions of this thesis are in two main directions, namely cooperative fault estimation and cooperative fault accommodation, which have been explained briefly as follows:

- Contributions on cooperative fault estimation [117], [118], [119], [120], [121], [122], [123]:

    1. The problem of cooperative fault estimation is investigated by utilizing distributed estimation filters, namely *sub-observers* whose cooperation and data fusion are maintained by a high-level (HL) supervisor.
    2. A systematic approach based on the theories from directed graphs (digraphs) and structural observability is proposed to design the sub-observers (SOs).
    3. The notions of estimation (E), weighted estimation (WE), sub-observer dependency estimation (SODE), and weighted sub-observer dependency estimation (WSODE) digraphs are developed to formulate the role of a high-level (HL) supervisor. Moreover, the objective of the supervisor is formulated by the problem of determining (optimal) paths on the corresponding digraphs.
    4. In cases of float, lock-in-place, and hard-over actuator failures, the overall fault-augmented state space model is shown to be in the general form of a linear time-invariant (LTI) system; hence, the estimation problem falls in the linear filtering category. Conditions are derived based on the decentralized fixed mode (DFM) to examine feasibility of cooperative sub-observers that guarantees stability of the overall estimation problem. Once the overall distributed estimation problem is shown to be feasible, the robust H_∞ linear filtering technique is used to design the distributed sub-observers.
    5. In case of the loss-of-effectiveness actuator failures, the overall fault-augmented state space model is shown to be in the general form of a bilinear system from the observability perspective. However, from the estimation point of view, the overall fault-augmented state space model is shown to be in the general form of a linear time-varying system, and therefore Kalman filtering (KF) technique

is utilized to design the local sub-observers. The concept of an *acyclic* digraph is used to guarantee the ultimate boundedness of the cooperative estimation system by using a proper Lyapunov function candidate. If the ranges of some sub-observers are overlapping, then certain states are being estimated by multiple sub-observers. In such cases, the fusion feedback (FF) optimization problem is introduced to fuse the data from all the range-overlapping sub-observers and feed the updated data back to the range-overlapping sub-observers for adjustments to the estimation process. Moreover, a closed form solution is developed for the fusion feedback optimization problem, and the modifications are made to the Kalman filters to guarantee stability in the presence of fusion feedback procedure.

- Contributions on cooperative fault accommodation [124], [125], [126], [127], [128]:

  1. The performance monitoring (PM) module is introduced at the high level (HL) module in order to identify the *partially low-level (LL) recovered* vehicles, whose tracking performances violate the given *error specification* of the formation mission. Based on the information regarding the LL-recovered vehicles from the PM module, the supervisor decides on activation of the formation-level fault recovery (FLFR) module.
  2. The formation-level fault recovery (FLFR) module is proposed that accounts for the performance degradation of a partially low-level (LL) recovered vehicle at the cost of other healthy vehicles being through certain criteria on their input signals. The proposed FLFR mechanism is used to accommodate the possible loss-of-effectiveness actuator failures.
  3. In case of a formation flight system with relative measurements among the vehicles, both the *centralized* and *decentralized* control approaches are considered and developed. In case of a single actuator failure, a robust H_∞ controller is designed in which the parameters of the controller are adjusted to accommodate the partially LL-recovered vehicle by enforcing the other healthy vehicles expending more control energy to compensate for the performance degradation of the faulty vehicle. In case of multiple actuator failures, a robust controller is designed to stabilize the nominal state space model of the formation, and a constraint is imposed on the desired input vector to satisfy the error specification of the formation mission.
  4. In case of a formation flight of unmanned vehicles with absolute measurements, the notion of *adjacency matrix* is developed to represent both the centralized and decentralized control approaches. In case of a single actuator failure, a

method is proposed to accommodate the fault by reconfiguring the formation structure in terms of the weighted absolute measurement formation (WAMF) digraph, activating a robust controller for the partially LL-recovered vehicle, and imposing a constraint on the desired inputs in order to compensate for the performance degradation of the formation mission. In case of multiple actuator failures, the notion of a supporting neighbor (SN) is introduced and explained, whose desired input vector is adjusted (or constrained) in order to accommodate the performance deficiencies of all the partially LL-recovered vehicles.

1.5 Organization of the Thesis

This thesis is organized as follows:

1) In Chapter 2, background information is presented that includes formation digraph, decentralized fixed mode (DFM), and linear matrix inequality (LMI). Moreover, some useful notations are introduced that will be used throughout this thesis. The problem formulation is presented in terms of the state space model of the formation with a certain formation digraph and the actuator failure model. The technical problems are described for both cases of cooperative fault estimation and accommodation in a formation flight of unmanned vehicles. Finally, an overview of the approaches is provided that will be used in the subsequent chapters to tackle the technical problems in this thesis.

2) In Chapter 3, the problem of simultaneous state and actuator fault estimation is considered in formation flight of unmanned vehicles with relative state measurements and subject to float, lock-in-place, and hard-over actuator failures. The fault parameters are augmented to the system states to form an overall LTI fault-augmented state space model. A novel framework is proposed for distributed and cooperative estimation of general LTI systems subject to process dynamics and sensor measurement unreliabilities. Within this framework, estimation digraphs are proposed based on which a high level supervisor can make decisions regarding the set of sub-observers to utilize under different unreliable information scenarios.

3) In Chapter 4, the problem of simultaneous state and actuator fault estimation is considered in formation flight of unmanned vehicles with relative state measurements subject to actuator failures including the loss-of-effectiveness. The fault parameters are augmented to the system states to form an overall bilinear fault-augmented state space

model. Our proposed distributed and cooperative estimation framework is extended to the general class of bilinear systems.

4) In Chapter 5, the problem of cooperative actuator fault accommodation in formation flight of unmanned vehicles with relative state measurements is studied. It is assumed that the actuator fault is partially estimated by our proposed estimation framework in the previous Chapters 3 and 4. In other words, it is assumed that the fault estimates are biased and not accurate enough to satisfy the error specifications of the formation mission, and hence the corresponding faulty vehicle is partially recovered. Therefore, a methodology is proposed to accommodate the partially recovered (estimated) vehicle at the expense of other healthy vehicles being through certain criteria on their input signals.

5) In Chapter 6, our proposed cooperative actuator fault accommodation methodology is extended to the case of formation flight of unmanned vehicles with absolute state measurements. The proposed method accommodates the partially recovered vehicle at the costs of some changes in the absolute measurement formation (AMF) digraph and some constraints on the desired trajectories of other healthy vehicles.

6) In Chapter 7, our theoretical methodologies are applied to a simulated formation flight of multiple satellites in deep space (DS) and planetary orbital environment (POE). Simulation results confirm the effectiveness of our analytical work in the previous chapters.

Chapter 2

Background Information, Problem Formulation and Methodology

2.1 Background Information

2.1.1 Formation Directed Graph (Digraph)

In this section, we first present some preliminary definitions from graph theory [129], [130]. A *Digraph* $G(V, E)$ is represented by a set of *vertices* V, which are connected together by a set of directed *edges* E. For a vertex v_i in a digraph $G(V, E)$, the *outdegree* and *indegree* are the numbers of outgoing edges $e_{ik} \in E$ and incoming edges $e_{ki} \in E$ ($v_k \in V$), respectively. A *source vertex* is a vertex with indegree zero, while a *sink vertex* is a vertex with outdegree zero.

Definition 2.1. *In a* Digraph$G(V, E)$*, a* directed path $P = (v_{p_0}, v_{p_1}, \ldots, v_{p_{(l-1)}}, v_{p_l})$ *from a vertex* v_{p_0} *to a vertex* v_{p_l} *is a sequence of edges* (v_{p_0}, v_{p_l})*,* (v_{p_1}, v_{p_2})*, ...,* $(v_{p_{(l-2)}}, v_{p_{(l-1)}})$*,* $(v_{p_{(l-1)}}, v_{p_l})$ *such that*

- $v_{p_k} \in V$ *for* $k = 0, 1, ..., l$*, and*
- $(v_{p_{(k-1)}}, v_{p_k}) \in E$ *for* $k = 0, 1, ..., l$*.*

A source-to-sink *path is a path that initiates at a source vertex and terminates at a sink vertex.*

Definition 2.2. *In some applications of formation missions, the objective is to maintain a proper* relative *positioning among the vehicles. For example, in the deep space multiple spacecraft interferometer [2] one may require centimeter level relative spacecraft positioning, but the inertial position of the entire formation may drift arbitrarily. These applications are defined as* relative-measurement formation missions*. In some other applications of formation missions, such as the planetary orbital environment (POE) satellite*

formation [6] and the unmanned aerial vehicle (UAV) formation missions [131], the objective is to maintain a proper relative positioning among the vehicles while the vehicles move about the desired absolute trajectories in their inertial framework. These applications are defined as absolute-measurement formation missions. *In such applications, if the desired absolute trajectories of the vehicles are not properly taken into the control loop, then undesirable absolute positioning and catastrophic clashes may take place. This is not an issue of concern for the relative-measurement formation missions.*

For the two cases of relative and absolute measurements among the vehicles of a formation (as per Definition 2.2), the *formation digraph* is defined independently.

Definition 2.3. *The relative and absolute measurement formation directed graphs (digraphs) are defined as follows:*

a) The relative measurement formation (RMF) digraph *is defined by* $G_{RMF}(V_{RMF}, E_{RMF})$, *where the vertex* v_i *represents the vehicle #*i *and the edge* e_{ij} *represents the relative measurement of the states of the sink vehicle #*j *with respect to the source vehicle #*i.

b) The absolute measurement formation (AMF) digraph *is defined by* $G_{AMF}(V_{AMF}, E_{AMF})$, *where the vertex* v_i *represents the vehicle #*i *and the edge* e_{ij} *represents the fact that the sink vehicle #*j, *in its control loop, requires the feedback from the states of the source vehicle #*i.

Definition 2.4. *For a formation flight of* N *vehicles with relative measurements, the nearest neighbor set* $\mathscr{N}(\{i\})$ *of a vehicle #*i *is defined as the index set of all the vehicles #*k *such that either* $e_{ki} \in E_{RMF}$ *or* $e_{ik} \in E_{RMF}$ *as per Definition 2.3, that is*

$$\mathscr{N}(\{i\}) = \{k \in \{1, ..., N\} |\ \textit{either } e_{ik} \in E_{RMF} \textit{ or } e_{ki} \in E_{RMF}\}$$

Definition 2.5. *For a formation flight of unmanned vehicles with absolute measurements, we define the parameter* ω_{ki} *(*$0 \leq \omega_{ki} \leq 1$*) as the* formation weight *of the vehicle #*i *with respect to the vehicle #*k. *The weight* ω_{ki} *is nonzero (*$0 < \omega_{ki} \leq 1$*) if and only if the vehicle #*i, *in its control loop, requires the feedback from the* ω_{ki}*-weighted states of the vehicle #*k. *In other words, the vehicle #*i *is maintaining a* ω_{ki}*-weighted desired position with respect to the vehicle #*k.

Definition 2.6. *For a formation flight of* N *vehicles with absolute measurements, the nearest (first-order) neighbor set of a vehicle #*i *is defined as the index set of all the vehicles #*k *such that* $\omega_{ki} \neq 0$, *that is* $\mathscr{N}(\{i\}) = \{k \in \{1, ..., N\} | \omega_{ki} \neq 0\}$. *For the index set* $\{i_1, ..., i_k\} \in \{1, ..., N\}$, *we define* $\mathscr{N}(\{i_1, ..., i_k\}) = \mathscr{N}(\{i_1\}) \cup \cdots \cup \mathscr{N}(\{i_k\})$ *and the*

inclusive nearest neighbor set $\mathscr{N}^{+}(\{i_1,...,i_k\}) = \mathscr{N}(\{i_1,...,i_k\}) \cup \{i_1,...,i_k\}$. *The normalized formation weights* ω_{ik} *satisfy* $\forall \mathrm{i} : \sum_{k \in \mathscr{N}^{+}(\{i\})} \omega_{ki} = 1$. *The general s-order neighbor set is defined as*

$$\mathscr{N}^{s}(\{i_1,...,i_k\}) = \underbrace{\mathscr{N}(\mathscr{N}(...\mathscr{N}}_{s\ times}(\{i_1,...,i_k\}))),$$

the full-order neighbor set is defined as

$$\mathscr{N}^{[1,\infty]}(\{i_1,...,i_k\}) = \bigcup_{s=1}^{\infty} \mathscr{N}^{s}(\{i_1,...,i_k\}),$$

and the inclusive full-order neighbor set is defined as

$$\mathscr{N}^{+[1,\infty]}(\{i_1,...,i_k\}) = \mathscr{N}^{[1,\infty]}(\{i_1,...,i_k\}) \cup (\{i_1,...,i_k\})$$

Definition 2.7. *For a formation flight of unmanned vehicles with absolute measurements, the* weighted absolute measurement formation (WAMF) directed graph (digraph) *is defined by* $G_{WAMF}(V_{WAMF}, E_{WAMF})$*, in which the vertex* v_i *represents the vehicle #i and the edge* e_{ij} *represents the fact that the source vehicle #i is in the nearest neighbor set of the sink vehicle #j with the formation weight* $\omega_{ij} \neq 0$*. Moreover, the adjacency matrix* Ω *is defined as [132]:*

$$\Omega = \begin{bmatrix} 0 & \omega_{21} & \cdots & \omega_{N1} \\ \omega_{12} & 0 & \cdots & \omega_{N2} \\ \vdots & \vdots & \ddots & \vdots \\ \omega_{1N} & \omega_{2N} & \cdots & 0 \end{bmatrix}$$

2.1.2 Decentralized Fixed Mode

Consider the general form of a linear system that is represented by the triplet (A, B, C) as follows

$$\begin{aligned} \dot{X} &= AX + \begin{bmatrix} B_1 & \cdots & B_{N_s} \end{bmatrix} \overbrace{\begin{bmatrix} U_1 \\ \vdots \\ U_{N_s} \end{bmatrix}}^{U} \\ \underbrace{\begin{bmatrix} Y_1 \\ \vdots \\ Y_{N_s} \end{bmatrix}}_{Y} &= \begin{bmatrix} C_1 \\ \vdots \\ C_{N_s} \end{bmatrix} X \end{aligned} \tag{2.1}$$

where $X(t) \in R^n$, $U(t) \in R^r$, and $Y(t) \in R^m$ are the state, input, and output vectors, respectively. Moreover, we have $B_i \in R^{n \times r_i}$, $C_i \in R^{m_i \times n}$, $U_i(t) \in R^{r_i}$, and $Y_i(t) \in R^{m_i}$

(with $\sum_{i=1}^{N_s} r_i = r$ and $\sum_{i=1}^{N_s} m_i = m$). Consider the feedback gain matrix $K \in \mathbf{K}$ with the following structure

$$\mathbf{K} = \left\{ K \in R^{r\times m} \middle| \, K = diag(\mathrm{K_i})_{i=1}^{N}, \mathrm{K_i} \in R^{r_i \times m_i}, i = 1, ..., N_s, \sum_{i=1}^{N_s} r_i = r, \sum_{i=1}^{N_s} m_i = m \right\} \quad (2.2)$$

The complex number $\lambda \in C$ is a *decentralized fixed mode (DFM)* [133] of the system (2.1) with respect to the feedback gain matrix $\mathbf{K}$ in (2.2) if

$$\lambda \in \bigcap_{K\in\mathbf{K}} eigs\,(A - BKC) \quad (2.3)$$

where $eigs\,(M)$ denotes the set of all eigenvalues of the matrix M.

Theorem 2.1. *([133]) There exists a decentralized linear time-invariant controller for the system* (2.1) *such that all the poles of the closed-loop system are in the left half plane if and only if the decentralized fixed modes of the system* (2.1) *are contained in the left half plane.*

2.1.3 Linear Matrix Inequality

The LMI technique is applicable to a wide range of constrained convex optimization fields including the control engineering [134]. A linear matrix inequality (LMI) is an inequality of the following form

$$A(y) = A_0 + \sum_{i=1}^{M} A_i y_i \leq 0$$

where $y = \begin{bmatrix} y_1 & \cdots & y_M \end{bmatrix}^T$ is the vector of unknown variables, namely the decision or optimization variables, and A_i, $i = 0, ..., M$ are the given symmetric matrices. $A(y)$ is negative semidefinite if and only if the largest eigenvalue of $A(y)$ is smaller than or equal to zero. According to [135], the largest eigenvalue of $A(y)$ is a convex function of y, and so the solution of the LMI condition $A(y) \leq 0$ is a convex set. Therefore, finding a solution y to the LMI condition $A(y)$ is a convex optimization problem.

The following lemmas will be used in the following chapters.

Lemma 2.1. *(Schur Complement) Consider a matrix H as follows*

$$H = \begin{bmatrix} H_{11} & H_{12} \\ H_{12}^T & H_{22} \end{bmatrix}, \; (H_{11} = H_{11}^T \; and \; H_{22} = H_{22}^T)$$

The matrix H is positive definite if and only if one of the two equivalent condition sets $\{H_{11} > 0, H_{22} - H_{12}^T H_{11}^{-1} H_{12} > 0\}$ or $\{H_{22} > 0, H_{11} - H_{12} H_{22}^{-1} H_{12}^T > 0\}$ is verified.

The matrix H is negative definite if and only if one of the two equivalent condition sets $\{H_{11} < 0, H_{22} - H_{12}^T H_{11}^{-1} H_{12} < 0\}$ or $\{H_{22} < 0, H_{11} - H_{12} H_{22}^{-1} H_{12}^T < 0\}$ is verified.

Proof: *Refer to [136].* ■

Lemma 2.2. *(Bounded Real Lemma) Consider a continuous-time transfer function $H(s) = D + C(sI - A)^{-1}B$. There exists a positive scalar $\gamma > 0$ such that $||H(s)||_\infty < \gamma$ and $\mathrm{Re}(eig(A)) < 0$, where $\mathrm{Re}(.)$ represents the real part of a real number and $eig(.)$ represents the eigenvalue of a matrix, if and only if there exists a positive definite matrix X that satisfies one of the following equivalent LMIs:*

$$\begin{bmatrix} A^T X + XA & XB & C^T \\ B^T X & -\gamma I & D^T \\ C & D & -\gamma I \end{bmatrix} < 0 \text{ or } \begin{bmatrix} AX + XA^T & B & XC^T \\ B^T & -\gamma I & D^T \\ CX & D & -\gamma I \end{bmatrix} < 0$$

Proof: *Refer to [136].* ■

Lemma 2.3. *Consider a linear time-invariant system*

$$\begin{cases} \dot{x} = Ax + Bu \\ y = Cx \end{cases}$$

with the initial condition $x(0)$, and the linear quadratic cost function

$$J_{LQR}(u, Q, R) = \int_0^\infty x^T Q x + u^T R u$$

where $Q > 0$ and $R > 0$. Taking the state feedback $u = Kx$, there exists a positive scalar $\gamma > 0$ such that $J(u) < \gamma$ if there exist a positive definite matrix X and a matrix Y that form the feedback gain $K = YX^{-1}$ and satisfy the following LMIs:

$$\begin{bmatrix} AX + XA^T + BY + Y^T B^T & X & Y^T \\ X & -Q^{-1} & 0 \\ Y & 0 & -R^{-1} \end{bmatrix} \leq 0$$

$$\begin{bmatrix} \gamma & x^T(0) \\ x(0) & X \end{bmatrix} \geq 0$$

Proof: *Refer to [134].* ■

2.1.4 Some Useful Notations

The following definitions introduce some notations that will be used in this thesis for sake of simplicity and brevity.

Definition 2.8. *The submatrices $M_{[i,j]_{a\times b}}$, $M_{[i,:]_a}$, $M_{[:,i]_a}$ and $M_{[i_1:i_2,j_1:j_2]}$ and the subvectors $M_{[i]_a}$ and $M_{[i_1:i_2]}$ are defined as follows:*

a) The submatrix $M_{[i,j]_{a\times b}}$ is defined as the matrix including all those elements of the matrix M that are limited to the rows $\#((i-1)a+1), ..., \#ia$ and the columns $\#((j-1)b+1), ..., \#jb$ (as a special case, $M_{[i,j]}$ represents the element $\#ij$ of the matrix M).

b) The submatrix $M_{[i,:]_a}$ is defined as the matrix including all those elements of the matrix M that are limited to the rows $\#((i-1)a+1), ..., \#ia$ (as a special case, $M_{[i,:]}$ represents the row $\#i$ of the matrix M).

c) The submatrix $M_{[:,i]_a}$ is defined as the matrix including all those elements of the matrix M that are limited to the columns $\#((i-1)a+1), ..., \#ia$ (as a special case, $M_{[:,i]}$ represents the column $\#i$ of the matrix M).

d) The submatrix $M_{[i_1:i_2,j_1:j_2]}$ is defined as the matrix including all those elements of the matrix M that are limited to the rows $\#i_1, ..., \#i_2$ and the columns $\#j_1, ..., \#j_2$.

e) The subvector $M_{[i]_a}$ is defined as the vector including all those elements of the vector M that are limited to the elements $\#((i-1)a+1), ..., \#ia$ (as a special case, $M_{[i]}$ represents the element $\#i$ of the vector M).

f) The subvector $M_{[i_1:i_2]}$ is defined as the vector including all those elements of the vector M that are limited to the elements $\#i_1, ..., \#i_2$.

Definition 2.9. *For a given matrix $M \in R^{n\times m}$ if one eliminates the rows $r_1, ..., r_i$ $(1 \leq r_1 < \cdots < r_i \leq n)$ and the columns $c_1, ..., c_j$ $(1 \leq c_1 < \cdots < c_j \leq m)$, the resulting matrix is represented and denoted by*

$$M^{(-\{r_1,...,r_i\},-\{c_1,...,c_j\})} = \begin{bmatrix} M_{[1:r_1-1,1:c_1-1]} & M_{[1:r_1-1,c_1+1:c_2-1]} & \cdots & M_{[1:r_1-1,c_j+1:m]} \\ M_{[r_1+1:r_2-1,1:c_1-1]} & M_{[r_1+1:r_2-1,c_1+1:c_2-1]} & \cdots & M_{[r_1+1:r_2-1,c_j+1:m]} \\ \vdots & \vdots & \ddots & \vdots \\ M_{[r_i+1:n,1:c_1-1]} & M_{[r_i+1:n,c_1+1:c_2-1]} & \cdots & M_{[r_i+1:n,c_j+1:m]} \end{bmatrix} \in R^{(n-i)\times(m-j)}$$

where $M_{[r_i:r_j,c_i:c_j]}$ denotes the submatrix of M which includes the elements up to and including the rows r_i and r_j, and the columns c_i and c_j.

2.2 Problem Formulation and Methodology

In this section, the research problem is formulated by presenting the state space model of a multi-vehicle formation and the classes of actuator failures that are considered in this thesis. The methodologies to tackle the relevant problems in our proposed cooperative fault estimation and accommodation framework are explained.

2.2.1 Problem Formulation

Consider a formation of N vehicles with the relative measurement formation (RMF) digraph $G_{RMF}(V_{RMF}, E_{RMF})$ as per Definition 2.3. The linear state space model of the formation is as follows:

$$\begin{aligned} \dot{X}_i &= AX_i + B_iU_i + W_i \quad (i = 1, ..., N) \\ Y_{ij} &= C_0(X_j - X_i) + V_{ij} \quad (j = 1, ..., N \ ; \ \mathrm{e_{ij}} \in E_{RMF}) \end{aligned} \tag{2.4}$$

where $X_i \in R^{n_0}$, $Y_i \in R^{m_0}$, and $U_i = \begin{bmatrix} u_{i,1} & \cdots & u_{i,r_0} \end{bmatrix}^T \in R^{r_0}$ are the state, input, and output vectors, respectively, in the local inertial frame, and the output matrix $C_0 \in R^{m_0 \times n_0}$ is the relative measurement matrix. The environmental disturbances and sensor noise are represented by $W_i \in R^{n_0}$ and $V_{ij} \in R^{m_0}$, respectively, and the actuators are modeled as ideal gains $B_i \in R^{n_0 \times r_0}$. The nominal (fault-free) value of B_i is represented by $\bar{B}$.

For the model (2.4), the actuator faults can be classified into four categories [137]: lock-in-place (LIP), hard-over failure (HOF), float, and loss-of-effectiveness (LOE). These types of actuator failure can be mathematically represented as follows:

$$B_iU_i = \begin{cases} \bar{B}U_i & \text{No Failure} \\ (\bar{B} + f_i)U_i = \bar{B}(I_{r_0 \times r_0} + \Pi_i)U_i & \text{Loss-Of-Effectiveness (LOE)} \\ 0_{n_0 \times 1} & \text{Float} \\ \bar{B}U_{Lock} & \text{Lock-In-Place (LIP)} \\ \bar{B}U_{Min} \text{ or } \bar{B}\mathrm{U_{Max}} & \text{Hard-Over Failure (HOF)} \end{cases} \tag{2.5}$$

where $f_i = \bar{B}\Pi_i \in R^{n_0 \times r_0}$, the negative semi-definite diagonal matrix $\Pi_i = diag(\pi_i) \in R^{r_0 \times r_0}$ with $\pi_i = \begin{bmatrix} \pi_{i1} & \cdots & \pi_{ir_0} \end{bmatrix}^T$ includes the LOE scalar parameters π_{ij}, $\bar{B}$ is the nominal value of the actuator gain, U_{Min} and $\mathrm{U_{Max}}$ are the minimum and maximum actuation, and U_{Lock} ($U_{Min} < U_{Lock} < U_{Max}$) is a constant level of actuation. The dynamic equation of the actuator fault parameters π_{ij} can be represented by

$$\dot{\pi}_i = 0 + W_i^f \tag{2.6}$$

where $W_i^f \in R^{r_0}$ is the corresponding vector of unreliabilities, which include the possible variations of π_i with time (if π_i is time invariant then $W_i^f = 0$). We define the *fault status operator* $\mathscr{F}\{.\}$ as below

$$\mathscr{F}\{i\} = \begin{cases} 1 & \text{LOE in vehicle } \#i \\ 0 & \text{Float/LIP/HOF in vehicle } \#i \end{cases} \tag{2.7}$$

Using the fault status operator $\mathscr{F}\{.\}$ in (2.7), the actuator failure model (2.5) can

be simplified as follows

$$B_i U_i = \begin{cases} \bar{B}(I_{r_0 \times r_0} + \Pi_i) U_i & \mathscr{F}\{i\} = 1 \\ \bar{B}\Pi_i & \mathscr{F}\{i\} = 0 \end{cases} \tag{2.8}$$

where for the case of $\mathscr{F}\{i\} = 0$ (Float, LIP, and HOF) we have

$$B_i U_i = \bar{B}\Pi_i = \begin{cases} 0_{n_0 \times 1} & \text{Float} \\ \bar{B} U_{Lock} & \text{LIP} \\ \bar{B} U_{Min} \text{ or } \bar{B}\mathrm{U}_{\mathrm{Max}} & \text{HOF} \end{cases} \tag{2.9}$$

In the following, the simplified general model of actuator failures in (2.8) will be utilized to form the overall fault-augmented state space model of the relative-measurement formation (Definition 2.2). Defining the relative state as $X_{ij} = X_j - X_i$ ($\forall e_{ij} \in E_{RMF}$ as per Definition 2.3, or equivalently, $\forall i, j \in \{1, ..., N\}$ such that either $i \in \mathscr{N}(\{j\})$ or $j \in \mathscr{N}(\{i\})$ as per Definition 2.4) and taking the overall fault-augmented state, environmental disturbances, process unreliabilities, input, output, and noise vectors, respectively, as

$$X = \begin{bmatrix} [X_{ij}]_{e_{ij} \in E_{RMF}} \\ [\pi_i]_{i=1}^{N} \end{bmatrix} \in R^{n_1} \ , \ W = \begin{bmatrix} [W_j - W_i]_{e_{ij} \in E_{RMF}} \\ 0_{Nr_0 \times 1} \end{bmatrix} \in R^{n_1}$$

$$\bar{W} = \begin{bmatrix} 0_{(N-1)n_0} \\ \left[W_i^f\right]_{i=1}^{N} \end{bmatrix} \in R^{n_1} \ , \ U = \begin{bmatrix} U_1 \\ \vdots \\ U_N \end{bmatrix} \in R^{r_1}$$

$$Y = [Y_{ij}]_{e_{ij} \in E_{RMF}} \in R^{m_1} \ , \ V = [V_{ij}]_{e_{ij} \in E_{RMF}} \in R^{m_1}$$

where $n_1 = (N-1)n_0 + Nr_0$, $r_1 = Nr_0$, and $m_1 = (N-1)m_0$, the overall fault-augmented state space model of the formation becomes

$$\begin{aligned} \dot{X} &= A_0 X + \sum_{i'=1}^{N} \sum_{j'=1}^{r_0} u_{i',j'} A_{i',j'} X + BU + W + \bar{W} \\ Y &= CX + V \end{aligned} \tag{2.10}$$

where we have

$$A_0 = \begin{bmatrix} diag(A)_{i=1}^{N-1} & \left[I_{ij}^A\right]_{e_{ij} \in E_{RMF}} \\ 0_{Nr_0 \times (N-1)n_0} & 0_{Nr_0 \times Nr_0} \end{bmatrix} \in R^{n_1 \times n_1}$$

$$I^A_{ij[:,k]_{r_0}} = \begin{cases} -\left(1 - \mathscr{F}\{i\}\right)\bar{B} & k = i \\ \left(1 - \mathscr{F}\{j\}\right)\bar{B} & k = j \\ 0_{n_0 \times r_0} & \text{otherwise} \end{cases}$$

$$A_{i',j'} = \begin{bmatrix} 0_{(N-1)n_0 \times (N-1)n_0} & \left[I_{ij}^{i',j'} \right]_{e_{ij} \in E_{RMF}} \\ 0_{Nr_0 \times (N-1)n_0} & 0_{Nr_0 \times Nr_0} \end{bmatrix} \in R^{n_1 \times n_1}$$

$$I_{ij[:,k]_{r_0}}^{i',j'} = \begin{cases} -\mathscr{F}\{i'\} \bar{B} I_{j'} & k = i = i' \\ \mathscr{F}\{i'\} \bar{B} I_{j'} & k = j = i' \\ 0_{n_0 \times r_0} & \text{otherwise} \end{cases}$$

$$I_{j'} = diag \underbrace{\left(\begin{bmatrix} 0 & \cdots & 1 & \cdots & 0 \end{bmatrix} \right)}_{\substack{j'^{th} \text{ element is one} \\ r_0 - 1 \text{ zeros totally}}} \in R^{r_0 \times r_0}$$

$$B = \begin{bmatrix} \left[I_{ij}^{B} \right]_{e_{ij} \in E_{RMF}} \\ 0_{Nr_0 \times Nr_0} \end{bmatrix} \in R^{n_1 \times r_1}$$

$$I_{ij[:,k]_{r_0}}^{B} = \begin{cases} -\mathscr{F}\{i\} \bar{B} & k = i \\ \mathscr{F}\{i\} \bar{B} & k = j \\ 0_{n_0 \times r_0} & \text{otherwise} \end{cases}$$

$$C = \begin{bmatrix} diag(C_0)_{i=1}^{N-1} & 0_{m_0 \times r_0 n_0} \\ 0_{m_0 \times r_0 n_0} & 0_{m_0 \times r_0 n_0} \end{bmatrix} \in R^{m_1 \times n_1}$$

If $\mathscr{F}\{i\} = 0$ ($\forall i \in \{1, ..., N\}$, corresponding to the float, LIP, and HOF types of actuator failure), then the system (2.10) is in the form of a linear time invariant (LTI) system. Therefore, in this case we consider the general equivalent state space representation of a LTI system S as follows:

$$S : \begin{cases} \dot{X} = AX + BU + W + \bar{W} \\ Y = CX + V \end{cases} \tag{2.11}$$

where

$$B = \begin{bmatrix} B_1 & \cdots & B_r \end{bmatrix}_{n \times r}, \; C = \begin{bmatrix} C_1 \\ \vdots \\ C_m \end{bmatrix}_{m \times n}$$

Moreover, $X = \begin{bmatrix} x_1 & \cdots & x_n \end{bmatrix}^T \in R^n$, $Y = \begin{bmatrix} y_1 & \cdots & y_m \end{bmatrix}^T \in R^m$, and $U = \begin{bmatrix} u_1 & \cdots & u_r \end{bmatrix}^T \in R^r$ are the state, output, and input vectors, respectively. In addition, $W = \begin{bmatrix} w_1 & \cdots & w_n \end{bmatrix}^T \in R^n$ and $V = \begin{bmatrix} v_1 & \cdots & v_m \end{bmatrix}^T \in R^m$ are the process disturbances and sensor noises, respectively.

On the other hand, if $\exists i \in \{1, ..., N\}$ such that $\mathscr{F}\{i\} \neq 0$ (corresponding to the LOE type of actuator failure), then the system (2.10) is in the form of a bilinear system. Therefore, in this case we consider the general equivalent state space representation of a bilinear system S as follows:

$$S : \begin{cases} \dot{X} = A_0 X + \sum_{i=1}^{r} u_i A_i X + BU + W + \bar{W} \\ Y = CX + V \end{cases} \tag{2.12}$$

Consider the overall fault-augmented state space model of the relative-measurement formation in equations (2.11) and (2.12). The cooperative fault estimation problem is to design a supervisory cooperative estimation framework as shown in Figure 2.1, in which the low-level fault estimation (LLFE) modules are called *sub-observers*. These LLFE sub-observers can cooperate in the sense of information exchange among themselves through communication channels that constitute the formation-level fault estimation (FLFE) scheme. The cooperation (information exchange) among the sub-observers is supervised by a high-level (HL) supervisor that is provided with information from a performance monitoring (PM) module. The PM module determines the estimation performance by receiving the status of unmodeled uncertainties and disturbances from a fault detection and isolation (FDI) module. One major problem is how to design sub-observers for each case of linear and bilinear models (2.11) and (2.12), respectively. To this end, a formal procedure is required to split the overall formation model among the cooperative local sub-observers. Moreover, a supervisor is needed to choose the proper set of sub-observers such that the convergence of the cooperative estimation scheme is guaranteed.

Based on the fault estimates (accomplished by the LLFE and FLFE modules as in Figure 2.1), the low-level fault recovery (LLFR) controllers are to be designed. In the case of relative-measurement formation missions (as per Definition 2.2), both the centralized and decentralized approaches are to be implemented in order to design the LLFR controllers by using the relative measurement formation (RMF) digraph (as per Definition 2.3). The tradeoffs between the centralized and decentralized approaches are to be discussed in order to justify the application of each approach in different failure situations.

In the case of absolute-measurement formation missions (as per Definition 2.2), LLFR controllers are to be designed based on the weighted absolute measurement formation (WAMF) digraph (as per Definition 2.7). The number of nonzero elements on a certain row $\#i$ of the formation adjacency matrix Ω determines the number of vehicles from which the vehicle $\#i$ requires to get feedback in order to generate its LLFR controller output. The tradeoffs between the number (and position) of nonzero elements

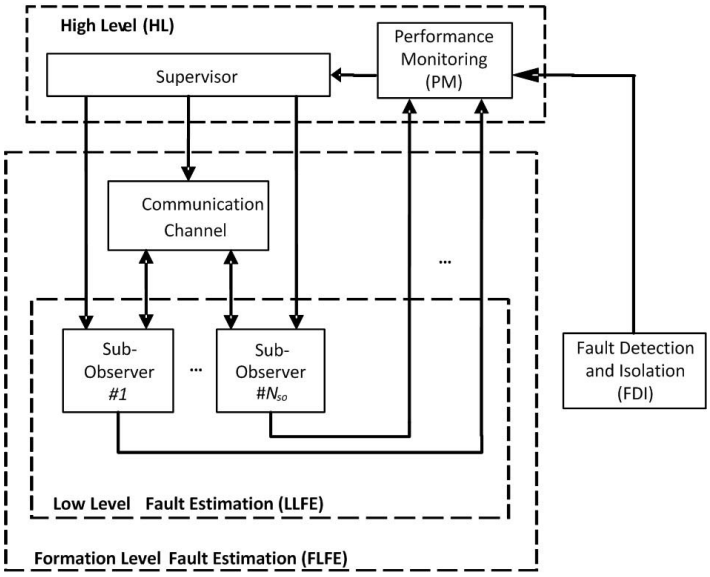

Figure 2.1: Structure of the proposed cooperative fault estimation system where N_{so} represents the total number of sub-observers.

in the adjacency matrix Ω and the performance of the formation under different failure scenarios are to be discussed.

If a fault in the vehicle $\#i$ is not properly estimated by the LLFE and FLFE modules, then the fault estimate is inaccurate or biased. Once the inaccurate (biased) fault estimate is incorporated in the LLFR controller, the output tracking error may exceed the desired error specification (as denoted by e_s) of the formation mission. The performance monitoring (PM) module (as shown in Figure 1.6) detects this violation of the error specification and identifies the *partially low-level (LL) recovered* vehicle $\#i$.

Definition 2.10. *In a formation flight of unmanned vehicles if a vehicle violates the error specification that is imposed on the formation due to incorporating inaccurate (biased) fault estimate (provided by the LLFE and FLFE modules) in the LLFR controller, then the vehicle is defined as a partially low-level (LL) recovered vehicle.*

The performance monitoring (PM) module sends the information about the partially LL-recovered vehicle to the supervisor (as shown in Figure 1.6). The supervisor in turn activates the formation level fault recovery (FLFR) module to compensate for the resulting performance degradation of the formation. The FLFR module is required to offer a systematic procedure to redesign the controllers, impose constraints on the desired input vectors, and reconfigure the formation digraph if necessary as discussed in subsequent sections and chapters.

2.2.2 Cooperative Fault Estimation Approach

Consider the vehicle $\#i$ in equation (2.4) and assume that the fault vector π_i in equations (2.5) and (2.6) is constant or slowly time-varying. In order to simultaneously estimate the state $X_i \in R^n$ and the fault parameter $\pi_i \in R^n$, the fault vector π_i can be augmented to the state of the system to form the fault-augmented state space model (2.10), to which the joint state and parameter estimation method [138], [139] can be applied.

In the three cases of float, LIP, and HOF, the fault-augmented state space model is in the form of a linear time-varying (LTI) system as in equation (2.11). In order to study the observability of the LTI model, the structural observability theorems [140], [141], [142] are applied to the system. These theorems are used along with the Grammian theorem [143] to develop a procedure to study the feasibility of the distributed and cooperative estimation units, namely the *sub-observers*, whose cooperation is in terms of information exchange on their local state estimates. The feasibility of distributed sub-observers is analyzed by using the notion of decentralized fixed mode (DFM) [133].

In order to design sub-observers in our proposed estimation framework, the differential operators (as in the differential algebra theory [113]) are avoided by implementing linear filtering techniques to prevent the negative impact of the sensor noise on the multiple differential operators. This is done based on the robust H_∞ Luenberger observer and linear matrix inequality (LMI) approaches [134], [135], [136] in order to perform the joint state and parameter estimation [138], [139] (using the fault-augmented state space model (2.11)). In case that a state is estimated by multiple sub-observers, due to the LTI model of the system the linear combination method [144], [145], [146], [147], [148] will be used to fuse the data from all the sub-observers. Moreover, a supervisor is assigned to select a subset of sub-observers to estimate all the states of the system while the effects of process dynamics and sensor measurement unreliabilities are confined. The role of the supervisor is explained by introducing the (E) estimation and weighted estimation (WE) digraphs. These issues will be discussed in Chapter 3.

In the case of actuator failures of the LOE type, the fault-augmented state space model is in the form of a bilinear system as shown in equation (2.12). The structural observability theorems [149], [150], [151] and the Grammian observability theorem [143] are used to study the structural observability of the distributed and cooperative estimation units, namely the *sub-observers*. The bilinear system (2.12) is in fact equivalent to a linear time-varying system from the estimation perspective. Therefore, Kalman filtering technique is used to design each sub-observer in order to perform the joint state and parameter estimation [138], [139] (using the fault-augmented state space model (2.12)). In case that a state is estimated by multiple sub-observers, due to the probabilistic model

of the system the probabilistic fusion method [144], [152] will be used to fuse the data from all the sub-observers. The convergence of the cooperative distributed (Kalman) sub-observers is analyzed by defining the sub-observer dependency (SOD) digraph and assuming that the SOD digraph is acyclic [153].

The cooperation among the sub-observers is in terms of information exchanges regarding their local state estimates. Similar to the case of a LTI system, a supervisor is designed based on graph theory to select a subset of the designed sub-observers. The role of the supervisor is formulated by the proposed sub-observer dependency estimation (SODE) and weighted sub-observer dependency estimation (WSODE) digraphs. These issues will be discussed in Chapter 4.

2.2.3 Cooperative Fault Accommodation Approach

Consider the four-vehicle formation whose digraph is depicted in Figure 2.2. Assume that vehicle #2 is subject to an actuator fault. Furthermore, it is only partially recovered by the low-level fault recovery (LLFR) controller due to the presence of possible biased and inaccurate fault estimates (provided by the LLFE and FLFE modules). As a result, vehicle #2 tracks the desired trajectory within an error bound of radius r, which is greater than the error specification e_s that is defined for the mission (that is, $r > e_s$). The main purpose of the formation-level fault recovery (FLFR) module is to reduce the error bound r so that the overall error specification of the formation mission is guaranteed (that is, $r < e_s$).

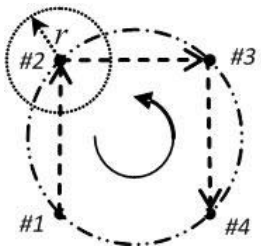

Figure 2.2: A four-vehicle formation flight.

In case of formation flight of unmanned vehicles with relative measurements (as per Definition 2.2), either a centralized or a decentralized recovery controller can be designed. The centralized approach is preferable to the decentralized one in the sense that it constrains the effect of a local failure and prevents the propagation of the resulting error to the entire formation. The decentralized method is preferable to the centralized one in the sense that it requires less communication efforts among the vehicles but a local failure can lead to a global manifestation of the resulting error. These issues will be

explained in detail in Chapters 5 and 6.

In a formation of multiple vehicles with relative measurements, a centralized controller can be designed based on the LMI-based robust H_∞ state feedback control techniques [134], [135], [136], in order to minimize the effects of the disturbances on the tracking errors. It will be shown that due to relative measurements, there exists a degree of freedom in designing the control signals. This degree of freedom can be used to accommodate a partially low-level (LL) recovered vehicle, which is defined as a faulty vehicle with inaccurate or biased fault estimates. The accommodation is accomplished by restricting the control effort of the partially LL-recovered vehicle at the expense of other healthy vehicles being imposed to some criteria on their input signals to account for the performance degradation of the partially LL-recovered vehicle. The centralized method requires all-to-all communication links but its advantage is that it constrains the effect of a local failure to the local vehicles.

In a formation of multiple vehicles with relative measurements, a decentralized controller can also be designed based on the LMI-based robust H_∞ state feedback control techniques [134], [135], [136], and the notion of the nearest neighbor sets. The nearest neighbor set (Definition 2.4) of a vehicle $\#i$ is defined as the set of all vehicles with respect to which the vehicle $\#i$ makes the relative measurements (Definition 2.2). Therefore, there exist local communication links that make the decentralized technique communicationally more efficient as compared with the centralized approach. However, this communication efficiency is at the cost of the disadvantage of the decentralized controller, which is due to the error propagation of a local failure to the entire formation.

In a formation of multiple vehicles with absolute measurements (as per Definition 2.2), the formation adjacency matrix [132] can be defined based on the formation weights (as per Definition 2.7), which determines the s-order neighbor sets (as in Definition 2.6). A controller can be designed based on the adjacency matrix of a formation, and the structure of the adjacency matrix determines whether the controller is centralized or decentralized. Therefore, the formation system will be studied merely based on its adjacency matrix regardless of the "centralized" or "decentralized" contexts. However, a centralized controller is preferable in the sense that it can accommodate more fault scenarios than a decentralized controller. This advantage is at the cost of all-to-all communication links for a centralized controller.

In a formation of multiple vehicles with absolute measurements and a partially LL-recovered vehicle, the formation weights need to be adjusted such that the impact of a faulty vehicle on the formation performance will be managed. Once the weights are selected, a robust H_∞ controller [134], [135], [136] can be designed to account for the uncertainties in the estimated fault parameters. Finally, some constraints are imposed on the overall desired inputs of some vehicles, which are in the nearest neighbor set of the

partially LL-recovered vehicle, in order to compensate for the performance degradations of the entire formation mission.

2.3 Conclusions

In this chapter, background information is presented that includes formation digraph, decentralized fixed mode (DFM), and linear matrix inequality (LMI). Moreover, some useful notations are introduced that will be used throughout this thesis. The problem formulation is presented in terms of the state space model of the formation with a certain formation digraph and actuator failure model. The technical problems are described for both cases of cooperative fault estimation and accommodation in a formation flight of unmanned vehicles. Finally, an overview of the approaches is provided that will be used in the subsequent chapters to tackle the technical problems in this thesis.

Chapter 3

Distributed and Cooperative Estimation of Formation Flight of Unmanned Vehicles with Relative Measurements Subject to Float, Lock-in-Place, and Hard-Over Actuator Faults

In this chapter, a novel framework is proposed for cooperative estimation of formation flight of unmanned vehicles with relative measurements subject to actuator failures of float, lock-in-place (LIP), and hard-over failure (HOF) types. This framework is developed based on the notion of *sub-observers* and is applicable to a large class of multi-agent linear time invariant (LTI) systems. We introduce a group of sub-observers where each sub-observer is estimating certain states that are conditioned on a given input, output, and state information. The state dependency (SD) digraph of the system is used to simplify and visualize the structure of sub-observers and the interconnection among them. The feasibility of the cooperative estimation scheme is analyzed using the concept of decentralized fixed mode from the decentralized control theory. We model the overall estimation task by an *estimation (E) digraph*. By selecting an appropriate path in the estimation digraph, the supervisor can select and configure a set of sub-observers to successfully estimate all the system states, while the feasibility of the overall integrated cooperative sub-observers is guaranteed. In presence of large disturbances and noise, some sub-observers become invalid, and so the supervisor reconfigures the set of selected sub-observers by selecting a new path in the estimation digraph, such that the impacts of

large disturbances and noise are managed and confined to the local estimates, and hence prevent them from propagation to the estimation performance of the entire formation.

In the next section, preliminary definitions and concepts that are required to develop our cooperative estimation framework are reviewed.

3.1 Preliminaries

In this section, the general case of a multiple vehicle formation flight system subject to float, lock-in-place, and hard-over actuator failures is formulated as a linear time-invariant (LTI) state space model as described in detail in Chapter 2, Section 2.2.1. The (SD) digraph of a LTI system is presented in order to simplify the study of the system properties by using the graph-based approaches. Based on the SD digraph of the formation flight system, structural observability is presented that will help the development of our proposed distributed and cooperative estimation framework in the subsequent sections.

3.1.1 LTI Fault-Augmented State Space Model of Formation Flight of Unmanned Vehicles

Consider a formation of N vehicles with the relative measurement formation (RMF) digraph $G_{RMF}(V_{RMF}, E_{RMF})$ as per Definition 2.3. The linear state space model of the formation is given by equation (2.4). In the following, the cases of float, LIP, and HOF is considered for all the vehicles and the simplified general model of actuator failures in (2.9) is utilized to form the overall fault-augmented state space model of the formation as given by equation (2.10). Moreover, it is assumed that $\dot{\pi}_i = 0$ ($W_i^f = 0$ in equation (2.6) whose effect will be analyzed later in this chapter).

If $\mathscr{F}\{i\} = 0$ ($\forall i \in \{1, ..., N\}$, corresponding to the float, LIP, and HOF types of actuator failure), then $A_{i',j'} = 0_{n_1 \times n_1}$ ($i' = 1, ..., N$ and $j' = 1, ..., r_0$) and therefore system (2.10) is in the form of a linear time invariant (LTI) system. Hence, in this case we consider the general equivalent state space representation of a LTI system S as follows:

$$S : \begin{cases} \dot{X} = AX + BU + W \\ Y = CX + V \end{cases} \tag{3.1}$$

where

$$B = \begin{bmatrix} B_1 & \cdots & B_r \end{bmatrix}_{n \times r}, \; C = \begin{bmatrix} C_1 \\ \vdots \\ C_m \end{bmatrix}_{m \times n}$$

Moreover, $X = \begin{bmatrix} x_1 & \cdots & x_n \end{bmatrix}^T \in R^n$, $Y = \begin{bmatrix} y_1 & \cdots & y_m \end{bmatrix}^T \in R^m$, and $U = \begin{bmatrix} u_1 & \cdots & u_r \end{bmatrix}^T \in R^r$ are the state, output, and input vectors, respectively. In addition, $W = \begin{bmatrix} w_1 & \cdots & w_n \end{bmatrix}^T \in R^n$ and $V = \begin{bmatrix} v_1 & \cdots & v_m \end{bmatrix}^T \in R^m$ are the process disturbances and sensor noises, respectively.

3.1.2 State Dependency (SD) Digraph for Formation Flight of Unmanned Vehicle Systems

In the following, the associated state dependency (SD) directed graph (digraph) of the linear formation vehicle system (3.1) is introduced [140], [141].

Definition 3.1. *For a LTI system S represented by the triplet matrices (A, B, C), the associated state dependency (SD) directed graph $G_{SD}(V_{SD}, E_{SD})$ is defined as follows:*

- *The* vertex *set is $V_{SD} = Set(U) \cup Set(X) \cup Set(Y)$ where U, X, and Y are the input, state, and output vectors, respectively, and $Set(\Psi)$ denotes the set of the elements of the vector Ψ.*
- *The* edge *set is defined as the union of* input-state, state-state, *and* state-output *edges as follows*

$$E_{SD} = \{(u_i, x_j) | b_{ji} \neq 0\} \cup \{(x_i, x_j) | a_{ji} \neq 0\} \cup \{(x_i, y_j) | c_{ji} \neq 0\} \tag{3.2}$$

  where a_{ji}, b_{ji}, and c_{ji} are the corresponding elements of the matrices A, B, and C, respectively.

Definition 3.2. *Consider a LTI system S and its directed graph G. A* directed path *$P = (v_{p_0}, v_{p_1}, \ldots, v_{p_{(l-1)}}, v_{p_l})$ from a vertex v_{p_0} to a vertex v_{p_l} is a sequence of edges (v_{p_0}, v_{p_l}), (v_{p_1}, v_{p_2}), ..., $(v_{p_{(l-2)}}, v_{p_{(l-1)}})$, $(v_{p_{(l-1)}}, v_{p_l})$ such that*

- *$v_{p_k} \in V$ for $k = 0, 1, ..., l$, and*
- *$(v_{p_{(k-1)}}, v_{p_k}) \in E$ for $k = 0, 1, ..., l$.*

Definition 3.3. *A path with $v_{p_0} \in U$ and $v_{p_l} \in Y$ is called an* input-output path. *Similarly, a path with $v_{p_0} \in X$ and $v_{p_l} \in Y$ is called a* state-output path. *A path with $v_{p_0} = v_{p_l}$ is called a* circuit. *Two edges $e_1 = (v_1, v_1') \in E$ and $e_1 = (v_1, v_1') \in E$ are said to be* vertex disjoint *if $v_1 \neq v_2$ and $v_1' \neq v_2'$. Note that e_1 and e_2 can be vertex disjoint even if $v_1' = v_2$ and $v_1 = v_2'$. Two paths $P_1 = (v_{p_{1,0}}, v_{p_{1,1}}, \ldots, v_{p_{1,(l_1-1)}}, v_{p_{1,l_1}})$ and $P_2 = (v_{p_{2,0}}, v_{p_{2,1}}, \ldots, v_{p_{2,(l_2-1)}}, v_{p_{2,l_2}})$ are said to be* vertex disjoint *if all of their edges $(v_{p_{1,(k_1-1)}}, v_{p_{1,k_1}})$, $k_1 = 0, 1, ..., l_1$, and $(v_{p_{2,(k_2-1)}}, v_{p_{2,k_2}})$, $k_2 = 0, 1, ..., l_2$, are mutually vertex*

disjoint. The length *of a path is the number of the consecutive edges required to complete the path.*

3.1.3 Observability and Structural Observability of the Formation Flight of Unmanned Vehicle Systems

For the class of systems with the same associated digraph (Definition 3.1), one can apply graph theory to study generic (or structural) properties. The graph-based properties simplify the study of system properties specifically when the dimensions of the system are large. However, the graph-based structural properties are true for almost all systems in the class of systems with the same graph, except for some pathological parameter matching cases that constitute a finite number of nontrivial polynomials in the system parameters. Therefore, conventional non-graph-based properties of a system are always required to be studied in order to confirm the results on the graph-based properties of that system. Among all the graph-based structural properties [140], [141], [142] we are interested in the structural observability that will be investigated next.

Proposition 3.1. *([141], [142]) Let S be a LTI system that is represented by the triplet (A, B, C) with its associated digraph G_{SD}. The system (or equivalently, the pair (C, A)) is* structurally observable *if and only if the following two conditions hold:*

- *There exists at least one state-output path originating from any state vertex in X; and*
- *There exists a set of vertex disjoint circuits and state-output paths which cover all state vertices.*

It should be noted that if a system S is structurally unobservable, then its associated digraph represents a class of systems that are all (including the system S itself) unobservable. But once a system is guaranteed to be structurally observable, its observability should be further validated by using the conventional Grammian theorem [143]. The Grammian theory provides a fundamental necessary/sufficient condition for observability of dynamical systems. In this thesis, although we introduce and use structural observability and graph-based analysis to demonstrate and visualize the feasibility of an observer, one needs to always verify the observability of the system by using the Grammian theory.

Using the properties of directed graph and structural observability presented here, the notion of *sub-observers* is defined in the next section to be utilized in our proposed distributed and cooperative estimation framework. Moreover, we present results to guarantee the feasibility of the overall cooperative sub-observers.

3.2 Distributed and Cooperative Sub-Observers in Formation Flight of Unmanned Vehicle Systems

In this section, a cooperative estimation framework is presented. In this framework, a set of multiple estimation agents, namely the *sub-observers*, are designed and a supervisor is developed. The objective of the supervisor is to select a subset of sub-observers that can estimate all the system states in presence of unreliable process dynamics and sensor measurements. The cooperation among the sub-observers is defined as the exchange of information on their local state estimates that aims at restricting the process dynamics and sensor measurement unreliabilities. In the following, the definition of sub-observers is presented and the notions of directed graph, observability, and structural observability that were discussed in the previous section are used to design and verify the feasibility of integrated sub-observers for the LTI fault-augmented state space model of a formation flight of vehicles subject to HOF, LIP, and float actuator failures.

Definition 3.4. *A sub-observer #i that is represented by* $SO^{(i)}(R^{(i)}|I^{(i)}, O^{(i)}, D^{(i)})$ *is a linear filter that is defined as*

$$\dot{\hat{X}}^{(i)} = A^{(i)}\hat{X}^{(i)} + \sum_{j \in \mathscr{N}(\{i\})} A^{(ij)}\hat{X}^{(j)} + B^{(i)}U^{(i)} + K^{(i)}(Y^{(i)} - C^{(i)}\hat{X}^{(i)}) \tag{3.3}$$

The range $R^{(i)}$ *is the set of state estimates that are being accomplished by* $SO^{(i)}$*. The* domain $D^{(i)}$ *is the set of state estimates that are not being accomplished by* $SO^{(i)}$ *but are received from the ranges* $R^{(j)}$ $(j \neq i)$ *of other sub-observers* $SO^{(j)}$ *as they directly affect the state estimates in* $R^{(i)}$ *through the dynamic equations of the system,* $\hat{X}^{(i)} \in R^{n^{(i)}}$ *and* $\hat{X}^{(j)} \in R^{n^{(j)}}$ *are the vectors of all the states in* $R^{(i)}$ *and* $D^{(j)}$*, respectively, and* $A^{(i)}(t) \in R^{n^{(i)} \times n^{(i)}}$ *and* $A^{(ij)}(t) \in R^{n^{(i)} \times n^{(j)}}$ *represent the partitions of the matrix* $A(t)$ *that correspond to the dependency of the states* $\hat{X}^{(i)}$ *(of* $SO^{(i)}$*) on itself and on the states* $\hat{X}^{(j)}$ *(of* $SO^{(j)}$*), respectively, as follows*

$$A^{(i)} = A^{(-S,-S)}\ ,\ S = \left\{ k \in \{1, ..., n\} |\, \hat{x}_k^{(i)} \notin D^{(i)} \right\} \tag{3.4}$$

$$A^{(ij)} = A^{(-S,-T)}\ ,\ T = \left\{ k \in \{1, ..., n\} | \hat{x}_k^{(j)} \notin R^{(j)} \right\} \tag{3.5}$$

The input set $I^{(i)} \subset Set(U)$ *and output set* $O^{(i)} \subset Set(Y)$ *are those that are required by* $SO^{(i)}$ *in order to make the state estimates in* $R^{(i)}$*. In addition,* $U^{(i)} \in R^{r^{(i)}}$ *is the vector of all the entities in* $I^{(i)}$ $(I^{(i)} = Set(U^{(i)}))$*, and* $B^{(i)} \in R^{n^{(i)} \times r^{(i)}}$ *represents the partition of the matrix* B *that corresponds to the dependency of the inputs* $U^{(i)}$ *on the states* $\hat{X}^{(i)}$ *as*

follows

$$\begin{aligned} B^{(i)} &= B^{(-S,-T)} \\ S &= \left\{k \in \{1,...,n\} | \hat{x}_k^{(i)} \notin D^{(i)}\right\} \\ T &= \left\{k \in \{1,...,r\} | u_k \notin I^{(i)}\right\} \end{aligned} \tag{3.6}$$

Moreover, $Y^{(i)} \in R^{m^{(i)}}$ *is the vector of all the entities in* $O^{(i)}$ *(*$O^{(i)} = Set(Y^{(i)})$*), and* $C^{(i)} \in R^{m^{(i)} \times n^{(i)}}$ *represents the partition of the matrix* C *that corresponds to the dependency of the outputs* $Y^{(i)}$ *on the states* $\hat{X}^{(i)}$ *as follows:*

$$\begin{aligned} C^{(i)} &= C^{(-S,-T)} \\ S &= \left\{k \in \{1,...,m\} | y_k \notin O^{(i)}\right\} \\ T &= \left\{k \in \{1,...,n\} | \hat{x}_k^{(i)} \notin D^{(i)}\right\} \end{aligned} \tag{3.7}$$

The matrix $K^{(i)}(t) \in R^{n^{(i)} \times m^{(i)}}$ *is the sub-observer dynamic gain. Given (conditioned on) availability of the information on* $I^{(i)}$*,* $O^{(i)}$*, and* $D^{(i)}$*, all the states of the overall system* S *whose estimates belong to* $R^{(i)}$ *are observable by using the sub-observer* $SO^{(i)}$*. The* nearest neighbor set $\mathscr{N}(\{i\})$ *and the* x_k-corresponding nearest neighbor set $\mathscr{N}_k(\{i\})$ *of a sub-observer* $SO^{(i)}$ *are defined, respectively, as follows*

$$\begin{aligned} \mathscr{N}(\{i\}) &= \left\{j \in \{1,...,N_{so}\} \mid \exists k \in \{1,...,n\}; \hat{x}_k^{(i)} \in D^{(i)}, \hat{x}_k^{(j)} \in R^{(j)}, \hat{x}_k^{(j)} \rightsquigarrow \hat{x}_k^{(i)}\right\} \\ &= \bigcup_{k \in \{1,...,n\}} \mathscr{N}_k(\{i\}) \\ \mathscr{N}_k(\{i\}) &= \left\{j \in \{1,...,N_{so}\} \mid \hat{x}_k^{(i)} \in D^{(i)}, \hat{x}_k^{(j)} \in R^{(j)}, \hat{x}_k^{(j)} \rightsquigarrow \hat{x}_k^{(i)}\right\} \end{aligned}$$

where $\hat{x}_k^{(j)} \rightsquigarrow \hat{x}_k^{(i)}$ *represents the fact that* $\hat{x}_k^{(j)} \in R^{(j)}$ *is sent from* $SO^{(j)}$ *to* $SO^{(i)}$ *in order to calculate* $\hat{x}_k^{(i)} \in D^{(i)}$*. Similar to Definition 2.6, for the index set* $\{i_1,...,i_k\} \in \{1,...,N_{so}\}$*, we define* $\mathscr{N}(\{i_1,...,i_k\}) = \mathscr{N}(\{i_1\}) \cup \cdots \cup \mathscr{N}(\{i_k\})$*. Moreover, the general* s-order neighbor set *is defined (similar to Definition 2.6) as*

$$\mathscr{N}^s(\{i_1,...,i_k\}) = \underbrace{\mathscr{N}(\mathscr{N}(...\mathscr{N}}_{s \text{ times}}(\{i_1,...,i_k\})))$$

If a state estimate $\hat{x}_p$, $p \in \{1,...,n\}$ is in the range of $SO^{(j)}$, then we write $\hat{x}_p^{(j)} \in R^{(j)}$. Moreover, if $\hat{x}_p$ is in the domain of another sub-observer $SO^{(i)}$, then we write $\hat{x}_p^{(i)} \in D^{(i)}$. In addition, the inputs $u_s \in I^{(i)}$, $s \in \{1,...,r\}$, and outputs $y_q \in O^{(i)}$, $q \in \{1,...,m\}$ of sub-observer $SO^{(i)}$ are members of the $Set(U)$ and $Set(Y)$ in equation (3.1), respectively.

Let us now provide further description to the problem of a given state being estimated by multiple sub-observers. Each state x_j, $j = 1,...,n$ could be estimated by one (multiple) sub-observer(s) $SO^{(k)}$ (i.e., $\hat{x}_j^{(k)} \in R^{(k)}$). In case that the estimate of x_j is required by the sub-observer $SO^{(l)}$ (i.e., $\hat{x}_j^{(l)} \in D^{(l)}$), a data fusion technique is required to combine all the estimates of x_j that are made by the sub-observers in $\mathscr{N}_j(\{l\})$.

Quite a few data fusion techniques [144] such as those based on linear combination, probabilistic fusion, Markov chain, and multiple criteria approaches have been proposed in the literature depending on the way the system is modeled. Due to the linear model that is considered in this chapter, the linear combination method with its different choices of the weights [144], [145], [146], [147], [148], and that represents a general class of information fusion including estimation versions ranking [154], weighted decision method (voting technique), and Bayesian inference technique [155], will be used in the following. Therefore, a linear combination of all the sub-observers $SO^{(k)}$ which estimate x_j is made, that is

$$\forall l \in S_{so} \triangleq \{1, ..., N_{so}\}, \forall j \in \{1, ..., n\}; \hat{x}_j^{(l)} \in D^{(l)}, \hat{x}_j^{(l)} = \sum_{k \in \mathcal{N}_j(\{l\})} \alpha_j^{(lk)} \hat{x}_j^{(k)} \tag{3.8}$$

where $0 \leq \alpha_j^{(lk)} \leq 1$ are the normalized weights that satisfy

$$\sum_{k \in \mathcal{N}_j(\{l\})} \alpha_j^{(lk)} = 1$$

The linear combination in equation (3.8) will be incorporated in the linear analysis that will be presented in Lemma 3.1 later in this chapter. Moreover, the weights will be considered as the design parameters by Lemma 3.2 in order to design an H_∞ robust observer.

For the sub-observer $SO^{(i)}$ in Definition 3.4, the expressions for $A^{(i)}$, $A^{(ij)}$, $B^{(i)}$, and $C^{(i)}$ in equations (3.4), (3.5), (3.6), and (3.7), respectively, can be used to provide the dynamic state space model of $X^{(i)}$ as follows:

$$\begin{aligned} \dot{X}^{(i)} &= A^{(i)} X^{(i)} + \sum_{j \in \mathcal{N}(\{i\})} A^{(ij)} X^{(j)} + B^{(i)} U^{(i)} + W^{(i)} \\ Y^{(i)} &= C^{(i)} \hat{X}^{(i)} + V^{(i)} \end{aligned} \tag{3.9}$$

where $W^{(i)} \in R^{n^{(i)}}$ and $V^{(i)} \in R^{m^{(i)} \times 1}$ are defined as follows:

$$W^{(i)} = W^{(-S,-\{\})} \ , \ S = \left\{ k \in \{1, ..., n\} | \hat{x}_k^{(i)} \notin D^{(i)} \right\} \tag{3.10}$$

$$V^{(i)} = V^{(-S,-\{\})} \ , \ S = \left\{ k \in \{1, ..., m\} | y_k \notin O^{(i)} \right\} \tag{3.11}$$

In fact, a sub-observer $SO^{(i)} : (I^{(i)}, O^{(i)}, D^{(i)}) \rightarrow R^{(i)}$ is a map that cannot operate independently if $D^{(i)} \neq \emptyset$. In such a case, $SO^{(i)}$ requires the information on state estimates $\hat{x}_m^{(i)} \in D^{(i)}$ from other sub-observers $SO^{(j)}$ ($\hat{x}_m^{(i)} := \hat{x}_m^{(j)}$; $\hat{x}_m^{(j)} \in R^{(j)}$). This implies that one needs to design and develop a cooperative framework for the sub-observers in the sense that they share and exchange information regarding their state estimates. The procedure presented below provides a constructive means for designing the sub-observers.

Procedure 3.1. *Consider the LTI system in equation* (3.1) *with the associated digraph as in Definition 3.1. A sub-observer simply constitutes a set of vertex disjoint circuits and state-output paths, such that there exists at least one state-output path originating from any state vertex of the sub-observer. Therefore, the sub-observers can be designed by following the proposed two steps, namely*

Step 1. The directed graph of the system is sketched according to the Definition 3.1.

Step 2. The sub-observer $SO^{(i)}$ is designed by choosing $I^{(i)} \subset Set(U)$, $O^{(i)} \subset Set(Y)$, and two sets of vertices from $Set(X)$ to form its domain $D^{(i)}$ and range $R^{(i)}$ such that the following three conditions are satisfied:

Condition 1. The states in $R^{(i)}$ and the output sensor measurements in $O^{(i)}$ should satisfy the conditions in Proposition 3.1.

Condition 2. The set of input vertices in $I^{(i)}$ and state vertices in $D^{(i)}$ should include all the vertices in $Set(U)$ and $Set(X)$, respectively, from which there exist incoming edges to the set of state vertices in $R^{(i)}$ and output vertices in $O^{(i)}$, unless the sub-observer $SO^{(i)}$ represents a direct measurement (namely y_p) of one state (namely x_p) where $R^{(i)} = \{\hat{x}_p^{(i)}\}$, $D^{(i)} = \{\}$, $I^{(i)} = \{\}$, and $O^{(i)} = \{y_p\}$.

Condition 3. Using the Grammian theorem [143], the states in $R^{(i)}$ should be observable upon the availability of the inputs $I^{(i)}$, outputs $O^{(i)}$, and state estimates $D^{(i)}$.

In its simplest graphic representation, a sub-observer consists of a set of vertex disjoint circuits and state-output paths, such that the observability of the states in the corresponding circuits and state-output paths is guaranteed.

Each sub-observer $SO^{(i)}$ can possibly be subject to unreliable information as follows:

$$\begin{aligned}\dot{\hat{X}}^{(i)} = A^{(i)}\hat{X}^{(i)} + \sum_{j \in \mathscr{N}(\{i\})} A^{(ij)}\hat{X}^{(j)} + B^{(i)}U^{(i)} \\ + K^{(i)}(Y^{(i)} - C^{(i)}\hat{X}^{(i)} + \bar{V}^{(i)}) - \bar{W}^{(i)}\end{aligned} \tag{3.12}$$

where the vectors $\bar{W}^{(i)}$ and $\bar{V}^{(i)}$ represent the uncertainties/unreliabilities in the process dynamics and sensor measurements of the sub-observer $SO^{(i)}$, respectively (in the fault-augmented state space model (3.1)). These uncertainties/unreliabilites can be due to the following sources:

- dynamic model of the augmented faults, e.g. $\bar{W} = \begin{bmatrix} 0_{1\times(N-1)n_0} & -\left[(W_i^f)^T\right]_{i=1}^{N} \end{bmatrix} \in R^{1\times n_1}$ (where W_i^f is defined in equation (2.6)) as in the fault-augmented state space model (2.10),
- communication delays (failures) in the transmission of input and output data, e.g. $\bar{W}^{(i)} = B^{(i)}(U^{(i)}(t) - U^{(i)}(t-\Delta t)) \in R^{n^{(i)}}$ and $\bar{V}^{(i)} = Y^{(i)}(t) - Y^{(i)}(t-\Delta t) \in R^{m^{(i)}}$ as in the sub-observer model (3.12), or

- communication delays (failures) in the transmission of the estimates $\hat{X}^{(j)}$ ($\forall j \in \{1, ..., N_{so}\}; D^{(i)} \cap R^{(j)} \neq \emptyset$) from $SO^{(j)}$ to $SO^{(i)}$, e.g. $\bar{W}^{(i)} = \sum_{j \in \mathscr{N}(\{i\})} A^{(ij)}(\hat{X}^{(j)}(t) - \hat{X}^{(j)}(t - \Delta t))$ as in the sub-observer model (3.12).

Taking $E^{(i)} = \hat{X}^{(i)} - X^{(i)}$ and using the model of $X^{(i)}$ from equation (3.9), the error dynamics for the sub-observer $SO^{(i)}$ is given by

$$\begin{aligned} \dot{E}^{(i)} = (A^{(i)} - K^{(i)}C^{(i)})E^{(i)} + K^{(i)}(V^{(i)} + \bar{V}^{(i)}) - (W^{(i)} + \bar{W}^{(i)}) \\ + \sum_{j \in \mathscr{N}(\{i\})} A^{(ij)} E^{(j)} \end{aligned} \tag{3.13}$$

In the next subsection, the sub-observer dependency (SOD) digraph will be defined for a group of sub-observers.

3.2.1 Sub-Observer Dependency (SOD) Digraph

In this subsection, the *sub-observer dependency (SOD) digraph* is introduced. For a set of sub-observers $\{SO^{(1)}, ..., SO^{(N_{so})}\}$, the associated SOD digraph $G_{\text{SOD}}(V_{\text{SOD}}, E_{\text{SOD}})$ is defined according to the following.

Vertex Set: The *vertex set* V_{SOD} includes the vertices v_i ($i = 1, 2, ..., N_{so}$), where the vertex v_i represents the sub-observer $SO^{(i)}$.

Edge Set: The *edge set* E_{SOD} includes the directed edges $e_{ij} = (v_i, v_j)$, where e_{ij} represents the information exchange from the sub-observer $SO^{(i)}$ to the sub-observer $SO^{(j)}$. In other words,

$$e_{ij} \in E_{\text{SOD}} \Longleftrightarrow i \in \mathscr{N}(\{j\}) \tag{3.14}$$

Definition 3.5. *A digraph is called* acyclic *if it has no cycles.*

Theorem 3.1. *([130]) Every acyclic digraph has at least one source vertex with zero in-degree and at least one sink vertex with zero out-degree.*

Theorem 3.2. *([130]) A digraph is acyclic if and only if its vertices can be ordered such that its adjacency matrix is upper (or lower) triangular.*

The sub-observers should be first validated before being used for the purpose of estimation. The *validity condition* of a sub-observer $SO^{(i)}$ depends on the uncertainties/unreliabilities $\bar{W}^{(i)}$ and $\bar{V}^{(i)}$ in the process dynamics and sensor measurements, respectively, which represents the accuracy of its state dynamic equations and measurement sensors. These notions are formally specified in the following subsection.

3.2.2 Validity Condition and Cost of a Sub-Observer

In this subsection, the *validity condition* and *cost* of a sub-observer are defined.

Definition 3.6. *The* validity condition $COND^{(i)}$ *of a sub-observer* $SO^{(i)}$ *is defined as follows:*

$$COND^{(i)} = \begin{cases} 0 \text{ (or } SO^{(i)} \text{ is valid)} & \text{if } \bar{W}^{(i)} = 0 \text{ and } \bar{V}^{(i)} = 0 \\ 1 \text{ (or } SO^{(i)} \text{ is invalid)} & \text{otherwise} \end{cases}$$

Implicit in Definition 3.6 is the fact that one requires availability of a diagnostic system for detecting the unreliabilities $\bar{W}^{(i)}$ and $\bar{V}^{(i)}$ to determine the validity conditions of the sub-observers as in the next assumption. However, a more detailed investigation on developing and designing these diagnosers (that are studied in [156]) are beyond the scope of this thesis and are not discussed any further.

Assumption 3.1. *It is assumed that an effective fault detection and isolation (FDI) module is available that, independent of the sub-observers, determines the validity conditions of the sub-observers (as formulated in Definition 3.6) by using change (fault) detection techniques.*

As discussed earlier, we would like to use a set of valid sub-observers to estimate all the system states. Therefore, the supervisor is required to take the information about the validity conditions from the FDI module (as per Assumption 3.1) and reconfigure a set of cooperative sub-observers, which are among the valid ones.

There may be cases in which the supervisor is not able to determine a set of sub-observers that can cooperatively estimate all the system states due to insufficiency of the number of valid sub-observers. In such cases, in order to select an appropriate set of sub-observers one may consider other criteria by assigning a cost to each sub-observer that is defined next.

Definition 3.7. *The* cost $COST^{(i)}$ *of a sub-observer* $SO^{(i)}$ *is defined as follows:*

$$COST^{(i)} = C_R COST_R^{(i)} + C_E COST_E^{(i)} + C_C COST_C^{(i)}$$

where the coefficients C_R, C_E, *and* C_C *are to be adjusted according to the significance of the* recovery cost $COST_R^{(i)}$, estimation cost $COST_E^{(i)}$, *and* communication cost $COST_C^{(i)}$ *of the sub-observer* $SO^{(i)}$, *respectively, which are defined as follows*

$$COST_R^{(i)} = \begin{cases} cost_r^{(i)} \in (0,\infty) & \mathscr{R}(i) = 1 \\ 0 & \mathscr{R}(i) = 0 \end{cases}$$

$$COST_E^{(i)} = \begin{cases} 0 & (COND^{(i)} = 0 \ or \ \mathscr{R}(i) = 1) \\ & and \\ & (\forall s > 0, \forall j \in \mathscr{N}^s(\{i\}) \text{: } COND^{(j)} = 0 \ or \ \mathscr{R}(j) = 1) \\ cost_e^{(i)} = n(R^{(i)}) & otherwise \end{cases}$$

$$COST_C^{(i)} = \begin{cases} cost_c^{(i)} = \sum\limits_{\substack{\forall k \in \{1,\ldots,n\}; \\ \exists j \in \mathscr{N}_k(\{i\})}} cost_{c,k}^{(i)} \in (0,\infty) & \exists j \in \mathscr{N}(\{i\}) \\ 0 & otherwise \end{cases}$$

where $n(.)$ *represents the cardinality value of a set, and the term* $\mathscr{R}(.)$ *is the* recovery status operator *that is defined as*

$$\mathscr{R}(i) = \begin{cases} 1 & \text{if } SO^{(i)} \text{ is invalid } (COND^{(i)} = 1) \text{ and recovered} \\ 0 & \text{if } SO^{(i)} \text{ is not recovered} \end{cases}$$

and the recovery of a sub-observer *is defined as repairment or replacement of its faulty sensors.*

These costs are to be interpreted as follows:

- $cost_r^{(i)} \in (0,\infty)$ is the recovery cost (e.g. sensor repairment or replacement cost) that is to be expensed to ensure $SO^{(i)}$ is valid by making $\bar{W}^{(i)} = 0$ and $\bar{V}^{(i)} = 0$ as in Definition 3.6.
- $cost_e^{(i)} = n(R^{(i)})$ is the estimation cost representing the number of states $n(R^{(i)})$ that are estimated by the sub-observer $SO^{(i)}$, where the sub-observer $SO^{(i)}$ is invalid ($COND^{(i)} = 1$) and not recovered ($\mathscr{R}(i) = 0$), or it has an invalid ($COND^{(j)} = 1$) and not recovered ($\mathscr{R}(j) = 0$) sub-observer $SO^{(j)}$ in its s-order neighbor set $\mathscr{N}^s(\{i\})$ (that is, $j \in \mathscr{N}^s(\{i\})$ for some $s > 0$).
- $cost_{c,k}^{(i)} \in (0,\infty)$ is the communication cost that is to be expensed to send the information about the estimate $\hat{x}_k^{(j)}$ from $SO^{(j)}$ to $SO^{(i)}$ (that is, $j \in \mathscr{N}_k(\{i\})$ or $e_{ji} \in E_{SOD}$ as in equation (3.14)).

We are now in a position to make the following assumption.

Assumption 3.2. *It is assumed that the supervisor is provided with information regarding the predefined costs* $cost_r^{(i)}$ *of the sub-observers in case of unreliable process dynamics and sensor measurements.*

In the next section, the role of a supervisor is explained by using the definitions of estimation (E) and weighted estimation (WE) digraphs.

3.3 The Role of a Supervisor

In this section, the objective and purpose of a supervisor is presented by defining the *estimation (E)* and *weighted estimation (WE) digraphs* for the cases of given sub-observer conditions $COND^{(i)}$ (as in Definition 3.6) and sub-observer costs $COST^{(i)}$ (as in Definition 3.7), respectively.

3.3.1 Estimation (E) Digraph

For a set of sub-observers $\{SO^{(1)}, ..., SO^{(N_{so})}\}$, the associated estimation digraph $G_E(V_E, E_E)$ is defined as following.

Vertex Set: The vertex set V_E includes all the vertices v_i, where $i = 1, 2, ..., 2^n$ and n is the dimension of the state vector in equation (3.1). Each vertex is assigned to a vector $\mathbf{v}_i \in R^n$ with the "1" and "0" entities that denote the "estimated" and "unestimated" status of the states, respectively, as follows:

$$\mathbf{v}_{i,[k]} = Logic\{x_k \text{ is estimated at vertex } \mathrm{v_i} \text{ or a preceding vertex}\} \quad (k = 1, ..., n)$$

where $\mathbf{v}_{i,[k]}$ represents the element $\#k$ of the vector $\mathbf{v}_i$ (as defined in Definition 2.8), and

$$Logic\{EXPRESSION\} = \begin{cases} 1 & \text{if Expression} \equiv \text{TRUE} \\ 0 & \text{otherwise} \end{cases}$$

In fact $\mathbf{v}_i$ identifies those states that are already estimated at vertex v_i or at any preceding vertices. Accordingly, the source vertex v_{source} and the sink vertex v_{sink} are assigned with the vectors $\mathbf{v}_{source} = 0_{n\times 1}$ and $\mathbf{v}_{sink} = 1_{n\times 1}$, respectively, where $0_{n\times 1}$ and $1_{n\times 1}$ denote $n \times 1$ vectors of zeros and ones, respectively. This implies that none of the states are estimated at v_{source} but all of the states are estimated at v_{sink} or a preceding vertex.

Edge Set: The edge set E_E includes all the directed edges $e^{(i)}_{a,b} = ((v_a, v_b), SO^{(i)}, COND^{(i)})$, where

- (v_a, v_b) indicates that the directed edge $e^{(i)}_{a,b}$ is a transition from v_a to v_b

- $SO^{(i)}$ indicates that the transition (v_a, v_b) along the directed edge $e^{(i)}_{a,b}$ is due to the implementation of the sub-observer $SO^{(i)}$ so that additional states are now estimated in v_b as compared to v_a according to $\mathbf{v}_b = OR\left\{\mathbf{v}_a, R^{(i)}_x\right\}$, where $R^{(i)}_{x,[k]} = Logic\left\{\hat{x}^{(i)}_k \in R^{(i)}\right\}$ $(k = 1, ..., n)$ and $(OR\{X, \mathrm{Y}\})_{[k]} = Logic\left\{(X)_{[k]} + (Y)_{[k]} \neq 0\right\}$ (the index $[k]$ is defined in Definition 2.8)

- $COND^{(i)} \in \{0, 1\}$ indicates that the transition (v_a, v_b) along the directed edge $e^{(i)}_{a,b}$ is conditioned on $COND^{(i)} = 0$ (as in Definition 3.6)

In the estimation digraph, the objective of the supervisor is to obtain information about the conditions $COND^{(i)}$ from the FDI module (as per Assumption 3.1), and to find a directed path $P = (V_P, E_P)$, which includes the vertex set $V_P = \{v_{source}, v_{i_1}, ..., v_{i_{p-1}}, v_{sink}\}$ and the directed edge set $E_P = \{e^{(j_1)}_{source,i_1}, e^{(j_2)}_{i_1,i_2}, ..., e^{(j_{p-1})}_{i_{p-2},i_{p-1}}, e^{(j_p)}_{i_{p-1},sink}\}$ (p is the length of the path P), that starts at v_{source} and ends at v_{sink} in the estimation digraph, while the conditions $COND^{(k)} = 0$ are satisfied for $\forall k \in \{j_1, j_2, ..., j_p\}$. Thus, the objective of the supervisor is summarized as follows:

$$\begin{array}{ll} \text{Find} & P = (V_P, E_P) \text{ with} \\ & V_P = \{v_{source}, v_{i_1}, ..., v_{i_{p-1}}, v_{sink}\} \subset V_E \text{ and} \\ & E_P = \{e^{(j_1)}_{source,i_1}, e^{(j_2)}_{i_1,i_2}, ..., e^{(j_{p-1})}_{i_{p-2},i_{p-1}}, e^{(j_p)}_{i_{p-1},sink}\} \subset E_E \\ s.t. & COND^{(k)} = 0\ ,\ \forall k \in \{j_1, j_2, ..., j_p\} \end{array} \tag{3.15}$$

As discussed in the previous sections, besides the information on whether a sub-observer $SO^{(i)}$ can be implemented ($COND^{(i)} = 0$) or not ($COND^{(i)} = 1$, as per Definition 3.6), in some applications the supervisor is provided with the information about the implementation cost $COST^{(i)}$ (as per Definition 3.7) of the sub-observer $SO^{(i)}$ (as per Assumption 3.2). This problem requires a more general and extended digraph model of the supervisor that will be considered in the next section.

3.3.2 Weighted Estimation (WE) Digraph

In the previous section, the condition $COND^{(i)} \in \{0, 1\}$ (as per Definition 3.6) was assigned to each sub-observer $SO^{(i)} \in \{SO^{(1)}, ..., SO^{(N_{so})}\}$, based on which the supervisor determines whether $SO^{(i)}$ can be implemented ($COND^{(i)} = 0$) in the directed path $P_{\text{sup}} = (V_{\text{sup}}, E_{\text{sup}})$ or not ($COND^{(i)} = 1$). Instead, in this section we assign the cost $COST^{(i)} \in [0, \infty]$ (as per Definition 3.7) to the sub-observer $SO^{(i)}$, and introduce the *weighted estimation (WE) directed graph (digraph)*. The WE digraph $G_{WE}(V_{WE}, E_{WE})$ is defined as follows:

Vertex Set: The vertex set V_{WE} is defined similar to the vertex set V_E. Accordingly, the source vertex v_{source} and the sink vertex v_{sink} are assigned with the vectors $\mathbf{v}_{source} = 0_{n\times 1}$ and $\mathbf{v}_{sink} = 1_{n\times 1}$.

Edge Set: The edge set E_{WE} includes all the directed edges $e_{ab}^{(i)} = ((v_a, v_b), SO^{(i)}, COST^{(i)})$, where

- (v_a, v_b) indicates that the directed edge $e_{ab}^{(i)}$ is a transition from v_a to v_b,
- $SO^{(i)}$ indicates that the transition (v_a, v_b) along the directed edge $e_{a,b}^{(i)}$ is due to the implementation of the sub-observer $SO^{(i)}$ so that additional states are now estimated in v_b as compared to v_a according to $\mathbf{v}_b = OR\left\{\mathbf{v}_a, R_x^{(i)}\right\}$
- $COST^{(i)} \in [0, \infty]$ is the weight of the directed edge $e_{a,b}^{(i)}$ that indicates the cost of the transition (v_a, v_b) along the directed edge $e_{a,b}^{(i)}$ by using the sub-observer $SO^{(i)}$.

In the WE digraph, the objective of the supervisor is to receive information on the costs $COST^{(i)}$ (as per Assumption 3.2), and to obtain a directed path $P = (V_P, E_P)$, which includes the vertex set $V_P = \{v_{source}, v_{i_1}, ..., v_{i_{p-1}}, v_{sink}\}$ along the directed edge set $E_P = \{e_{source,i_1}^{(j_1)}, e_{i_1,i_2}^{(j_2)}, ..., e_{i_{p-2},i_{p-1}}^{(j_{p-1})}, e_{i_{p-1},sink}^{(j_p)}\}$ (p is the length of the path P_{sup}), that starts at v_{source} and ends at v_{sink} in the WE digraph, while the cumulative cost of $COST^{(k)}$ is minimized for $\forall k \in \{j_1, j_2, ..., j_p\}$. The objective of the supervisor is summarized as follows:

$$
\begin{aligned}
Min \quad & \sum_{k=j_1}^{j_p} COST^{(k)} \\
s.t. \quad & \mathscr{R}(k) \in \{0, 1\} \text{ and} \\
& \forall l \in \{1, ..., n\}; \hat{x}_l^{(k)} \in D^{(k)} : \emptyset \neq \mathscr{N}_l(\{k\}) \in \left\{k' \in S_{so} | \hat{x}_l^{(k')} \in R^{(k')}\right\} \\
& P = (V_P, E_P) \text{ with} \\
& V_P = \{v_{source}, v_{i_1}, ..., v_{i_{p-1}}, v_{sink}\} \subset V_{WE} \text{ and} \\
& E_P = \{e_{source,i_1}^{(j_1)}, e_{i_1,i_2}^{(j_2)}, ..., e_{i_{p-2},i_{p-1}}^{(j_{p-1})}, e_{i_{p-1},sink}^{(j_p)}\} \subset E_{WE}
\end{aligned}
\tag{3.16}
$$

In [119], [120], and [117], the design and analysis of a supervisor in the Discrete Event System (DES) framework [157] is proposed to solve the problems (3.15) and (3.16) by finding the correct path in the system automaton, however these results are beyond the scope of this thesis and are not pursued any further.

Our proposed framework is demonstrated below through a numerical example of an LTI system. All the concepts that have been presented so far in this chapter are discussed and illustrated in detail to provide a transparent and clear transition to the feasibility analysis in the next section.

Example 3.1. *This example shows how the sub-observers are designed and how the supervisor makes decision on the proper set of sub-observers according to the validity conditions of the sub-observers. Consider the following two systems, namely (a) the system* (A, B, C) *with two sensor measurements* $\{y_1, y_2\}$*, and (b) the system* $(\tilde{A}, \tilde{B}, \tilde{C})$ *with one sensor measurement* $\{y_1\}$*.*

$$A = \begin{bmatrix} a_{11} & a_{12} & a_{13} \\ 0 & a_{22} & 0 \\ 0 & 0 & a_{33} \end{bmatrix}, \; B = \begin{bmatrix} 0 & 0 \\ 0 & b_{22} \\ b_{31} & 0 \end{bmatrix}, \; C = \begin{bmatrix} c_{11} & 0 & 0 \\ 0 & 0 & c_{23} \end{bmatrix}$$

$$\tilde{A} = \begin{bmatrix} a_{11} & a_{12} & a_{13} \\ 0 & 0 & 0 \\ 0 & 0 & 0 \end{bmatrix}, \; \tilde{B} = \begin{bmatrix} 0 & 0 \\ 0 & b_{22} \\ b_{31} & 0 \end{bmatrix}, \; \tilde{C} = \begin{bmatrix} c_{11} & 0 & 0 \end{bmatrix}$$

The directed graphs of the corresponding systems are shown in Figure 3.1-(a) and (b), respectively. In Figure 3.1-(a), the two vertex disjoint state-output paths (x_2, x_1, y_1) *and* (x_3, y_2) *cover all the states, and hence, guarantee the structural observability of the system (Proposition 3.1). In contrast, in Figure 3.1-(b) no such set of vertex disjoint circuits and state-output paths exist that cover all the states (vertices), implying that the system is structurally unobservable. Therefore, for further analysis we only consider the directed graph of the system* (A, B, C)*.*

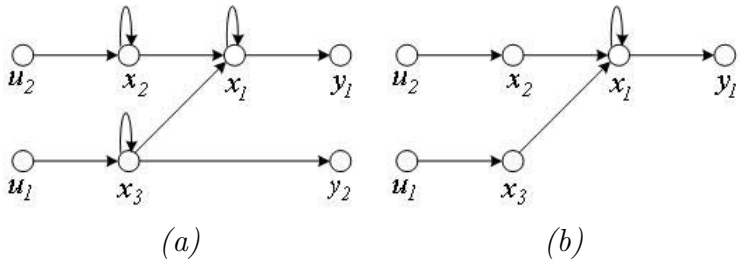

Figure 3.1: The directed graphs of the two systems (a) (A, B, C) *and (b)* $(\tilde{A}, \tilde{B}, \tilde{C})$

Let us now investigate the application of Procedure 3.1 for the structurally observable system (A, B, C)*. In step 1 of Procedure 3.1, the directed graph of the system* (A, B, C) *is constructed as shown in Figure 3.1-(a). According to the directed graph of the system it turns out that at most* <u>nine</u> *sub-observers, which are shown in Figure 3.2, can be designed in step 2 of Procedure 3.1 that* simultaneously *satisfy the conditions 1, 2, and 3.*

In Figure 3.2, the dashed lines represent the information that the sub-observer $SO^{(i)}$ *requires to receive regarding certain inputs* $u_s \in I^{(i)}$ *(*$s \in \{1, ..., r\}$*), outputs* $y_q \in O^{(i)}$ *(*$q \in \{1, ..., m\}$*), and state estimates* $\hat{x}_p^{(i)} \in D^{(i)}$ *(*$p \in \{1, ..., n\}$*) from other sub-observers* $SO^{(j)}$ *(such that* $\hat{x}_p^{(j)} \in R^{(j)}$ *and* $\hat{x}_p^{(i)} := \hat{x}_p^{(j)}$*). The solid lines represent the dynamic relations among the states* $\hat{x}_p^{(i)} \in R^{(i)}$ *of the sub-observer* $SO^{(i)}$*. Using Proposition 3.1*

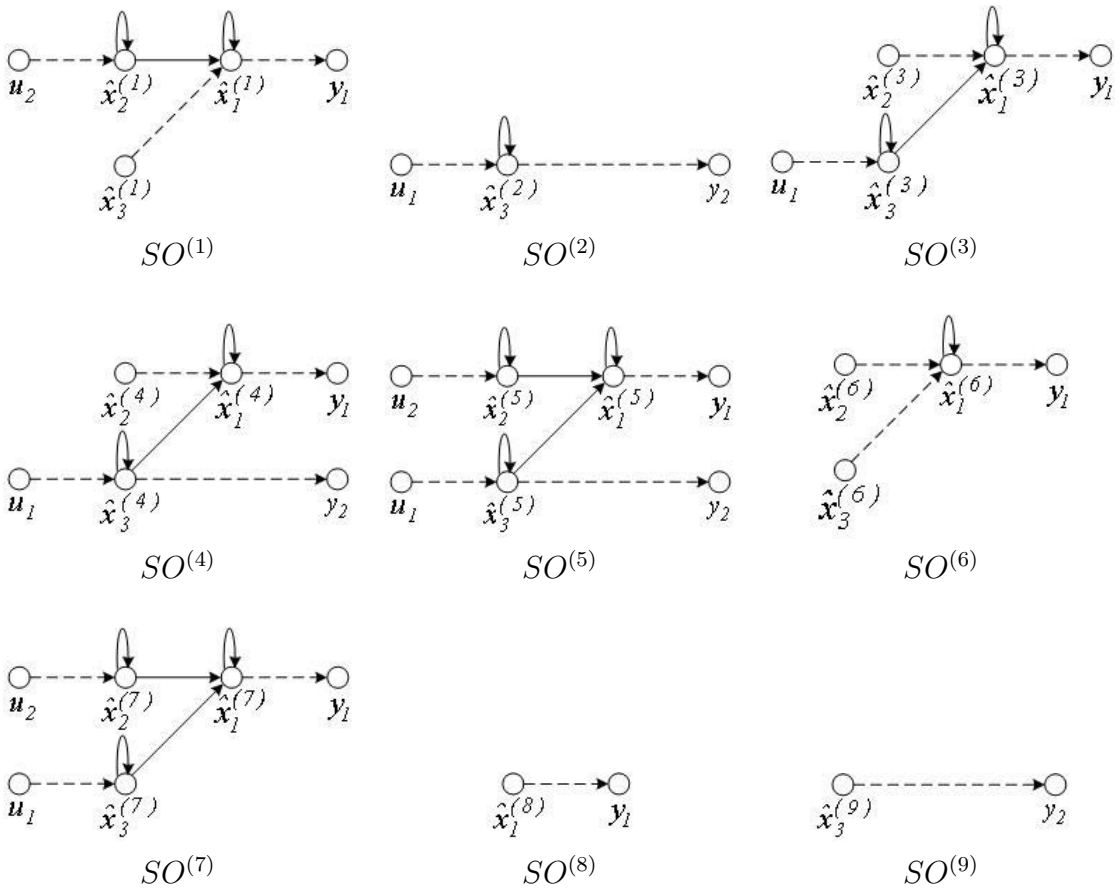

Figure 3.2: The directed graphs of the nine sub-observers for the system (A, B, C).

and the Grammian theorem [143] for each sub-observer $SO^{(i)}$, it is easy to verify that the graph representing $SO^{(i)}$ satisfies the conditions of the Proposition 3.1. The nine sub-observers are formally represented as follows:

$$
\begin{array}{ll}
(i) & SO^{(1)}(R^{(1)}|I^{(1)}, O^{(1)}, D^{(1)}) \\
 & R^{(1)} = \{\hat{x}_1^{(1)}, \hat{x}_2^{(1)}\}, I^{(1)} = \{u_2\}, O^{(1)} = \{y_1\}, D^{(1)} = \{\hat{x}_3^{(1)}\} \\
(ii) & SO^{(2)}(R^{(2)}|I^{(2)}, O^{(2)}, D^{(2)}) \\
 & R^{(2)} = \{\hat{x}_3^{(2)}\}, I^{(2)} = \{u_1\}, O^{(2)} = \{y_2\}, D^{(2)} = \{\} \\
(iii) & SO^{(3)}(R^{(3)}|I^{(3)}, O^{(3)}, D^{(3)}) \\
 & R^{(3)} = \{\hat{x}_1^{(3)}, \hat{x}_3^{(3)}\}, I^{(3)} = \{u_1\}, O^{(3)} = \{y_1\}, D^{(3)} = \{\hat{x}_2^{(3)}\} \\
(iv) & SO^{(4)}(R^{(4)}|I^{(4)}, O^{(4)}, D^{(4)}) \\
 & R^{(4)} = \{\hat{x}_1^{(4)}, \hat{x}_3^{(4)}\}, I^{(4)} = \{u_1\}, O^{(4)} = \{y_1, y_2\}, D^{(4)} = \{\hat{x}_2^{(4)}\} \\
(v) & SO^{(5)}(R^{(5)}|I^{(5)}, O^{(5)}, D^{(5)}) \\
 & R^{(5)} = \{\hat{x}_1^{(5)}, \hat{x}_2^{(5)}, \hat{x}_3^{(5)}\}, I^{(5)} = \{u_1, u_2\}, O^{(5)} = \{y_1, y_2\}, D^{(5)} = \{\} \\
(vi) & SO^{(6)}(R^{(6)}|I^{(6)}, O^{(6)}, D^{(6)}) \\
 & R^{(6)} = \{\hat{x}_1^{(6)}\}, I^{(6)} = \{\}, O^{(6)} = \{y_1\}, D^{(6)} = \{\hat{x}_2^{(6)}, \hat{x}_3^{(6)}\} \\
(vii) & SO^{(7)}(R^{(7)}|I^{(7)}, O^{(7)}, D^{(7)}) \\
 & R^{(7)} = \{\hat{x}_1^{(7)}, \hat{x}_2^{(7)}, \hat{x}_3^{(7)}\}, I^{(7)} = \{u_1, u_2\}, O^{(7)} = \{y_1\}, D^{(7)} = \{\} \\
(viii) & SO^{(8)}(R^{(8)}|I^{(8)}, O^{(8)}, D^{(8)}) \\
 & R^{(8)} = \{\hat{x}_1^{(8)}\}, I^{(8)} = \{\}, O^{(8)} = \{y_1\}, D^{(8)} = \{\} \\
(ix) & SO^{(9)}(R^{(9)}|I^{(9)}, O^{(9)}, D^{(9)}) \\
 & R^{(9)} = \{\hat{x}_3^{(9)}\}, I^{(9)} = \{\}, O^{(9)} = \{y_2\}, D^{(9)} = \{\}
\end{array}
$$

In each of the sub-observers $SO^{(8)}$ and $SO^{(9)}$, there is only one sensor that is involved in the observation resulting in having no specific dynamics associated with them. Consequently, $SO^{(8)}$ and $SO^{(9)}$ should be interpreted as direct measurements of the states. A portion of the estimation digraph of the system is depicted in Figure 3.3. In this figure, without loss of generality, some vertices and edges are eliminated in order to avoid redundant paths and simplify the understanding of the corresponding definitions and concepts.

In Figure 3.3, the vertices are assigned with the following vectors

$$
\mathbf{v}_{source} = \begin{bmatrix} 0 \\ 0 \\ 0 \end{bmatrix}, \ \mathbf{v}_{sink} = \begin{bmatrix} 1 \\ 1 \\ 1 \end{bmatrix}, \ \mathbf{v}_1 = \begin{bmatrix} 1 \\ 1 \\ 0 \end{bmatrix}
$$

$$
\mathbf{v}_2 = \begin{bmatrix} 0 \\ 0 \\ 1 \end{bmatrix}, \ \mathbf{v}_3 = \begin{bmatrix} 1 \\ 0 \\ 1 \end{bmatrix}, \ \mathbf{v}_4 = \begin{bmatrix} 1 \\ 0 \\ 0 \end{bmatrix}
$$

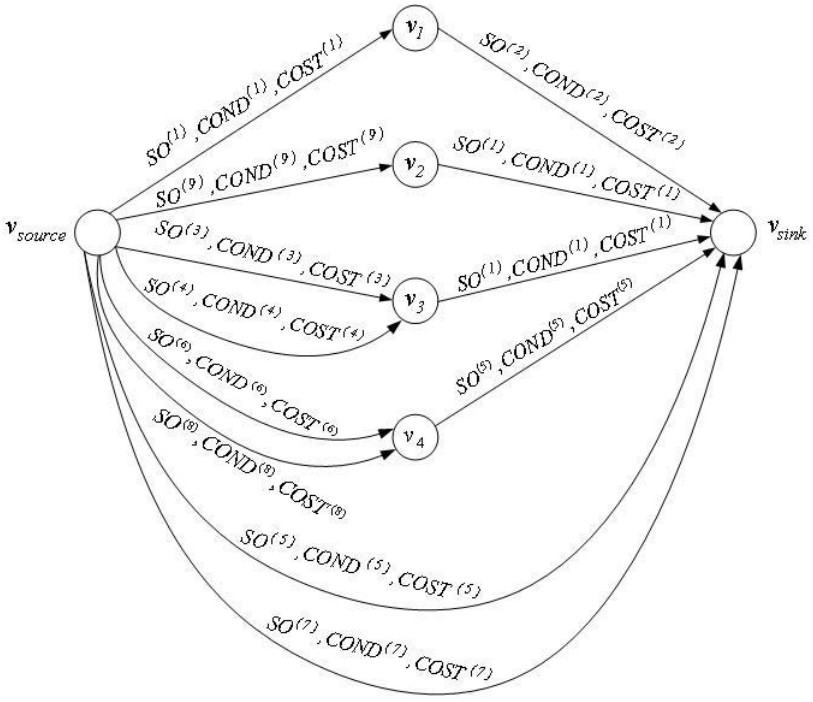

Figure 3.3: A portion of the combined estimation (E) and weighted estimation (WE) digraphs of the system (A, B, C). The edges are labeled with $(SO^{(i)}, COND^{(i)})$ and $(SO^{(i)}, COST^{(i)})$ for the E and WE digraphs, respectively.

Although for system (A, B, C), there are nine possible sub-observers, however, one only needs a subset of them to cooperatively estimate all the states of the system. For instance, in the normal operation mode the supervisor suggests an initial set of sub-observers $\{SO^{(1)}, SO^{(2)}\}$ with $\mathscr{N}(\{1\}) = \{2\}$ and $\mathscr{N}(\{2\}) = \{\}$, which corresponds to the path $\mathbf{v}_{source}\mathbf{v}_1\mathbf{v}_{sink}$ in the estimation digraph of Figure 3.3, that can cooperatively estimate all the system states.

Let us now assume that the process dynamics uncertainty/unreliability $\bar{W}^{(i)} \neq 0$ occurs in the sub-observers $SO^{(i)}$, $i \in \{2, 3, 4, 5, 7\}$ (as in equation (3.12) and Definition 3.6). These uncertainties originate from the dynamic equation of the state x_3 subject to the process dynamics unreliability $\bar{W}_3^{(i)} \neq 0$, where $\bar{W}_3^{(i)}$ represents the x_3-corresponding element of $\bar{W}^{(i)}$.

In the first approach, consider the estimation (E) digraph in Figure 3.4. The sub-observers $SO^{(i)}$, $i \in \{2, 3, 4, 5, 7\}$ become invalid ($COND^{(i)} = 1$ as per Definition 3.6) and hence should not be used any further for constructing the state estimates. Consequently, in order to achieve the objective in equation (3.15) the supervisor eliminates all the sub-observer sets in which the invalid sub-observers are employed. The eliminated sub-observers are denoted by the dashed edges in the E digraph in Figure 3.4, where the supervisor proposes the modified set of sub-observers $\{SO^{(1)}, SO^{(9)}\}$, with $\mathscr{N}(\{1\}) = \{9\}$ and $\mathscr{N}(\{2\}) = \{\}$, corresponding to the path $\mathbf{v}_{source}\mathbf{v}_2\mathbf{v}_{sink}$. Therefore, the information on the uncertain dynamic state x_3 is not incorporated in the modified set of sub-observers $\{SO^{(1)}, SO^{(9)}\}$.

In the second approach, consider the weighted estimation (WE) digraph in Figure 3.5. The sub-observers $SO^{(i)}$, $i \in \{2, 3, 4, 5, 7\}$ are costly ($COST^{(i)} \neq 0$ as per Definition 3.7). By taking the coeficients $C_R = 0$ (no recovery available), $C_C = 0$ (no communication cost), and $C_E = 1$ as explained in Definition 3.7, the cost of invalid sub-observers $SO^{(i)}$ are equal to $n(R^{(i)})$ as indicated in Figure 3.5. These costs should be incorporated in the cooperative estimation scheme. Consequently, in order to achieve the objective in equation (3.16), the supervisor minimizes the cumulative cost of the sub-observers and proposes the modified set of sub-observers $\{SO^{(1)}, SO^{(9)}\}$ with $\mathscr{N}(\{1\}) = \{9\}$ and $\mathscr{N}(\{2\}) = \{\}$, which corresponds to the path $\mathbf{v}_{source}\mathbf{v}_2\mathbf{v}_{sink}$ with the minimum cost of $COST^{(1)} + COST^{(9)} = 0$ as shown in Figure 3.5.

For this example, the results of the E and WE digraphs are the same. Note that one still needs to verify the feasibility of the overall observation task that is achieved by the supervisor-selected initial set of sub-observers $\{SO^{(1)}, SO^{(2)}\}$ (the path $\mathbf{v}_{source}\mathbf{v}_1\mathbf{v}_{sink}$ shown in Figure 3.3) in the normal operation mode, and the supervisor-reconfigured set of sub-observers $\{SO^{(1)}, SO^{(9)}\}$ (the path $\mathbf{v}_{source}\mathbf{v}_2\mathbf{v}_{sink}$ shown in Figure 3.4 and Figure 3.5) in the process dynamics uncertainty/unreliability situation. Subsequently, in the next section, we will provide guidelines to transform the overall cooperative sub-observers scheme

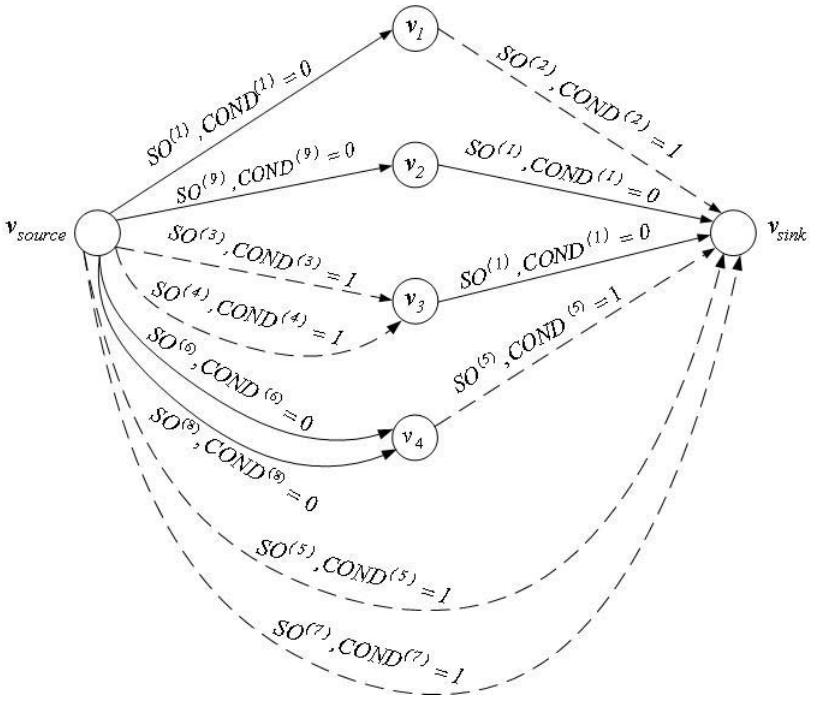

Figure 3.4: The estimation (E) digraph in which the solid and dashed edges represent the valid ($COND^{(i)} = 0$) and invalid ($COND^{(i)} = 1$) sub-observers, respectively.

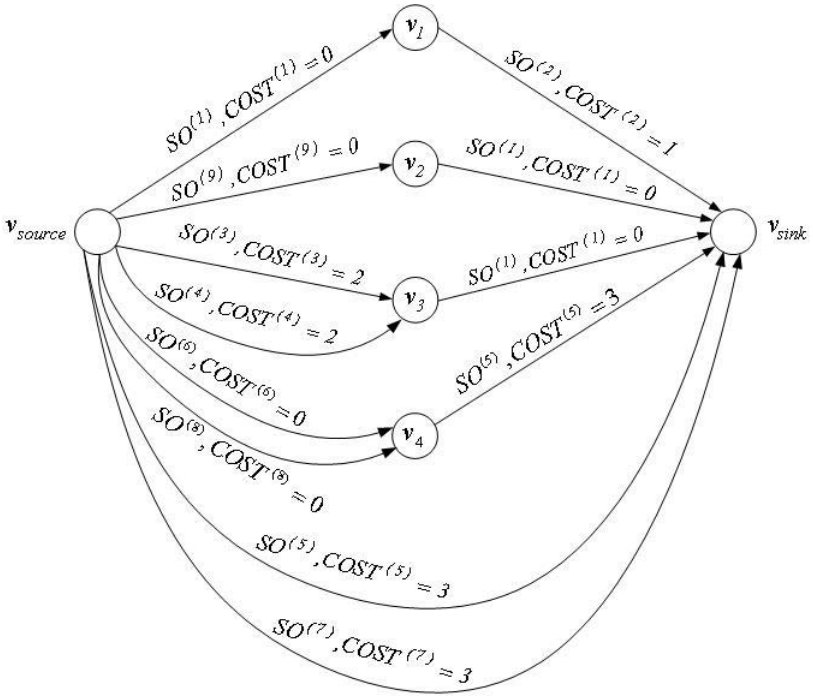

Figure 3.5: The weighted estimation (WE) digraph.

into an equivalent centralized estimation scheme having an observer gain matrix $\bar{K}$ with a certain block-diagonal structure (Example 3.2). Then, we will also provide a test to verify the feasibility of the equivalent centralized estimation scheme having a block-diagonal observer gain matrix $\bar{K}$ (Example 3.3). ■

To summarize, we have proposed a supervisory technique that selects a set of valid sub-observers for cooperatively estimating all the states of the system in presence of process dynamics and sensor measurement uncertainties/unreliabilities. The cooperation among the sub-observers is defined as the exchange of information on their local state estimates that aims at restricting the process dynamics and sensor measurement uncertainties/unreliabilities. It should be noted that it is possible to define the sub-observers only based on the Grammian observability theorem. However, the advantage of the structural observability is in the graphic representation that helps improve the intuition behind the concepts. If a system is structurally unobservable, then it is unobservable for all the values of the system parameters. However, if the system is structurally observable, then it is not guaranteed that the system is observable for all the values of the system. In such cases, the Grammian theory should still be employed to verify the observability of the system. On the other hand, the intention of our proposed framework is to use the structural (graph based) and Grammian approaches in parallel as follows. First, the graph based approach is used to ease the sub-observer design by visualizing the interactions among the states. Next, the Grammian approach is used to verify the observability of the overall cooperative sub-observer scheme.

We are now in the position to formally verify that the overall integration of the cooperative sub-observers in the selected set will lead to an overall stable (convergent) system. In the next section, feasibility of our proposed cooperative estimation scheme is investigated.

3.4 Feasibility Analysis and Design of Distributed Cooperative Sub-Observers

In this section, our goal is to verify the feasibility of the cooperative estimation scheme that is constructed from the set of selected valid sub-observers for LTI systems. The feasibility of a set of cooperative sub-observers is verified by investigating the feasibility of its equivalent centralized estimation scheme, which is performed through the following steps.

1) Lemma 3.1 provides guidelines on how to transform the overall cooperative sub-observers (3.13) into an equivalent centralized estimation scheme for only the sake

of analysis. The observer gain matrix $\bar{K}$ has a certain block-diagonal structure $\bar{\mathbf{K}}$, i.e. $\bar{K} \in \bar{\mathbf{K}}$.

2) Lemma 3.3 and Lemma 3.4 provide a test for verifying the feasibility of the equivalent centralized estimation scheme having a block-diagonal observer gain matrix $\bar{K} \in \bar{\mathbf{K}}$ when a sensor measurement and a dynamic equation are uncertain, respectively.

Consequently, a set of cooperative sub-observers is feasible if and only if the equivalent centralized estimation scheme, which is formed by using Lemma 3.1, is verified to be feasible by using equation (3.29), Lemma 3.3 and Lemma 3.4.

Lemma 3.1. *For an observable multi-input multi-output (MIMO) system that is represented by the triplet (A, B, C), the feasibility of a cooperative estimation scheme that is designed according to the Procedure 3.1 is equivalent to the feasibility of a centralized estimation problem having an observer gain matrix $\bar{K}(s) \in \bar{\mathbf{K}}$ with a certain sparse structure $\bar{\mathbf{K}} = diag\left(K^{(1)}(s), ..., K^{(N_{so})}(s)\right)$, where $K^{(i)}(s)$ is the gain of $SO^{(i)}$ and N_{so} is the total number of sub-observers.*

Proof: *Consider a linear MIMO system that is given by equation* (3.1) *and the sub-observer $SO^{(l)}$, $l = 1, ..., N_{so}$ with its state vector $\hat{X}^{(l)} \in R^{n^{(l)}}$ ($n^{(l)}$ is the dimension of $\hat{X}^{(l)}$) that includes and concatenates all its states $\hat{x}_i^{(l)} \in R^{(l)}$, $i \in \{1, ..., n\}$. For all the states $\hat{x}_i^{(l)} \in R^{(l)}$, we have*

$$\dot{\hat{x}}_i^{(l)} = \sum_{\substack{\forall j \in \{1,...,n\}; \\ \hat{x}_j^{(l)} \in R^{(l)}}} a_{ij} \hat{x}_j^{(l)} + \sum_{\substack{\forall j \in \{1,...,n\}; \\ \hat{x}_j^{(l)} \in D^{(l)}}} \underbrace{\sum_{k \in \mathcal{N}_j(\{l\})} a_{ij} \alpha_j^{(lk)} \hat{x}_j^{(k)}}_{\hat{x}_j^{(l)}} + B_i U$$
$$+ K_i^{(l)}(Y^{(l)} - C^{(l)} \hat{X}^{(l)}) - \bar{W}_i^{(l)} + K_i^{(l)} \bar{V}^{(l)} \tag{3.17}$$

where a_{ij} is the $(ij)^{th}$ element of A, $K_i^{(l)}$ is the x_i-corresponding element of the sub-observer matrix gain $K^{(l)}$, $\hat{X}^{(l)}$ is the estimate of $X^{(l)} \in R^{n^{(l)}}$, which is the vector of all states $\hat{x}_i^{(l)} \in R^{(l)}$, and $Y^{(l)} \in R^{m^{(l)}}$ is the vector of all local measurements, which are in terms of their corresponding uncertainties $V^{(l)}$ and estimated states in $R^{(l)}$ through the measurement matrix $C^{(l)}$, that is $Y^{(l)} = C^{(l)} X^{(l)} + V^{(l)}$.

Taking the state estimation error as $e_i^{(l)} = \hat{x}_i^{(l)} - x_i$, the corresponding error dynamics now becomes

$$\dot{e}_i^{(l)} = \sum_{\substack{\forall j \in \{1,...,n\}; \\ \hat{x}_j^{(l)} \in R^{(l)}}} a_{ij} e_j^{(l)} + \sum_{\substack{\forall j \in \{1,...,n\}; \\ \hat{x}_j^{(l)} \in R^{(l)}}} \sum_{k \in \mathcal{N}_j(\{l\})} a_{ij} \alpha_j^{(lk)} e_j^{(k)}$$
$$- K_i^{(l)} C^{(l)} E^{(l)} + K_i^{(l)}(V^{(l)} + \bar{V}^{(l)}) + (w_i - \bar{W}_i^{(l)}) \tag{3.18}$$

where $E^{(l)} = \hat{X}^{(l)} - X^{(l)}$ *is the vector of all estimation errors* $e_i^{(l)}$*. Now, augmenting all the error equations in equation* (3.18) *(for* $i = 1, ..., n^{(l)}$ *and* $l = 1, ..., N_{so}$*) and* neglecting *the effects of uncertainties, disturbances, and unmodeled dynamics results in a compact form and representation of the estimation error dynamics, namely*

$$\dot{E} = \left(\bar{A} - \bar{K}\bar{C}\right) E \tag{3.19}$$

where E *has the dimension* $n_{N_{so}} \times 1$*,* $\bar{A}$ *has the dimension* $n_{N_{so}} \times n_{N_{so}}$*,* $\bar{K}$ *has the dimension* $n_{N_{so}} \times m_{N_{so}}$*, and* $\bar{C}$ *has the dimension* $m_{N_{so}} \times n_{N_{so}}$ *(*$n_{N_{so}} = \Sigma_{l=1}^{N_{so}} n^{(l)}$ *and* $m_{N_{so}} = \Sigma_{l=1}^{N_{so}} m^{(l)}$*) are defined as follows:* $\forall l \in S_{so}, \forall i'_l \in N; 0 < i'_l < n^{(l)}$ *and* $\forall k \in S_{so}, \forall j'_k \in N; 0 < j'_k < n^{(k)}$*;*

$$E_{[n_{l-1}+i'_l]} = E^{(l)}_{[i'_l]} \tag{3.20}$$

$$\bar{A}_{[n_{l-1}+i'_l, n_{k-1}+j'_k]} = \begin{cases} a_{ij} & l = k, \exists\{x_i, x_j\} \subset Set(X); \hat{X}^{(l)}_{[i'_l]} = \hat{x}^{(l)}_i, \hat{X}^{(k)}_{[j'_k]} = \hat{x}^{(k)}_j \\ a_{ij}\alpha_j^{(lk)} & l \neq k, \exists\{x_i, x_j\} \subset Set(X); \hat{X}^{(l)}_{[i'_l]} = \hat{x}^{(l)}_i, \hat{X}^{(k)}_{[j'_k]} = \hat{x}^{(k)}_j \\ 0 & otherwise \end{cases} \tag{3.21}$$

$$\bar{C} = diag\left(C^{(1)}, ..., C^{(N_{so})}\right) \tag{3.22}$$

$$\bar{K} = diag\left(K^{(1)}, ..., K^{(N_{so})}\right) \tag{3.23}$$

in which the index $[i]$ *denotes the* i^{th} *element of a vector, the index* $[i, j]$ *denotes the* $(ij)^{th}$ *element of a matrix, and* $n_l = \Sigma_{s=1}^{l} n^{(s)}$ *is the dimension of the cumulative state up to the* l^{th} *sub-observer. Therefore, the cooperative estimation scheme is equivalent to a centralized estimation problem for the pair* $(\bar{A}, \bar{C})$ *by using a block-diagonal observer gain matrix* $\bar{K} \in \bar{\mathbf{K}}_{n_{N_{so}} \times m_{N_{so}}}$ *where*

$$\bar{\mathbf{K}}_{n_{N_{so}} \times m_{N_{so}}} = \left\{ diag(K^{(1)}, ..., K^{(N_{so})}) \middle| \, K^{(1)} \in R^{n^{(l)} \times m^{(l)}}, ..., K^{(N_{so})} \in R^{n^{(N_{so})} \times m^{(N_{so})}} \right\} \tag{3.24}$$

This completes the proof of the lemma. ■

The example below demonstrates and illustrates in detail the application of Lemma 3.1 by transforming the overall cooperative sub-observers scheme into an equivalent centralized estimation scheme having a block-diagonal observer gain matrix $\bar{K} \in \bar{\mathbf{K}}_{n_{N_{so}} \times m_{N_{so}}}$.

Example 3.2. *Consider the system that is introduced in Example 3.1 with the triplet matrices* (A, B, C)*, and the initial supervisor-selected set of sub-observers* $\{SO^{(1)}, SO^{(2)}\}$ *in the normal operation mode and the supervisor-reconfigured set of sub-observers* $\{SO^{(1)}, SO^{(9)}\}$ *in the presence of process dynamics uncertainty/unreliability. For this example, the equivalent centralized observer structure for each of the two sets of sub-observers is obtained. For the initial set of sub-observers* $\{SO^{(1)}, SO^{(2)}\}$*, we have*

$$SO^{(1)}: \frac{d}{dt}\begin{bmatrix} \hat{x}_1^{(1)} \\ \hat{x}_2^{(1)} \end{bmatrix} = \begin{bmatrix} a_{11} & a_{12} \\ 0 & a_{22} \end{bmatrix}\begin{bmatrix} \hat{x}_1^{(1)} \\ \hat{x}_2^{(1)} \end{bmatrix} + \begin{bmatrix} 0 \\ b_{22} \end{bmatrix} u_2 + \begin{bmatrix} a_{13} \\ 0 \end{bmatrix} \hat{x}_3^{(2)} + \begin{bmatrix} k_{11} \\ k_{21} \end{bmatrix} (y_1 - c_{11}\hat{x}_1^{(1)}) \tag{3.25}$$

$$SO^{(2)}: \frac{d}{dt}\hat{x}_3^{(2)} = a_{33}\hat{x}_3^{(2)} + b_{31}u_1 + k_{32}(y_2 - c_{23}\hat{x}_3^{(2)})$$

Neglecting the effects of uncertainties, disturbances, and unmodeled dynamics, the corresponding estimation error dynamics are now governed by

$$SO^{(1)}: \frac{d}{dt}\begin{bmatrix} e_1^{(1)} \\ e_2^{(1)} \end{bmatrix} = \begin{bmatrix} a_{11} & a_{12} \\ 0 & a_{22} \end{bmatrix}\begin{bmatrix} e_1^{(1)} \\ e_2^{(1)} \end{bmatrix} + \begin{bmatrix} a_{13} \\ 0 \end{bmatrix} e_3^{(2)} - \begin{bmatrix} k_{11} \\ k_{21} \end{bmatrix} c_{11}e_1^{(1)} \tag{3.26}$$

$$SO^{(2)}: \frac{d}{dt}e_3^{(2)} = a_{33}e_3^{(2)} - k_{32}c_{23}e_3^{(2)}$$

By augmenting the two error equations we obtain

$$\frac{d}{dt}\begin{bmatrix} e_1^{(1)} \\ e_2^{(1)} \\ e_3^{(2)} \end{bmatrix} = \left(\bar{A} - \begin{bmatrix} k_{11} & 0 \\ k_{21} & 0 \\ 0 & k_{32} \end{bmatrix}\bar{C}\right)\begin{bmatrix} e_1^{(1)} \\ e_2^{(1)} \\ e_3^{(2)} \end{bmatrix} \tag{3.27}$$

or equivalently, $\dot{e} = \left(\bar{A} - \bar{K}\bar{C}\right)e$*, where* $\bar{A} = A$ *and* $\bar{C} = C$*. Therefore, according to Lemma 3.1, the feasibility of the cooperative estimation scheme by using the supervisor-selected initial set of sub-observers* $\{SO^{(1)}, SO^{(2)}\}$ *as in equation* (3.25) *is equivalent to the feasibility of the centralized estimation problem given by equation* (3.27) *with an observer gain* $\bar{K}$ *having a sparse block-diagonal structure as follows*

$$\bar{K} \in \bar{\mathbf{K}}_{3\times 2} = \left\{ diag\left(\begin{bmatrix} k_{11} \\ k_{21} \end{bmatrix}, k_{32}\right) \middle| \begin{bmatrix} k_{11} \\ k_{21} \end{bmatrix} \in R^2, k_{32} \in R \right\} \tag{3.28}$$

In this example, since each state is estimated by one and only one sub-observer, the pair $(\bar{A}, \bar{C})$ *of the overall augmented error dynamics* (3.27) *is identical to the one obtained from the pair* (A, C) *of the original system. For the supervisor-reconfigured set of sub-observers* $\{SO^{(1)}, SO^{(9)}\}$*, it is easy to show that the resulting equivalent centralized observer has the same block-diagonal observer gain structure* $\bar{K}$ *as given in equation* (3.28)*.*

■

Up to this point, we have shown that the feasibility of the cooperative set of sub-observers (that are selected by the supervisor) are equivalent to the centralized estimation

scheme with a sparse block-diagonal gain $\bar{K}$. In the following, we investigate the feasibility of a centralized estimation scheme having the gain $\bar{K} \in \bar{\mathbf{K}}_{n_{N_{so}} \times m_{N_{so}}}$ in equation (3.24).

According to [133], for a given MIMO linear system that is represented by the triplet $(\bar{A}, \bar{B}, \bar{C})$, a centralized estimation solution that is obtained by using an observer gain matrix $\bar{K}$ having a certain sparse structure ($\bar{K} \in \bar{\mathbf{K}}_{n_{N_{so}} \times m_{N_{so}}}$) is feasible if the overall estimation error dynamics (3.19) does not have any decentralized fixed modes with respect to the structured gain matrix $\bar{K} \in \bar{\mathbf{K}}_{n_{N_{so}} \times m_{N_{so}}}$, that is

$$\bigcap_{\bar{K} \in \bar{\mathbf{K}}_{n_{N_{so}} \times m_{N_{so}}}} eigs\left(\bar{A} - \bar{K}\bar{C}\right) = \emptyset \tag{3.29}$$

where $eigs\,(M)$ denotes the set of all eigenvalues of the matrix M.

Note that in this section the feasibility of cooperative sub-observers is guaranteed by using Lemma 3.1. Now, an H_∞ robust observer matrix $\bar{K}$ is designed for the distributed sub-observers that have the overall structure $\bar{\mathrm{K}} = \mathrm{diag}(K^{(i)})_{i=1}^{N_{so}}$ (as in equation (3.23)) associated with the closed-loop matrix $(\bar{A} - \bar{K}\bar{C})$ in equation (3.19). The matrices $\bar{A}$ and $\bar{C}$ are defined by equations (3.21) and (3.22), respectively, in the proof of Lemma 3.1. In this regard, we consider the following lemma.

Lemma 3.2. *Consider the distributed sub-observers with the overall structure* $\bar{\mathrm{K}} = \mathrm{diag}(K^{(i)})_{i=1}^{N_{so}}$ *and the overall error dynamics* $\dot{E} = \left(\bar{A} - \bar{K}\bar{C}\right) E$ *given by equation* (3.19). *The distributed state feedback matrix* $\bar{K} = YX^{-1}$ *(or equivalently* $K^{(i)} = Y_i X_i^{-1}$*) stabilizes the system and minimizes the positive parameter* γ*, which represents an upper bound on the* H_∞ *norm of the transfer function from the disturbance to the estimation error, if there exist a block-diagonal matrix* $\mathrm{Y} = \mathrm{diag}(\mathrm{Y_i})_{i=1}^{N_{so}}$ *and a positive definite block-diagonal matrix* $\mathrm{X} = \mathrm{diag}(\mathrm{X_i})_{i=1}^{N_{so}} > 0$ *that satisfy the following optimization problem*

$$\begin{aligned}
&\textit{Minimize} \quad \gamma \\
&\textit{subject to} \\
&X > 0 \\
&\begin{bmatrix} \bar{A}^T X + X\bar{A} + \bar{C}^T Y^T + Y\bar{C} & X & I \\ X & -\gamma I & 0 \\ I & 0 & -\gamma I \end{bmatrix} < 0 \\
&\forall l \in S_{so}, \forall \hat{x}_j^{(l)} \in R^{(l)}, \forall k \in \mathscr{N}_j(\{l\}) : 0 \leq \alpha_j^{(lk)} \leq 1 \\
&\forall l \in S_{so}, \forall \hat{x}_j^{(l)} \in R^{(l)} : \textstyle\sum_{k \in \mathscr{N}_j(\{l\})} \alpha_j^{(lk)} = 1
\end{aligned}$$

Proof: *Follows from the results in [136] and those in Lemma 2.2. The last two convex constraints are those that are already explained for the linear combination in equation* (3.8). ■

In case of process dynamics and sensor measurement uncertainties/unreliabilities (as per Definition 3.6), the necessary and sufficient condition in equation (3.29) is complemented by the following two lemmas.

Lemma 3.3. *Given that the j^{th} sensor measurement $y_j = Y_{[j]}$, $j = 1, ..., m$ is unreliable, a centralized estimation scheme by using an observer gain matrix $\bar{K}$ with a certain sparse block-diagonal structure ($\bar{K} \in \bar{\mathbf{K}}_{n_{N_{so}} \times m_{N_{so}}}$) is feasible if*

$$\bigcap_{\bar{K}^{sen} \in \bar{\mathbf{K}}^{sen}_{n_{N_{so}} \times m'_{N_{so}}}} eigs\left(\bar{A} - \bar{K}^{sen}\bar{C}^{sen}\right) = \emptyset$$

where $\bar{C}^{sen} = \bar{C}^{(-T^{sen}, -\{\})}$, and $\bar{K}^{sen}_{n_{N_{so}} \times m'_{N_{so}}} = \{\bar{K}^{(-\{\}, -T^{sen})} | \bar{K} \in \bar{\mathbf{K}}_{n_{N_{so}} \times m_{N_{so}}}\}$, in which $T^{sen} = \{k \in \{1, ..., m\} | \exists l \in S_{so}; Y^{(l)}_{[k]} = y_j\}$, and $m'_{N_{so}} = m_{N_{so}} - n(T^{sen})$, with $n(.)$ denoting the cardinality of a set.

Proof: *Follows from the results in [133] and those in Lemma 3.1.* ■

Lemma 3.4. *Given that the i^{th} dynamic equation*

$$\dot{x}_i = \dot{X}_{[i]} = A_{[i,:]}X + B_i U + w_i$$

is unreliable (where $|w_i| > B_W$ as per Definition 3.6), where the index $[i, :]$ represents the i^{th} row of the associated matrix, a centralized estimation scheme that is obtained by using an observer gain matrix $\bar{K}$ with a certain sparse block-diagonal structure $\bar{K} \in \bar{\mathbf{K}}_{n_{N_{so}} \times m_{N_{so}}}$ is feasible if

- *The state x_i is directly measured by a sensor, namely y_q, that is $\forall q \in \{1, ..., m\}$; $y_q = C_q X + v_q = x_i + v_q$.*
- *The following eigenvalue condition holds*

$$\bigcap_{\bar{K}^{eq} \in \bar{\mathbf{K}}^{eq}_{n'_{N_{so}} \times m'_{N_{so}}}} eigs\left(\bar{A}^{eq} - \bar{K}^{eq}\bar{C}^{eq}\right) = \emptyset$$

where $\bar{A}^{eq} = \bar{A}^{(-s^{eq}, -s^{eq})}$, $\bar{C}^{eq} = \bar{C}^{(-T^{eq}, -s^{eq})}$, and $\bar{K}^{eq}_{n'_{N_{so}} \times m'_{N_{so}}} = \{\bar{K}^{(-S^{eq}, -T^{eq})} | \bar{K} \in \bar{\mathbf{K}}_{n_{N_{so}} \times m_{N_{so}}}\}$, in which $S^{eq} = \{k \in \{1, ..., n\} | \exists l \in S_{so}; E_{[k]} = e^{(l)}_i\}$, $T^{eq} = \{k \in \{1, ..., m\} | \exists l \in S_{so}; Y^{(l)}_{[k]} = y_q\}$, $n'_{N_{so}} = n_{N_{so}} - n(S^{eq})$, and $m'_{N_{so}} = m_{N_{so}} - n(T^{eq})$, with $n(.)$ denoting the cardinality *of a set.*

Proof: *Follows from the results in [133] and those in Lemma 3.1.* ■

For the j^{th} sensor uncertainty, Lemma 3.3 is motivated by the fact that the uncertain sensor should be disregarded in the estimation process, that is the y_j-corresponding columns should be eliminated from the matrix $\bar{K}$ to yield the modified matrix $\bar{K}^{sen}$, and

the y_j-corresponding rows should be eliminated from the matrix $\bar{C}$ to yield the modified matrix $\bar{C}^{sen}$, which should subsequently be used to verify the eigenvalue condition (3.29). Similarly, for the i^{th} uncertain dynamic equation, Lemma 3.4 is motivated by the fact that the uncertain state x_i should be directly measured by a sensor, namely y_q, since the uncertain dynamic equation should not be incorporated in the estimation of x_i. Therefore, the estimation process proceeds with the remaining system states excluding x_i and y_q. In other words, the x_i-corresponding columns and rows should be eliminated from the matrix $\bar{A}$ to yield $\bar{A}^{eq}$, the x_i-corresponding columns and y_q-corresponding rows should be eliminated from the matrix $\bar{C}$ to yield $\bar{C}^{eq}$, and the x_i-corresponding rows and y_q-corresponding columns should be eliminated from the matrix $\bar{K}$ to yield $\bar{K}^{eq}$. Consequently, the matrices $\bar{A}^{eq}$, $\bar{C}^{eq}$, and $\bar{K}^{eq}$ should be used to subsequently verify the eigenvalue condition (3.29).

Remark 3.1. *In case of process dynamics and sensor measurement uncertainties/unreliabilities (as per Definition 3.6), the H_∞ optimal observer matrices $\bar{K}^{sen}$ and $\bar{K}^{eq}$ can be designed for the distributed sub-observers associated with the closed-loop matrices $(\bar{A} - \bar{K}^{sen}\bar{C}^{sen})$ (in Lemma 3.3) and $(\bar{A}^{eq} - \bar{K}^{eq}\bar{C}^{eq})$ (in Lemma 3.4), respectively. To this end, Lemma 3.2 can be used to design the matrices $\bar{K}^{sen}$ and $\bar{K}^{eq}$ by substituting the pair $(\bar{A}, \bar{C})$ in this lemma with $(\bar{A}, \bar{C}^{sen})$ and $(\bar{A}^{eq}, \bar{C}^{eq})$, respectively.*

The following example illustrates how Lemma 3.3 and Lemma 3.4 enable one to determine whether a system with process dynamics and sensor measurement uncertainties/unreliabilities is observable with respect to an observer gain matrix $\bar{K}$ having a certain block-diagonal structure $\bar{K} \in \bar{\mathbf{K}}_{n_{N_{so}} \times m_{N_{so}}}$.

Example 3.3. *Consider the system that is introduced in Example 3.1, whose state space representation matrices A and C are given by*

$$A = \begin{bmatrix} -0.1 & 0.1 & 0.1 \\ 0 & -0.2 & 0 \\ 0 & 0 & -0.2 \end{bmatrix}, \; C = \begin{bmatrix} 1 & 0 & 0 \\ 0 & 0 & 1 \end{bmatrix}$$

The supervisor-selected initial set of sub-observers are $\{SO^{(1)}, SO^{(2)}\}$ in the absence of process dynamics unreliability and the supervisor-reconfigured set of sub-observers are $\{SO^{(1)}, SO^{(9)}\}$ in the presence of process dynamics unreliability. In Example 3.2, the equivalent centralized observer structure of these two sets of sub-observers are provided in equation (3.27) *with the sparse block-diagonal gain structure $\bar{\mathbf{K}}_{3\times 2}$ given by equation* (3.28)*. In this example, this equivalent centralized observer structure is used to study the feasibility of the two sets of sub-observers.*

For the initial set of sub-observers $\{SO^{(1)}, SO^{(2)}\}$ we have

$$\bigcap_{\bar{K} \in \bar{\mathbf{K}}} eigs\left(\bar{A} - \bar{K}\bar{C}\right) = \emptyset$$

Therefore, the system is observable by using the supervisor-selected initial set of sub-observers in the absence of any process dynamics and sensor measurement unreliabilities. For the supervisor-reconfigured set of sub-observers $\{SO^{(1)}, SO^{(9)}\}$, $S^{eq} = \{3\}$ *corresponds to the unreliability in the dynamic equation of* x_3, *and* $T^{eq} = \{2\}$ *corresponds to the sensor* y_2 *which directly measures* x_3. *We have*

$$\bar{A}^{eq} = \begin{bmatrix} -0.1 & 0.1 \\ 0 & -0.2 \end{bmatrix}, \ \bar{C}^{eq} = \begin{bmatrix} 1 & 0 \end{bmatrix}, \ \bar{\mathbf{K}}^{eq} = \left\{ \bar{\mathrm{K}}^{eq} = \begin{bmatrix} k_{11} \\ k_{21} \end{bmatrix} \middle| k_{11}, k_{21} \in R \right\}$$

$$\bigcap_{\bar{K}^{eq} \in \bar{\mathbf{K}}^{eq}} eigs\left(\bar{A}^{eq} - \bar{K}^{eq}\bar{C}^{eq}\right) = \emptyset$$

Therefore, the system is observable by using the supervisor-reconfigured set of sub-observers $\{SO^{(1)}, SO^{(9)}\}$ *in the presence of process dynamic uncertainty/unreliability.* ■

3.5 Conclusions

In this chapter, we have proposed a framework in which a set of sub-observers can be selected by a supervisor to cooperatively estimate all the fault parameters and states of a formation flight of unmanned vehicle system, while confining the effects of the process dynamics and sensor measurement uncertainties/unreliabilities. We have shown how to systematically design the distributed sub-observers in our cooperative estimation scheme. After the feasibility of cooperative sub-observers is guaranteed by using the equivalent centralized estimation scheme, H_∞ optimal sub-observer matrices are designed. Moreover, our proposed cooperative estimate scheme is shown to be applicable to cases in which the process dynamics and sensor measurement unreliabilities are present in the formation flight system.

Chapter 4

Distributed and Cooperative Estimation of Formation Flight of Unmanned Vehicles with Relative Measurements Subject to Loss-of-Effectivenss Actuator Failures

In this chapter, we extend the proposed framework in the previous chapter to the case of formation flight of unmanned vehicles with relative measurements subject to actuator failures of the loss-of-effectiveness type. The main difference with the previous chapter is that in presence of the loss-of-effectiveness (LOE) failures the fault augmented state space model is in a bilinear form, which makes the design and analysis of the cooperative sub-observers different from those in the previous chapter. From the estimation point of view, the bilinear fault-augmented system is in the form of a linear time-varying representation. Therefore, the linear time-invariant observer approach (as in the previous chapter) cannot be used here, and instead the Kalman filtering technique is used to design the sub-observers. In order to guarantee the ultimate boundedness of the estimation errors in the convergence analysis section of this chapter, the sub-observer dependency (SOD) digraph (as defined later in this chapter) is assumed to be acyclic, which is a confining condition to select a sub-set of cooperative sub-observers as opposed to the feasibility analysis section of the previous chapter, where no such confining conditions are imposed. Moreover, in case that the ranges of some sub-observers are overlapping, a fusion feedback (FF) procedure is developed to satisfy the constrained-state conditions in parallel

to the time evolution of the Kalman filter equations of the sub-observers. We first start by presenting some preliminaries.

4.1 Preliminaries

In this section, the general case of a multiple vehicle formation flight system subject to actuator failures of the loss-of-effectiveness type is formulated as a bilinear state space model. The state dependency (SD) digraph of the bilinear system is presented in order to simplify the study of system properties by using the graph-based approaches. Based on the SD digraph of the formation flight system, structural observability is presented that will help us in the development of our proposed distributed and cooperative estimation framework in the subsequent sections.

4.1.1 Bilinear Fault-Augmented State Space Model of Formation Flight of Unmanned Vehicles

Consider a formation of N vehicles with the relative measurement formation (RMF) digraph $G_{RMF}(V_{RMF}, E_{RMF})$ as per Definition 2.3. The linear state space model of the formation is given by equation (2.4). In the following, the case of LOE is considered for all the vehicles, and the general model of LOE actuator failures given in equations (2.5) and (2.8) is utilized to form the overall fault-augmented state space model of the formation as shown in equation (2.10). Moreover, it is assumed that $\dot{\pi}_i = 0$ ($W_i^f = 0$ in equation (2.6) whose effect will be analyzed later in this chapter).

If $\mathscr{F}\{i\} = 1$ ($\forall i \in \{1, ..., N\}$, corresponding to the LOE type of actuator failure), then the system (2.10) is in the form of a bilinear system. Therefore, in this case we consider the general equivalent state space representation of a bilinear system S as follows:

$$S : \begin{cases} \dot{X} = A_0 X + \sum_{i=1}^{r} u_i A_i X + BU + W \\ Y = CX + V \end{cases} \tag{4.1}$$

where

$$B = \begin{bmatrix} B_1 & \cdots & B_r \end{bmatrix}_{n \times r}, \; C = \begin{bmatrix} C_1 \\ \vdots \\ C_m \end{bmatrix}_{m \times n}$$

Moreover, $X = \begin{bmatrix} x_1 & \cdots & x_n \end{bmatrix}^T \in R^n$, $Y = \begin{bmatrix} y_1 & \cdots & y_m \end{bmatrix}^T \in R^m$, and $U = \begin{bmatrix} u_1 & \cdots & u_r \end{bmatrix}^T \in R^r$ are the state, output, and input vectors, respectively. In addition, $W = \begin{bmatrix} w_1 & \cdots & w_n \end{bmatrix}^T \in$

R^n and $V = \begin{bmatrix} v_1 & \cdots & v_m \end{bmatrix}^T \in R^m$ are the process disturbance and sensor noise, respectively.

4.1.2 State Dependency (SD) Digraph of Bilinear Systems

In the following, the associated state dependency (SD) directed graph (digraph) of the bilinear system (4.1) is introduced [137].

Definition 4.1. *For a bilinear system S in equation* (4.1)*, the associated state dependency (SD) directed graph $G_{SD}(V_{SD}, E_{SD})$ is defined as follows:*

- *The* vertex *set is $V_{SD} = Set(U) \cup Set(X) \cup Set(Y)$ where U, X, and Y are the input, state, and output vectors, respectively, and $Set(\Psi)$ denotes the set of the elements of the vector Ψ.*
- *The* edge *set is defined as the union of* input-state*,* state-state*, and* state-output *edges as follows*

$$E_{SD} = \{(u_i, x_j) | b_{ji} \neq 0\} \cup \left\{(x_i, x_j)_k | a_{k,ji} \neq 0\right\} \cup \{(x_i, y_j) | c_{ji} \neq 0\} \tag{4.2}$$

  where $a_{k,ji}$, b_{ji}, and c_{ji} are the corresponding elements of the matrices A_k ($k = 0, ..., r$), B, and C, respectively.

Definition 4.2. *Two edges $e_1 = (v_1, v_1')_{k_1} \in E$ and $e_2 = (v_2, v_2')_{k_2} \in E$ are said to be A-disjoint if the condition $v_1 \neq v_2$ and at least one of the conditions $v_1' \neq v_2'$ and $k_1 \neq k_2$ are satisfied. In general, n ($n \geq 2$) edges are A-disjoint if they are mutually A-disjoint.*

4.1.3 Observability and Structural Observability of Bilinear Systems

For the class of systems with the same associated digraph (Definition 4.1), one can apply graph theory to study generic (or structural) properties. The graph-based properties simplify the study of system properties specifically when the dimensions of the system are large. However, the graph-based structural properties are valid for almost all systems in the class of systems with the same graph, except for some pathological parameter matching cases that constitute a finite number of nontrivial polynomials in the system parameters. Therefore, the conventional non-graph-based properties of a system are always required to be studied in order to confirm the results of the graph-based properties. The following theorem relates to the structural (generic) observability of bilinear systems.

Theorem 4.1. *[149] Consider the bilinear system given by equation* (4.1)*. For piecewise continuous input signals U, the bilinear system* (4.1) *is observable if and only if $g\_rank(O(C, A_0, A_1, ..., A_r)) = n$, where*

$$O(C, A_0, A_1, ..., A_m) =$$
$$col(C, CA_0, CA_1, ..., CA_r, CA_0^2, CA_0A_1, ..., CA_0A_r, CA_1A_0, ..., CA_r^{n-1})$$

is the observability matrix of system (4.1) *and $g\_rank(M)$ denotes the generic rank of a matrix M.* ■

In the graph theory domain, there is a graph-based technique to check the structural observability of a bilinear system as will be described next.

Proposition 4.1. *[150] Let S be a bilinear system that is given by* (4.1) *with its associated digraph G_{SD}. The bilinear system S is* structurally (generically) observable *if and only if the following two conditions hold:*

- *There exists at least one state-output path originating from any state vertex in X; and*
- *There exists a set of n A-disjoint state-state and state-output edges in G_{SD}.*

It should be noted that if a bilinear system S is structurally unobservable, then its associated digraph represents a class of systems that are all (including the system S itself) unobservable. But once a system is guaranteed to be structurally observable, its observability should be further validated by using the Grammian-based observability theorem [151], [158]. This observability theorem provides a fundamental necessary/sufficient condition for observability of dynamical bilinear systems. In this thesis, although we introduce and use structural observability and graph-based analysis to demonstrate and visualize the feasibility of an observer, one needs to always verify the system observability by using the observability theorem.

4.2 Distributed and Cooperative Sub-Observers in Bilinear Systems

In this section, our proposed cooperative estimation framework in the previous chapter is extended to the case of bilinear systems. Similar to the previous chapter, this framework is based on a set of multiple sub-observers (Definition 3.4) and a supervisor which selects a subsubset of sub-observers that can estimate all the states of the system in presence of unreliable process dynamics and sensor measurements. The cooperation among the sub-observers is defined as the exchange of information on their local state

estimates that aim at restricting the effect of process dynamics and measurement sensor uncertainties/unreliabilities.

Consider the bilinear system given by equation (4.1). This system can be equivalently represented by the following linear time-varying model

$$\begin{cases} \dot{X} = \underbrace{\left(A_0 + \sum_{i=1}^{r} u_i(t) A_i\right)}_{A(t)} X + BU + W \\ Y = CX + V \end{cases} \tag{4.3}$$

where $(A(t), B, C)$ represent the triplet matrices of the equivalent linear time-varying model (4.3) of the bilinear model (4.1). The sub-observers are defined according to the Definition 3.4.

Inherited from the bilinear model of the system, each sub-observer $SO^{(i)}$ is represented by a bilinear dynamic equation as follows:

$$\begin{aligned} \dot{\hat{X}}^{(i)} &= \underbrace{\left(A_0^{(i)} + \sum_{i'=1}^{r} u_{i'}(t) A_{i'}^{(i)}\right)}_{A^{(i)}(t)} \hat{X}^{(i)} + \sum_{j \in \mathscr{N}(\{i\})} \underbrace{\left(A_0^{(ij)} + \sum_{i'=1}^{r} u_{i'}(t) A_{i'}^{(ij)}\right)}_{A^{(ij)}(t)} \hat{X}^{(j)} \\ &\quad + B^{(i)} U^{(i)} + K^{(i)}(Y^{(i)} - C^{(i)} \hat{X}^{(i)}) \\ &= A^{(i)}(t) \hat{X}^{(i)} + \sum_{j \in \mathscr{N}(\{i\})} A^{(ij)}(t) \hat{X}^{(j)} + B^{(i)} U + K^{(i)}(Y^{(i)} - C^{(i)} \hat{X}^{(i)}) \end{aligned} \tag{4.4}$$

where $\hat{X}^{(i)}$ and $\hat{X}^{(j)}$ are the vectors of all the states in $R^{(i)}$ and $D^{(i)}$, respectively, and $A^{(i)}(t)$ and $A^{(ij)}(t)$ represent the partitions of the matrix $A(t)$ that correspond to the dependency of the states $\hat{X}^{(i)}$ (of $SO^{(i)}$) on itself and on the states $\hat{X}^{(j)}$ (of $SO^{(j)}$), respectively, as follows:

$$\begin{aligned} &A^{(i)} = A^{(-S,-S)} \ , \ A_{i'}^{(i)} = A^{(-S,-S)} \ \ (i' = 0, ..., r) \\ &S = \left\{ k \in \{1, ..., n\} | \hat{x}_k^{(i)} \notin D^{(i)} \right\} \end{aligned} \tag{4.5}$$

$$\begin{aligned} &A^{(ij)} = A^{(-S,-T)} \ , \ A_{i'}^{(ij)} = A^{(-S,-T)} \ \ (i' = 0, ..., r) \\ &T = \left\{ k \in \{1, ..., n\} | \hat{x}_k^{(j)} \notin R^{(j)} \right\} \end{aligned} \tag{4.6}$$

In addition, $U^{(i)}$ is the vector of all entities in $I^{(i)}$ ($I^{(i)} = set(U^{(i)})$), and $B^{(i)}$ represents the partition of the matrix B that corresponds to the dependency of the inputs $U^{(i)}$ on the states $\hat{X}^{(i)}$ as follows:

$$\begin{aligned} &B^{(i)} = B^{(-S,-T)} \\ &S = \left\{ k \in \{1, ..., n\} | \hat{x}_k^{(i)} \notin D^{(i)} \right\} \\ &T = \left\{ k \in \{1, ..., r\} | u_k \notin I^{(i)} \right\} \end{aligned} \tag{4.7}$$

Moreover, $Y^{(i)}$ is the vector of all entities in $O^{(i)}$ ($O^{(i)} = set(Y^{(i)})$), and $C^{(i)}$ represents the portion of the matrix C that corresponds to the dependency of the states $\hat{X}^{(i)}$ on the outputs $Y^{(i)}$ as follows:

$$\begin{aligned} C^{(i)} &= C^{(-S,-T)} \\ S &= \left\{k \in \{1,...,m\} | y_k \notin O^{(i)}\right\} \\ T &= \left\{k \in \{1,...,n\} | \hat{x}_k^{(i)} \notin D^{(i)}\right\} \end{aligned} \tag{4.8}$$

The matrix $K^{(i)}(t) \in R^{n^{(i)} \times m^{(i)}}$ is the sub-observer dynamic gain. Given (conditioned on) availability of the information on $I^{(i)}$, $O^{(i)}$, and $D^{(i)}$, all the states of the overall system S whose estimates belong to $R^{(i)}$ are observable by using the sub-observer $SO^{(i)}$.

For the sub-observer $SO^{(i)}$ given in Definition 3.4, the expressions for $A^{(i)}$, $A^{(ij)}$, $B^{(i)}$, and $C^{(i)}$ in equations (4.5), (4.6), (4.7), and (4.8), respectively, can be used to give the dynamic state space model of $X^{(i)}$ as follows:

$$\begin{aligned} \dot{X}^{(i)} &= A^{(i)}(t)X^{(i)} + \sum_{j \in \mathcal{N}(\{i\})} A^{(ij)}(t)\hat{X}^{(j)} + B^{(i)}U + W^{(i)} \;\; Y^{(i)} \\ &= C^{(i)}\hat{X}^{(i)} + V^{(i)} \end{aligned} \tag{4.9}$$

where $W^{(i)} \in R^{n^{(i)}}$ and $V^{(i)} \in R^{m^{(i)} \times 1}$ are defined as follows:

$$W^{(i)} = W^{(-S,-\{\})} \;,\; S = \left\{k \in \{1,...,n\} | \hat{x}_k^{(i)} \notin D^{(i)}\right\} \tag{4.10}$$

$$V^{(i)} = V^{(-S,-\{\})} \;,\; S = \left\{k \in \{1,...,m\} | y_k \notin O^{(i)}\right\} \tag{4.11}$$

Similar to the previous chapter, the notions of directed graph and structural observability in the previous sections are used in the following to design the sub-observers for a class of bilinear systems. The following procedure provides a constructive means for designing the sub-observers.

Procedure 4.1. *Consider the case of a bilinear system as given by equation* (4.1)*, whose equivalent linear time-varying model is presented by equation* (4.3)*, with the associated digraph as given in Definition 4.1. A sub-observer simply constitutes a set of A-disjoint state-state and state-output edges, such that there exists at least one state-output path originating from any state vertex of the sub-observer. Therefore, the sub-observers can be designed by following the proposed two steps, namely*

Step 1. The directed graph of the system is sketched according to the Definition 4.1.

Step 2. The sub-observer $SO^{(i)}$ is designed by choosing $I^{(i)} \subset Set(U)$, $O^{(i)} \subset Set(Y)$, and two sets of vertices from $Set(X)$ to form its domain $D^{(i)}$ and range $R^{(i)}$ such that the following three conditions are satisfied:

Condition 1. *The states in $R^{(i)}$ and the output sensor measurements in $O^{(i)}$ should satisfy the conditions in Proposition 4.1.*

Condition 2. *The set of input vertices in $I^{(i)}$ and state vertices in $D^{(i)}$ should include all the vertices in $Set(U)$ and $Set(X)$, respectively, from which there exist incoming edges to the set of state vertices in $R^{(i)}$ and output vertices in $O^{(i)}$, unless the sub-observer $SO^{(i)}$ represents a direct measurement (namely y_p) of one state (namely x_p) where $R^{(i)} = \{\hat{x}_p^{(i)}\}$, $D^{(i)} = \{\}$, $I^{(i)} = \{\}$, and $O^{(i)} = \{y_p\}$.*

Condition 3. *Using Theorem 4.1, the states in $R^{(i)}$ should be observable upon the availability of inputs $I^{(i)}$, outputs $O^{(i)}$, and state estimates $D^{(i)}$.*

Each sub-observer $SO^{(i)}$ can possibly be subject to unreliable information. Inherited from the bilinear model of the system, each sub-observer $SO^{(i)}$ is represented by a bilinear dynamic equation as follows:

$$\begin{aligned}\dot{\hat{X}}^{(i)} = A^{(i)}(t)\hat{X}^{(i)} + \sum_{j\in\mathscr{N}(\{i\})} A^{(ij)}(t)\hat{X}^{(j)} + B^{(i)}U \\ + K^{(i)}(Y^{(i)} - C^{(i)}\hat{X}^{(i)} + \bar{V}^{(i)}) - \bar{W}^{(i)}\end{aligned} \tag{4.12}$$

where the vectors $\bar{W}^{(i)}$ and $\bar{V}^{(i)}$, respectively, represent the process dynamics measurement sensor unreliabilities of the sub-observer $SO^{(i)}$ (in the fault-augmented state space model (4.1)). These unreliabilites can be due to the following sources:

- dynamic model of the augmented faults, e.g. $\bar{W} = \left[\begin{array}{cc} 0_{1\times(N-1)n_0} & -\left[(W_i^f)^T\right]_{i=1}^{N} \end{array}\right] \in R^{1\times n_1}$ (where W_i^f is defined as in equation (2.6)) is as in the fault-augmented state space model (2.10),
- communication delays (failures) in the transmission of input and output data, e.g. $\bar{W}^{(i)} = B^{(i)}(U^{(i)}(t) - U^{(i)}(t-\Delta t)) \in R^{n^{(i)}}$ and $\bar{V}^{(i)} = Y^{(i)}(t) - Y^{(i)}(t-\Delta t) \in R^{m_1}$ are as in the sub-observer model (4.12), or
- communication delays (failures) in the transmission of the estimates $\hat{X}^{(j)}$ ($\forall j \in \{1,...,N_{so}\}; D^{(i)}\cap R^{(j)} \neq \emptyset$) from $SO^{(j)}$ to $SO^{(i)}$, e.g. $\bar{W}^{(i)} = \sum_{j\in\mathscr{N}(\{i\})} A^{(ij)}(\hat{X}^{(j)}(t) - \hat{X}^{(j)}(t-\Delta t))$ are as in the sub-observer model (4.12).

Taking $E^{(i)} = \hat{X}^{(i)} - X^{(i)}$ and using the dynamic equation of $X^{(i)}$ from equation (4.9), the error dynamics for the sub-observer $SO^{(i)}$ is

$$\begin{aligned}\dot{E}^{(i)} = (A^{(i)}(t) - K^{(i)}C^{(i)})E^{(i)} - (W^{(i)} + \bar{W}^{(i)}) + K^{(i)}(V^{(i)} + \bar{V}^{(i)}) \\ + \sum_{j\in\mathscr{N}(\{i\})} A^{(ij)}(t)E^{(j)}\end{aligned} \tag{4.13}$$

Similar to the Definition 3.6 and Definition 3.7 in the previous chapter, the sub-observers $SO^{(i)}$ are assigned with the validity conditions $COND^{(i)}$ and costs $COST^{(i)}$, which are provided to the supervisor (as per Assumption 3.1 and Assumption 3.2) in order to be considered in our proposed cooperative estimation framework.

In equation (4.13), the Kalman gain $K^{(i)}$ can be chosen to minimize the trace of the covariance matrix $P^{(i)}$ so that the sub-observer $SO^{(i)}$ is now designed as follows:

$$\begin{aligned}
&\dot{\hat{X}}^{(i)} = A^{(i)}(t)\hat{X}^{(i)} + B^{(i)}U + K^{(i)}(Y^{(i)} - C^{(i)}\hat{X}^{(i)}) + \sum_{j\in\mathscr{N}(\{i\})} A^{(ij)}(t)\hat{X}^{(j)} \\
&K^{(i)} = P^{(i)}(C^{(i)})^T(R^{(i)})^{-1} \\
&\dot{P}^{(i)} = A^{(i)}(t)P^{(i)} + P^{(i)}(A^{(i)}(t))^T + Q^{(i)} - P^{(i)}(C^{(i)})^T(R^{(i)})^{-1}C^{(i)}P^{(i)} + \hbar^{(i)} \\
&\hbar^{(i)} = \sum_{j\in\mathscr{N}(\{i\})} \hbar^{(ij)} \\
&\hbar^{(ij)} = A^{(ij)}(\mathrm{t})(P^{(ij)})^T + P^{(ij)}(A^{(ij)}(t))^T \ , \ P^{(ij)} = \mathscr{E}\{(E^{(i)})(E^{(j)})^T\}
\end{aligned} \tag{4.14}$$

where $\mathscr{E}\{.\}$ represents the expected value of a random variable. $Q^{(i)} > 0$, $R^{(i)} > 0$, and $P^{(i)} > 0$ are the covariance matrices of $W^{(i)}$, $V^{(i)}$, and $E^{(i)}$, respectively. The information about $P^{(ij)}$ is unknown and unavailable to $SO^{(i)}$. Instead, an estimate of the term $\hbar^{(ij)} = A^{(ij)}(\mathrm{t})P^{(ij)^T} + P^{(ij)}(A^{(ij)}(t))^T$ in (4.14) is made by using the information about $P^{(j)}$ which is sent from $SO^{(j)}$ to $SO^{(i)}$.

For the covariance matrix $P^{(ij)}$ we have

$$|P^{(ij)}_{[a,b]}| \leq \sqrt{P^{(i)}_{[a,a]}P^{(j)}_{[b,b]}} \tag{4.15}$$

where the index $[a, b]$ is defined in Definition 2.8. Consequently, the term $\hbar^{(ij)} = A^{(ij)}(\mathrm{t})(P^{(ij)})^T + P^{(ij)}(A^{(ij)}(t))^T$ in (4.14) is estimated by $\hat{\hbar}^{(ij)}$ below

$$\hat{\hbar}^{(ij)} = A^{(ij)}(\mathrm{t})(\hat{P}^{(ij)})^T + \hat{P}^{(ij)}(A^{(ij)}(t))^T \tag{4.16}$$

in which $\hat{P}^{(ij)}$ corresponds to the worst case scenario for the eigenvalues of $\hat{\hbar}^{(ij)}$ subject to the constraint (4.15) as in the following optimization problem:

$$\begin{aligned}
\hat{P}^{(ij)} = \arg\ \max\ & \hbar_{min} \\
s.t.\ & |\hat{P}^{(ij)}_{[a,b]}| \leq \sqrt{P^{(i)}_{[a,a]}P^{(j)}_{[b,b]}} \\
& \lambda_{min}(\hat{\hbar}^{(ij)}) \geq \hbar_{min} \\
& \lambda_{max}(\hat{\hbar}^{(ij)}) \leq \hbar_{max} \\
& \hat{\hbar}^{(ij)} \geq 0
\end{aligned}$$

where $\lambda_{min}(.)$ and $\lambda_{max}(.)$ represent the minimum and maximum eigenvalues of a matrix, respectively, $\hbar_{min}$ is a lower bound on the eigenvalues of $\hat{\hbar}^{(ij)}$, and the upper bound $\hbar_{max}$

is imposed on $\lambda_{max}(\hat{\hbar}^{(ij)})$ (or equivalently $||\hat{\hbar}^{(ij)}||$) in order to guarantee stability of the estimation system as will be shown later in Theorem 4.2.

Taking $\hat{P}^{(ij)} = A^{(ij)}M$ where M is a transformation matrix, we get:

$$\begin{aligned}
|\hat{P}^{(ij)}_{[a,b]}| \leq \sqrt{P^{(i)}_{[a,a]}P^{(j)}_{[b,b]}} &\iff A^{(ij)}_{[a,:]}M_{[:,b]} \leq \sqrt{P^{(i)}_{[a,a]}P^{(j)}_{[b,b]}} \\
\lambda_{min}(\hat{\hbar}^{(ij)}) \geq \hbar_{min} &\iff A^{(ij)}(M+M^T)(A^{(ij)})^T - \hbar_{min}I \geq 0 \\
\lambda_{max}(\hat{\hbar}^{(ij)}) \leq \hbar_{max} &\iff A^{(ij)}(M+M^T)(A^{(ij)})^T - \hbar_{max}I \leq 0 \\
\forall A^{(ij)} \in R^{n^{(i)}\times n^{(i)}} : \hat{\hbar}^{(ij)} \geq 0 &\iff M + M^T \geq 0
\end{aligned}$$

where I represents the identity matrix with appropriate dimensions and the indices $[a,:]$ and $[:,b]$ are defined in Definition 2.8. Therefore, $\hat{P}^{(ij)}$ is the solution to the following constrained optimization problem:

$$\begin{aligned}
\hat{P}^{(ij)} = A^{(ij)}M = \arg\ \max\ & \hbar_{min} \\
s.t.\ & A^{(ij)}_{[a,:]}M_{[:,b]} \leq \sqrt{P^{(i)}_{[a,a]}P^{(j)}_{[b,b]}} \\
& A^{(ij)}(M+M^T)(A^{(ij)})^T - \hbar_{min}I \geq 0 \\
& A^{(ij)}(M+M^T)(A^{(ij)})^T - \hbar_{max}I \leq 0 \\
& M + M^T \geq 0
\end{aligned}$$

Using the estimate $\hat{\hbar}^{(ij)}$ in (4.16), the equation (4.14) of the sub-observer $SO^{(i)}$ becomes

$$\begin{aligned}
\dot{\hat{X}}^{(i)} &= A^{(i)}(t)\hat{X}^{(i)} + B^{(i)}U + K^{(i)}(Y^{(i)} - C^{(i)}\hat{X}^{(i)}) \\
&\quad + \sum_{j\in\mathscr{N}(\{i\})} A^{(ij)}(t)\hat{X}^{(j)} \\
K^{(i)} &= P^{(i)}(C^{(i)})^T(R^{(i)})^{-1} \\
\dot{P}^{(i)} &= A^{(i)}(t)P^{(i)} + P^{(i)}(A^{(i)}(t))^T + Q^{(i)} - P^{(i)}(C^{(i)})^T(R^{(i)})^{-1}C^{(i)}P^{(i)} + \hat{\hbar}^{(i)} \\
\hat{\hbar}^{(i)} &= \sum_{j\in\mathscr{N}(\{i\})} \hat{\hbar}^{(ij)} \qquad (\hat{\hbar}^{(i)} \geq 0)
\end{aligned} \tag{4.17}$$

In the next section, the role of the supervisor is explained by using the definitions of sub-observer dependency estimation (SODE) and weighted sub-observer dependency estimation (WSODE) digraphs.

4.3 The Role of a Supervisor

Similar to the previous chapter, in this chapter the role of a supervisor is explained by introducing the *sub-observer dependency estimation (SODE)* and *weighted sub-observer*

dependency estimation (WSODE) directed graph (digraph), respectively, for the cases of given sub-observer conditions $COND^{(i)}$ (as in Definition 3.6) and sub-observer costs $COST^{(i)}$ (as in Definition 3.7).

4.3.1 Sub-Observer Dependency Estimation (SODE) Digraph

In this section, the role of a supervisor is described by introducing the sub-observer dependency estimation (SODE) directed graph (digraph). For a set of sub-observers $\{SO^{(1)}, ..., SO^{(N_{so})}\}$, the associated SODE digraph $G_{SODE}(V_{SODE}, E_{SODE})$ is defined in the following.

Vertex Set: The vertex set V_{SODE} is defined similar to the vertex set V_E in the previous chapter. Accordingly, the source vertex v_{source} and the sink vertex v_{sink} are assigned with the vectors $\mathbf{v}_{source} = 0_{n\times 1}$ and $\mathbf{v}_{sink} = 1_{n\times 1}$.

Edge Set: The edge set E_{SODE} includes all the directed edges $e^{(i)}_{a,b} = ((v_a, v_b), SO^{(i)}, COND^{(i)})$, where

- (v_a, v_b) indicates that the directed edge $e^{(i)}_{a,b}$ is a transition from v_a to v_b
- $SO^{(i)}$ indicates that the transition (v_a, v_b) along the directed edge $e^{(i)}_{a,b}$ is due to the implementation of the sub-observer $SO^{(i)}$ so that additional states are now estimated in v_b as compared to v_a according to $\mathbf{v}_b = OR\left\{\mathbf{v}_a, R^{(i)}_x\right\}$, where

$$R^{(i)}_{x,[k]} = Logic\left\{\hat{x}^{(i)}_k \in R^{(i)}\right\} \ (k = 1, ..., n)$$

$$(OR\{X, \mathrm{Y}\})_{[k]} = Logic\left\{(X)_{[k]} + (Y)_{[k]} \neq 0\right\}$$

- $SO^{(i)}$ also indicates that the transition (v_a, v_b) along the directed edge $e^{(i)}_{a,b}$ due to the implementation of the sub-observer $SO^{(i)}$ is conditioned on that in v_a all the required state estimates in the domain $D^{(i)}$ of the sub-observer $SO^{(i)}$ are available, that is $\forall k \in \{1, ..., n\}$: if $\hat{x}^{(\mathrm{i})}_{\mathrm{k}} \in D^{(i)} \Rightarrow \mathbf{v}_{a,[k]} = 1$
- $COND^{(i)} \in \{0, 1\}$ indicates that the transition (v_a, v_b) along the directed edge $e^{(i)}_{a,b}$ is conditioned on $COND^{(i)} = 0$.

Similar to the previous chapter, the objective of the supervisor is summarized as follows:

$$\begin{array}{ll} \text{Find} & P = (V_P, E_P) \text{ with} \\ & V_P = \{v_{source}, v_{i_1}, ..., v_{i_{p-1}}, v_{sink}\} \subset V_{SODE} \text{ and} \\ & E_P = \{e^{(j_1)}_{source,i_1}, e^{(j_2)}_{i_1,i_2}, ..., e^{(j_{p-1})}_{i_{p-2},i_{p-1}}, e^{(j_p)}_{i_{p-1},sink}\} \subset E_{SODE} \\ s.t. & COND^{(k)} = 0 \ , \ \forall k \in \{j_1, j_2, ..., j_p\} \end{array} \tag{4.18}$$

As discussed in the previous chapter, besides the information on whether a sub-observer $SO^{(i)}$ can be implemented ($COND^{(i)} = 0$) or not ($COND^{(i)} = 1$, as per Definition 3.6), in some applications the supervisor is provided with the information on the implementation cost $COST^{(i)}$ (as per Definition 3.7) of the sub-observer $SO^{(i)}$ (as per Assumption 3.2). This problem requires a more general and extended digraph model for the supervisor that will be considered in the next section.

4.3.2 Weighted Sub-Observer Dependency Estimation (WSODE) Digraph

In the previous section, the condition $COND^{(i)} \in \{0, 1\}$ (as per Definition 3.6) was assigned to each sub-observer $SO^{(i)} \in \{SO^{(1)}, ..., SO^{(N_{so})}\}$, based on which the supervisor determines whether $SO^{(i)}$ can be implemented ($COND^{(i)} = 0$) in the directed path $P_{\text{sup}} = (V_{\text{sup}}, E_{\text{sup}})$ or not ($COND^{(i)} = 1$). Instead, in this section we assign the cost $COST^{(i)} \in [0, \infty]$ (as per Definition 3.7) to the sub-observer $SO^{(i)}$ (as per Assumption 3.2), and introduce the *weighted sub-observer dependency estimation (WSODE) directed graph (digraph)*. The WSODE digraph $G_{WSODE}(V_{WSODE}, E_{WSODE})$ is defined as follows:

Vertex Set: The *vertex set* V_{WSODE} is defined similar to the vertex set V_{SODE}. Accordingly, the source vertex v_{source} and the sink vertex v_{sink} are assigned to the vectors $\mathbf{v}_{source} = 0_{n\times 1}$ and $\mathbf{v}_{sink} = 1_{n\times 1}$.

Edge Set: The *edge set* E_{WSODE} includes all the directed edges $e^{(i)}_{a,b} = ((v_a, v_b), SO^{(i)}, COND^{(i)})$, where

- (v_a, v_b) indicates that the directed edge $e^{(i)}_{a,b}$ is a transition from v_a to v_b
- $SO^{(i)}$ indicates that the transition (v_a, v_b) along the directed edge $e^{(i)}_{a,b}$ is due to the implementation of the sub-observer $SO^{(i)}$ so that additional states are now estimated in v_b as compared to v_a according to $\mathbf{v}_b = OR\left\{\mathbf{v}_a, R^{(i)}_x\right\}$
- $SO^{(i)}$ also indicates that the transition (v_a, v_b) along the directed edge $e^{(i)}_{a,b}$ due to the implementation of the sub-observer $SO^{(i)}$ is conditioned on that in v_a all the required state estimates in the domain $D^{(i)}$ of the sub-observer $SO^{(i)}$ are available, that is $\forall k \in \{1, ..., n\}$: if $\hat{\mathrm{x}}^{(\mathrm{i})}_{\mathrm{k}} \in D^{(i)} \Rightarrow \mathbf{v}_{a,[k]} = 1$
- $COST^{(i)} \in [0, \infty]$ is the weight of the directed edge $e^{(i)}_{a,b}$ that indicates the cost of the transition (v_a, v_b) along the directed edge $e^{(i)}_{a,b}$ by using the sub-observer $SO^{(i)}$.

Similar to the previous chapter, the objective of the supervisor is summarized as follows:

$$
\begin{aligned}
Min \quad & \sum_{k=j_1}^{j_p} COST^{(k)} \\
s.t. \quad & \mathscr{R}(k) \in \{0,1\} \text{ and} \\
& \forall l \in \{1,...,n\}; \hat{x}_l^{(k)} \in D^{(k)} : \emptyset \neq \mathscr{N}_l(\{k\}) \in \left\{k' \in S_{so} | \hat{x}_l^{(k')} \in R^{(k')}\right\} \\
& P = (V_P, E_P) \text{ with} \\
& V_P = \{v_{source}, v_{i_1}, ..., v_{i_{p-1}}, v_{sink}\} \subset V_{WSODE} \text{ and} \\
& E_P = \{e^{(j_1)}_{source,i_1}, e^{(j_2)}_{i_1,i_2}, ..., e^{(j_{p-1})}_{i_{p-2},i_{p-1}}, e^{(j_p)}_{i_{p-1},sink}\} \subset E_{WSODE}
\end{aligned}
\tag{4.19}
$$

In [119], [120], and [117], the design and analysis of a supervisor in the Discrete Event System (DES) framework [157] is proposed to solve the problems (4 22) and (4 23) by finding the correct path in the system automaton, however these results are beyond the scope of this thesis and are therefore not pursued any further.

So far, we have indicated how to design sub-observers for the general case of a bilinear state space representation. We have also presented the role of a supervisor that is governed by equations (4.18) and (4.19) based on the SODE and WSODE digraphs, respectively. We are now in the position to formally verify that the overall integration of the cooperative sub-observers in the selected set will lead to an overall stable (convergent) system. In the next section, the convergence of our cooperative estimation scheme will be analyzed.

4.4 Convergence Analysis of Cooperative Sub-Observers in Bilinear Systems

In this section, the results on convergence analysis of cooperative sub-observers are based on the assumption that the sub-observer dependency (SOD) digraph is acyclic (as per Definition 3.5). Our goal now is to investigate the convergence of cooperative sub-observers given by equation (4.17) for the bilinear system (4.1), whose equivalent linear time-varying model is given by equation (4.3). The following lemma is provided from the results in [159].

Lemma 4.1. *([159]) Consider the dynamic system $\dot{X} = f(X,t)$, where $f(X,t)$ is piecewise continuous in t and locally Lipschitz in X. Let $V(X(t),t)$ be a continuously differentiable Lyapunov function such that*

a) $\exists \alpha, \beta > 0$ *such that* $\forall X(t) \in R^n$, $\alpha||X(t)||^2 < V(X(t),t) < \beta||X(t)||^2$

b) $\exists \bar{\gamma} > 0$ *such that* $\forall \mathrm{X(t)} \in D_X^{\gamma} = \{X(t) \in R^n; ||\mathrm{X(t)}|| > \bar{\gamma}\}$, $\dot{V}(\mathrm{X(t)}, \mathrm{t}) < 0$

Then $\forall X(t_0) \in R^n$*:* $\exists t_b = t_b(X(t_0), \bar{\gamma})$ *such that* $X(t) \in D_{\mathrm{X}}^{\mathrm{b}} = \{X(t) \in R^n; ||\mathrm{X(t)}|| < \mathrm{B_X} = \bar{\gamma}\beta/\alpha\}$ *for* $\forall t \geq t_b$*.*

Theorem 4.2. *Consider the equivalent linear time-varying model* (4.3) *of the bilinear system* (4.1)*, whose states are being cooperatively estimated by the sub-observers governed by equation* (4.17)*. The estimation errors are uniformly ultimately bounded if the sub-observer dependency (SOD) digraph is acyclic (as per Definition 3.5).*

Proof: *According to the Condition 3 in Procedure 4.1, the pair* $(A^{(i)}, C^{(i)})$ *of the sub-observer* $SO^{(i)}$ *(given in equation 4.17) is observable. If the sub-observer* $SO^{(i)}$ *is initialized with a positive definite covariance matrix* $P^{(i)}(0)$*, and if the matrices* $Q^{(i)}$*,* $R^{(i)}$ *and* $\hat{\hbar}^{(i)}$ *are positive semi-definite and bounded, then the covariance matrix* $P^{(i)}$ *remains positive definite and bounded for all time [160], [161]. We define the following Lyapunov function candidate for the sub-observer* $SO^{(i)}$*:*

$$V^{(i)}(E^{(i)}, t) = {E^{(i)}}^T {P^{(i)}}^{-1} E^{(i)} \tag{4.20}$$

Using the equation

$$\frac{d}{dt}\left({P^{(i)}}^{-1}\right) = {P^{(i)}}^{-1} \dot{P}^{(i)} {P^{(i)}}^{-1}$$

and using the equations (4.17) *and* (4.13) *for* $K^{(i)}$ *and* $\dot{E}^{(i)}$*, respectively, we get*

$$\begin{aligned}
&\dot{V}^{(i)}(E^{(i)}, t) \\
&= {E^{(i)}}^T \left({P^{(i)}}^{-1} A^{(i)} + {A^{(i)}}^T {P^{(i)}}^{-1} - 2{C^{(i)}}^T {R^{(i)}}^{-1} C^{(i)} - {P^{(i)}}^{-1} \dot{P}^{(i)} {P^{(i)}}^{-1}\right) E^{(i)} \\
&- {E^{(i)}}^T {P^{(i)}}^{-1} W^{(i)} - {W^{(i)}}^T {P^{(i)}}^{-1} E^{(i)} + {E^{(i)}}^T {C^{(i)}}^T {R^{(i)}}^{-1} V^{(i)} + {V^{(i)}}^T {R^{(i)}}^{-1} C^{(i)} E^{(i)} \\
&+ \sum_{j \in \mathscr{N}(\{i\})} \left({E^{(i)}}^T {P^{(i)}}^{-1} A^{(ij)} E^{(j)} + {E^{(j)}}^T {A^{(ij)}}^T {P^{(i)}}^{-1} E^{(i)}\right)
\end{aligned}$$

Using equation (4.17) *for* $\dot{P}^{(i)}$*, we have*

$$\begin{aligned}
&\dot{V}^{(i)}(E^{(i)}, t) \\
&= {E^{(i)}}^T \left(-{P^{(i)}}^{-1} Q^{(i)} {P^{(i)}}^{-1} - {P^{(i)}}^{-1} \hat{\hbar}^{(i)} {P^{(i)}}^{-1} - {C^{(i)}}^T {R^{(i)}}^{-1} C^{(i)}\right) E^{(i)} \\
&- {E^{(i)}}^T {P^{(i)}}^{-1} W^{(i)} - {W^{(i)}}^T {P^{(i)}}^{-1} E^{(i)} + {E^{(i)}}^T {C^{(i)}}^T {R^{(i)}}^{-1} V^{(i)} + {V^{(i)}}^T {R^{(i)}}^{-1} C^{(i)} E^{(i)} \\
&+ \sum_{j \in \mathscr{N}(\{i\})} \left({E^{(i)}}^T {P^{(i)}}^{-1} A^{(ij)} E^{(j)} + {E^{(j)}}^T {A^{(ij)}}^T {P^{(i)}}^{-1} E^{(i)}\right)
\end{aligned}$$

Taking $||W^{(i)}|| < B_{W^{(i)}}$ *and* $||V^{(i)}|| < B_{V^{(i)}}$ *the following inequality holds:*

$$
\begin{aligned}
&\dot{V}^{(i)}(E^{(i)},t) < \\
&-\left(\underbrace{(\lambda_{\min}(Q^{(i)})+\lambda_{\min}(\hat{h}^{(i)}))\inf_{t>0}\lambda_{\max}^{-2}(P^{(i)})}_{\omega_L^{i,i}}+\lambda_{\max}^{-1}(R^{(i)})\lambda_{\min}({C^{(i)}}^T C^{(i)})\right)||E^{(i)}||^2 \\
&+\underbrace{\left(\sup_{t>0}2\lambda_{\min}^{-1}(P^{(i)})B_{W^{(i)}}+2\lambda_{\min}^{-1}(R^{(i)})\lambda_{\max}^{1/2}({C^{(i)}}^T C^{(i)})B_{V^{(i)}}\right)}_{\omega_L^{i}}||E^{(i)}|| \\
&+\sum_{j\in\mathscr{N}(\{i\})}\underbrace{\sup_{t>0}2\lambda_{\max}^{1/2}({A^{(ij)}}^T A^{(ij)})\sup_{t>0}\lambda_{\min}^{-1}(P^{(i)})}_{\omega_L^{i,j}}||E^{(i)}||||E^{(j)}||
\end{aligned}
\tag{4.21}
$$

If the sub-observer dependency (SOD) digraph is acyclic, then the Lyapunov function candidate in (4.20) *can be taken independently for each sub-observer* $SO^{(i)}$*. Since the adjacency matrix is upper triangular (as per Theorem 3.2), the estimation error analysis and evaluations can be done hierarchically starting at the source sub-observer vertices (with zero in-degrees as per Theorem 3.1) and ending at the sink sub-observer vertices (with zero out-degrees as per Theorem 3.1) in the SOD digraph, while the estimation errors are propagated hierarchically in the source-to-sink directions of the paths in the acyclic SOD digraph. In other words, there are no estimation error cycles throughout the SOD digraph, and so once the ultimate boundedness of the estimation errors are guaranteed and achieved for each sub-observer independently, then it will be preserved in the overall scheme. In order to perform the independent estimation error calculations, we have*

$$
\begin{aligned}
\dot{V}^{(i)}(E^{(i)},t) &< -\underbrace{\left(\omega_L^{i,i}+\lambda_{\max}(R^{(i)})\lambda_{\min}({C^{(i)}}^T C^{(i)})\right)}_{A_L^i}||E^{(i)}||^2+\underbrace{\left(\omega_L^{i}+\Omega_{\mathrm{L}}^{i}\right)}_{B_L^i}||E^{(i)}|| \\
&= -A_L^i||E^{(i)}||^2+B_L^i||E^{(i)}||
\end{aligned}
\tag{4.22}
$$

where

$$
\Omega_{\mathrm{L}}^{i}=\sum_{j\in\mathscr{N}(\{i\})}\omega_L^{i,j}\sup_{t>0}||E^{(j)}||
$$

For the Lyapunov function candidate $V^{(i)}$ *and its derivative* $\dot{V}^{(i)}$ *in equations* (4.20) *and* (4.22)*, respectively, we apply Lemma 4.1 by using the parameters* $\alpha=\inf_{t\in R^+}\lambda_{\min}((P^{(i)})^{-1})$*,* $\beta=\sup_{t\in R^+}\lambda_{\max}((P^{(i)})^{-1})$*, and* $\bar{\gamma}=B_L^i/A_L^i$*, and get*

$$
||E^{(i)}|| < B_{E^{(i)}}=\frac{\sup\limits_{t\in R^+}\lambda_{\max}(P^{(i)})B_L^i}{\inf\limits_{t\in R^+}\lambda_{\min}(P^{(i)})A_L^i}
\tag{4.23}
$$

Therefore, all the estimation errors $E^{(i)}$ converge to within the error bounds $B_{E^{(i)}}$, and the proof of the theorem is complete. ■

The following example demonstrates the concepts and theories that have been presented so far in this chapter.

Example 4.1. *This example shows how the sub-observers are designed and how the supervisor makes decision on the proper set of sub-observers according to the costs of the sub-observers. Consider the system that is presented by equation* (4.1) *(or* (4.3)*) with the state vector $X = [x_1\ x_2]^T$, input vector $U = [u_1\ u_2]^T$ ($r = 2$), and output vector $Y = [y_1\ y_2]^T$, and the system matrices*

$$A_0 = \begin{bmatrix} a_{0,11} & 0 & 0 \\ 0 & 0 & 0 \\ 0 & 0 & a_{0,33} \end{bmatrix},\ A_1 = \begin{bmatrix} 0 & a_{1,12} & 0 \\ 0 & 0 & 0 \\ 0 & 0 & 0 \end{bmatrix},\ A_2 = \begin{bmatrix} 0 & 0 & 0 \\ 0 & 0 & 0 \\ 0 & a_{2,32} & 0 \end{bmatrix}$$

$$B = \begin{bmatrix} b_{11} & 0 \\ 0 & 0 \\ 0 & b_{32} \end{bmatrix},\ C = \begin{bmatrix} c_{11} & 0 & 0 \\ 0 & 0 & c_{23} \end{bmatrix}$$

The directed graphs of the systems is shown in Figure 4.1. In this figure, the two state-output paths (x_2, x_1, y_1) and (x_2, x_3, y_2) cover all the states, and there exist $n = 3$ A-disjoint vertices (x_1, y_1), (x_3, y_2), and $(x_2, y_1)_1$. Therefore, the structural observability of the system (Proposition 4.1) is guaranteed.

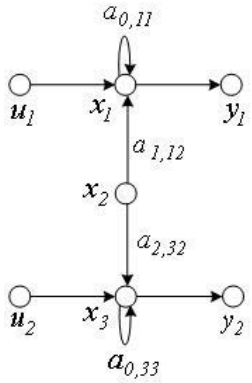

Figure 4.1: The directed graph of the bilinear system with the matrices A_0, A_1, A_2, B, and C.

Let us now investigate the application of Procedure 4.1 for the structurally observable bilinear system above. In step 1 of Procedure 4.1, the directed graph of the system is constructed as shown in Figure 4.1. According to the directed graph of the system it turns

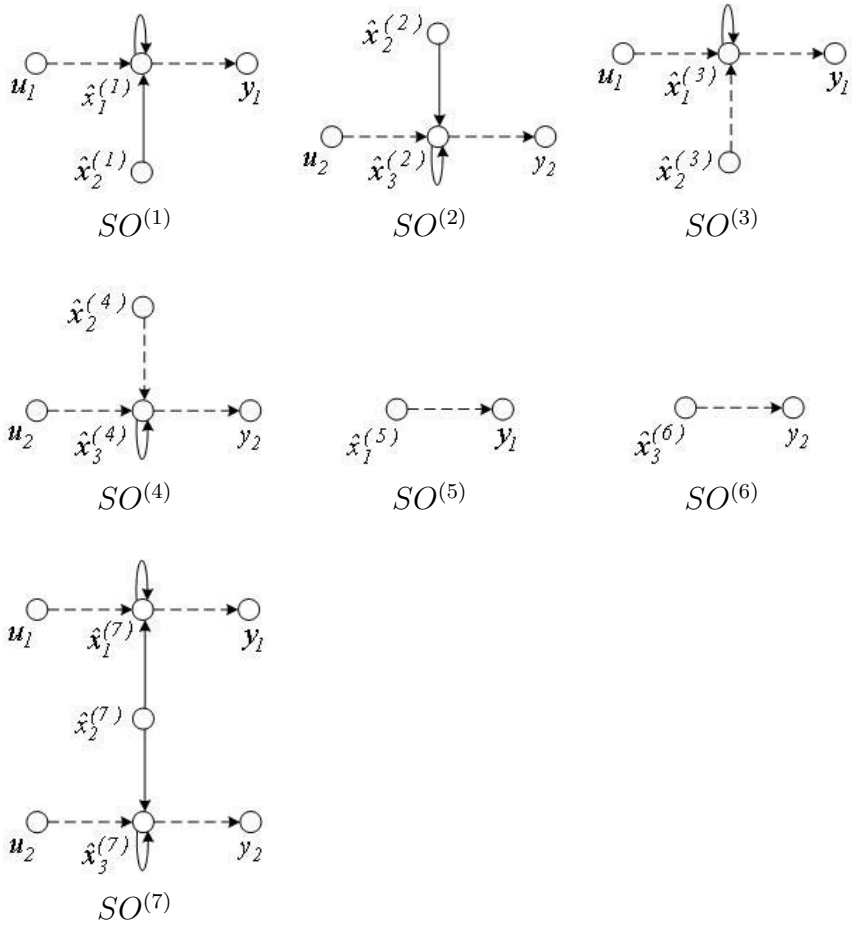

Figure 4.2: The directed graphs of the seven sub-observers for the system (A, B, C).

out that at most seven sub-observers, which are shown in Figure 4.2, can be designed in step 2 of Procedure 4.1 that simultaneously *satisfy the conditions 1, 2, and 3.*

In Figure 4.2, the dashed lines represent the information that the sub-observer $SO^{(i)}$ requires to receive regarding certain inputs $u_s \in I^{(i)}$ ($s \in \{1, ..., r\}$), outputs $y_q \in O^{(i)}$ ($q \in \{1, ..., m\}$), and state estimates $\hat{x}_p^{(i)} \in D^{(i)}$ ($p \in \{1, ..., n\}$) from other sub-observers $SO^{(j)}$ (such that $\hat{x}_p^{(j)} \in R^{(j)}$ and $\hat{x}_p^{(i)} := \hat{x}_p^{(j)}$). The solid lines represent the dynamic relations among the states $\hat{x}_p^{(i)} \in R^{(i)}$ of the sub-observer $SO^{(i)}$. Using Proposition 4.1 for each sub-observer $SO^{(i)}$, it is easy to verify that the graph representing $SO^{(i)}$ satisfies the conditions of the Proposition 4.1. The seven sub-observers are formally represented as follows:

$$
\begin{array}{ll}
(i) & SO^{(1)}(R^{(1)}|I^{(1)}, O^{(1)}, D^{(1)}) \\
 & R^{(1)} = \{\hat{x}_1^{(1)}, \hat{x}_2^{(1)}\}, I^{(1)} = \{u_1\}, O^{(1)} = \{y_1\}, D^{(1)} = \{\} \\
(ii) & SO^{(2)}(R^{(2)}|I^{(2)}, O^{(2)}, D^{(2)}) \\
 & R^{(2)} = \{\hat{x}_2^{(2)}, \hat{x}_3^{(2)}\}, I^{(2)} = \{u_2\}, O^{(2)} = \{y_2\}, D^{(2)} = \{\} \\
(iii) & SO^{(3)}(R^{(3)}|I^{(3)}, O^{(3)}, D^{(3)}) \\
 & R^{(3)} = \{\hat{x}_1^{(3)}\}, I^{(3)} = \{u_1\}, O^{(3)} = \{y_1\}, D^{(3)} = \{\hat{x}_2^{(3)}\} \\
(iv) & SO^{(4)}(R^{(4)}|I^{(4)}, O^{(4)}, D^{(4)}) \\
 & R^{(4)} = \{\hat{x}_3^{(4)}\}, I^{(4)} = \{u_2\}, O^{(4)} = \{y_2\}, D^{(4)} = \{\hat{x}_2^{(4)}\} \\
(v) & SO^{(5)}(R^{(5)}|I^{(5)}, O^{(5)}, D^{(5)}) \\
 & R^{(5)} = \{\hat{x}_1^{(5)}\}, I^{(5)} = \{\}, O^{(5)} = \{y_1\}, D^{(5)} = \{\} \\
(vi) & SO^{(6)}(R^{(6)}|I^{(6)}, O^{(6)}, D^{(6)}) \\
 & R^{(6)} = \{\hat{x}_3^{(6)}\}, I^{(6)} = \{\}, O^{(6)} = \{y_2\}, D^{(6)} = \{\} \\
(vii) & SO^{(7)}(R^{(7)}|I^{(7)}, O^{(7)}, D^{(7)}) \\
 & R^{(7)} = \{\hat{x}_1^{(7)}, \hat{x}_2^{(7)}, \hat{x}_3^{(7)}\}, I^{(7)} = \{u_1, u_2\}, O^{(7)} = \{y_1, y_2\}, D^{(7)} = \{\}
\end{array}
$$

In each of the sub-observers $SO^{(5)}$ and $SO^{(6)}$, there is only one sensor that is involved in the observation resulting in having no specific dynamics associated with them. Consequently, $SO^{(5)}$ and $SO^{(6)}$ should be interpreted as direct measurements of the states. A portion of the estimation digraph of the system is depicted in Figure 4.3. In this figure, without loss of generality, some vertices and edges are eliminated in order to avoid redundant paths and simplify the understanding of the corresponding definitions and concepts.

In Figure 4.3, the vertices are assigned with the following vectors

$$
\mathbf{v}_{source} = \begin{bmatrix} 0 \\ 0 \\ 0 \end{bmatrix}, \ \mathbf{v}_{sink} = \begin{bmatrix} 1 \\ 1 \\ 1 \end{bmatrix}, \ \mathbf{v}_1 = \begin{bmatrix} 1 \\ 1 \\ 0 \end{bmatrix}, \ \mathbf{v}_2 = \begin{bmatrix} 0 \\ 1 \\ 1 \end{bmatrix}
$$

Although for this bilinear system, there are seven possible sub-observers, however, one only needs a subset of them to cooperatively estimate all the states of the system.

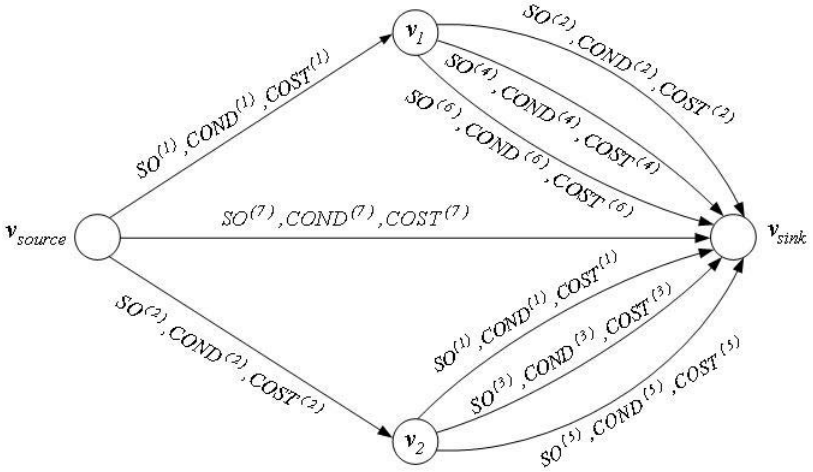

Figure 4.3: A portion of the combined sub-observer dependency estimation (SODE) and weighted sub-observer dependency estimation (WSODE) digraphs of the bilinear system with the matrices A_0, A_1, A_2, B, and C. The edges are labeled with $(SO^{(i)}, COND^{(i)})$ and $(SO^{(i)}, COST^{(i)})$ for the SODE and WSODE digraphs, respectively.

For instance, in the normal operation mode the supervisor suggests an initial set of sub-observers $\{SO^{(2)}, SO^{(3)}\}$ with $\mathscr{N}(\{2\}) = \{\}$ and $\mathscr{N}(\{3\}) = \{2\}$, which corresponds to the path $\mathbf{v}_{source}\mathbf{v}_2\mathbf{v}_{sink}$ in the SODE digraph of Figure 4.3, that can cooperatively estimate all the system states.

Let us now assume that the process dynamics uncertainty/unreliability $\bar{W}^{(i)} \neq 0$ occurs in the sub-observers $SO^{(i)}$, $i \in \{2, 4, 7\}$ (as given in equation (4.12) and Definition 3.6). These uncertainties originate from the dynamic equation of the state x_3 subject to the process dynamics uncertainty/unreliability $\bar{W}_3^{(i)} \neq 0$, where $\bar{W}_3^{(i)}$ represents the x_3-corresponding element of $\bar{W}^{(i)}$.

In the first approach, consider the SODE digraph in Figure 4.4. The sub-observers $SO^{(i)}$, $i \in \{2, 4, 7\}$ become invalid ($COND^{(i)} = 1$ as per Definition 3.6) and hence should not be used any further for constructing the state estimates. Consequently, in order to achieve the objective in equation (4.18) the supervisor eliminates all the sub-observer sets, in which the invalid sub-observers are employed. The eliminated sub-observers are denoted by the dashed edges in the SODE digraph in Figure 4.4, where the supervisor proposes the modified set of sub-observers $\{SO^{(1)}, SO^{(6)}\}$, with $\mathscr{N}(\{1\}) = \{\}$ and $\mathscr{N}(\{6\}) = \{\}$, corresponding to the path $\mathbf{v}_{source}\mathbf{v}_1\mathbf{v}_{sink}$. Therefore, the information about the uncertain dynamic state x_3 is not incorporated in the modified set of sub-observers $\{SO^{(1)}, SO^{(6)}\}$.

In the second approach, consider the weighted WSODE digraph in Figure 4.5. The sub-observers $SO^{(i)}$, $i \in \{2, 4, 7\}$ are costly ($COST^{(i)} \neq 0$ as per Definition 3.7). By taking the coeficients $C_R = 0$ (no recovery available), $C_C = 0$ (no communication cost), and

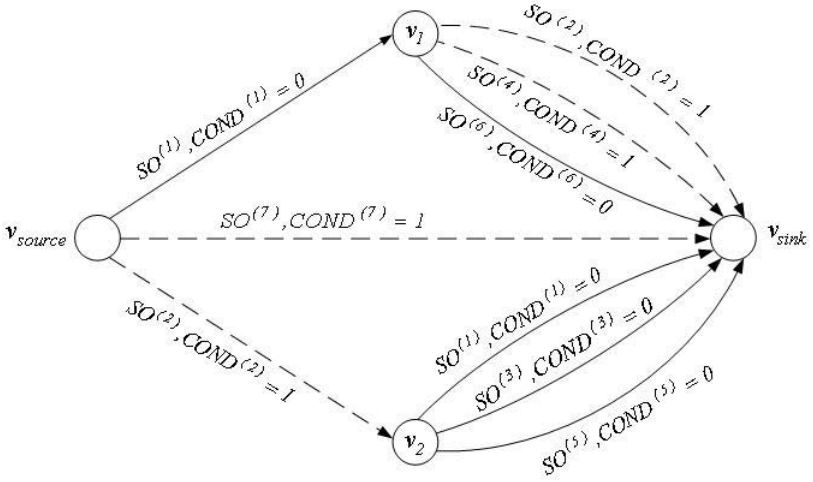

Figure 4.4: The SODE digraph in which the solid and dashed edges represent the valid ($COND^{(i)} = 0$) and invalid ($COND^{(i)} = 1$) sub-observers, respectively.

$C_E = 1$ *as explained in Definition 3.7, the cost of invalid sub-observers* $SO^{(i)}$ *are equal to* $n(R^{(i)})$ *that are indicated in Figure 4.5. These costs should be incorporated in the cooperative estimation scheme. Consequently, in order to achieve the objective in equation* (4.19) *the supervisor minimizes the cumulative cost of the sub-observers and proposes the modified set of sub-observers* $\{SO^{(1)}, SO^{(6)}\}$ *with* $\mathscr{N}(\{1\}) = \{\}$ *and* $\mathscr{N}(\{6\}) = \{\}$*, which corresponds to the path* $\mathbf{v}_{source}\mathbf{v}_1\mathbf{v}_{sink}$ *with the minimum cost of* $COST^{(1)} + COST^{(6)} = 0$ *as shown in Figure 4.5.*

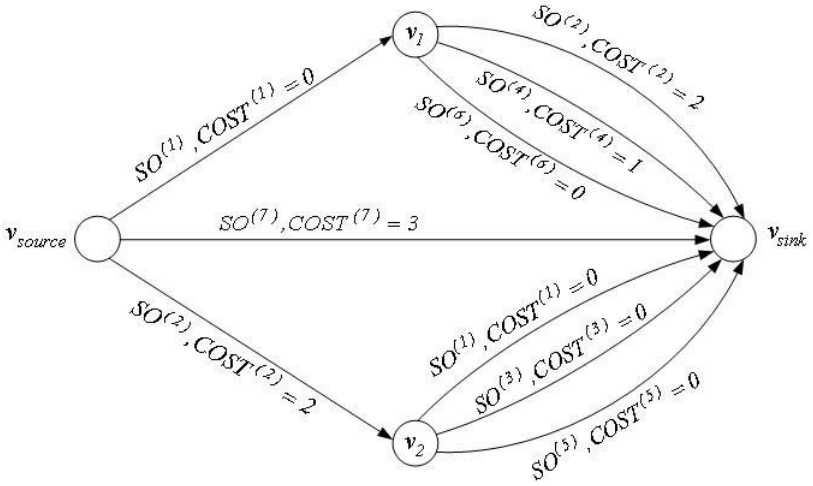

Figure 4.5: The WSODE digraph.

In this example, the results of the SODE and WSODE digraphs are the same. Note

that one still needs to verify the uniformly ultimate boundedness of the overall observation task that is achieved by the supervisor-selected initial set of sub-observers $\{SO^{(2)}, SO^{(3)}\}$ *(the path* $\mathbf{v}_{source}\mathbf{v}_2\mathbf{v}_{sink}$ *shown in Figure 4.3) in the normal operation mode, and the supervisor-reconfigured set of sub-observers* $\{SO^{(1)}, SO^{(6)}\}$ *(the path* $\mathbf{v}_{source}\mathbf{v}_1\mathbf{v}_{sink}$ *shown in Figure 4.4 and Figure 4.5) in the process dynamics unreliability situation. In Figure 4.6, the acyclic condition of Theorem 4.2 is verified for the sub-observer dependency (SOD) digraphs of the two sets of sub-observers* $\{SO^{(2)}, SO^{(3)}\}$ *and* $\{SO^{(1)}, SO^{(6)}\}$*. As can be seen from Figure 4.6 (and Theorem 4.2), both SOD digraphs are acyclic that guarantee the uniformly ultimate boundedness of the estimation task by using either of the sub-observer sets* $\{SO^{(2)}, SO^{(3)}\}$ *and* $\{SO^{(1)}, SO^{(6)}\}$*.* ■

(a) *(b)*

Figure 4.6: The sub-observer dependency (SOD) digraphs of (a) the supervisor-selected initial set of sub-observers $\{SO^{(2)}, SO^{(3)}\}$ *in the normal operation mode and (b) the supervisor-reconfigured set of sub-observers* $\{SO^{(1)}, SO^{(6)}\}$ *in the process dynamics unreliability mode.*

If the ranges of some sub-observers are overlapping, then certain states are being estimated by multiple sub-observers. In such cases, one needs a procedure to fuse the data from all the range-overlapping sub-observers and feed the updated data back to the range-overlapping sub-observers for adjustments to the estimation approach. In the next section, this fusion feedback procedure is described for the range-overlapping sub-observers.

4.5 Distributed and Cooperative Range-Overlapping Sub-Observers with Fusion Feedback (FF)

In this section, the distributed estimation technique is extended to the case of *range-overlapping* sub-observers [118]. This method can be applied to a number of large-scale systems including sensor networks and formation flight of unmanned vehicles missions. So far, we have shown that a system can be cooperatively estimated by a group of sub-observers. If the ranges of some of the sub-observers are overlapping, then those sub-observers are called constrained-state sub-observers (CSSOs) which simultaneously estimate some common states. In order for the CSSOs to achieve consensus over the estimates of the common states, additional information exchange links are required among the range-overlapping sub-observers rather than the information exchange links that are

already included in the sub-observer dependency (SOD) digraph. These additional information exchange links will be embedded into a fusion feedback (FF) procedure that aims at satisfying the constrained-state conditions simultaneously with the time evolution of the Kalman filter expressions of the CSSOs.

4.5.1 Constrained-State Sub-Observer (CSSO)

We can distinguish two types of states, namely local and common, that will be defined in the following.

Definition 4.3. *Consider a state x_p, $p \in \{1, ..., n\}$ and the set $\vartheta(p) \subset \{1, ..., N_{so}\}$ of all the sub-observers which estimate x_p, that is $\forall l \in \vartheta(p) : \hat{x}_p^{(l)} \in R^{(l)}$ and $\forall l \in \{1, ..., N_{so}\} - \vartheta(p) : \hat{x}_p^{(l)} \notin R^{(l)}$.*

- *If $n(\vartheta(p)) = 1$, then x_p is a* local state*, $\vartheta(p)$ is the* sub-observer (SO) set *of x_p, and $SO^{(l)}$ ($l \in \vartheta(p)$) is a sub-observer (SO) of x_p ($n(.)$ denotes the* cardinality *of a set).*
- *If $n(\vartheta(p)) \geq 2$, then x_p is a* common state*, $\vartheta(p)$ is the* constrained-state sub-observer (CSSO) set *of x_p, and $SO^{(l)}$ ($l \in \vartheta(p)$) is a* constrained-state sub-observer (CSSO) *of x_p.*

For a given common state x_p, $p \in \{1, ..., n\}$ and its associated CSSO set $\vartheta(p) \subset \{1, ..., N_{so}\}$, a *constrained-state condition* is imposed on the value of the estimates $\hat{x}_p^{(i)}$, $\forall i \in \vartheta$ that is

$$\forall \mathrm{x_p} \text{ “common” } , \forall \{i, j\} \subset \vartheta(p) : \hat{x}_p^{(i)} = \hat{x}_p^{(j)} \tag{4.24}$$

The CSSOs in the CSSO set $\vartheta(p)$ (as in Definition 4.3) cooperatively estimate the states of the system, while simultaneously satisfying the constrained-state condition of x_p (as in equation (4.24)) through solving local optimization problems. This cooperation is in the sense of information exchanges on the local state estimates. For the CSSO $SO^{(i)}$, $i \in \{1, ..., N_{so}\}$ with the range $R^{(i)} = \{\hat{x}_{i_1}^{(i)}, \hat{x}_{i_2}^{(i)}, ..., \hat{x}_{i_{n^{(i)}}}^{(i)}\}$, the Kalman filter gain

$$K^{(i)} = \begin{bmatrix} K_{i_1}^{(i)} & K_{i_2}^{(i)} & \cdots & K_{i_{n^{(i)}}}^{(i)} \end{bmatrix}^T$$

is calculated next by minimizing the variances of the “common” states.

Denoting $\hat{\sigma}_j^{(i)} = \underset{x_j}{Col}\, \underset{x_j}{Row}(\hat{P}^{(i)})$ as the variance of the state estimate $x_j^{(i)}$ made by the sub-observer $SO^{(i)}$, where $\underset{x_j}{Row}$ and $\underset{x_j}{Col}$ represent the x_j-corresponding row and column, respectively, we now introduce the **centralized optimization problem** as follows:

$$
\begin{aligned}
&\forall x_p \in \{x_{i_1}, x_{i_2}, ..., x_{i_{n(i)}}\} \text{ “local” :} \\
&\quad K_p^{(i)} = \arg\ \min\ \dot{\hat{\sigma}}_p^{(i)}(t) \\
&\qquad = \underset{x_p}{Row}\left(\hat{P}^{(i)}(C^{(i)})^T(R^{(i)})^{-1}\right) \\
&\qquad = \underset{x_p}{Row}(\hat{P}^{(i)})(C^{(i)})^T(R^{(i)})^{-1} \\
&\qquad = \hat{P}_p^{(i)}(C^{(i)})^T(R^{(i)})^{-1} \qquad (4.25) \\
&\forall x_p \in \{x_{i_1}, x_{i_2}, ..., x_{i_{n(i)}}\} \text{ “common” ,} \\
&\vartheta(p) = \{i, \vartheta_2, ..., \vartheta_\mu\}(\mathrm{n}(\vartheta(p)) = \mu > 2) : \\
&\quad \left((K_p^{(i)}, K_p^{(\vartheta_2)}, ..., K_p^{(\vartheta_\mu)})\right) = \arg\ \min\ \dot{\hat{\sigma}}_p^{(i)} + \dot{\hat{\sigma}}_p^{(\vartheta_2)} + \cdots + \dot{\hat{\sigma}}_p^{(\vartheta_\mu)} \\
&\qquad\qquad s.t.\ \exists \hat{x}_p(t) \in R, \forall l \in \vartheta : \hat{x}_p^{(l)} \to \hat{x}_p(t)
\end{aligned}
$$

where $Q^{(i)}$ and $R^{(i)}$ are zero-mean white Gaussian random processes representing the state dynamic disturbance and sensor noise of the sub-observer $SO^{(i)}$, respectively. The value $n(.)$ denotes the *cardinality* of a set, and we have $K_j^{(i)} = \underset{x_j}{Row}(K^{(i)})$ and $\hat{P}_j^{(i)} = \underset{x_j}{Row}(\hat{P}^{(i)})$. Moreover, $\hat{x}_j$ is the estimate of the common state x_j to which all CSSOs $SO^{(i)}$ with $\hat{x}_j^{(i)} \in R^{(i)}$ will converge to, so that the constrained-state condition is satisfied.

In equation (4.25), for a local state x_p with $\hat{x}_p^{(i)} \in R^{(i)}$, the row vector $K_p^{(i)}$ is calculated locally and independently for only the sub-observer $SO^{(i)}$. For a common state x_p with $\hat{x}_p^{(l)} \in R^{(l)}$ $(\forall l \in \vartheta(p))$, the row vectors $K_p^{(l)}$ $(\forall l \in \vartheta(p))$ should be calculated simultaneously in a centralized manner. Therefore, the calculation of the row vectors $K_p^{(l)}$ $(\forall l \in \vartheta(p))$ requires stringent communication among the sub-observers $SO^{(l)}$ $(\forall l \in \vartheta(p))$ that results in performance that is highly dependent on the computational and communication delays and failures. In the following section, the robustness of our proposed CSSO technique as governed by equation (4.25) is improved through the use of a fusion feedback.

4.5.2 Fusion Feedback (FF)

In this section, *constrained-state sub-observer with fusion feedback (CSSOFF)* is introduced to improve the performance of the CSSO scheme. As shown in Figure 4.7, our proposed CSSOFF is realized in four steps, namely “prediction”, “observation”, “fusion”, and “feedback” that are performed synchronously for all the sub-observers. Moreover, it is assumed that the communication delay is negligible.

The first two steps are similar to the general Kalman filtering technique as given below:

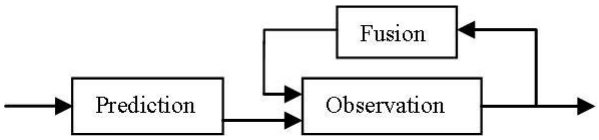

Figure 4.7: CSSOFF procedure that includes "prediction", "observation", "fusion", and "feedback" steps.

Steps 1-2. Prediction and Observation:

$$\begin{aligned}
&\bar{X}^{(i)} = \hat{X}^{(i)} \ , \ \bar{P}^{(i)} = \hat{P}^{(i)} \\
&\dot{\bar{X}}^{(i)} = A^{(i)}\bar{X}^{(i)} + B^{(i)}U^{(i)} + \bar{K}^{(i)}(Y^{(i)} - C^{(i)}\bar{X}^{(i)}) + \sum_{j\in\mathscr{N}(\{i\})} A^{(ij)}(t)\bar{X}^{(j)} \\
&\dot{\bar{P}}^{(i)} = A^{(i)}\bar{P}^{(i)} + \bar{P}^{(i)}(A^{(i)})^T + Q^{(i)} - \bar{P}^{(i)}(C^{(i)})^T(R^{(i)})^{-1}C^{(i)}\bar{P}^{(i)} + \hat{h}^{(i)}
\end{aligned}$$

where

$$\bar{K}^{(i)} = \bar{P}^{(i)}(C^{(i)})^T(R^{(i)})^{-1} \tag{4.26}$$

In the last two steps, the estimates of the common states are fused and the fusion results are fed back to the corresponding sub-observers to modify their observation step accordingly in order to ensure that the constrained-state conditions (4.24) on the common states (as per Definition 4.3) are satisfied. In other words, we have:

Step 3. Fusion: Quite a few data fusion techniques [144] such as linear combination, probabilistic fusion, Markov chain-based, and multiple criteria approaches have been proposed in the literature based on how a system is modeled. Due to the stochastic nature of the model that is considered in this chapter, the probabilistic fusion method [152] will be used in the following. Taking

$$\bar{x}_p^{(i)} = \underset{x_p}{Row}\,\bar{X}^{(i)} \ , \ \bar{\sigma}_p^{(i)} = \underset{x_p}{Col}\,\underset{x_p}{Row}(\bar{P}^{(i)})$$

the data fusion is achieved according to

$$\begin{aligned}
&\forall x_p \in \{x_1, ..., x_n\}\text{ "common" :} \\
&\quad \sigma_p^{(f)} = \left(\sum_{l\in\vartheta(p)} (\bar{\sigma}_p^{(l)})^{-1}\right)^{-1} \\
&\quad x_p^{(f)} = \sigma_p^{(f)}\left(\sum_{l\in\vartheta(p)} (\bar{\sigma}_p^{(l)})^{-1}\bar{x}_p^{(l)}\right) = \sum_{l\in\vartheta(p)} \underbrace{\frac{\sigma_p^{(f)}}{\bar{\sigma}_p^{(l)}}}_{\alpha_p^{(l)}}\bar{x}_p^{(l)} = \sum_{l\in\vartheta(p)} \alpha_p^{(l)}\bar{x}_p^{(l)}
\end{aligned} \tag{4.27}$$

where $\sum_{l\in\vartheta(p)} \alpha_p^{(l)} = 1$, $x_p^{(f)}$ and $\sigma_p^{(f)}$ are the fused estimate and error covariance of the state x_p, and $\vartheta(p)$ is the CSSO set of the common state x_p that provides the estimates $\bar{x}_p^{(j)}$ $(j \in \vartheta(p))$ for fusion. The vector $x_p^{(f)}$ is now fed back to the sub-observers in the CSSO set $\vartheta(p)$ in order to ensure that the constrained-state conditions (4.24) on the common states (as per Definition 4.3) are satisfied.

Step 4. Feedback:

$$\begin{aligned}
\dot{\hat{X}}^{(i)} &= A^{(i)}\hat{X}^{(i)} + B^{(i)}U^{(i)} + K^{(i)}(Y^{(i)} - C^{(i)}\hat{X}^{(i)}) + \sum_{j\in\mathscr{N}(\{i\})} A^{(ij)}(t)\hat{X}^{(j)} \\
\dot{\hat{P}}^{(i)} &= (A^{(i)} - K^{(i)}C^{(i)})\hat{P}^{(i)} + \hat{P}^{(i)}((A^{(i)})^T - (C^{(i)})^T(K^{(i)})^T) \\
&\quad + Q^{(i)} + C^{(i)}R^{(i)}(C^{(i)})^T + \hat{\hbar}^{(i)}
\end{aligned} \tag{4.28}$$

where $R^{(i)} = \{\hat{x}_{i_1}^{(i)}, \hat{x}_{i_2}^{(i)}, ..., \hat{x}_{i_{n^{(i)}}}^{(i)}\}$ and the Kalman filter gain

$$K^{(i)} = \begin{bmatrix} K_{i_1}^{(i)} & K_{i_2}^{(i)} & \cdots & K_{i_{n^{(i)}}}^{(i)} \end{bmatrix}^T$$

is calculated by using the **fusion feedback (FF) optimization problem** as follows:

$$\begin{aligned}
&\forall x_p \in \{x_{i_1}, x_{i_2}, ..., x_{i_{n^{(i)}}}\} \text{ “local” :} \\
&\quad K_p^{(i)} = \arg\ \min\ \dot{\hat{\sigma}}_p^{(i)}(t) \\
&\qquad = \underset{x_p}{Row}\left(\hat{P}^{(i)}(C^{(i)})^T(R^{(i)})^{-1}\right) \\
&\qquad = \underset{x_p}{Row}(\hat{P}^{(i)})(C^{(i)})^T(R^{(i)})^{-1} \\
&\qquad = \hat{P}_p^{(i)}(C^{(i)})^T(R^{(i)})^{-1} \\
&\forall x_p \in \{x_{i_1}, x_{i_2}, ..., x_{i_{n^{(i)}}}\} \text{ “common” ,} \\
&\vartheta(p) = \{i, \vartheta_2, ..., \vartheta_\mu\}(\mathrm{n}(\vartheta(p)) = \mu > 2) : \\
&\quad \forall i \in \vartheta(p) : K_p^{(i)} = \arg\ \min\ \dot{\hat{\sigma}}_p^{(i)} \\
&\qquad\qquad s.t.\ \hat{x}_p^{(i)} + \dot{\hat{x}}_p^{(i)}\tau = x_p^{(f)} + \dot{x}_p^{(f)}\tau
\end{aligned} \tag{4.29}$$

where $\tau > 0$ is a predefined time constant which delays the convergence of the estimate $\hat{x}_p^{(i)}(t)$ to the fusion data $x_p^{(f)}(t)$ (given in equation (4.27)). This delay results from the transient response of the differential equation $\hat{x}_p^{(i)} + \dot{\hat{x}}_p^{(i)}\tau = x_p^{(f)} + \dot{x}_p^{(f)}\tau$ that is obtained as follows:

$$\hat{x}_p^{(i)}(t) = x_p^{(f)}(t) + \left(\hat{x}_p^{(i)}(0) - x_p^{(f)}(0)\right)\exp(-t/\tau)$$

This delay is required to prevent the propagation of the transient estimation error of a sub-observer to the entire estimation system.

In equation (4.29), for a common state x_p with $\hat{x}_p^{(l)} \in R^{(l)}$ $(\forall l \in \vartheta(p))$, the row vectors $K_p^{(l)}$ $(\forall l \in \vartheta(p))$ are calculated locally and independently for each sub-observer

$SO^{(l)}$ ($\forall l \in \vartheta(p)$) in the "feedback" step. The local and independent calculations are the main advantages of the fusion feedback (FF) optimization problem (4.29) in our proposed CSSOFF procedure which alleviate the stringent communication requirements that exist in the centralized optimization problem goverened by equation (4.25). Moreover, there exists a closed-form solution to the local FF optimization problem given by equation (4.29). This closed-form solution will be obtained in the next section.

4.5.3 Closed-Form Solution to the Fusion Feedback (FF) Optimization Problem

The constrained state sub-observer with fusion feedback (CSSOFF) was introduced and discussed in the previous section, and the fusion feedback (FF) optimization problem was formally defined in (4.29). Considering a common state x_p with $\hat{x}_p^{(i)} \in R^{(i)}$ ($\forall i \in \vartheta(p)$), we start constructing the closed-form solution to the local optimization problem (4.29). Using the equation (4.27), the corresponding optimization constraint is now restated as

$$\hat{x}_p^{(i)} + \dot{\hat{x}}_p^{(i)}\tau = \sum_{l\in\vartheta(p)} \alpha_p^{(l)}\bar{x}_p^{(l)} + \sum_{l\in\vartheta(p)} \alpha_p^{(l)}\dot{\bar{x}}_p^{(l)}\tau$$

or equivalently

$$\dot{\hat{x}}_p^{(i)} = \sum_{l\in\vartheta(p)} \alpha_p^{(l)}\dot{\bar{x}}_p^{(l)} + \sum_{l\in\vartheta(p)} \alpha_p^{(l)}(\bar{x}_p^{(l)} - \hat{x}_p^{(i)})/\tau \tag{4.30}$$

Defining $\underset{x_p}{Row}(M)$ as the x_p-corresponding row of the matrix M, from (4.28) we have

$$\begin{aligned}\underset{x_p}{Row}(\dot{\hat{X}}^{(i)}) = \underset{x_p}{Row}(A^{(i)})\hat{X}^{(i)} + \underset{x_p}{Row}(B^{(i)})U^{(i)} + \underset{x_p}{Row}(K^{(i)})(Y^{(i)} - C^{(i)}\hat{X}^{(i)}) \\ + \sum_{j\in\mathcal{N}(\{i\})} \underset{x_p}{Row}(A^{(ij)})\hat{X}^{(j)}\end{aligned}$$

or equivalently

$$\dot{\hat{x}}_p^{(i)} = A_p^{(i)}\hat{X}^{(i)} + B_p^{(i)}U^{(i)} + K_p^{(i)}(Y^{(i)} - C^{(i)}\hat{X}^{(i)}) + \sum_{j\in\mathcal{N}(\{i\})} A_p^{(ij)}\hat{X}^{(j)} \tag{4.31}$$

where $A_p^{(i)} = \underset{x_p}{Row}(A^{(i)})$, $B_p^{(i)} = \underset{x_p}{Row}(B^{(i)})$, $K_p^{(i)} = \underset{x_p}{Row}(K^{(i)})$, and $A_p^{(ij)} = \underset{x_p}{Row}(A^{(ij)})$. From the equations (4.30) and (4.31) it can be concluded that

$$\sum_{l\in\vartheta(p)} \alpha_p^{(l)}\dot{\bar{x}}_p^{(l)} + \sum_{l\in\vartheta(p)} \alpha_p^{(l)}(\bar{x}_p^{(l)} - \hat{x}_p^{(i)})/\tau = A_p^{(i)}\hat{X}^{(i)} + B_p^{(i)}U^{(i)} + K_p^{(i)}\underbrace{(Y^{(i)} - C^{(i)}\hat{X}^{(i)})}_{\Delta Y^{(i)}} + \sum_{j\in\mathscr{N}(\{i\})} A_p^{(ij)}\hat{X}^{(j)}$$

or equivalently

$$\sum_{l\in\vartheta(p)} \alpha_p^{(l)}\dot{\bar{x}}_p^{(l)} + \sum_{l\in\vartheta(p)} \alpha_p^{(l)}(\bar{x}_p^{(l)} - \hat{x}_p^{(i)})/\tau - A_p^{(i)}\hat{X}^{(i)} - B_p^{(i)}U^{(i)} - \sum_{j\in\mathscr{N}(\{i\})} A_p^{(ij)}\hat{X}^{(j)} \triangleq \underbrace{\Delta x_p^{(i)}}_{x} = \underbrace{K_p^{(i)}}_{K}\underbrace{\Delta Y^{(i)}}_{Y} \tag{4.32}$$

For sake of notational simplicity, we continue with an alternate formulation of $KY = x$ in the right hand side of equation (4.32) as given in the derivations below

$$\underbrace{\begin{bmatrix} k_1 & \cdots & k_n \end{bmatrix}}_{K_{so}}\underbrace{\begin{bmatrix} y_1 & \cdots & y_n \end{bmatrix}^T}_{Y} = x \tag{4.33}$$

We conclude that

$$\begin{aligned} K &= \begin{bmatrix} k_1 & k_2 & \cdots & k_{n-1} & \frac{x-k_1y_1-k_2y_2-\cdots-k_{n-1}y_{n-1}}{y_n} \end{bmatrix} \\ &= \underbrace{\begin{bmatrix} 0 & 0 & \cdots & 0 & x/y_n \end{bmatrix}}_{M} + \underbrace{\begin{bmatrix} k_1 & k_2 & \cdots & k_{n-1} \end{bmatrix}}_{K_{red}} \\ &\times \underbrace{\begin{bmatrix} 1 & 0 & \cdots & 0 & -y_1/y_n \\ 0 & 1 & \cdots & 0 & -y_2/y_n \\ \vdots & \vdots & \ddots & \vdots & \vdots \\ 0 & 0 & \cdots & 1 & -y_{n-1}/y_n \end{bmatrix}}_{N} = M + K_{red}N \end{aligned} \tag{4.34}$$

where K_{red} is the reduced Kalman filter row-vector gain. The problem is now reduced to finding K_{red} such that the cost function of the fusion feedback (FF) optimization problem in (4.29) is minimized. Replacing for $K_p^{(i)} = K$ from (4.34) into (4.31) we have

$$\begin{aligned} \dot{\hat{x}}_p^{(i)} &= A_p^{(i)}\hat{X}^{(i)} + B_p^{(i)}U^{(i)} + K_p^{(i)}(Y^{(i)} - C^{(i)}\hat{X}^{(i)}) + \sum_{j\in\mathscr{N}(\{i\})} A_p^{(ij)}\hat{X}^{(j)} \\ &= A_p^{(i)}\hat{X}^{(i)} + B_p^{(i)}U^{(i)} + (M + K_{red}N)(Y^{(i)} - C^{(i)}\hat{X}^{(i)}) + \sum_{j\in\mathscr{N}(\{i\})} A_p^{(ij)}\hat{X}^{(j)} \\ &= A_p^{(i)}\hat{X}^{(i)} + B_p^{(i)}U^{(i)} + (M + K_{red}N)(C^{(i)}X^{(i)} + V^{(i)} - C^{(i)}\hat{X}^{(i)}) + \sum_{j\in\mathscr{N}(\{i\})} A_p^{(ij)}\hat{X}^{(j)} \end{aligned}$$

Therefore, we have

$$\underbrace{\left(\dot{\hat{x}}_p^{(i)} - \dot{x}_p\right)}_{\dot{\hat{e}}_p^{(i)}} = \left(A_p^{(i)} - (M + K_{red}N)C^{(i)}\right) \underbrace{\left(\hat{X}^{(i)} - X^{(i)}\right)}_{\hat{E}^{(i)}} - W_p^{(i)} + (M + K_{red}N)V^{(i)} + \sum_{j \in \mathcal{N}(\{i\})} A_p^{(ij)} \underbrace{(\hat{X}^{(j)} - X^{(j)})}_{\hat{E}^{(j)}}$$

This is the dynamic equation for the estimation error $\hat{e}_p^{(i)} = \underset{x_p}{Row}\, \hat{E}^{(i)}$, which represents the x_p-corresponding row of the vector $\hat{E}^{(i)}$. Now, we want to develope the variance dynamic equation $\dot{\hat{\sigma}}_p^{(i)} = \mathrm{E}\left\{(\hat{e}_p^{(i)})^2\right\} = \underset{x_p}{Row}\, \underset{x_p}{Col}\, \dot{P}^{(i)}$, which represents the x_p-corresponding diagonal element of the derivative of the matrix $P^{(i)} = \mathrm{E}\left\{\hat{E}^{(i)}(\hat{E}^{(i)})^T\right\}$, as follows

$$\begin{aligned}
\dot{\hat{\sigma}}_p^{(i)} &= \mathrm{E}\left\{\dot{\hat{e}}_p^{(i)}\hat{e}_p^{(i)}\right\} + \mathrm{E}\left\{\hat{e}_p^{(i)}\dot{\hat{e}}_p^{(i)}\right\} \\
&= \left(A_p^{(i)} - (M + K_{red}N)C^{(i)}\right)\mathrm{E}\left\{\hat{E}^{(i)}\hat{e}_p^{(i)}\right\} \\
&+ \mathrm{E}\left\{\hat{e}_p^{(i)}(\hat{E}^{(i)})^T\right\}\left(A_p^{(i)} - (M + K_{red}N)C^{(i)}\right)^T \\
&+ \mathrm{E}\left\{(\mathrm{W}_\mathrm{p}^{(\mathrm{i})})^2\right\} + (M + K_{red}N)\mathrm{E}\left\{V^{(i)}(V^{(i)})^T\right\}(M + K_{red}N)^T \\
&+ \sum_{j \in \mathcal{N}(\{i\})} A_p^{(ij)}\mathrm{E}\left\{\hat{E}^{(j)}\hat{e}_p^{(i)}\right\} + \mathrm{E}\left\{\hat{e}_p^{(i)}(\hat{E}^{(j)})^T\right\}(A_p^{(ij)})^T
\end{aligned}$$

Taking

$$\begin{aligned}
P_p^{(i)} &= \underset{x_p}{Row}(P^{(i)}) = \mathrm{E}\left\{\hat{e}_p^{(i)}(\hat{E}^{(i)})^T\right\} \\
Q_{p,p}^{(i)} &= \underset{x_p}{Row}\, \underset{x_p}{Col}\, \mathrm{E}\left\{\mathrm{W}^{(i)}(W^{(i)})^T\right\} = \mathrm{E}\left\{(\mathrm{W}_\mathrm{p}^{(\mathrm{i})})^2\right\} \\
R^{(i)} &= \mathrm{E}\left\{V^{(i)}(V^{(i)})^T\right\} \\
\hbar_{p,p}^{(i)} &= \underset{x_p}{Row}\, \underset{x_p}{Col}\left(\hbar^{(i)}\right)
\end{aligned}$$

(with $\hbar^{(i)}$ introduced in equation (4.14)) where $\mathrm{E}\{.\}$ denotes the expectation operation and $\underset{x_p}{Col}(M)$ is the only column of matrix M that corresponds to the state x_p, we have

$$\begin{aligned}
\dot{\hat{\sigma}}_p^{(i)} &= (A_p^{(i)} - (M + K_{red}N)C^{(i)})(P_p^{(i)})^T + P_p^{(i)}(A_p^{(i)} - (M + K_{red}N)C^{(i)})^T \\
&+ Q_{p,p}^{(i)} + (M + K_{red}N)R^{(i)}(M + K_{red}N)^T + \hbar_{p,p}^{(i)}
\end{aligned} \tag{4.35}$$

The variance dynamic equation $\dot{\hat{\sigma}}_p^{(i)}$ in equation (4.35) is a convex function of the gain K_{red}. Therefore, in order to minimize $\dot{\hat{\sigma}}_p^{(i)}$ we take its derivative with respect to K_{red} and set it equal to zero. The solution yields

$$K_{red} = \left(P_p^{(i)}(C^{(i)})^T N^T - MR^{(i)}N^T\right)\left(NR^{(i)}N^T\right)^{-1} \tag{4.36}$$

Comparing the optimal Kalman filter gain given in equation (4.26) with the Kalman filter gain K_{so} given in equations (4.34) and (4.36), the later is sub-optimal in the sense that it does not give the optimal solution to the local Kalman filter, but instead it achieves consensus over the constrained state among the local Kalman filters at the cost of sub-optimality. In other words, the Kalman filter gain K_{so} given in equations (4.34) and (4.36) is achieved by deviating from the optimal Kalman filter gain given in equation (4.26), and this deviation may cause instability of the covariance values. In the next section, our proposed Kalman filter gain given in equations (4.34) and (4.36) is modified by imposing an upper bound on its deviation from the optimal Kalman filter gain given in equation (4.26) in order to guarantee the stability of the covariance value $\hat{\sigma}_p^{(i)}$.

4.5.4 Modification of the Kalman Filter Gain to Guarantee Stability

In this section, we modify the Kalman filter gain K_{so} given by equations (4.34) and (4.36) by imposing an upper bound on its deviation from the optimal Kalman filter gain given by equation (4.26) in order to avoid instability (unboundedness) of the covariance value $\hat{\sigma}_p^{(i)}$ in our proposed estimation method. Consider the fusion feedback (FF) optimization problem given in (4.29). From (4.34) and (4.35) we have

$$\begin{aligned}\dot{\hat{\sigma}}_p^{(i)} &= (A_p^{(i)} - K_p^{(i)}C^{(i)})(P_p^{(i)})^T + P_p^{(i)}(A_p^{(i)} - K_p^{(i)}C^{(i)})^T \\ &\quad + Q_{p,p}^{(i)} + K_p^{(i)}R^{(i)}(K_p^{(i)})^T + \hbar_{p,p}^{(i)}\end{aligned}$$

or equivalently

$$\begin{aligned}\dot{\hat{\sigma}}_p^{(i)} &= \underbrace{A_p^{(i)}(P_p^{(i)})^T + P_p^{(i)}(A_p^{(i)})^T + Q_{p,p}^{(i)} + \hbar_{p,p}^{(i)}}_{\Theta} \\ &\quad - \underbrace{K_p^{(i)}}_{K}\underbrace{C^{(i)}P_p^{(i)}}_{0.5\Phi} - \underbrace{P_p^{(i)}(C^{(i)})^T}_{0.5\Phi^T}\underbrace{(K_p^{(i)})^T}_{K^T} + \underbrace{K_p^{(i)}}_{K}\underbrace{R^{(i)}}_{0.5\Psi}\underbrace{(K_p^{(i)})^T}_{K^T} \\ &= \Theta - K\Phi + 0.5K\Psi K^T\end{aligned} \tag{4.37}$$

The variance dynamic equation $\dot{\hat{\sigma}}_p^{(i)}$ given in equation (4.37) is a convex function of the gain K. Using the notation above and equation (4.33), the FF optimization problem (4.29) can be restated as follows:

$$\forall x_p \in \{x_{i_1}, x_{i_2}, ..., x_{i_{n^{(i)}}}\} \text{ “common” },$$
$$\vartheta(p) = \{i, \vartheta_2, ..., \vartheta_\mu\} (\mathrm{n}(\vartheta(p)) = \mu > 2) :$$
$$\forall i \in \vartheta(p) : K_p^{(i)} = \arg \min \left(\dot{\hat{\sigma}}_j^{(m)} = \Theta - K\Phi + 0.5K\Psi K^T \right)$$
$$s.t.\ KY = x$$

The graphical interpretation of the above constrained optimization problem is shown in Figure 4.8. Since the matrix Ψ is positive definite, the equation $\dot{\hat{\sigma}}_j^{(m)} = \Theta - K\Phi + 0.5K\Psi K^T$ represents a hyper-ellipsoid in the hyper-space $K \in R^{m^{(i)}}$ ($m^{(i)}$ is the dimension of $K = K_p^{(i)}$) as shown in Figure 4.8. In this figure, the center point $\bar{K}_p^{(i)} = \Phi^T \Psi^{-1} = P_p^{(i)} (C^{(i)})^T (R^{(i)})^{-1}$ (as in equation (4.26)) is the locally optimum solution that yields the optimum value $\dot{\bar{\sigma}}_p^{(i)}$ and ensures stability of the local filters without fusion feedback.

Once the fusion data is fed back to the local filters, the local values $\dot{\hat{\sigma}}_p^{(i)}$ deviate from the locally optimum value $\dot{\bar{\sigma}}_p^{(i)}$ according to the closed-form solution for the gain $K_{so} = M + K_{red}N$ as given in equations (4.34) and (4.36). This deviation may cause instability (unboundedness) of the covariance value $\hat{\sigma}_p^{(i)}$. In order to guarantee stability (boundedness) of the covariance value $\hat{\sigma}_p^{(i)}$ in our proposed estimation method, in the following we impose an upper bound on the deviation of $\dot{\hat{\sigma}}_p^{(i)}$ from the locally optimum value $\dot{\bar{\sigma}}_p^{(i)}$. This upper bound is centered at $\dot{\bar{\sigma}}_p^{(i)}$ and surrounded by the *boundary hyper-ellipsoid* as follows

$$\Theta - K\Phi + 0.5K\Psi K^T = \ell \dot{\bar{\sigma}}_p^{(i)}|_{\bar{K}_p^{(i)} = \Phi^T \Psi^{-1}} \stackrel{\Delta}{=} \dot{\sigma}_b \ (\ell > 1) \tag{4.38}$$

It should be noted that $\ell = 1$ gives the optimum solution $\dot{\bar{\sigma}}_p^{(i)}$ itself, and so ℓ should be chosen greater than one in order to make the the boundary hyper-ellipsoid given in equation (4.38). This boundary hyper-ellipsoid is shown by the dashed lines in Figure 4.8 and Figure 4.9. Therefore, the solution $K_{so} = M + K_{red}N$ (equations (4.34) and (4.36)), which is the tangent point K_{so} in Figure 4.8, is valid only if the hyper-plane $KY = x$ intersects with the boundary hyper-ellipsoid (4.38) in at least one point, which implies that $\dot{\hat{\sigma}}_p^{(i)}|_{K_{so}} < \ell \dot{\bar{\sigma}}_p^{(i)}$. Otherwise, if no such intersection exists, as shown in Figure 4.9, then we have to search among all the hyper-planes that are parallel to $KY = x$, and find the one which is closest to $KY = x$ and has intersection with the boundary hyper-ellipsoid (4.38). This closest hyper-plane is denoted by the equation $K_{bound,1} Y = x_{b1}$ in Figure 4.9.

The solution $K_{so} = K_{bound}$ is calculated in the case shown in Figure 4.9, in which the hyper-plane $KY = x$ does not have an intersection with the boundary hyper-ellipsoid (4.38). We calculate the two extreme boundary tangent points $K_{bound,i}$ ($i = 1, 2$) in the following manner ($\exists \chi \in R$):

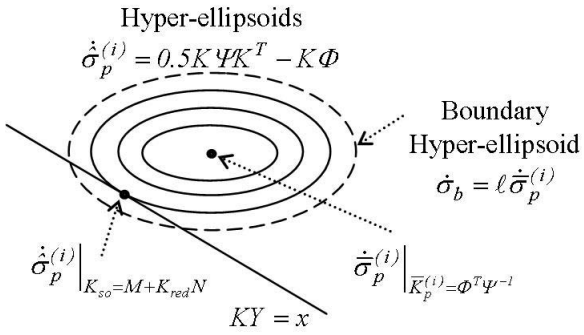

Figure 4.8: Graphical interpretation of the constrained optimization problem (4.29).

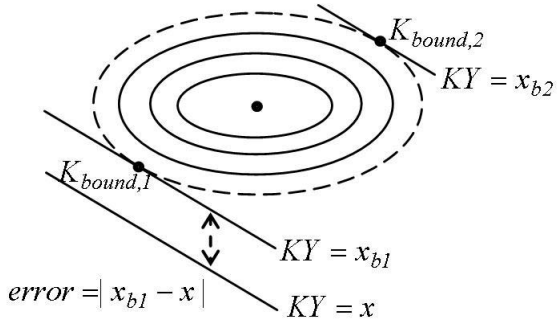

Figure 4.9: Boundary hyper-ellipsoid and the two boundary tangent points.

$$\frac{\partial}{\partial K}(hyper-ellipsoid)\Big|_{K_{bound,i}} = \chi\frac{\partial}{\partial K}(hyper-plane)\Big|_{K_{bound,i}}$$
$$\Rightarrow \quad \frac{\partial}{\partial K}(\Theta - K\Phi + 0.5K\Psi K^T)\Big|_{K_{bound,i}} = \chi\frac{\partial}{\partial K}(KY)\Big|_{K_{bound,i}}$$
$$\Rightarrow \quad \Psi K_{bound,i}^T - \Phi = \chi Y \quad \Rightarrow \quad K_{bound,i}^T = \Psi^{-1}(\chi Y + \Phi)$$

Replacing the matrix $K_{bound,i}^T$ from the equation above into the boundary hyper-ellipsoid (4.38) results in

$$0.25Y^T\Psi^{-1}Y\chi^2 = \sigma_b + 0.25\Phi^T\Psi^{-1}\Phi$$
$$\Rightarrow \quad \chi = \pm\sqrt{\frac{4\sigma_b + \Phi^T\Psi^{-1}\Phi}{Y^T\Psi^{-1}Y}}$$

Therefore, the two boundary tangent points $K_{bound,i}$ $(i = 1, 2)$ are calculated according to

$$K_{bound,i}^T = \Psi^{-1}\left(\pm\sqrt{\frac{\sigma_b + 0.5\Phi^T\Psi^{-1}\Phi}{0.25Y^T\Psi^{-1}Y}}Y + \Phi\right)$$

Finally, the gain $K_{so} = K_{bound}$ is calculated as follows

$$K_{bound} = \arg \min_{\substack{K_{bound}\in \\ \{K_{bound,1},K_{bound,2}\}}} \{|K_{bound,1}Y - x|, |K_{bound,2}Y - x|\} \tag{4.39}$$

From the scenarios shown in Figure 4.8 and Figure 4.9, the gain K_{so} is now designed according to

$$K_{so} = \begin{cases} M + K_{red}\mathrm{N} & \text{if } x_{b,min} < x < x_{b,max} \\ K_{bound} & \text{otherwise} \end{cases} \tag{4.40}$$

where $x_{b,\min} = \min(K_{bound,1}Y, K_{bound,2}Y)$, $x_{b,\max} = \max(K_{bound,1}Y, K_{bound,2}Y)$, the term $M + K_{red}\mathrm{N}$ is taken from equations (4.34) and (4.36), and K_{bound} is taken from equation (4.39).

Remark 4.1. *It should be noted that the results of this chapter are applicable to the formation flights of unmanned vahicles in which all four types of actuator failures including float, LIP, HOF, and LOE [137] exist simultaneously as indicated in equation* (2.5)*. In this situation, by defining the fault status operator* $\mathscr{F}\{.\}$ *as in equation* (2.7)*, the overall fault-augmented state space model of the formation flight system can be formulated as in equation* (2.10)*. This equation is in the form of a general bilinear state space model as in equation* (4.1) *of this chapter. Therefore, all the theories that are developed in this chapter are applicable to the system* (2.10)*, which represents the case*

of all four types of actuator faults present in the formation flight system. However, the acyclic sub-observer dependency (SOD) digraph remains a necessary condition as explained in Theorem 4.2.

To summarize, in this section the stability (boundedness) of the covariance matrix for the case of range-overlapping constrained-state sub-observers (CSSOs) in our cooperative and distributed estimation framework is ensured, and a method is developed that selects the sub-observer Kalman filter gains as provided by equation (4.40) for the range-overlapping CSSOs.

In this chapter, we have proposed a framework in which a set of distributed sub-observers can be selected by a supervisor to cooperatively estimate all the states of a bilinear system, while confining the effects of process dynamics and sensor measurement unreliabilities.

4.6 Conclusions

In this chapter, we extended the proposed cooperative and distributed estimation framework from the previous chapter to the formation flight of unmanned vehicles with relative measurements subject to loss-of-effectiveness (LOE) actuator failures. The fault augmented state space model was shown to be in a bilinear form, which made the design and analysis of the cooperative sub-observers different from those developed in the previous chapter. From the estimation point of view, the bilinear fault-augmented system was expressed in the form of a linear time-varying model, for which a set of sub-observers were designed based on the Kalman filtering technique. A subset of these sub-observers was selected by a supervisor to cooperatively estimate all the fault parameters and states of a formation flight system, while confining the effects of process dynamics and sensor measurement uncertainties/unreliabilities. The ultimate boundedness of the estimation errors was guaranteed by using the concept of acyclic sub-observer dependency (SOD) digraph. Moreover, in case that the ranges of some of the sub-observers were overlapping, namely constrained-state sub-observers (CSSOs), a fusion feedback (FF) procedure was developed to satisfy the constrained-state conditions simultaneously with the time evolution of the Kalman filter equations of the CSSOs.

Chapter 5

Cooperative Actuator Fault Accommodation in Formation Flight of Unmanned Vehicles With Relative Measurements

In some applications of formation flight missions, the objective is to maintain a proper relative positioning among the vehicles. For example, a deep space multiple spacecraft interferometer [2] may require centimeter level relative spacecraft positioning, although the inertial position of the entire formation may drift arbitrarily. Consider the four-vehicle formation with relative measurements, whose digraph is depicted in Figure 2.2. Assume that vehicle #2 is subject to an actuator fault. Furthermore, it is only partially recovered by the low-level fault recovery (LLFR) module due to the presence of possible biased and inaccurate fault estimates. Therefore, vehicle #2 tracks the desired trajectory within an error bound of radius r, which is greater than the error specification e_s that is defined for the mission (that is, $r > e_s$ in Figure 2.2). The main purpose of the formation-level fault recovery (FLFR) module is to demonstrate that by restricting the control effort of vehicle #2, at the expense of higher control efforts from other vehicles, one can reduce the error bound r so that the overall error specifications of the formation mission is guaranteed (that is, r in Figure 2.2).

In this chapter, the main results are presented for the two cases of centralized and decentralized cooperative fault accommodation in formation flight of unmanned vehicles with relative measurements and relative measurement formation (RMF) digraph (as in Definition 2.3).

5.1 Preliminaries

5.1.1 Centralized State Space Model

In this section, we consider the general N-vehicle formation with the relative measurement formation (RMF) digraph $G_{RMF}(V_{RMF}, E_{RMF})$ (as per Definition 2.3), whose special four-vehicle case is depicted in Figure 2.2. For the case of centralized cooperative fault accommodation, the dynamic equations of vehicles $\#i$, $i \in \{1, ..., N\}$ (N is the total number of vehicles) and the relative state measurements are represented by a linear state space model as follows:

$$\begin{aligned} \dot{X}_i &= AX_i + B_iU_i + D_{ext} \quad (i = 1, ..., N) \\ Y_{ij} &= CX_{ij} + V_{ij} = C(X_j - X_i) + V_{ij} \quad (i = 1, ..., N-1\ ,\ j = i+1) \end{aligned} \tag{5.1}$$

where $X_i \in R^n$ and $U_i \in R^r$ are the state and input vectors, respectively, in the local inertial frame, and $Y_{ij} \in R^m$ is the output measurement of the relative state $X_{ij} = X_j - X_i$. The output matrix $C = I_{n\times n}$ ($I_{n\times n}$ is the identity matrix) denotes that the relative state vector is fully measured by the output sensors. The environmental disturbances and measurement noises are represented by $D_{ext} \in R^n$ and $V_{ij} \in R^n$, respectively. The actuators are modeled as ideal gains $B_i \in R^{n\times r}$ which are assumed to have full column rank (the system is not overactuated). The nominal (fault-free) value of B_i is represented by $\bar{B}$. In other words $B_i = \bar{B} + f_i$, where $f_i \in R^{n\times r}$ represents a fault in the actuator B_i. In this regards, the following remark is presented.

Remark 5.1. *In the case of float, hard-over failure (HOF), and lock-in-place (LIP) actuator failures (as per equation* (2.5)*), the failure is modeled by* $B_iU_i = \bar{B}\Pi_i$ *(as per equation* (2.9)*), where* $\bar{B}\Pi_i$ *is a constant scalar or matrix. Consequently, there is a loss of controllability that prevents any controller from actuating the system, unless the trivial recovery solution of a redundant actuator is available. Therefore, our fault accommodation method will be mainly focused on the loss-of-effectiveness (LOE) actuator failure (as per equation* (2.5)*).*

In equation (5.1), the relative measurements are made between the consecutive vehicles. Even if in practice the measurements are made between the neighboring vehicles, they can be transformed by using a linear transformation matrix into the relative measurements between the consecutive vehicles due to the centralized availability of the sensor information.

5.1.2 Decentralized State Space Model

For the case of decentralized cooperative fault accommodation in an N-vehicle formation with the relative measurement formation (RMF) digraph $G_{RMF}(V_{RMF}, E_{RMF})$ (as per Definition 2.3), the dynamic equations of vehicles $\#i$, $i \in \{1, ..., N\}$ (N is the total number of vehicles) and the relative state measurements are represented by a linear state space model as follows:

$$\begin{aligned} &\dot{X}_i = AX_i + B_iU_i + D_{ext} \quad (i = 1, ..., N) \\ &Y_{ij} = CX_{ij} + V_{ij} = C(X_j - X_i) + V_{ij} \quad (j = 1, ..., N \ ; \ e_{ij} \in E_{RMF}) \end{aligned} \tag{5.2}$$

where $e_{ij} \in E_{RMF}$ (as per Definition 2.3) is equivalent to $i \in \mathcal{N}(\{j\})$ or $j \in \mathcal{N}(\{i\})$ (as per Definition 2.4). For simplicity, the following analysis ignores the effects of the environmental disturbances D_{ext}. However, these effects are subsequently analyzed and taken into account later in this chapter.

5.2 Centralized Cooperative Actuator Fault Accommodation

The dashed edges in Figure 2.2 represent the system output measurements, based on which a linear controller is designed. In the general case of equation (5.1), in order to avoid output redundancy the output measurements are made between the vehicles $\#i$ and $\#j$, for $i = 1, ..., N-1$ and $j = i+1$ (e.g. the three outputs corresponding to the three dashed edges for the special case of the four-vehicle formation in Figure 2.2). This makes the relative measurement formation (RMF) digraph (as shown in Figure 2.2) a connected tree. For each dashed edge, the corresponding desired relative state and relative error dynamics are obtained as

$$\begin{aligned} &\dot{X}^d_{ij} = AX^d_{ij} + \bar{B}U^d_{ij} \\ &\dot{E}^d_{ij} = AE^d_{ij} - B_iU_i + B_jU_j - \bar{B}U^d_{ij} \end{aligned} \tag{5.3}$$

where $X_{ij} = X_j - X_i$ and $E_{ij} = X_{ij} - X^d_{ij}$ are the relative state and relative error between the vehicles $\#i$ and $\#j$, respectively, and X^d_{ij} and U^d_{ij} are the desired relative state and desired input vectors, respectively. In the compact matrix form the overall error dynamics can be expressed as (by neglecting the environmental disturbances D_{ext})

$$\underbrace{\begin{bmatrix} \dot{E}_{12} \\ \dot{E}_{23} \\ \vdots \\ \dot{E}_{(N-1)N} \end{bmatrix}}_{\dot{E}} = \underbrace{\begin{bmatrix} A & 0_{n\times n} & \cdots & 0_{n\times n} \\ 0_{n\times n} & A & \cdots & 0_{n\times n} \\ \vdots & \vdots & \ddots & \vdots \\ 0_{n\times n} & 0_{n\times n} & \cdots & A \end{bmatrix}}_{A_T} \underbrace{\begin{bmatrix} E_{12} \\ E_{23} \\ \vdots \\ E_{(N-1)N} \end{bmatrix}}_{\dot{E}}$$

$$+ \underbrace{\begin{bmatrix} -B_1 & B_2 & 0_{n\times r} & \cdots & 0_{n\times r} & 0_{n\times r} \\ 0_{n\times r} & -B_2 & B_3 & \cdots & 0_{n\times r} & 0_{n\times r} \\ \vdots & \vdots & \vdots & \ddots & \vdots & \vdots \\ 0_{n\times r} & 0_{n\times r} & 0_{n\times r} & \cdots & -B_{N-1} & B_N \end{bmatrix}}_{J(B_1,\ldots,B_N)} \underbrace{\begin{bmatrix} U_1 \\ U_2 \\ U_3 \\ \vdots \\ U_{N-1} \\ U_N \end{bmatrix}}_{U} \tag{5.4}$$

$$- \underbrace{\begin{bmatrix} \bar{B} & 0_{n\times r} & \cdots & 0_{n\times r} \\ 0_{n\times r} & \bar{B} & \cdots & 0_{n\times r} \\ \vdots & \vdots & \ddots & \vdots \\ 0_{n\times r} & 0_{n\times r} & \cdots & \bar{B} \end{bmatrix}}_{\bar{B}_T} \underbrace{\begin{bmatrix} U_{12}^d \\ U_{23}^d \\ \vdots \\ U_{(N-1)N}^d \end{bmatrix}}_{U^d}$$

Therefore, the control laws that utilize the error vectors E_{ij} are derived based on

$$\begin{bmatrix} -B_i & B_j \end{bmatrix} \begin{bmatrix} U_i \\ U_j \end{bmatrix} = \bar{B}U_{ij}^d + \bar{B}KE_{ij} \triangleq P_{ij}(t) \tag{5.5}$$

that when applied to equation (5.4) result in the closed-loop characteristic polynomials $\det(sI - A + \bar{B}K) = 0$ for the error dynamics E_{ij}, where $\det(.)$ represents the determinant of a matrix. Therefore, controllability of the pair (A, B) is a necessary and sufficient condition for feasibility of a stabilizing controller. Moreover, it is necessary that $Columns(B_i) \subset span\left(Columns(\bar{B})\right)$, where $Columns(.)$ represents the set of all column vectors of a matrix, in order for the equality (5.5) above to be valid. In other words, there exists an invertible transformation matrix $(I_{r_0\times r_0} + \prod_i)$ such that $B_i = \bar{B}(I_{r_0\times r_0} + \prod_i)$ as in equation (5.2).

By choosing the proper feedback gain K, one can ensure that the closed-loop error dynamics is asymptotically stable. In the matrix form the control laws (5.5) corresponding to the relative measurements (e.g. the three dashed edges for the special case of the four-vehicle formation shown in Figure 2.2) are given as follows

$$JU = P(t) \tag{5.6}$$

where $P(t) = \begin{bmatrix} P_{12}^T(t) & P_{23}^T(t) & \cdots & P_{(N-1)N}^T(t) \end{bmatrix}^T$. The above equation is used in our following discussions to design control laws for the vehicles in the formation.

In the subsequent sections, the focus is on the loss-of-effectiveness (LOE) actuator failure (as per equation (5.2)). If the vehicle $\#i$ is subject to one of the other three types of actuator failures, namely float, lock-in-place (LIP), and hard-over failure (HOF) (as per equation (5.2)), then the following control command can be designed based on the model $B_i U_i = \bar{B}\Pi_i$ from equation (2.9) to recover the fault:

$$U = \underbrace{\begin{bmatrix} J \\ \mathrm{J}^0 \end{bmatrix}_{left}^{-1}}_{\tilde{J}_{left}^{-1}} \times \begin{bmatrix} P(t) \\ \bar{B}\Pi_i \end{bmatrix} \tag{5.7}$$

where $M_{left}^{-1} = (M^T M)^{-1} M^T$ is the left inverse of the matrix M, and

$$\mathrm{J}^0 = \underbrace{\begin{bmatrix} 0_{n\times r} & \cdots & 0_{n\times r} & B_i & 0_{n\times r} & \cdots & 0_{n\times r} \end{bmatrix}}_{\substack{\text{only the } i^{th} \text{ block is nonzero} \\ \text{out of the } N \text{ blocks}}}$$

$$rank\left(\tilde{J}\right) = rank\left(\begin{bmatrix} J \\ \mathrm{J}^0 \end{bmatrix}_{Nn\times Nr}\right) = Nr$$

The matrix $\tilde{J}$ has full column rank since the matrices B_i, $i = 1, ..., N$, which constitute the columns of the matrix $\tilde{J}$, are assumed to have full column ranks (this assumption was made earlier for equation (5.1)). Therefore, the left inverse $\tilde{J}_{left}^{-1}$ exists in equation (5.7). By applying the control command (5.7) to the error dynamics in equation (5.4), the relative error dynamics in equation (5.3) maintains the closed-loop characteristic polynomials $\det(sI - A + \bar{B}K) = 0$ for each of the relative error dynamics E_{ij}. However, since the faulty vehicle $\#i$ has a constant level of actuation $B_i U_i = \bar{B}\Pi_i$ as in equation (2.9), there is a loss of control energy as compared to the fault free scenario.

In the following sections, the problem of fault recovery for a loss-of-effectiveness (LOE) actuator failure (as given in equation (5.2)) will be investigated.

5.2.1 Centralized Low-Level Fault Recovery (LLFR) Controller

In this section, we assume that the system is fault free or one has an accurate fault estimate. In the later, we assume that the actuators of vehicle $\#i$ are subject to loss-of-effectiveness (LOE) failures as given in equation (5.2), that is $B_i = \bar{B} + f_i$. The estimates of the actuator faults f_i that are provided by the fault identification filter or module are represented by $\hat{f}_i$. Therefore, the estimates of the faulty actuator gains are represented

by $\hat{B}_i = \bar{B} + \hat{f}_i$. We assume that the estimates of faulty actuator gains are unbiased, that is $\hat{f}_i = f_i$ or $\hat{B}_i = B_i$. These unbiased estimates are used in the LLFR controller.

Replacing for $P_{ij}(t)$ from equation (5.5) into (5.4), each subsystem becomes in the following form

$$\begin{cases} \dot{E}_{ij} = (A + \bar{B}K)E_{ij} + D_{ext} \\ Y_{ij} = E_{ij} \end{cases} \tag{5.8}$$

The following lemma is used to design an H_∞ optimal state feedback matrix K that is used in equations (5.5) and (5.6) in order to minimize the effects of the disturbances on the tracking errors.

Lemma 5.1. *Consider the system governed by equation* (5.8) *with the initial state* $E_{ij}(0)$. *The state feedback matrix* $K = YX^{-1}$ *stabilizes the system and minimizes* $\gamma_1 + \gamma_2$, *where* γ_1 *is an upper bound on the* H_∞ *norm of the transfer function from the disturbance to the output of the system and* γ_2 *is an upper bound on the linear quadratic cost function* $J_{LQR}(KE_{ij}, Q, R)$ *in Lemma 2.3, if and only if there exist a matrix* Y *and a positive definite matrix* $X > 0$ *that satisfy the following optimization problem*

$$\begin{aligned} &Minimize \quad \gamma_1 + \gamma_2 \\ &subject\ to \\ &X > 0 \\ &\begin{bmatrix} AX + XA^T + \bar{B}Y + Y^T\bar{B}^T & I & X \\ I & -\gamma_1 I & 0 \\ X & 0 & -\gamma_1 I \end{bmatrix} < 0 \\ &\begin{bmatrix} AX + XA^T + \bar{B}Y + Y^T\bar{B}^T & X & Y^T \\ X & -Q^{-1} & 0 \\ Y & 0 & -R^{-1} \end{bmatrix} \leq 0 \\ &\begin{bmatrix} \gamma_2 & E_{ij}^T(0) \\ E_{ij}(0) & X \end{bmatrix} \geq 0 \end{aligned}$$

Proof: *Follows from the results in [136] and [134], and those in Lemmas 2.2 and 2.3.* ■

Now that the state feedback matrix K is designed in Lemma 5.1, one has an infinite number of solutions for determining the control signal U in equation (5.6). Therefore, a significant degree of freedom is available to the LLFR module to choose the control law. We take advantage of this flexibility to optimize the fuel consumption across the formation. The following cost function is considered in the constrained optimization problem

$$\underset{U_i \in R^r}{Minimize} \quad \sum_{i=1}^{N} \frac{\alpha_i}{2} U_i^T U_i \quad \text{subject to (5.6)} \tag{5.9}$$

where the positive scalar coefficients $\alpha_i > 0$, $i = 1, ..., N$ are the respective control effort weights or gains. The solution to the above minimization problem is obtained by using the Lagrange multiplier method as follows:

$$U = \begin{bmatrix} -\hat{B}_1 & \hat{B}_2 & 0_{n\times r} & \cdots & 0_{n\times r} & 0_{n\times r} \\ 0_{n\times r} & -\hat{B}_2 & \hat{B}_3 & \cdots & 0_{n\times r} & 0_{n\times r} \\ \vdots & \vdots & \vdots & \cdots & \vdots & \vdots \\ 0_{n\times r} & 0_{n\times r} & 0_{n\times r} & \ddots & -\hat{B}_{N-1} & \hat{B}_N \\ (\hat{B}_1^{\mathrm{T}})^{-1}_{right}\alpha_1 & (\hat{B}_2^{\mathrm{T}})^{-1}_{right}\alpha_2 & (\hat{B}_3^{\mathrm{T}})^{-1}_{right}\alpha_3 & \cdots & (\hat{B}_{N-1}^{\mathrm{T}})^{-1}_{right}\alpha_{N-1} & (\hat{B}_N^{\mathrm{T}})^{-1}_{right}\alpha_N \end{bmatrix}^{-1}_{left} \tag{5.10}$$

$$\times \begin{bmatrix} P_{12}(t) \\ P_{23}(t) \\ P_{34}(t) \\ \vdots \\ P_{(N-1)N}(t) \\ 0_{r\times 1} \end{bmatrix} = \hat{J}(\hat{B}_1, ..., \hat{B}_N)^{-1}_{left} \begin{bmatrix} P_{12}(t) \\ P_{23}(t) \\ P_{34}(t) \\ \vdots \\ P_{(N-1)N}(t) \\ 0_{r\times 1} \end{bmatrix}$$

where $M^{-1}_{left} = (M^T M)^{-1} M^T$ and $M^{-1}_{right} = M^T (M M^T)^{-1}$ are the left and right inverses of the matrix M, respectively, and $\hat{B}_i$, $i = 1, ..., N$ represents the estimate of the faulty actuator gain B_i, which is determined from the fault severity estimator following the detection process of the actuator fault. Note that $\hat{B}_i = B_i$ implies that the actuator is fault free or that one has an accurate estimate of the fault. Under this situation by substituting equation (5.10) into equation (5.4), one gets $\dot{E}_{ij} = (A + \bar{B}K)E_{ij}$, for $i = 1, ..., N-1$ and $j = i + 1$.

In the absence of any environmental disturbances and modeling uncertainties, the above error dynamics shows that asymptotic stability of the closed-loop system is achieved by the LLFR controller if the fault is accurately estimated (that is $\hat{f}_i = f_i$ or $\hat{B}_i = B_i$). However, when one makes an inaccurate estimate of the fault (that is $\hat{f}_i \neq f_i$ or $\hat{B}_i \neq B_i$), asymptotic stability of the error dynamics is no longer achieved. In this case, instead an ultimate boundedness of the closed-loop system can be guaranteed. These results are discussed next, where the FLFR module is qualitatively and quantitatively introduced to handle and compensate for any possible violation of the overall mission error specifications.

5.2.2 Centralized Formation-Level Fault Recovery (FLFR) Module

To illustrate the main idea behind the FLFR module, let us consider the case of a partially LL-recovered vehicle $\#k$ due to the biased estimate of its actuator fault, that is, assume that $\hat{f}_k \neq f_k$ ($\hat{B}_k \neq B_k$) or $\hat{f}_k = f_k + \varepsilon_k$ (or $\hat{B}_k = B_k + \varepsilon_k$), where ε_k is an unknown function but bounded (that is $||\varepsilon_k|| < B_{\varepsilon_k}$ with B_{ε_k} known). The closed-loop system becomes

$$\dot{E} = (A_T + \bar{B}_T K_T)E + D\Big[\ P_{12}^T(t) \quad P_{23}^T(t) \quad \cdots \quad P_{(N-1)N}^T(t) \quad 0_{1\times r}\ \Big]^T \tag{5.11}$$

where

$$\begin{aligned} &\bar{B}_T = diag(\bar{B})_{i=1}^{N-1}\ ,\ K_T = diag(K)_{i=1}^{N-1} \\ &D = \underbrace{\Big(J(B_1,...,B_k,...,B_N) - J(B_1,...,\hat{B}_k,...,B_N)\Big)}_{D^0}\hat{J}(B_1,...,\hat{B}_k,...,B_N)_{left}^{-1} \end{aligned} \tag{5.12}$$

The matrix D has the following structure

$$D^0_{[i,j]_{n\times r}} = \begin{cases} -\varepsilon_k & \text{if } j = k \text{ and } i = k-1 \geq 1 \\ \varepsilon_k & \text{if } j = k \text{ and } i = k \leq N-1 \\ 0_{n\times r} & \text{otherwise} \end{cases} \tag{5.13}$$

It should be noted that for a formation of N vehicles, there are totally $N-1$ relative state dynamics. For example, for the special case of the four-vehicle formation in Figure 2.2, we have

$$\bar{B}_T = \begin{bmatrix} \bar{B} & 0_{n\times r} & 0_{n\times r} \\ 0_{n\times r} & \bar{B} & 0_{n\times r} \\ 0_{n\times r} & 0_{n\times r} & \bar{B} \end{bmatrix}\ ,\ K_T = \begin{bmatrix} K & 0_{r\times n} & 0_{r\times n} \\ 0_{r\times n} & K & 0_{r\times n} \\ 0_{r\times n} & 0_{r\times n} & K \end{bmatrix}$$

$$D^0 = \begin{bmatrix} 0_{n\times r} & -\varepsilon_2 & 0_{n\times r} & 0_{n\times r} \\ 0_{n\times r} & +\varepsilon_2 & 0_{n\times r} & 0_{n\times r} \\ 0_{n\times r} & 0_{n\times r} & 0_{n\times r} & 0_{n\times r} \end{bmatrix}$$

Therefore, the matrix D in equation (5.12) has the following structure

$$D_{B^{n\times r}[i,:]} = \begin{cases} \Big[\ d_1 \quad \cdots \quad d_N\ \Big] & \text{if } i = k-1 \geq 1 \\ -\Big[\ d_1 \quad \cdots \quad d_N\ \Big] & \text{if } i = k \leq N-1 \\ \Big[\ 0 \quad \cdots \quad 0\ \Big] & \text{otherwise} \end{cases} \tag{5.14}$$

where $d_1, ..., d_N \in R^{n\times r}$ are the nonzero blocks of the matrix D. In comparison with the closed loop of the system (5.4) and the controller (5.6), the presence of the term D in equation (5.11) (due to an inaccurate fault estimate) does impact and loosen the asymptotic stability of the closed-loop system. Equation (5.11) consists of two perturbed subsystems ($E_{(k-1)k}$ and $E_{k(k+1)}$), and the remainder subsystems $E_{i(i+1)}$ (for $i \neq k-1$

and $i \neq k$) are asymptotically stable. Therefore, we will only concentrate on analysis of the perturbed subsystems.

The dynamics of the perturbed subsystems $E_{(k-1)k}$ and $E_{k(k+1)}$ can be expressed as

$$\begin{aligned} \dot{E}_{\{k\}}(t) &= A_{clp}E_{\{k\}}(t) + D_{\{k\}}(t) \\ A_{clp} &= A_{\{k\}} + (I_{2n\times 2n} + \Delta)\bar{B}_{\{k\}}K_{\{k\}} \end{aligned} \tag{5.15}$$

where

$$E_{\{k\}} = \begin{bmatrix} E_{(k-1)k} \\ E_{k(k+1)} \end{bmatrix},\ D_{\{k\}} = \begin{bmatrix} d_1 & \cdots & d_{N-1} \\ -d_1 & \cdots & -d_{N-1} \end{bmatrix} B_T U^d$$

$$A_{\{k\}} = \begin{bmatrix} A & 0 \\ 0 & A \end{bmatrix},\ \bar{B}_{\{k\}} = \begin{bmatrix} \bar{B} & 0 \\ 0 & \bar{B} \end{bmatrix}$$

$$K_{\{k\}} = \begin{bmatrix} K & 0 \\ 0 & K \end{bmatrix},\ \Delta = \begin{bmatrix} d_{k-1} & d_k \\ -d_{k-1} & -d_k \end{bmatrix}$$

We are now in a position to state our first result of this subsection.

Lemma 5.2. *Assume that the positive parameters α_i, $i = 1, ..., N$ in the cost function* (5.9) *are lower bounded by a positive value, namely $\alpha_i \geq 1$, and that the matrix $\hat{J}(\hat{B}_1, ..., \hat{B}_N)$ in equation* (5.10) *is invertible (or $\hat{J}(\hat{B}_1, ..., \hat{B}_N)^{-1}_{left}$ exists) for all values of the parameters $\alpha_i \geq 1$, $i = 1, ..., N$. Assume that the faulty vehicle #k is partially recovered by the LLFR module by using the biased estimate of the actuator gain $\hat{B}_k \neq B_k$. The norm of the matrix D in equation* (5.12) *is upper bounded by a monotonically decreasing function of the coefficient α_k. Therefore, to maximally reduce the norm and effects of D on the error dynamics* (5.11) *the coefficient α_k in the cost function* (5.9) *should be selected sufficiently large.*

Proof: *Equations* (5.12) *and* (5.13) *can be used to calculate the disturbance term D as follows*

$$D = \varepsilon_k I^0 \begin{bmatrix} (\hat{J}^{-1}_{left})_{[k,1]_{r\times n}} & (\hat{J}^{-1}_{left})_{[k,2]_{r\times n}} & \cdots & (\hat{J}^{-1}_{left})_{[k,N]_{r\times n}} \end{bmatrix} \triangleq \varepsilon_k I^0 (\hat{J}^{-1}_{left})_{[k,:]_r}$$

where

$$I^0_{[i]_r} = \begin{cases} I_{r\times r} & \text{if } i = k-1 \geq 1 \\ -I_{r\times r} & \text{if } i = k \leq N-1 \\ 0_{r\times r} & \text{otherwise} \end{cases}$$

and the indices $[i]_a$, $[i,j]_{a\times b}$, and $[i,:]_a$ are defined in Definition 2.8. We have

$$\begin{bmatrix} (\hat{J}^{-1}_{left})_{[k,1]_{r\times n}} & \cdots & (\hat{J}^{-1}_{left})_{[k,k-1]_{r\times n}} & (\hat{J}^{-1}_{left})_{[k,k]_{r\times n}} & (\hat{J}^{-1}_{left})_{[k,k+1]_{r\times n}} & \cdots & (\hat{J}^{-1}_{left})_{[k,N]_{r\times n}} \end{bmatrix}$$

$$\times \begin{bmatrix} J_{[1,1]_{n\times r}} & \cdots & J_{[1,k-1]_{n\times r}} & J_{[1,k]_{n\times r}} & J_{[1,k+1]_{n\times r}} & \cdots & J_{[1,N]_{n\times r}} \\ \vdots & \ddots & \vdots & \vdots & \vdots & \iddots & \vdots \\ J_{[k-1,1]_{n\times r}} & \cdots & J_{[k-1,k-1]_{n\times r}} & J_{[k-1,k]_{n\times r}} & J_{[k-1,k+1]_{n\times r}} & \cdots & J_{[k-1,N]_{n\times r}} \\ J_{[k,1]_{n\times r}} & \cdots & J_{[k,k-1]_{n\times r}} & J_{[k,k]_{n\times r}} & J_{[k,k+1]_{n\times r}} & \cdots & J_{[k,N]_{n\times r}} \\ J_{[k+1,1]_{n\times r}} & \cdots & J_{[k+1,k-1]_{n\times r}} & J_{[k+1,k]_{n\times r}} & J_{[k+1,k+1]_{n\times r}} & \cdots & J_{[k+1,N]_{n\times r}} \\ \vdots & \ddots & \vdots & \vdots & \vdots & \iddots & \vdots \\ J_{[N,1]_{n\times r}} & \cdots & J_{[N,k-1]_{n\times r}} & J_{[N,k]_{n\times r}} & J_{[N,k+1]_{n\times r}} & \cdots & J_{[N,N]_{n\times r}} \end{bmatrix}$$

$$= \underbrace{\begin{bmatrix} 0_{r\times r} & \cdots & 0_{r\times r} & I_{r\times r} & 0_{r\times r} & \cdots & 0_{r\times r} \end{bmatrix}}_{\substack{only\ k^{th}\ block\ is\ identity \\ out\ of\ the\ N\ blocks}}$$

The above equation can be rewritten as

$$\begin{bmatrix} (\hat{J}^{-1}_{left})_{[k,-N]_{r\times n}} & (\hat{J}^{-1}_{left})_{[k,N]_{r\times n}} \end{bmatrix} \times \begin{bmatrix} J_{11} & J_{1k} \\ J_{k1} & (\hat{B}^T_k)^{-1}_{right}\alpha_k \end{bmatrix} = \begin{bmatrix} 0_{r\times(N-1)r} & I_{r\times r} \end{bmatrix}$$

where

$$J_{11} = \begin{bmatrix} J_{[1,1]_{n\times r}} & \cdots & J_{[1,k-1]_{n\times r}} & J_{[1,k+1]_{n\times r}} & \cdots & J_{[1,N]_{n\times r}} \\ \vdots & \ddots & \vdots & \vdots & \ddots & \vdots \\ J_{[N-1,1]_{n\times r}} & \cdots & J_{[N-1,k-1]_{n\times r}} & J_{[N-1,k+1]_{n\times r}} & \cdots & J_{[N-1,N]_{n\times r}} \end{bmatrix}$$

$$J_{1k} = \begin{bmatrix} J_{[1,k]_{n\times r}} \\ \vdots \\ J_{[N-1,k]_{n\times r}} \end{bmatrix}$$

$$J_{k1} = \begin{bmatrix} J_{[N,1]_{n\times r}} & \cdots & J_{[N,k-1]_{n\times r}} & J_{[N,k+1]_{n\times r}} & \cdots & J_{[N,N]_{n\times r}} \end{bmatrix}$$

$$(\hat{J}^{-1}_{left})_{[k,-N]_{r\times n}} = \begin{bmatrix} (\hat{J}^{-1}_{left})_{[k,1]_{r\times n}} & \cdots & (\hat{J}^{-1}_{left})_{[k,N-1]_{r\times n}} \end{bmatrix}$$

The solution is

$$(\hat{J}^{-1}_{left})_{[k,N]_{r\times n}} = \left((\hat{B}^T_k)^{-1}_{right}\alpha_k - J_{k1}(J_{11})^{-1}_{left}J_{1k}\right)^{-1}_{left}$$

$$(\hat{J}^{-1}_{left})_{[k,-N]_{r\times n}} = -\left((\hat{B}^T_k)^{-1}_{right}\alpha_k - J_{k1}(J_{11})^{-1}_{left}J_{1k}\right)^{-1}_{left} J_{k1}(J_{11})^{-1}_{left}$$

or equivalently,

$$(\hat{J}_{left}^{-1})_{[k,:]_r} = \left[\begin{array}{cc} (\hat{J}_{left}^{-1})_{[k,-N]_{r\times n}} & (\hat{J}_{left}^{-1})_{[k,N]_{r\times n}} \end{array} \right]$$

$$= \left((\hat{B}_k^T)_{right}^{-1}\alpha_k - J_{k1}(J_{11})_{left}^{-1}J_{1k}\right)_{left}^{-1} \left[\begin{array}{cc} -J_{k1}(J_{11})_{left}^{-1} & I_{n\times n} \end{array} \right]$$

Therefore, by factoring out the parameter α_k we have

$$||D|| = \left\| \varepsilon_k I^0 (\hat{J}_{left}^{-1})_{[k,:]_r} \right\|$$

$$\leq \frac{||\varepsilon_k||}{\alpha_k} \sup_{\alpha_k \geq 1} \left\| I^0 \left((\hat{B}_k^T)_{right}^{-1} - J_{k1}(J_{11})_{left}^{-1}J_{1k}/\alpha_k \right)_{left}^{-1} \left[\begin{array}{cc} -J_{k1}(J_{11})_{left}^{-1} & I_{n\times n} \end{array} \right] \right\|$$

This implies that the matrix D is upper bounded by a monotonically decreasing function of α_k, which completes the proof. ■

We are now in a position to state our main results in the following two theorems.

Theorem 5.1. *To stabilize the nominal (disturbance free) error dynamics system $\dot{E}_{\{k\}}(t) = [A_{\{k\}} + (I_{2n\times 2n} + \Delta)\bar{B}_{\{k\}}K_{\{k\}}]E_{\{k\}}(t)$ in equation (5.15), the FLFR module should choose a sufficiently large coefficient α_k in the cost function (5.9) corresponding to the partially LL-recovered vehicle #k by using the biased actuator gain estimate $\hat{B}_k \neq B_k$.*

Proof: *We rearrange the nominal error dynamic system $\dot{E}_{\{k\}} = (A_{\{k\}} + (I_{2n\times 2n} + \Delta)\bar{B}_{\{k\}}K_{\{k\}})E_{\{k\}}$ (note that $A_{\{k\}} + \bar{B}_{\{k\}}K_{\{k\}}$ is Hurwitz) into an equivalent closed-loop configuration of the system S and the controller CON as follows:*

$$S : \left\{ \begin{array}{l} \dot{E}_{\{k\}} = (A_{\{k\}} + \bar{B}_{\{k\}}K_{\{k\}})E_{\{k\}} + U \\ Y = B_{\{k\}}K_{\{k\}}E_{\{k\}} \end{array} \right. , \; CON : U = \Delta Y$$

where the system S is controllable and observable allowing a proper choice of $K_{\{k\}} = diag(K, K)$. Let us take

$$\gamma_1 = \sup_{\omega \in R} \sigma_{\max}[S(j\omega)]$$

where $\sigma_{\max}$ denotes the maximum singular value of a complex matrix, and where γ_1 is finite since $S(j\omega)$ is Hurwitz. Taking $||\Delta||_\infty \leq \gamma_2$, it then follows readily that the controller CON satisfies $||U||_\infty \leq \gamma_2||Y||_\infty$.

According to the small-gain theorem [159], a sufficient condition for stability of the overall closed-loop system is $\gamma_1\gamma_2 < 1$. Taking $B_\Delta = 1/\gamma_1$, this condition becomes $||\Delta||_\infty < B_\Delta$, which is equivalent to appropriately decreasing $||\Delta||_\infty$, or alternatively,

appropriately decreasing $||D||_\infty$. The latter can be achieved by using Lemma 5.2 where the coefficient α_k is selected to be sufficiently large. ■

Theorem 5.2. *Let the nominal error dynamics system $\dot{E}_{\{k\}}(t) = [A_{\{k\}} + (I_{2n\times 2n} + \Delta)\bar{B}_{\{k\}}K_{\{k\}}]E_{\{k\}}(t)$ in equation (5.15) be stable according to Theorem 5.1. The norm of $E_{\{k\}}(t)$ is upper bounded by a monotonically decreasing function of the coefficient α_k in the cost function (5.9). Therefore, in order to make the norm of the tracking error $E_{\{k\}}$ smaller than the predefined specification given by e_s, the FLFR module should select a sufficiently large coefficient α_k in the cost function (5.9) corresponding to the partially LL-recovered vehicle #k by using the biased actuator gain estimate $\hat{B}_k \neq B_k$.*

Proof: *The Laplace transform of the error state $E_{\{k\}}$ governed by the dynamical system $\dot{E}_{\{k\}}(t) = A_{clp}E_{\{k\}}(t) + D_{\{k\}}$, is given by*

$$E_{\{k\}}(s) = (sI_{2n\times 2n} - A_{clp})^{-1}D_{\{k\}}(s) = G(s)D_{\{k\}}(s)$$

where $G(s)$ is the system transfer function matrix. Using the definition of $D_{\{k\}}(t)$ in (5.15), and d_i ($i = 1, ..., N-1$) from equation (5.12) and Lemma 5.2, we have

$$E_{\{k\}}(s) = G(s)\varepsilon_k \begin{bmatrix} -I_{r\times r} \\ I_{r\times r} \end{bmatrix} \left((\hat{B}_k^T)_{right}^{-1}\alpha_k - J_{k1}(J_{11})_{left}^{-1}J_{1k}\right)_{left}^{-1}$$

$$\times \begin{bmatrix} -J_{k1}(J_{11})_{left}^{-1} & I_{n\times n} \end{bmatrix} \begin{bmatrix} I_{(N-1)n\times(N-1)n} \\ 0_{n\times(N-1)n} \end{bmatrix} B_T\mathscr{L}\{U^d(t)\}$$

where $\mathscr{L}\{.\}$ denotes the Laplace transform of a given signal. Let us define

$$H \triangleq \sup_{\substack{t\in R^+ \\ |\varepsilon_k|<B_{\varepsilon_k} \\ \alpha_k\geq 1}} \int_{\tau=0}^{t} \left\{ \|G(t-\tau)\| \left\| \begin{bmatrix} -I_{r\times r} \\ I_{r\times r} \end{bmatrix} \left((\hat{B}_k^T)_{right}^{-1} - J_{k1}(J_{11})_{left}^{-1}J_{1k}/\alpha_k\right)^{-1} \right. \right. \tag{5.16}$$

$$\left. \left. \times \begin{bmatrix} -J_{k1}(J_{11})_{left}^{-1} & I_{n\times n} \end{bmatrix} \begin{bmatrix} I_{(N-1)n\times(N-1)n} \\ 0_{n\times(N-1)n} \end{bmatrix} B_T U^d(\tau) \right\| \right\} d\tau$$

We now can express the tracking error $E_{\{k\}}$ in the time domain as follows

$$||E_{\{k\}}(t)|| \leq \frac{||\varepsilon_k||H}{\alpha_k} \triangleq B_{E_{\{k\}}} \tag{5.17}$$

It follows that $||E_{\{k\}}(t)||$ is bounded by a monotonically decreasing function of the parameter $\alpha_k \geq 1$. In order for the norm of the tracking error $E_{\{k\}}$ be smaller than the specification e_s, a solution based on equation (5.17) can be obtained as follows

$$\frac{\max||\varepsilon_k||H}{\alpha_k} \leq e_s$$

Therefore, in the absence of any disturbances the desired domain for the parameter α_k *is given by*

$$\alpha_k \geq \frac{B_{\varepsilon_k} H}{e_s} \tag{5.18}$$

Let us now assume that an external (environmental) disturbance $D_{ext,T} = \begin{bmatrix} D_{ext}^T & D_{ext}^T \end{bmatrix}^T$, *where* D_{ext} *is introduced earlier in equation* (5.1) *and* $D_{ext,T}$ *is bounded by* B_{ext} *(i.e.,* $||D_{ext,T}|| < B_{ext}$*), is applied to the system* (5.15) *as given by* $\dot{E}_{\{k\}}(t) = A_{clp}E_{\{k\}}(t) + D_{\{k\}} + D_{ext,T}$. *Following along similar steps as those above, equation* (5.17) *is now modified as follows*

$$||E_{\{k\}}(t)|| \leq B_{E_{\{k\}}} + T_{E_{\{k\}}} = B_{tot} \tag{5.19}$$

where

$$T_{E_{\{k\}}} \triangleq \sup_{\substack{t \in R^+ \\ |\varepsilon_k| < B_{\varepsilon_k} \\ \alpha_k \geq 1}} \left\| \int_{\tau=0}^{t} G(t-\tau) B_{ext} d\tau \right\|$$

One immediate observation that can be made is that by using the above method one cannot certainly get a better (smaller) error than $T_{E_{\{k\}}}$. *Therefore, in the presence of the disturbances the desired domain for the parameter* α_k *is given by*

$$\alpha_k \geq \frac{B_{\varepsilon_k} H}{e_s - T_{E_{\{k\}}}} \tag{5.20}$$

This completes the proof of the theorem. ■

The results presented in this section correspond to the centralized FLFR module for a single partially LL-recovered vehicle, in which case the other healthy vehicles are required to expend more control resource to compensate for the performance degradation of the faulty vehicle. In the next section, our proposed centralized FLFR module is formulated for the case of multiple partially LL-recovered vehicles by designing a new robust controller and imposing a constraint on the desired input vector.

5.2.3 Centralized FLFR Module for Multiple Actuator Failures

In this section, we present the FLFR module for the case of multiple partially LL-recovered vehicles $\#k$, $k \in \{1, ..., N\}$ due to the biased estimates of actuator faults. Assume that $||\hat{f}_k - f_k|| \geq 0$ (equivalently, $||\hat{B}_k - B_k|| \geq 0$) or $\hat{f}_k = f_k + \varepsilon_k$ (equivalently, $\hat{B}_k = B_k + \varepsilon_k$)

for $k = 1, ..., N$, where ε_k is an unknown function but bounded ($||\varepsilon_k|| \leq B_{\varepsilon_k}$ with B_{ε_k} known). This is a general formulation of the problem that represents either cases of 0, 1, ..., or N partially LL-recovered vehicles, such that the number of partially LL-recovered vehicles is equal to the number of vehicles $\#k$, $k = 1, ..., N$ for which $B_{\varepsilon_k} \neq 0$ and the non-faulty (or fully LL-recovered) vehicles $\#k$, $k = 1, ..., N$ are identified by $B_{\varepsilon_k} = 0$. Using the input vector U in equation (5.10) with $\alpha_k = 1$ for $k = 1, ..., N$, the closed-loop system in equation (5.11) becomes

$$\dot{E} = (A_T + \bar{B}_T K_T)E + D\begin{bmatrix} P_{12}^T(t) & P_{23}^T(t) & \cdots & P_{(N-1)N}^T(t) & 0_{1\times r} \end{bmatrix}^T \tag{5.21}$$

where

$$\begin{aligned} &\bar{B}_T = diag(\bar{B})_{i=1}^{N-1} \ , \ K_T = diag(K_i)_{i=1}^{N-1} \\ &D = \underbrace{\Big(J(B_1, ..., B_N) - J(\hat{B}_1, ..., \hat{B}_N)\Big)}_{D^0} \hat{J}(\hat{B}_1, ..., \hat{B}_N)_{left}^{-1} \end{aligned} \tag{5.22}$$

where

$$D^0_{[i,j]_{n\times r}} = \begin{cases} -\varepsilon_k & \text{if } j = k \text{ and } i = k-1 \geq 1 \\ \varepsilon_k & \text{if } j = k \text{ and } i = k \leq N-1 \\ 0_{n\times r} & \text{otherwise} \end{cases} \tag{5.23}$$

Using the definition of $P_{ij}(t)$ in equation (5.5), the closed-loop system dynamics (5.21) can be reformulated as

$$\dot{E}(t) = \left(A_T + \bar{B}_T K_T + \underbrace{D\Delta_T \bar{B}_T}_{\Delta\bar{B}_T} K_T \right) E(t) + D_T \tag{5.24}$$

where

$$\begin{aligned} &E(t) = \begin{bmatrix} \mathrm{E}_{12}^{\mathrm{T}} & \cdots & E_{(N-1)N}^T \end{bmatrix}^{\mathrm{T}} \ , \ D_T = D\Delta_T B_T U^d \\ &A_T = diag\,(A)_{i=1}^{N-1} \ , \ \bar{B}_T = diag\,\big(\bar{B}\big)_{i=1}^{N-1} \\ &K_T = diag\,(K_i)_{i=1}^{N-1} \ , \ \Delta_T = \begin{bmatrix} I_{(N-1)n\times(N-1)n} \\ 0_{r\times(N-1)n} \end{bmatrix} \end{aligned}$$

Now, we assume that the error specification e_s of the formation mission is violated by the partially LL-recovered vehicles $\#k$, $k \in \{1, ..., N\}$. As explained at the beginning of this subsection, this is a general formulation of the problem that represents either cases

of 0, 1, ..., or N partially LL-recovered vehicles, such that the number of partially LL-recovered vehicles is equal to the number of vehicles $\#k$, $k = 1, ..., N$ for which $B_{\varepsilon_k} \neq 0$ and the non-faulty (or fully LL-recovered) vehicles $\#k$, $k = 1, ..., N$ are identified by $B_{\varepsilon_k} = 0$. In order to simultaneously design the controllers for faulty and non-faulty vehicles, in the following two theorems will be presented in which a robust controller is designed to stabilize the nominal state space model in equation (5.24), and a constraint is imposed on the desired input vector to satisfy the error specification e_s of the formation mission.

Theorem 5.3. *Consider the formation vehicles $\#k$, $k = 1, ..., N$, with $B_{\varepsilon_k} \neq 0$ and $B_{\varepsilon_k} = 0$ pertaining to a partially LL-recovered vehicle and a non-faulty vehicle, respectively, whose nominal (disturbance-free) state space model is represented by $\dot{E} = (A_T + \bar{B}_T K_T + \Delta\bar{B}_T K_T)E$ as in equation (5.24). The nominal model of the system is stable by using the state feedback gain $K_T = (\hat{B}_T)^T P$ if there exists a block-diagonal matrix $P = diag\,(P_i)_{i=1}^{N-1}$ that satisfies the following LMI conditions*

$$\begin{cases} \begin{bmatrix} A_T P + P(A_T)^T + Q & P\bar{B}_T \\ (\bar{B}_T)^T P & -I \end{bmatrix} < 0 & \text{if } \lambda_{\mathrm{M}} \leq 0 \\ \begin{bmatrix} A_T P + P(A_T)^T + Q & P\bar{B}_T \\ (\bar{B}_T)^T P & -I \end{bmatrix} < 0 \text{ and } \begin{bmatrix} -Q & \sqrt{\lambda_M} P \\ \sqrt{\lambda_M} P & -I \end{bmatrix} < 0 & \text{if } \lambda_{\mathrm{M}} > 0 \end{cases} \tag{5.25}$$

where $P > 0$ and $Q > 0$ are positive definite matrices, and

$$\lambda_M = \sup_{||\varepsilon_i|| < B_{\varepsilon_i}} \lambda_{\max}\{(\bar{B}_T + \Delta\bar{B}_T)(\bar{B}_T + \Delta\bar{B}_T)^T\} - \inf_{||\varepsilon_i|| < B_{\varepsilon_i}} \lambda_{\min}\{(\Delta\bar{B}_T)(\Delta\bar{B}_T)^T\}$$

with λ_{max} and λ_{min} representing the maximum and minimum eigenvalues of a matrix, respectively.

Proof: *We start with the following Lyapunov function candidate*

$$V = E^T P E\ ,\ P > 0$$

Using the feedback gain matrix $K_i = \hat{B}_i^T P$ we have

$$\begin{aligned} \dot{V} = E^T \Big(& P A_T + (A_T)^T P + P\bar{B}_T(\bar{B}_T)^T P \\ & + P(\bar{B}_T + \Delta\bar{B}_T)(\bar{B}_T + \Delta\bar{B}_T)^T P - P\Delta\bar{B}_T(\Delta\bar{B}_T)^T P \Big) E \end{aligned}$$

Taking the matrix algebraic Riccati inequality $A_T P + P(A_T)^T + P\bar{B}_T(\bar{B}_T)^T P + Q < 0$ with $P > 0$ and $Q > 0$ that correspond to the LMI condition

$$\begin{bmatrix} A_T P + P(A_T)^T + Q & P\bar{B}_T \\ (\bar{B}_T)^T P & -I \end{bmatrix} < 0 \tag{5.26}$$

we get

$$\dot{V} \leq E^T \left(-Q + \lambda_M P^2\right) E \tag{5.27}$$

If $\lambda_M \leq 0$*, then the LMI condition* (5.26) *is the necessary condition in* (5.25) *to guarantee* $\dot{V} < 0$ *in equation* (5.27)*; otherwise if* $\lambda_M > 0$*, then the necessary condition in* (5.25) *is formed by augmenting the LMI condition* (5.26) *with the following LMI condition*

$$\begin{bmatrix} -Q & \sqrt{\lambda_M} P \\ \sqrt{\lambda_M} P & -I \end{bmatrix} < 0 \tag{5.28}$$

Therefore, the control gain $K_T = (\bar{B}_T)^T P$ *will asymptotically stabilize the system for all the values of the uncertainty* $\Delta\bar{B}_T$*. This completes the proof of the theorem.* ■

Theorem 5.4. *Assume that the error specification* (e_s) *of the formation mission is violated by the vehicles #*k*,* $k = 1, ..., N$*, with* $B_{\varepsilon_k} \neq 0$ *and* $B_{\varepsilon_k} = 0$ *pertaining to a partially LL-recovered vehicle and a non-faulty vehicle, respectively. Assume that the FLFR module implements the robust controller as in Theorem 5.3 for the partially LL-recovered and healthy vehicles #*k*,* $k = 1, ..., N$*. In order for the error specification* (e_s) *to be satisfied, the FLFR module needs to impose a constraint on the desired input vector* $U^d(t)$ *in equation* (5.4)*.*

Proof: *Using the robust controller as in Theorem 5.3, the tracking error dynamics of the overall formation system becomes*

$$\dot{E} = (A_T + \bar{B}_T K_T + \Delta\bar{B}_T K_T)E + D\Delta_T B_T U^d$$

whose Laplace transform (by neglecting the initial conditions) is given by

$$E(s) = \underbrace{(sI - A_T - (\bar{B}_T + \Delta\bar{B}_T)K_k)^{-1}}_{G_T(s)} D\Delta_T B_T U^d(s)$$

where $G_T(s)$ *is the transfer function matrix. We take*

$$H_T \stackrel{\Delta}{=} \sup_{\substack{t\in R^+ \\ \forall k\in\{1,...,N\}; \\ ||\varepsilon_k||<B_{\varepsilon_k}}} \left\| \int_{\tau=0}^{t} G_T(t-\tau) D\Delta_T B_T d\tau \right\|$$

Therefore, in the absence of any disturbances we get

$$||E(t)|| \leq H_T \sup_{t\in R^+} ||U^d(t)|| = B_E \tag{5.29}$$

Let us now assume that an external (environmental) disturbance

$$D_{ext,T} = \underbrace{\left[\begin{array}{ccc} D_{ext}^T & \cdots & D_{ext}^T \end{array}\right]^T}_{N-1 \text{ times}}$$

where D_{ext} is introduced earlier in equation (5.1) *and $D_{ext,T}$ is bounded by B_{ext} (i.e., $||D_{ext,T}|| < B_{ext}$), is applied to the system* (5.24) *as given by $\dot{E} = (A_T + \bar{B}_T K_T + \Delta\bar{B}_T K_T)E + D_T + D_{ext,T}$. Following along similar steps as those above, equation* (5.29) *is now modified as follows*

$$||E(t)|| \leq B_E + T_E = B_{tot} \tag{5.30}$$

where

$$T_E \triangleq \sup_{\substack{t\in R^+ \\ \forall k\in\{1,\ldots,N\}; \\ ||\varepsilon_k||<B_{\varepsilon_k}}} \left\| \int_{\tau=0}^{t} G(t-\tau)B_{ext}d\tau \right\|$$

In order that the condition $B_{tot} \leq e_s$ in equation (5.30) *holds, B_E is replaced from equation* (5.29) *and B_{tot} is replaced by e_s as follows*

$$\sup_{t\in R^+} ||U^d(t)|| \leq \frac{e_s - T_E}{H_T} \tag{5.31}$$

which requires the FLFR module to impose the constraint (5.31) *on the desired input vector $U^d(t)$. This completes the proof of the theorem.* ■

The results presented in this section correspond to the centralized FLFR module, which is mostly applicable to the formations of only a very few vehicles with a requirement of having adequate communication resources. As the number of vehicles in the fleet increases and the communication resources become more constrained and limited, the motivation for implementing decentralized LLFR controller and decentralized FLFR module becomes more pronounced. Towards this end, a decentralized cooperative fault accommodation strategy is discussed and developed in the next section given the availability of relative measurements among the formation flight of unmanned vehicles.

5.3 Decentralized Cooperative Actuator Fault Accommodation

Consider the general N-vehicle formation with relative measurements, RMF digraph as per Definition 2.3, and the state space model of the vehicle $\#i$ as represented by (5.2). For simplicity, the effects of the environmental disturbances D_{ext} in (5.2) are ignored in

the following analysis, but these effects will be analyzed later in the subsequent sections. The relative states X_{ij} are measured and used in the formation feedback loop. In order to avoid redundant measurements, we assume that the RMF digraph (as per Definition 2.3) is connected. To each edge $X_{ij} = X_j - X_i$ representing the relative state measurement of the vehicle $\#j$ with respect to the vehicle $\#i$, we assign a scalar parameter $\alpha_{ij} \in R$ and two matrices $\beta_{ij}^i, \beta_{ij}^j \in R^{r\times n}$ for designing a decentralized controller and define the following vectors

$$U^d \triangleq \begin{bmatrix} \vdots \\ U_{ij}^d \\ \vdots \end{bmatrix}_{(N-1)r\times 1}, \; E \triangleq \begin{bmatrix} \vdots \\ E_{ij} \\ \vdots \end{bmatrix}_{(N-1)n\times 1}$$
$$\alpha \triangleq \begin{bmatrix} \vdots \\ \alpha_{ij} \\ \vdots \end{bmatrix}_{(N-1)\times 1}, \; \beta \triangleq \begin{bmatrix} \vdots \\ \beta_{ij}^i \\ \beta_{ij}^j \\ \vdots \end{bmatrix}_{2(N-1)r\times n} \tag{5.32}$$

where the vectors $U_{ij}^d \in R^r$, $E_{ij} \in R^n$, scalar $\alpha_{ij} \in R$, and matrix $\left[(\beta_{ij}^i)^T \; (\beta_{ij}^j)^T\right]^T \in R^{2r\times n}$ are on the same corresponding row blocks of the vectors U^d, E, α, and matrix β, respectively. The states U_{ij}^d and E_{ij} are introduced earlier in equation (5.3). Similar to the compact matrix form of the error dynamics equations in (5.4), in the general case of N vehicles we have

$$\dot{E} = A_T E + J(B_1, ..., B_N)U - \bar{B}_T U^d \tag{5.33}$$

where the input vector U and the matrix J are given by

$$U = \begin{bmatrix} U_1 \\ \vdots \\ U_N \end{bmatrix}, \; J_{[i,j]_{n\times r}} = \begin{cases} B_j & \text{if } \exists k \in \mathscr{N}(\{j\}); E_{[i]_n} = E_{kj} \\ -B_j & \text{if } \exists k \in \mathscr{N}(\{j\}); E_{[i]_n} = E_{jk} \\ 0 & \text{otherwise} \end{cases}$$

with the indices $[i,j]_{a\times b}$ and $[i]_a$ are defined as in Definition 2.8, and the nearest neighbor set $\mathscr{N}(\{r\})$ is defined in Definition 2.4.

It should be noted that the dynamics of individual vehicles are coupled through their relative state measurements. For example, in the special case of the four-vehicle formation in Figure 2.2, the error dynamics is given by

$$\underbrace{\begin{bmatrix}\dot{E}_{12}\\ \dot{E}_{23}\\ \dot{E}_{34}\end{bmatrix}}_{\dot{E}} = \underbrace{\begin{bmatrix}A & 0_{n\times n} & 0_{n\times n}\\ 0_{n\times n} & A & 0_{n\times n}\\ 0_{n\times n} & 0_{n\times n} & A\end{bmatrix}}_{A_T}\underbrace{\begin{bmatrix}E_{12}\\ E_{23}\\ E_{34}\end{bmatrix}}_{E} + \underbrace{\begin{bmatrix}-B_1 & B_2 & 0 & 0\\ 0 & -B_2 & B_3 & 0\\ 0 & 0 & -B_3 & B_4\end{bmatrix}}_{J(B_1,B_2,B_3,B_4)}\underbrace{\begin{bmatrix}U_1\\ U_2\\ U_3\\ U_4\end{bmatrix}}_{U}$$
$$- \underbrace{\begin{bmatrix}\bar{B} & 0_{n\times r} & 0_{n\times r}\\ 0_{n\times r} & \bar{B} & 0_{n\times r}\\ 0_{n\times r} & 0_{n\times r} & \bar{B}\end{bmatrix}}_{\bar{B}_T}\underbrace{\begin{bmatrix}U_{12}^d\\ U_{23}^d\\ U_{34}^d\end{bmatrix}}_{U^d}$$

5.3.1 Decentralized Low-Level Fault Recovery (LLFR) Controller

In this section, we assume that the system is fault free or one has an accurate fault estimate. In the later case of accurate fault estimate, we assume that the actuators of vehicles $\#i$ are subject to loss-of-effectiveness (LOE) actuator failures as in equation (5.2), that is $B_i = \bar{B} + f_i$, and the estimates of faulty actuator gains are unbiased, that is $\hat{B}_i = B_i$. These unbiased estimates are used in the LLFR controller. In the following, a decentralized control strategy is proposed and implemented in order to meet the restrictive communication constraints that are imposed due to the availability of only local relative state measurements. Motivated by conventional linear control design techniques, a decentralized controller is designed in which the control signal U_i of vehicle $\#i$ is specified in terms of local relative state measurements and the desired trajectories of the vehicles in its nearest neighbor set.

To design the decentralized controller, the LLFR module incorporates the actuator fault estimates $\hat{B}_i$ into the matrix J that yields $J(\hat{B}_1, ..., \hat{b}_N)$ and generates the overall input vector $U = [U_1^T \ ... \ U_N^T]^T$ as follows

$$U = U_d + U_s \tag{5.34}$$

The actuator gain B_i is now replaced by its estimate $\hat{B}_i$ (that is, $\hat{B}_i = \bar{B} + \hat{f}_i$) by incorporating the fault estimate $\hat{f}_i$. Moreover, $\hat{B}_i = B_i$ when the system is fault free or when one has an accurate fault estimate. The control terms $U_d \in R^{(N-1)r\times 1}$ and $U_s \in R^{(N-1)n\times 1}$ are the desired input control and the stabilizing control, respectively, which are defined as follows

$$U_d = (\mathrm{A}(\alpha) \otimes I_{r\times r})U^d$$
$$U_s = \mathrm{B}(\beta)E$$

where $\otimes$ represents the Kronecker product, the tracking error E and the desired input U^d are defined as in equation (5.32), and

$$\mathrm{A}(\alpha) = \begin{bmatrix} A_1^T(\alpha) \\ \vdots \\ A_N^T(\alpha) \end{bmatrix}_{N\times(N-1)}, \ \mathrm{B}(\beta) = \begin{bmatrix} B_1^T(\beta) \\ \vdots \\ B_N^T(\beta) \end{bmatrix}_{Nr\times(N-1)n} \tag{5.35}$$

with $\mathrm{A}(\alpha)$ and $\mathrm{B}(\beta)$ denoting the design matrices.

In order to construct a decentralized controller one needs to appropriately design the above matrices such that the control signals satisfy the communication restrictions of a decentralized control scheme. In other words we need to generate the control U_i of vehicle $\#i$ merely in terms of the information on the local relative state measurements and the desired trajectories of the vehicles in its nearest neighbor set. The matrices $\mathrm{A}(\alpha)$ and $\mathrm{B}(\beta)$ are computed and specified next.

For calculating the vectors $\mathrm{A}_i(\alpha)$, $i = 1, ..., N$ in (5.35), one vehicle, namely vehicle $\#r$, is arbitrarily chosen as the reference and is assigned with $\mathrm{A}_r(\alpha) = \alpha$. For each α_{ij}, an associated vector T_{ij}^{α} is defined according to $\alpha^T T_{ij}^{\alpha} = \alpha_{ij}$. For any given vehicle $\#j$ in the nearest neighbor set ($j \in \mathscr{N}(\{r\})$), we evaluate

$$\mathrm{A}_j(\alpha) = A_r(\alpha) + T_{rj}^{\alpha}$$

with the consideration that $T_{rj}^{\alpha} = -T_{jr}^{\alpha}$. This neighboring calculation can be accomplished by induction through the RMF digraph (as per Definition 2.3) of the entire formation, so that all the vectors $\mathrm{A}_i(\alpha)$, $i = 1, ..., N$ are specified to form the matrix $\mathrm{A}(\alpha)$ in (5.35).

For calculating $B_i^T(\beta) = \begin{bmatrix} B_{[i,1]_{r\times n}} & \cdots & B_{[i,N-1]_{r\times n}} \end{bmatrix}$ in (5.35), we take

$$B_{[i,k]_{r\times n}} = \begin{cases} \beta_{ij}^i & \text{if } \exists j \in \mathscr{N}(\{i\}); E_{[k]_n} = E_{ij} \\ \beta_{ji}^i & \text{if } \exists j \in \mathscr{N}(\{i\}); E_{[k]_n} = E_{ji} \\ 0 & \text{otherwise} \end{cases}$$

For example, in the special case of the four-vehicle formation in Figure 2.2, the matrices $\mathrm{A}(\alpha)$ and $B(\beta)$ have the following structures

$$A(\alpha) = \begin{bmatrix} \alpha_{12}-1 & \alpha_{23}-1 & \alpha_{34}-1 \\ \alpha_{12} & \alpha_{23}-1 & \alpha_{34}-1 \\ \alpha_{12} & \alpha_{23} & \alpha_{34}-1 \\ \alpha_{12} & \alpha_{23} & \alpha_{34} \end{bmatrix}, \ B(\beta) = \begin{bmatrix} \beta_{12}^1 & 0 & 0 \\ \beta_{12}^2 & \beta_{23}^2 & 0 \\ 0 & \beta_{23}^3 & \beta_{34}^3 \\ 0 & 0 & \beta_{34}^4 \end{bmatrix} \tag{5.36}$$

In the following, the decentralized controller (5.34) is designed for the system (5.33) in either cases of a fault free formation or a formation with unbiased fault estimates.

Lemma 5.3. *Consider a fault free vehicle formation or the formation that is equipped with unbiased fault estimates $\hat{f}_i = f_i$, where in both cases we can take $\hat{B}_i = B_i$. The state feedback matrix $B(\beta) = YX^{-1}$ stabilizes the closed-loop system* (5.33)-(5.34) *(with the initial state $E(0)$) for all values of the vector $\alpha \in R^{N-1}$ and minimizes $\gamma_1 + \gamma_2$, where γ_1 is an upper bound on the H_∞ norm of the transfer function from the disturbance to the output of the system and γ_2 is an upper bound on the linear quadratic cost function $J_{LQR}(U_s, Q, R)$ in Lemma 2.3, if there exist a matrix Y (with the same dimensions and structure as $B(\beta)$) and a positive definite block-diagonal matrix $X = diag(X_i)_{i=1}^{N-1} > 0$ that satisfy the following optimization problem*

$$
\begin{aligned}
&Minimize \quad \gamma_1 + \gamma_2 \\
&subject\ to \\
&X > 0 \\
&\begin{bmatrix} AX + XA^T + J(.)Y + Y^T J(.)^T & I & X \\ I & -\gamma_1 I & 0 \\ X & 0 & -\gamma_1 I \end{bmatrix} < 0 \\
&\begin{bmatrix} AX + XA^T + J(.)Y + Y^T J(.)^T & X & Y^T \\ X & -Q^{-1} & 0 \\ Y & 0 & -R^{-1} \end{bmatrix} \leq 0 \\
&\begin{bmatrix} \gamma_2 & E^T(0) \\ E(0) & X \end{bmatrix} \geq 0
\end{aligned}
\tag{5.37}
$$

in which the term $J(.)$ is defined (similar to the one in equation (5.33)*) as*

$$J(.) = J(\hat{B}_1, ..., \hat{B}_N)$$

Proof: *First, it should be pointed out that by substituting the control law U from equation* (5.34) *into* (5.33)*, the control U_d cancels out the terms U^d from the closed-loop system. The control U_s forms the nominal (disturbance free) closed-loop dynamical system that is given by*

$$\dot{E} = (A_T + J(.)B(\beta))E$$

By applying Lemmas 2.2 and 2.3 to the model above and by defining the new matrix $Y = B(\beta)X$, where Y has the same dimension and structure as $B(\beta)$, gives the optimization problem with LMI conditions that are stated in equation (5.37)*. Therefore, the solution to the H_∞ optimal feedback matrix $B(\beta)$ is calculated according to $B(\beta) = YX^{-1}$.*

■

In the next section, the vector $\alpha \in R^{N-1}$ is used as a degree of freedom for the purpose of fault accommodation in the formation flight of unmanned vehicles. It is shown

that imprecise estimates of actuator fault signals (in both cases of a single or multiple faults) will impact the performance of the overall formation flight system. This performance degradation is detected by the HL supervisor and, subsequently, the FLFR module is activated. We will formulate a decentralized cooperative fault accommodation in the FLFR module by using a controller that is similar to equation (5.34) and which guarantees that the desired error specifications in the presence of possible estimation inaccuracy and bias are maintained and satisfied.

5.3.2 Decentralized Formation-Level Fault Recovery (FLFR) Module

In this section, assume that the vehicle $\#i$ is faulty and partially recovered by the low-level fault recovery (LLFR), which implies that the corresponding fault estimate is biased and inaccurate. Therefore, vehicle $\#i$ tracks the desired trajectory within an error bound of radius r, which is greater than the mission error specification e_s ($r > e_s$ as in the special case of the four-vehicle formation in Figure 2.2). Our main objective here is to propose an FLFR module to compensate for the performance degradations of the partially LL-recovered vehicle.

Let us now consider a loss-of-effectiveness fault in vehicle $\#i$ actuator, and assume that the LLFR module has estimated the severity of this fault, however this value is biased and imprecise, that is $\hat{f}_i = f_i + \varepsilon_i$ or equivalently $\hat{B}_i = B_i + \varepsilon_i$, where ε_i is unknown but bounded (that is $||\varepsilon_i|| < B_{\varepsilon_i}$) with B_{ε_i} a known bound. This biased estimate will result in the overall formation performance degradations that are detected by the HL supervisor. The supervisor then activates the FLFR module in order to satisfy the desired mission error specifications.

In the following, we develop the FLFR module by investigating the stability and convergence of an N-vehicle formation flight system by using the decentralized controller (5.34) that is subject to the fact that the fault estimate in vehicle $\#i$ actuator is biased. Our main result of this section is stated in the following two theorems. Theorem 5.5 proposes a decentralized controller which is robust to the biased estimate of the fault parameter in vehicle $\#i$, and Theorem 5.6 proposes the selection criterion for the vector $\alpha \in R^{N-1}$ in order to satisfy the error specification e_s of the formation flight mission.

Theorem 5.5. *Let the actuator of vehicle $\#i$ be faulty, and let the corresponding fault parameter be estimated by a biased estimator such that $\hat{f}_i = f_i + \varepsilon_i$ (as given by equation (5.34)), where ε_i is unknown but bounded ($||\varepsilon_i|| < B_{\varepsilon_i}$) and B_{ε_i} is a known bound. In general, the matrix $\varepsilon_i \in R^{n\times r}$ includes N_{ε_i} ($N_{\varepsilon_i} \leq nr$) uncertain (nonzero) elements ε_{ij} ($j = 1, ..., N_{\varepsilon_i}$) and $nr - N_{\varepsilon_i}$ zero elements. Assume that the error specification (e_s) is violated implying that the vehicle $\#i$ is partially recovered by the LLFR module. The*

state feedback matrix $B(\beta) = YX^{-1}$ *stabilizes the closed-loop system* (5.33)-(5.34) *(with the initial state* $E(0)$*) for all values of the vector* $\alpha \in R^{N-1}$ *and minimizes* $\gamma_1 + \gamma_2$*, where* γ_1 *is an upper bound on the* H_∞ *norm of the transfer function from the disturbance to the output of the system and* γ_2 *is an upper bound on the linear quadratic cost function* $J_{LQR}(U_s, Q, R)$ *in Lemma 2.3, if there exist a matrix* Y *(with the same dimension and structure as* $B(\beta)$*) and a positive definite block-diagonal matrix* $X = diag(X_i)_{i=1}^{N-1} > 0$ *that satisfy the following optimization problem*

$$
\begin{aligned}
&\textit{Minimize } \gamma_1 + \gamma_2 \\
&\textit{s.t. } X > 0 \textit{ and for } \varepsilon_i \in \{\varepsilon_i^{j+}, \varepsilon_i^{j-}\}\ ,\ j = 1,...,\mathrm{N}_{\varepsilon_\mathrm{i}}: \\
&\begin{bmatrix} A_T X + X A_T^T + (J(.) - J_{\varepsilon_i})Y + Y^T (J(.) - J_{\varepsilon_i})^T & I & X \\ I & -\gamma_1 I & 0 \\ X & 0 & -\gamma_1 I \end{bmatrix} < 0 \\
&\begin{bmatrix} AX + XA^T + (J(.) - J_{\varepsilon_i})Y + Y^T (J(.) - J_{\varepsilon_i})^T & X & Y^T \\ X & -Q^{-1} & 0 \\ Y & 0 & -R^{-1} \end{bmatrix} \leq 0 \\
&\begin{bmatrix} \gamma_2 & E^T(0) \\ E(0) & X \end{bmatrix} \geq 0
\end{aligned}
\tag{5.38}
$$

in which the terms $J(.)$ *and* J_{ε_i} *are defined (similar to the one in equation* (5.33)*) as*

$$
\begin{aligned}
J(.) &= J(\hat{B}_1, ..., \hat{B}_N) \\
J_{\varepsilon_i} &= J\underbrace{(0, ..., \varepsilon_i, ..., 0)}_{\substack{\textit{only the } i^{th} \textit{ block} \\ \textit{is nonzero} \\ \textit{out of the N blocks}}}
\end{aligned}
$$

and the terms ε_i^{j+} *and* ε_i^{j-} *are defined as*

$$
\varepsilon_i^{j+} = \varepsilon_i|_{\varepsilon_{ij} = +N_{\varepsilon_i}^R B_{\varepsilon_i}, \varepsilon_{ik} = 0 (k \neq j)}\ ,\ \varepsilon_i^{j-} = \varepsilon_i|_{\varepsilon_{ij} = -N_{\varepsilon_i}^R B_{\varepsilon_i}, \varepsilon_{ik} = 0 (k \neq j)}
$$

where ε_{ij} *(*$\mathrm{j} = 1,...,\mathrm{N}_{\varepsilon_\mathrm{i}}$*) are the uncertain (nonzero) elements of the matrix* ε_i*, and* N_{ε_i} *and* $N_{\varepsilon_i}^R$ *represent the number of nonzero elements and rows of the matrix* ε_i*, respectively.*

Proof: *By substituting the control law* U *from equation* (5.34) *into* (5.33) *the resulting closed-loop system is obtained as*

$$
\dot{E} = (A_T + (J(.) - J_{\varepsilon_i})B(\beta))\, E + \bar{D}_{d,i}(t) \tag{5.39}
$$

where

$$
\bar{D}_{d,i}(t) = -J_{\varepsilon_i}(A_i^T(\alpha) \otimes I_{r \times r}) U^d(t) \tag{5.40}
$$

By applying Lemmas 2.2 and 2.3 to the system (5.39)*, a necessary condition for minimizing* $\gamma_1 + \gamma_2$ *is to find a matrix* Y *(with the same dimension and structure as* $B(\beta)$*) and a positive definite block-diagonal matrix* $X = diag(X_i)_{i=1}^{N-1} > 0$ *that satisfy the LMI conditions in equation* (5.38)*.*

The LMI conditions in equation (5.38) *cannot be directly verified since the matrix* ε_i *is unknown. However, the unknown matrix* ε_i *is bounded, that is* $||\varepsilon_i|| < B_{\varepsilon_i}$*. Therefore, the summation of the absolute values of the uncertain (nonzero) elements on each row of the matrix* ε_i *is less than* B_{ε_i}*. This implies that the sum of the absolute values of the uncertain (nonzero) elements on all* $N_{\varepsilon_i}^R$ *rows of the matrix* ε_i *is less than* $N_{\varepsilon_i}^R B_{\varepsilon_i}$*, that is*

$$\sum_{j=1}^{\mathrm{N}_{\varepsilon_\mathrm{i}}} ||\varepsilon_{ij}|| < N_{\varepsilon_i}^R B_{\varepsilon_i} \tag{5.41}$$

The condition (5.41) *can be represented by a convex polygon region in the* N_{ε_i}*-dimensional space corresponding to* $\begin{bmatrix} \varepsilon_{i1} & \varepsilon_{i2} & \cdots & \varepsilon_{iN_{\varepsilon_i}} \end{bmatrix}^T$*. This convex region is surrounded and covered by the vertices*

$$\begin{bmatrix} +N_{\varepsilon_i}^R B_{\varepsilon_i} \\ 0 \\ \vdots \\ 0 \end{bmatrix}, \begin{bmatrix} -N_{\varepsilon_i}^R B_{\varepsilon_i} \\ 0 \\ \vdots \\ 0 \end{bmatrix}, \begin{bmatrix} 0 \\ +N_{\varepsilon_i}^R B_{\varepsilon_i} \\ \vdots \\ 0 \end{bmatrix}, \begin{bmatrix} 0 \\ -N_{\varepsilon_i}^R B_{\varepsilon_i} \\ \vdots \\ 0 \end{bmatrix} \tag{5.42}$$
$$, ..., \begin{bmatrix} 0 \\ 0 \\ \vdots \\ +N_{\varepsilon_i}^R B_{\varepsilon_i} \end{bmatrix}, \begin{bmatrix} 0 \\ 0 \\ \vdots \\ -N_{\varepsilon_i}^R B_{\varepsilon_i} \end{bmatrix}$$

Now, if the LMI conditions in equation (5.38) *hold for the vertices in* (5.42)*, then they hold for all values of the unknown matrix* ε_i*. Therefore, if there exist a matrix* Y *(with the same dimension and structure as* $B(\beta)$*) and a positive definite block-diagonal matrix* $X = diag(X_i)_{i=1}^{N-1} > 0$ *that satisfy the LMI conditions in equation* (5.38) *for* $\varepsilon_i \in \{\varepsilon_i^{j+}, \varepsilon_i^{j-}\}$*,* $j = 1, ..., N_{\varepsilon_i}$*, then* Y *and* X *satisfy the LMI conditions in equation* (5.38) *for the unknown matrix* ε_i*, and therefore the solution to the* H_∞ *optimal feedback matrix* $B(\beta)$ *is calculated according to* $B(\beta) = YX^{-1}$*.* ■

Theorem 5.6. *Assume that the closed-loop formation flight system* (5.33)-(5.34) *with the partially LL-recovered vehicle #i is stabilized for all values of the vector* $\alpha \in R^{N-1}$ *by using the FLFR controller gain* $B(\beta) = YX^{-1}$ *according to Theorem 5.5. There exists nonzero* $\alpha \in R^{N-1}$ *given by equation* (5.47) *below in the control signal* U_d *such that the*

norm of the tracking error E remains smaller than the predefined specification given by e_s.

Proof: *Consider the closed-loop system* (5.39) *that is already shown to be stable according to the results in Theorem 5.5. Denoting* $A_{dclp,i} = (A_T + (J(.) - J_{\varepsilon_i})B(\beta))$ *in* (5.39)*, the tracking error E is governed by the dynamical system* $\dot{E}(t) = A_{dclp,i}E(t) + \bar{D}_{d,i}(t)$ *whose Laplace transform is given by*

$$E(s) = (sI - A_{dclp,i})^{-1}\bar{D}_{d,i}(s) = G_{d,i}(s)\bar{D}_{d,i}(s)$$

where $G_{d,i}(s)$ *is the transfer function matrix. By using the definition of* $\bar{D}_{d,i}(t)$ *from equation* (5.39)*, we have*

$$E(s) = -G_{d,i}(s)J_{\varepsilon_i}(A_i^T(\alpha) \otimes I_{r\times r})\mathscr{L}\{U^d(t)\}$$

where $\mathscr{L}\{.\}$ *denotes the Laplace transform of a given signal. Let us denote* $\mathrm{A}_i(\alpha) = ||\mathrm{A}_i(\alpha)||\hat{\mathrm{A}}_i(\alpha)$*, where* $\hat{\mathrm{A}}_i(\alpha)$ *is the normalized* $\mathrm{A}_i(\alpha)$*. We now obtain*

$$E(s) = -G_{d,i}(s)J_{\varepsilon_i}(||\mathrm{A}_i(\alpha)||\hat{\mathrm{A}}_i^T(\alpha) \otimes I_{r\times r})\mathscr{L}\{U^d(t)\}$$

Taking

$$H_{d,i}(\hat{\mathrm{A}}_i(\alpha)) \triangleq \sup_{\substack{t\in R^+ \\ ||\varepsilon_i||<B_{\varepsilon_i}}} \int_{\tau=0}^{t} \left\{ \|G_{d,i}(t-\tau)\| \left\| (\hat{\mathrm{A}}_i^T(\alpha) \otimes I_{r\times r})U^d(\tau) \right\| \right\} d\tau \tag{5.43}$$

we get

$$||E(t)|| \leq ||\varepsilon_i||H_{d,i}(\hat{\mathrm{A}}_i(\alpha))||\mathrm{A}_i(\alpha)|| \triangleq B_{E,i} \tag{5.44}$$

In order for the norm of the tracking error E be smaller than the specification e_s*, a solution based on equation* (5.44) *can be obtained as follows:*

$$\max ||\varepsilon_i||H_{d,i}(\hat{\mathrm{A}}_i(\alpha))||A_i^T(\alpha)|| \leq e_s$$

$$\Rightarrow \quad ||A_i^T(\alpha)|| \leq \frac{e_s}{B_{\varepsilon_i}H_{d,i}(\hat{\mathrm{A}}_i(\alpha))}$$

Therefore, in absence of any disturbances the desired domain for the parameter α *is given by*

$$D'_\alpha = \left\{ \alpha \in R^{N-1} \middle| \, ||A_i^T(\alpha)|| \leq \frac{e_s}{B_{\varepsilon_i}H_{d,i}(\hat{\mathrm{A}}_i(\alpha))} \right\} \tag{5.45}$$

Let us now assume that an external (environmental) disturbance

$$D_{ext,T} = \underbrace{\begin{bmatrix} D_{ext}^T & \cdots & D_{ext}^T \end{bmatrix}}_{N-1 \text{ times}}^T$$

where D_{ext} is introduced in equation (5.2) and $D_{ext,T}$ is bounded by B_{ext} (that is $||D_{ext,T}|| < B_{ext}$), is applied to the system (5.38) as given by $\dot{E} = (A_T + \bar{B}_T K_T + \Delta_d(\beta, \varepsilon_i))E + \bar{D}_{d,i}(t) + D_{ext}$. Following along similar steps as those followed earlier, equation (5.44) is modified as follows:

$$|E(t)| \leq B_{E,i} + T_{E,i} = B_{tot} \tag{5.46}$$

where

$$T_{E,i} \triangleq \sup_{\substack{t \in R^+ \\ |\varepsilon_i| < B_{\varepsilon_i} \\ \beta \in D'_\beta}} \left\| \int_{\tau=0}^{t} G_{d,i}(t-\tau) B_{ext} d\tau \right\|$$

One immediate conclusion is that one cannot certainly get a better (smaller) error bound than $T_{E,i}$. Therefore, in presence of the disturbances the desired domain for the parameter α is given by

$$D'_\alpha = \left\{ \alpha \in R^{N-1} \middle| \, ||A_i^T(\alpha)|| \leq \frac{e_s - T_{E,i}}{B_{\varepsilon_i} H_{d,i}(\hat{\mathrm{A}}_i(\alpha))} \right\} \tag{5.47}$$

This completes the proof of the theorem. ■

Remark 5.2. *The fact that not all the subsystems $E_{i(i+1)}$ (as in (5.15)) are perturbed in the centralized FLFR module is the main advantage of the centralized approach achieved at the expense of more stringent communication requirements. This is in contrast to the decentralized FLFR approach, which is communicationally more efficient but propagates the error to the entire subsystems (as shown in (5.39)).*

The results presented in this section correspond to the decentralized FLFR module for a single partially LL-recovered vehicle. In the next section, our proposed decentralized FLFR module is formulated for the case of multiple partially LL-recovered vehicles by designing a new robust controller and imposing a constraint on the desired input vector.

5.3.3 Decentralized FLFR Module for Multiple Actuator Failures

In this section, we present the FLFR module for the case of multiple partially LL-recovered vehicles $\#k$, $k \in \{1, ..., N\}$ due to the biased estimates of actuator faults. Assume that the vector α (as in equation (5.32)) is already designed for the case of a single actuator

failure by using Theorem 5.6. For the case of multiple actuator failures, assume that $||\hat{f}_k - f_k|| \geq 0$ (equivalently, $||\hat{B}_k - B_k|| \geq 0$) or $\hat{f}_k = f_k + \varepsilon_k$ (equivalently, $\hat{B}_k = B_k + \varepsilon_k$) for $k = 1, ..., N$, where ε_k is an unknown function but bounded ($||\varepsilon_k|| \leq B_{\varepsilon_k}$ with B_{ε_k} known). This is a general formulation of the problem that represents either cases of 0, 1, ..., or N partially LL-recovered vehicles, such that the number of partially LL-recovered vehicles is equal to the number of vehicles $\#k$, $k \in \{1, ..., N\}$ for which $B_{\varepsilon_k} \neq 0$ and the non-faulty (or fully LL-recovered) vehicles $\#k$, $k \in \{1, ..., N\}$ are identified by $B_{\varepsilon_k} = 0$.

Now, assume that the error specification e_s of the formation mission is violated by the partially LL-recovered vehicles $\#k$, $k \in \{1, ..., N\}$. In order to simultaneously design controllers for faulty and non-faulty vehicles, in the following two theorems will be presented in which a robust controller is designed to stabilize the nominal closed-loop state space model (5.33)-(5.34), and a constraint is imposed on the desired input vector to satisfy the error specification e_s of the formation mission.

Theorem 5.7. *Let the actuators of vehicles $\#i$, $i \in \{1, ..., N\}$ be faulty, and let the corresponding fault parameters be estimated by a biased estimator such that $\hat{f}_i = f_i + \varepsilon_i$ (as given by equation (5.34)), where ε_i is unknown but bounded ($||\varepsilon_i|| < B_{\varepsilon_i}$) and B_{ε_i} is a known bound. In general, the matrix $\varepsilon_i \in R^{n \times r}$ includes N_{ε_i} ($N_{\varepsilon_i} \leq nr$) uncertain (nonzero) elements ε_{ij} ($j = 1, ..., N_{\varepsilon_i}$) and $nr - N_{\varepsilon_i}$ zero elements. Assume that the error specification (e_s) is violated implying that the vehicles $\#i$, $i \in \{1, ..., N\}$ are partially recovered by the LLFR module. The state feedback matrix $B(\beta) = YX^{-1}$ stabilizes the closed-loop system (5.33)-(5.34) (with the initial state $E(0)$ and the value of the vector α calculated by using Theorem 5.5) and minimizes $\gamma_1 + \gamma_2$, where γ_1 is an upper bound on the H_∞ norm of the transfer function from the disturbance to the output of the system and γ_2 is an upper bound on the linear quadratic cost function $J_{LQR}(U_s, Q, R)$ in Lemma 2.3, if there exist a matrix Y (with the same dimension and structure as $B(\beta)$) and a positive definite block-diagonal matrix $X = diag(X_i)_{i=1}^{N-1} > 0$ that satisfy the following optimization problem*

$$
\begin{aligned}
&\textit{Minimize } \gamma_1 + \gamma_2 \\
&\textit{s.t. } X > 0 \textit{ and for } \forall i \in \{1, ..., N\}, \varepsilon_i \in \{\varepsilon_i^{j+}, \varepsilon_i^{j-}\}\ ,\ j = 1,...,\mathrm{N}_{\varepsilon_i} : \\
&\begin{bmatrix} A_T X + X A_T^T + (J(.) - J_{\varepsilon_i})Y + Y^T (J(.) - J_{\varepsilon_i})^T & I & X \\ I & -\gamma_1 I & 0 \\ X & 0 & -\gamma_1 I \end{bmatrix} < 0 \\
&\begin{bmatrix} AX + XA^T + (J(.) - J_{\varepsilon_i})Y + Y^T (J(.) - J_{\varepsilon_i})^T & X & Y^T \\ X & -Q^{-1} & 0 \\ Y & 0 & -R^{-1} \end{bmatrix} \leq 0 \\
&\begin{bmatrix} \gamma_2 & E^T(0) \\ E(0) & X \end{bmatrix} \geq 0
\end{aligned}
\tag{5.48}
$$

in which the terms $J(.)$ and J_{ε_i} are defined (similar to the one in equation (5.33)) as

$$J(.) = J(\hat{B}_1, ..., \hat{B}_N)$$
$$J_{\varepsilon_i} = J\underbrace{(0, ..., \varepsilon_i, ..., 0)}_{\substack{\text{only the } i^{th} \text{ block} \\ \text{is nonzero} \\ \text{out of the } N \text{ blocks}}}$$

and the terms ε_i^{j+} and ε_i^{j-} are defined as

$$\varepsilon_i^{j+} = \varepsilon_i|_{\varepsilon_{ij}=+N_{\varepsilon_i}^R B_{\varepsilon_i}, \varepsilon_{ik}=0(k\neq j)} \ , \ \varepsilon_i^{j-} = \varepsilon_i|_{\varepsilon_{ij}=-N_{\varepsilon_i}^R B_{\varepsilon_i}, \varepsilon_{ik}=0(k\neq j)}$$

where ε_{ij} (j = 1,...,N_{ε_i}) are the uncertain (nonzero) elements of the matrix ε_i, and N_{ε_i} and $N_{\varepsilon_i}^R$ represent the number of nonzero elements and rows of the matrix ε_i, respectively.

Proof: *The proof is similar to that of Theorem 5.5.* ■

Theorem 5.8. *Assume that the error specification (e_s) of the formation mission is violated by the partially LL-recovered vehicles #i, $i \in \{1, ..., N\}$, with $B_{\varepsilon_i} \neq 0$ and $B_{\varepsilon_i} = 0$ pertaining to a partially LL-recovered vehicle and a non-faulty vehicle, respectively. Assume that the FLFR module implements the robust controller as in Theorem 5.7 for the partially LL-recovered and healthy vehicles #i, $i = 1, ..., N$. In order for the error specification (e_s) to be satisfied, the FLFR module needs to impose a constraint on the desired input vector $U^d(t)$ as given by equation (5.32).*

Proof: *Using the robust controller as in Theorem 5.7, the tracking error dynamics of the overall formation system (as denoted in equation (5.39)) becomes*

$$\dot{E} = (A_T + (J(.) - J_\varepsilon)B(\beta))\, E - J_\varepsilon(A_i^T(\alpha) \otimes I_{r\times r})U^d(t) \tag{5.49}$$

in which the terms $J(.)$ and J_ε are defined (similar to the one in equation (5.33)) as

$$J(.) = J(\hat{B}_1, ..., \hat{B}_N)$$
$$J_\varepsilon = J(\varepsilon_1, ..., \varepsilon_N)$$

The Laplace transform of (5.49) (by neglecting the initial conditions) is given by

$$E(s) = \underbrace{-(sI - A_T - (J(.) - J_\varepsilon)B(\beta))^{-1}}_{G_T(s)} J_\varepsilon(A_i^T(\alpha) \otimes I_{r\times r})U^d(s)$$

where $G_T(s)$ is the transfer function matrix. We take

$$H_T \triangleq \sup_{\substack{t\in R^+ \\ \forall k\in\{1,...,N\}; \\ ||\varepsilon_k||<B_{\varepsilon_k}}} \left\| \int_{\tau=0}^{t} G_T(t-\tau) J_\varepsilon(A_i^T(\alpha) \otimes I_{r\times r}) d\tau \right\|$$

Therefore, in absence of any disturbances we get

$$||E(t)|| \leq H_T \sup_{t \in R^+} ||U^d(t)|| = B_E \tag{5.50}$$

Let us now assume that an external (environmental) disturbance

$$D_{ext,T} = \underbrace{\left[\begin{array}{ccc} D_{ext}^T & \cdots & D_{ext}^T \end{array} \right]^T}_{N-1 \text{ times}}$$

where D_{ext} *is introduced earlier in equation* (5.1) *and* $D_{ext,T}$ *is bounded by* B_{ext} *(i.e.,* $||D_{ext,T}|| < B_{ext}$*), is applied to the system* (5.39) *as given by* $\dot{E} = (A_T + (J(.) - J_\varepsilon)B(\beta))\, E + \bar{D}_{d,i}(t) + D_{ext,T}$*. Following along similar steps as those given for equation* (5.49) *above, equation* (5.50) *is now modified as follows*

$$||E(t)|| \leq B_E + T_E = B_{tot} \tag{5.51}$$

where

$$T_E \stackrel{\Delta}{=} \sup_{\substack{t \in R^+ \\ \forall k \in \{1,\ldots,N\}; \\ ||\varepsilon_k|| < B_{\varepsilon_k}}} \left\| \int_{\tau=0}^{t} G(t-\tau) B_{ext} d\tau \right\|$$

In order that the condition $B_{tot} \leq e_s$ *in equation* (5.51) *holds,* B_E *is replaced from equation* (5.50) *and* B_{tot} *is replaced by* e_s *as follows*

$$\sup_{t \in R^+} ||U^d(t)|| \leq \frac{e_s - T_E}{H_T} \tag{5.52}$$

which requires the FLFR module to impose the constraint (5.52) *on the desired input vector* $U^d(t)$*. This completes the proof of the theorem.* ■

In this chapter, the cases of centralized and decentralized cooperative fault accommodation strategies under relative measurements are proposed and developed. As mentioned in Remark 5.2, the decentralized approach is communicationally more efficient but propagates the effects of a local failure in the form of undesired tracking errors to all the subsystems of the formation. In contrast, the centralized approach confines the effects of a local failure and prevents its error propagation at the expense of more stringent communication requirements.

In the next chapter, the case of cooperative fault accommodation in a formation of multiple vehicles with absolute measurements will be formulated and studied.

5.4 Conclusions

In this chapter, a cooperative fault accommodation algorithm is proposed for formation flight of unmanned vehicles. Through this framework two recovery modules, namely low level fault recovery (LLFR) and formation level fault recovery (FLFR) modules are introduced. In the LLFR module, conventional recovery controllers are designed by incorporating fault severity estimation techniques. It is assumed that an estimate of an actuator fault parameter is available; however this estimate is possibly biased. Due to an inaccurate fault estimate and the resultant ineffective recovery controller, the HL supervisor detects violations of the formation flying mission performance specifications. The FLFR module is then activated to compensate for these performance degradations corresponding to the faulty and compromised vehicle by requiring that the healthy vehicles allocate and expend additional resources. Moreover, in case of multiple failures, the FLFR module implements robust controllers and imposes a constraint on the desired input vector. Therefore, actuator faults are cooperatively recovered through our proposed architecture, and the formation flight mission specifications are consequently satisfied.

Chapter 6

Cooperative Actuator Fault Accommodation in Formation Flight of Unmanned Vehicles with Absolute Measurements

In some applications of formation missions, such as the planetary orbital environment (POE) satellite formation [6] and the unmanned aerial vehicle (UAV) formation missions [131], the objective is to maintain a proper relative positioning among the vehicles while the vehicles move about the desired absolute trajectories in their inertial framework. In such applications, if the desired absolute trajectories of the vehicles are not properly taken into the control loop, then undesirable absolute positioning and catastrophic clashes may take place. This was not an issue of concern in the previous chapter for the case of relative-measurement formation applications such as deep-space satellite formations [6].

Consider the four-vehicle formation with absolute measurements, whose digraph is depicted in Figure 2.2. Assume that vehicle #2 is subject to an actuator fault. Furthermore, it is only partially recovered by the low-level fault recovery (LLFR) module due to the presence of possible biased and inaccurate fault estimates. Therefore, vehicle #2 tracks the desired trajectory within an error bound of radius r, which is greater than the error specification e_s that is defined for the mission (that is, $r > e_s$ as shown in Figure 2.2). The main purpose of the formation-level fault recovery (FLFR) module is to reconfigure the formation structure in terms of the weighted absolute measurement formation (WAMF) digraph (as per Definition 2.7), activate a robust controller for the partially LL-recovered vehicle, and impose a constraint on the desired inputs in order to compensate for the performance degradation of the formation mission (that is, $r < e_s$ as shown in Figure 2.2).

In the following sections, results are presented for the case of cooperative fault accommodation embedded with absolute measurements.

6.1 Preliminaries

6.1.1 State Space Model

In this section, we consider the general N-vehicle formation, whose special four-vehicle case is depicted in Figure 2.2. The vehicle $\#i$, $i \in \{1, ..., N\}$ (N is the total number of vehicles) is represented by a linear state space model as follows:

$$\begin{aligned} \dot{X}_i &= AX_i + B_iU_i + D_{ext} \\ Y_i &= CX_i = X_i \end{aligned} \tag{6.1}$$

where $X_i \in R^n$, $Y_i \in R^m$, and $U_i \in R^r$ are the state, input, and output vectors, respectively, in the local inertial frame, and the output matrix $C = I_{n\times n}$ ($I_{n\times n}$ is an identity matrix) denotes that the state vector is fully measured by the output sensors. The environmental disturbances are represented by $D_{ext} \in R^n$ and the actuators are modeled as ideal gains $B_i \in R^{n\times r}$ which are assumed to have full column rank (the system is not overactuated). The nominal (fault-free) value of B_i is represented by $\bar{B}$. In other words $B_i = \bar{B} + f_i$, where $f_i \in R^{n\times r}$ represents a loss-of-effectiveness actuator failure in the actuator B_i. According to Remark 5.1, our fault accommodation method will be mainly focused on the loss-of-effectiveness (LOE) actuator failure (as per equation (2.5)).

6.1.2 Centralized Scheme Versus Decentralized Scheme

In formation flight of N vehicles $\#i$, $i \in \{1, ..., N\}$ embedded with absolute measurements, the terminologies of an s-order neighbor set $\mathscr{N}^s$ (as in Definition 2.6) and adjacency matrix $\Omega = [\omega_{ij}]$ (as in Definition 2.7) can be applied to both centralized as well as decentralized controllers. Not withstanding the above, the differences are as follows:

- For the centralized controller we have $\forall i \in \{1, ..., N\}$: $\mathscr{N}(\{i\}) = \{1, ..., N\}$, whereas for the decentralized controller we have $\exists i \in \{1, ..., N\}$: $\mathscr{N}(\{i\}) \neq \{1, ..., N\}$ (or $\mathscr{N}(\{i\}) \subset \{1, ..., N\}$).
- For the centralized controller we have $\forall i \in \{1, ..., N\}$, $\forall j \in \{1, ..., N\}$: $\omega_{ij} \neq 0$, whereas for the decentralized controller we have $\exists i \in \{1, ..., N\}$, $\exists j \in \{1, ..., N\}$: $i \neq j$ and $\omega_{ij} = 0$.

This chapter is presented according to an absolute-measurement formation flight system having the general terms $\mathscr{N}^s$ and Ω regardless of being a centralized scheme or a

decentralized scheme. Therefore, the terms "centralized" and "decentralized" are omitted in the remainder of this chapter. This chapter results can be applied to both schemes alghough the outcomes will be normally different. In other words, based on this chapter results certain failure situations may be accommodated *only* by using a centralized control scheme whereas the decentralized control scheme may fail to accommodate the vehicles. One of the benefits of the centralized scheme over the decentralized scheme is minimized and nullified by the all-to-all communication requirement of this scheme.

6.2 Desired Formation Tracking Specifications

Consider that the desired trajectory of the vehicle $\#i$ is specified according to

$$\dot{X}_i^d = AX_i^d + \bar{B}U_i^d \tag{6.2}$$

where $X_i^d \in R^n$ and $U_i^d \in R^q$ are the desired state and input vectors, respectively. Therefore, the control signal

$$U_i = -K_i E_i + U_i^d \ , \ E_i = X_i - X_i^d$$

yields the following error dynamics

$$\dot{E}_i = (A - \bar{B}K_i)E_i$$

where K_i is the feedback gain that yields the desired closed-loop system by assuming that the pair (A, B) is controllable. For simplicity, in the following the effects of the environmental disturbances D_{ext} (as given in equation (6.1)) are ignored. However, these effects are analyzed and incorporated later in this chapter.

In formation missions, the reference trajectory X_i^r of the vehicle $\#i$ is a weighted summation of its own desired state X_i^d and its desired relative state $(X_k + X_{ki}^d)$, where $X_{ki}^d = X_i^d - X_k^d$, with respect to the vehicles $\#k$ $(\forall k \in \mathcal{N}(\{i\}))$ in its nearest neighbor set $\mathcal{N}(\{i\})$ (as per Definition 2.6). In other words, the reference trajectory X_i^r of the vehicle $\#i$ is calculated as follows:

$$X_i^r = \omega_{ii} X_i^d + \sum_{k \in \mathscr{N}(\{i\})} \omega_{ki}(X_k + X_i^d - X_k^d) \tag{6.3}$$

$$= \left(\sum_{k \in \mathscr{N}^+(\{i\})} \omega_{ki} \right) X_i^d + \sum_{k \in \mathscr{N}(\{i\})} \omega_{ki}(X_k - X_k^d)$$

$$= X_i^d + \sum_{k \in \mathscr{N}(\{i\})} \omega_{ki}(X_k - X_k^d)$$

$$= X_i^d - \sum_{k \in \mathscr{N}(\{i\})} \omega_{ki} E_k$$

where the nearest neighbor set $\mathscr{N}(\{i\})$ and inclusive nearest neighbor set $\mathscr{N}^+(\{i\})$ of the vehicle $\#i$ are defined in Definition 2.6. One immediate result that follows from the above equation is that

$$E_i^r = E_i - \sum_{k \in \mathscr{N}(\{i\})} \omega_{ki} E_k$$

where by taking $E^r = \begin{bmatrix} (E_1^r)^T & \cdots & (E_N^r)^T \end{bmatrix}^T$ and $E = \begin{bmatrix} (E_1)^T & \cdots & (E_N)^T \end{bmatrix}^T$ can be transformed into the following form

$$E^r = \left(\left(I_{N \times N} - \begin{bmatrix} 0 & \omega_{21} & \cdots & \omega_{N1} \\ \omega_{12} & 0 & \cdots & \omega_{N2} \\ \vdots & \vdots & \ddots & \vdots \\ \omega_{1N} & \omega_{2N} & \cdots & 0 \end{bmatrix} \right) \otimes I_{n \times n} \right) E \tag{6.4}$$

$$= \left((I_{N \times N} - \Omega) \otimes I_{n \times n} \right) E$$

where Ω is the adjacency matrix of the weighted absolute measurement formation (WAMF) digraph (as per Definition 2.7) and $\otimes$ denotes the Kronecker product. We present the following conditions to comply with the criteria of a formation mission.

Condition 6.1. *In a formation mission the following conditions must be satisfied:*

a) The WAMF digraph $G_{WAMF}(V_{WAMF}, E_{WAMF})$ (as per Definition 2.7) is connected.

b) $\det(I_{N \times N} - \Omega) \neq 0$.

c) In an ideal disturbance free environment if $E^r = 0$ *as* $t \to \infty$ *then* $E = 0$ *as* $t \to \infty$.

d) $\forall k \in \{1, ..., N\}$; $||E_k|| < e_s$, *where* e_s *represents the error specification of the formation mission.*

e) $|eig(\Omega)| < 1$, *where* $eig(.)$ *represents the eigenvalue of a matrix.*

Condition 6.1-(a) follows from the definition of any specific formation mission, Condition 6.1-(b) follows from the equation (6.4) to guarantee that the matrix Ω is full rank, and Condition 6.1-(c) guarantees that each vehicle state will finally converge to its desired trajectory although this reference trajectory is generated through getting feedback from all the vehicles in its nearest neighbor set. Condition 6.1-(e) guarantees that the series expansion of $\Sigma_{s=0}^{\infty}\Omega^{s}$ is valid and this property will be used later in the thesis. Regarding Condition 6.1-(d), the following remark is now stated.

Remark 6.1. *According to Condition 6.1-(d), the error specification* e_s *is to be satisfied in each vehicle #k with respect to the desired trajectory, that is* $||E_k|| < e_s$. *The equivalent condition for the reference trajectory tracking problem can be determined as follows. According to equation* (6.4), *we have* $E = ((I_{N\times N} - \Omega) \otimes I_{n\times n})^{-1} E^r$. *We conclude that*

$$||E_k|| < \Omega_{\max} \sum_{i=1}^{L_{\max}} ||E_i^r||$$

where $\Omega_{\max}$ *is the maximum element of the matrix* $((I_{N\times N} - \Omega) \otimes I_{n\times n})^{-1}$ *and* $L_{\max}$ *is the supremum over the maximum number of nonzero entities on the rows of* $((I_{N\times N} - \Omega) \otimes I_{n\times n})^{-1}$. *Therefore, a sufficient criterion to satisfy the Condition 6.1-(d) is*

$$||E_i^r|| < \frac{e_s}{\Omega_{\max} L_{\max}} \qquad \forall i \in \{1, ..., N\} \tag{6.5}$$

where $1 \leq \Omega_{\max}$ *and* $1 \leq L_{\max} \leq N$.

The reference state X_i^r of the vehicle $\#i$ forms the reference state space model as follows:

$$\dot{X}_i^r = AX_i^r + B_i U_i^r \tag{6.6}$$

The reference input vector U_i^r is derived by substituting for X_i^r from equation (6.3) into (6.6) to obtain

$$\left(\dot{X}_i^d + \sum_{k\in\mathcal{N}(\{i\})} \omega_{ki}(\dot{X}_k - \dot{X}_k^d)\right) = A\left(X_i^d + \sum_{k\in\mathcal{N}(\{i\})} \omega_{ki}(X_k - X_k^d)\right) + B_i U_i^r$$

$$\Rightarrow B_i U_i^r = (\dot{X}_i^d - AX_i^d) + \sum_{k\in\mathcal{N}(\{i\})} \omega_{ki}(\dot{X}_k - AX_k) - \sum_{k\in\mathcal{N}(\{i\})} \omega_{ki}(\dot{X}_k^d - AX_k^d) \tag{6.7}$$

$$\Rightarrow B_i U_i^r = B_i U_i^d + \sum_{k\in\mathcal{N}(\{i\})} \omega_{ki} B_k(U_k - U_k^d)$$

$$\Rightarrow U_i^r = U_i^d + \sum_{k\in\mathcal{N}(\{i\})} \omega_{ki}(B_i)_{left}^{-1} B_k(U_k - U_k^d)$$

where $(B_i)_{left}^{-1} = (B_i^T B_i)^{-1} B_i^T$ is the left inverse of the matrix B_i. Using the reference input U_k^r, the vehicle $\#k$ implements the control law

$$U_k = -K_k E_k^r + U_k^r \ , \ E_k^r = X_k - X_k^r$$

in order to yield the following error dynamics

$$\dot{E}_k^r = (A - B_k K_k) E_k^r$$

where K_k is the feedback gain that is designed according to the following lemma.

Lemma 6.1. *Consider the system governed by the dynamic equation $\dot{E}_k^r = (A - B_k K_k)E_k^r$ with the initial state $E_k^r(0)$. The state feedback matrix $K_k = YX^{-1}$ stabilizes the system and minimizes $\gamma_1 + \gamma_2$, where γ_1 is an upper bound on the H_∞ norm of the transfer function from the disturbance to the output of the system and γ_2 is an upper bound on the linear quadratic cost function $J_{LQR}(K_k E_k^r, Q, R)$ in Lemma 2.3, if and only if there exist a matrix Y and a positive definite matrix $X > 0$ that satisfy the following optimization problem*

$$\begin{aligned}
&Minimize \quad \gamma_1 + \gamma_2 \\
&subject\ to \\
&X > 0 \\
&\begin{bmatrix} AX + XA^T + B_k Y + Y^T {B_k}^T & I & X \\ I & -\gamma_1 I & 0 \\ X & 0 & -\gamma_1 I \end{bmatrix} < 0 \\
&\begin{bmatrix} AX + XA^T + B_k Y + Y^T {B_k}^T & X & Y^T \\ X & -Q^{-1} & 0 \\ Y & 0 & -R^{-1} \end{bmatrix} \leq 0 \\
&\begin{bmatrix} \gamma_2 & (E_k^r)^T(0) \\ E_k^r(0) & X \end{bmatrix} \geq 0
\end{aligned}$$

Proof: *Follows from the results in [136] and [134], and those in Lemmas 2.2 and 2.3.* ■

Therefore, we have

$$U_i^r = U_i^d + \sum_{k \in \mathscr{N}(\{i\})} \omega_{ki} (B_i)_{left}^{-1} B_k (-K_k E_k^r + U_k^r - U_k^d)$$

Taking $U^r = \begin{bmatrix} (U_1^r)^T & \cdots & (U_N^r)^T \end{bmatrix}^T$, $U^d = \begin{bmatrix} (U_1^d)^T & \cdots & (U_N^d)^T \end{bmatrix}^T$, and $K_T = diag \begin{pmatrix} K_1 & \cdots & K_N \end{pmatrix}$ the reference input vector U^r is obtained from

$$\begin{aligned} &(I_{Nr \times Nr} - \Omega_0) U^r = (I_{Nr \times Nr} - \Omega_0) U^d - \Omega_0 K_T E^r \\ &\Rightarrow U^r = U^d - (I_{Nr \times Nr} - \Omega_0)^{-1} \Omega_0 K_T E^r \end{aligned} \tag{6.8}$$

where $\Omega_0 = diag \left((B_i)_{left}^{-1} \right)_{i=1}^N (\Omega \otimes I_{r \times r}) \, diag \, (B_i)_{i=1}^N$. By invoking the matrix geometric series $(I - M)^{-1} = \Sigma_{s=0}^{\infty} \mathrm{M}^{\mathrm{s}}$ with $\mathrm{M}^0 \triangleq \mathrm{I}$, we get

$$U^r = U^d - \sum_{s=1}^{\infty} \Omega_0^s K_T E^r \tag{6.9}$$

In practice, equation (6.8) can be used to determine the reference inputs of the vehicles. However, equation (6.9) is used below to determine the information that is required to be exchanged among the vehicles in order to generate their reference inputs. The matrix Ω_0^s in equation (6.9) corresponds to all possible paths of length s in the WAMF digraph (as per Definition 2.7). The summation term in equation (6.9) adds up an infinite number of terms Ω_0^s $(s = 1, 2, ...)$. However, in reality only a finite number of terms Ω_0^s $(s < N)$ are used to determine the information requirement for each vehicle. This is due to the fact that in the WAMF digraph, the maximum length of a path with no redundant vertex is equal to $N - 1$.

Remark 6.2. *In equation* (6.9)*, the term* Ω_0^s *indicates that in a fault free and disturbance free environment (that is,* $B_i = \bar{B}$ *and* $D_{ext} = 0_{n \times 1}$*), each vehicle #i (*$i \in \{1, , ..., N\}$*) requires the error vectors* E_j^r *of vehicles #j,* $\forall j \in \mathscr{N}^{[1,\infty]}(\{i\}) = \cup_{s=1}^{\infty} \mathscr{N}^s(\{i\})$ *(as per Definition 2.6) in order to generate the reference input* U_i^r *for its reference model* (6.6)*.*

In the next section, the problem of actuator fault recovery is considered at the low level (LL) by incorporating the fault estimates in the LLFR controllers.

6.3 Low-Level Fault Recovery (LLFR) Controller

In this section, we assume that the system is fault free or that one has the index set $\{i_1, i_2, ..., i_{N_F}\}$ of all the N_F faulty vehicles #k, $k \in \{i_1, i_2, ..., i_{N_F}\}$ with an accurate fault

estimate. In the later case of N_F faulty vehicles, we assume that the actuators of the faulty vehicles $\#k$, $k \in \{i_1, ..., i_{N_F}\}$ are subject to loss-of-effectiveness (LOE) failures as in equation (6.2), that is $B_k = \bar{B} + f_k$. Moreover, we assume that the fault estimates are unbiased, that is $\hat{f}_k = f_k + \varepsilon_k$ (or $\hat{B}_k = B_k + \varepsilon_k$) with $\varepsilon_k = 0$. Therefore, these accurate estimates are incorporated into the controllers that are designed from Lemma 6.1 so that the LLFR controllers are obtained.

In case when $\varepsilon_k = 0_{n\times r}$, $k \in \{i_1, i_2, ..., i_{N_F}\}$, the reference input vector U_k^r in the reference model (6.6) should be calculated based on the existing estimate $\hat{B}_k = B_k$. For simplicity and without loss of generality, B_i ($i \in \{1, , ..., N\}$) can be replaced by $\hat{B}_i$ for both cases of a fault free vehicle $\#i$ ($i \in \{1, , ..., N\} - \{i_1, i_2, ..., i_{N_F}\}$) and a faulty vehicle $\#i$ ($i \in \{i_1, i_2, ..., i_{N_F}\}$) with an accurate fault estimate. This substitution is incorporated in equation (6.7) as follows

$$\hat{B}_i U_i^r = (\dot{X}_i^d - AX_i^d) + \sum_{k\in\mathscr{N}(\{i\})} \omega_{ki}(\dot{X}_k - AX_k) - \sum_{k\in\mathscr{N}(\{i\})} \omega_{ki}(\dot{X}_k^d - AX_k^d)$$

or equivalently

$$\hat{B}_i U_i^r = \bar{B}U_i^d + \sum_{k\in\mathscr{N}(\{i\})} \omega_{ki}\hat{B}_k U_k - \sum_{k\in\mathscr{N}(\{i\})} \omega_{ki}\bar{B}U_k^d \tag{6.10}$$

One now obtains

$$U_i^r = (\hat{B}_i)_{left}^{-1}\bar{B}U_i^d + \sum_{k\in\mathscr{N}(\{i\})} \omega_{ki}(\hat{B}_i)_{left}^{-1}\hat{B}_k \underbrace{(-K_k E_k^r + U_k^r)}_{U_k} - \sum_{k\in\mathscr{N}(\{i\})} \omega_{ki}(\hat{B}_i)_{left}^{-1}\bar{B}U_k^d$$

(K_k is designed according to Lemma 6.1) which gives

$$(I_{Nr\times Nr} - \hat{\Omega}_0)U^r = (I_{Nr\times Nr} - \hat{\Omega}_1)U^d - \hat{\Omega}_0 K_T E^r$$

This is equivalent to

$$U^r = (I_{Nr\times Nr} - \hat{\Omega}_0)^{-1}(I_{Nr\times Nr} - \hat{\Omega}_1)U^d - (I_{Nr\times Nr} - \hat{\Omega}_0)^{-1}\hat{\Omega}_0 K_T E^r \tag{6.11}$$

where

$$\hat{\Omega}_0 = diag\left((\hat{B}_i)_{left}^{-1}\right)_{\mathrm{i=1}}^{\mathrm{N}} (\Omega \otimes I_{r\times r})\, diag\left(\hat{B}_i\right)_{\mathrm{i=1}}^{\mathrm{N}}$$

$$\hat{\Omega}_1 = diag\left((\hat{B}_i)_{left}^{-1}\right)_{\mathrm{i=1}}^{\mathrm{N}} (\Omega \otimes I_{r\times r})\, diag\left(\bar{B}\right)_{\mathrm{i=1}}^{\mathrm{N}}$$

Using the matrix geometric series $(I-M)^{-1}=\Sigma_{s=0}^{\infty}\mathrm{M}^{\mathrm{s}}$ with $\mathrm{M}^{0}\triangleq\mathrm{I}$, we have

$$U^r=(\Sigma_{s=0}^{\infty}\hat{\Omega}_0^s)(I_{Nr\times Nr}-\hat{\Omega}_1)U^d-\left(\Sigma_{s=1}^{\infty}\hat{\Omega}_0^s\right)K_TE^r \tag{6.12}$$

$$=U^d+\Sigma_{s=0}^{\infty}\hat{\Omega}_0^s(\hat{\Omega}_0-\hat{\Omega}_1)U^d-\left(\Sigma_{s=1}^{\infty}\hat{\Omega}_0^s\right)K_TE^r$$

In practice, equation (6.11) can be used to determine the reference inputs of the vehicles. However, equation (6.12) is used below to determine the information that is required to be exchanged among the vehicles in order to generate their reference inputs.

Remark 6.3. *In equation* (6.12)*, the term* Ω_0^s *indicates that in a disturbance free environment, each vehicle #i (*$i\in\{1,,...,N\}$*) requires the error vectors* E_j^r *of vehicles #j (*$\forall j\in\mathscr{N}^{[1,\infty]}(\{i\})=\cup_{s=1}^{\infty}\mathscr{N}^s(\{i\})$ *as per Definition 2.6). Moreover, the term* $\hat{\Omega}_0^s(\hat{\Omega}_0-\hat{\Omega}_1)$ *indicates that each vehicle #i (*$i\in\{1,,...,N\}$*) requires the desired input vectors* U_k^d *of the faulty vehicles #k (*$\forall k\in\mathscr{N}^{[1,\infty]}(\{i\})=\cup_{s=1}^{\infty}\mathscr{N}^s(\{i\})$ *;* $k\in\{i_1,i_2,...,i_{N_F}\}$*) in order to generate the reference input* U_i^r *for its reference model* (6.6)*.*

In case that the actuator fault estimate of a faulty vehicle $\#k$, $k\in\{i_1,i_2,...,i_{N_F}\}$ is biased, that is $\varepsilon_k\neq 0$, and the error specification (e_s) of the formation flight of unmanned vehicles mission is violated, the vehicle $\#k$ is partially recovered by the LLFR module. Consequently, the formation level fault recovery (FLFR) module will be activated to account for the performance degradations of the partially LL-recovered vehicle $\#k$. The results for the cooperative FLFR module will be presented in the next section.

6.4 Formation-Level Fault Recovery (FLFR) Module

Consider the case of a partially LL-recovered vehicle $\#k$, $k\in\{i_1,i_2,...,i_{N_F}\}$ due to the biased estimate of its actuator fault, that is $\hat{f}_k\neq f_k$ $(\hat{B}_k\neq B_k)$ or $\hat{f}_k=f_k+\varepsilon_k$ (or $\hat{B}_k=B_k+\varepsilon_k$), where $\varepsilon_k\neq 0$ is an unknown function but bounded ($||\varepsilon_k||<B_{\varepsilon_k}$ with B_{ε_k} known). In order to accommodate a partially LL-recovered vehicle $\#k$, the FLFR module reconfigures the formation structure in terms of the weighted absolute measurement formation (WAMF) digraph (as per Definition 2.7) according to Theorem 6.1. It also activates a robust controller for the partially LL-recovered vehicle according to Theorem 6.2. Moreover, it imposes a constraint on the overall desired input vector of all the vehicles in the s-order ($s<N$) neighbor set of the partially LL-recovered vehicle according to Theorem 6.3 in order to compensate for the performance degradations of the formation flight of unmanned vehicles.

Theorem 6.1. *If a vehicle #k, $k \in \{i_1, i_2, ..., i_{N_F}\}$ is partially recovered by the LLFR module due to a biased estimate $\hat{B}_k = B_k + \varepsilon_k$ with $\varepsilon_k \neq 0_{n\times r}$, then the FLFR module needs to set $\omega_{ki} = 0$ ($\forall i \in \{1, , ..., N\}$; $i \neq k$) in order to satisfy the Condition 6.1-(c).*

Proof: *For a vehicle #i, $i \in \{1, , ..., N\}$ we start with the equation* (6.10)*. For simplicity and without loss of generality, the term $\hat{B}_k U_k$ ($k \in \{1, , ..., N\}$) in equation* (6.10) *can be replaced by $(B_k + \varepsilon_k)U_k$ for all the three cases of a fault free vehicle #k ($k \in \{1, , ..., N\} - \{i_1, i_2, ..., i_{N_F}\}$), a faulty vehicle #k ($k \in \{i_1, i_2, ..., i_{N_F}\}$) with accurate fault estimate, and a partially LL-recovered vehicle #k ($k \in \{i_1, i_2, ..., i_{N_F}\}$). It should be noted that only in the later case we have $\varepsilon_k \neq 0$. This replacement is incorporated in equation* (6.7) *as follows:*

$$\hat{B}_i U_i^r = \bar{B} U_i^d + \sum_{k\in\mathscr{N}(\{i\})} \omega_{ki}(B_k + \varepsilon_k)U_k - \sum_{k\in\mathscr{N}(\{i\})} \omega_{ki}\bar{B}U_k^d$$

$$\Rightarrow \hat{B}_i U_i^r = \bar{B} U_i^d + \sum_{k\in\mathscr{N}(\{i\})} \omega_{ki} B_k U_k - \sum_{k\in\mathscr{N}(\{i\})} \omega_{ki}\bar{B}U_k^d + \sum_{k\in\mathscr{N}(\{i\})} \omega_{ki}\varepsilon_k U_k$$

$$\Rightarrow \hat{B}_i U_i^r = (\dot{X}_i^d - AX_i^d) + \sum_{k\in\mathscr{N}(\{i\})} \omega_{ki}(\dot{X}_k - AX_k)$$

$$- \sum_{k\in\mathscr{N}(\{i\})} \omega_{ki}(\dot{X}_k^d - AX_k^d) + \sum_{k\in\mathscr{N}(\{i\})} \omega_{ki}\varepsilon_k U_k$$

$$\Rightarrow \underbrace{\hat{B}_i U_i^r}_{\dot{X}_i^r - AX_i^r} - \dot{X}_i^d - \sum_{k\in\mathscr{N}(\{i\})} \omega_{ki}(\dot{X}_k - \dot{X}_k^d) + AX_i^d + A\sum_{k\in\mathscr{N}(\{i\})} \omega_{ki}(X_k - X_k^d)$$

$$= \sum_{k\in\mathscr{N}(\{i\})} \omega_{ki}\varepsilon_k U_k$$

$$\Rightarrow \frac{d}{dt}\left(X_i^r - X_i^d - \sum_{k\in\mathscr{N}(\{i\})} \omega_{ki}(X_k - X_k^d)\right) - A\left(X_i^r - X_i^d - \sum_{k\in\mathscr{N}(\{i\})} \omega_{ki}(X_k - X_k^d)\right)$$

$$= \sum_{k\in\mathscr{N}(\{i\})} \omega_{ki}\varepsilon_k U_k$$

$$\Rightarrow X_i^r - X_i^d - \sum_{k\in\mathscr{N}(\{i\})} \omega_{ki}(X_k - X_k^d) = \sum_{k\in\mathscr{N}(\{i\})} \omega_{ki} \int_{\tau=0}^{t} \exp(-A\tau)\varepsilon_k U_k(t-\tau)d\tau \triangleq \chi_i(t)$$

Therefore, similar to equation (6.4) *we get*

$$E^r = ((I_{N\times N} - \Omega) \otimes I_{n\times n})\, E + \chi(t)\ ,\ \chi(t) = \left[\ \chi_1^T(t) \quad \cdots \quad \chi_N^T(t)\ \right]^T$$

which indicates that Condition 6.1-(c) is not satisfied. Therefore, if a vehicle #k ($k \in \{i_1, i_2, ..., i_{N_F}\}$) is partially LL-recovered, that is $\varepsilon_k \neq 0$, then one needs to choose $\omega_{ki} = 0$, $\forall i \neq k$ in order to obtain $\chi_i(t) = 0$, which guarantees the Condition 6.1-(c). ■

For a non-faulty or fully LL-recovered vehicle #i ($\varepsilon_i = 0_{n\times r}$), the local state feedback matrix K_i can be appropriately selected by using Lemma 6.1 such that the control signal $U_i = -U_i^r + K_i E_i^r$ results in the desired closed-loop error dynamics $\dot{E}_i^r = (A + \hat{B}_i K_i)E_i^r$.

Now, consider the overall formation flight mission dynamics and its reference model as follows

$$\dot{X} = A_T X + B_T U$$

$$\dot{X}^r = A_T X^r + \hat{B}_T U^r$$

where

$$A_T = diag(A)_{k=1}^N$$

$$K_T = diag(K_i)_{k=1}^N$$

$$B_T = diag(B_k)_{k=1}^N$$

$$\varepsilon = diag(\varepsilon_k)_{k=1}^N$$

$$\hat{B}_T = diag(\hat{B}_k)_{k=1}^N = B_T + \varepsilon$$

Due to the biased estimate of certain faults, that is $\varepsilon \neq 0_{Nn\times Nr}$, the overall closed-loop error dynamics becomes:

$$\dot{E}^r = (A_T + \hat{B}_T K_T - \varepsilon K_T)E^r + \varepsilon U^r$$

Using the reference input given by equation (6.11) we have

$$\dot{E}^r = \left(A_T + \hat{B}_T K_T \underbrace{-\varepsilon(I_{Nr\times Nr} + (I_{Nr\times Nr} - \hat{\Omega}_0)^{-1}\hat{\Omega}_0)}_{\Delta\hat{B}_T} K_T \right) E^r \tag{6.13}$$

$$+ \varepsilon(I_{Nr\times Nr} - \hat{\Omega}_0)^{-1}(I_{Nr\times Nr} - \hat{\Omega}_1)U^d$$

For a partially LL-recovered vehicle #i ($\varepsilon_i \neq 0_{n\times r}$), the nominal (disturbance-free) state space model is represented by $\dot{E}_i^r = (A + (\hat{B}_i + \Delta\hat{B}_i(\varepsilon_i))K_i)E_i^r$ with $\Delta\hat{B}_i(\varepsilon_i) =$

$(\Delta\hat{B}_T)_{[i,i]_{n\times r}}$, where the index $[i,j]_{a\times b}$ is defined according to Definition 2.8. In the following, a robust state feedback gain K_i is designed for the uncertain model (6.13) of the partially LL-recovered vehicle #i.

Theorem 6.2. *Consider a partially LL-recovered vehicle #i whose nominal (disturbance-free) state space model is represented by $\dot{E}_i^r = (A + (\hat{B}_i + \Delta\hat{B}_i(\varepsilon_i))K_i)E_i^r$ with the initial state $E_i^r(0)$, as in equation (6.13). In general, the matrix $\varepsilon_i \in R^{n\times r}$ includes N_{ε_i} ($N_{\varepsilon_i} \leq nr$) uncertain (nonzero) elements ε_{ij} ($j = 1, ..., N_{\varepsilon_i}$) and $nr - N_{\varepsilon_i}$ zero elements. The state feedback matrix $K_i = Y_i X_i^{-1}$ stabilizes the system and minimizes $\gamma_1 + \gamma_2$, where γ_1 is an upper bound on the H_∞ norm of the transfer function from the disturbance to the output of the system and γ_2 is an upper bound on the linear quadratic cost function $J_{LQR}(K_i E_i^r, Q, R)$ in Lemma 2.3, if there exist a matrix Y_i and a positive definite matrix $X_i > 0$ that satisfy the following optimization problem*

$$
\begin{aligned}
&\textit{Minimize } \gamma_1 + \gamma_2 \\
&\textit{s.t. } X_i > 0 \textit{ and for } \varepsilon_i \in \{\varepsilon_i^{j+}, \varepsilon_i^{j-}\}\ ,\ j = 1,...,\mathrm{N}_{\varepsilon_\mathrm{i}}: \\
&\begin{bmatrix} AX_\mathrm{i} + X_\mathrm{i}A^T + (\hat{B}_i + \Delta\hat{B}_i(\varepsilon_i))Y_\mathrm{i} + Y_i^T(\hat{B}_i + \Delta\hat{B}_i(\varepsilon_i))^T & I & X_\mathrm{i} \\ I & -\gamma_1 I & 0 \\ X_\mathrm{i} & 0 & -\gamma_1 I \end{bmatrix} < 0 \\
&\begin{bmatrix} AX_i + X_iA^T + (\hat{B}_i + \Delta\hat{B}_i(\varepsilon_i))Y_i + Y_i^T(\hat{B}_i + \Delta\hat{B}_i(\varepsilon_i))^T & X_i & Y_i^T \\ X_i & -Q^{-1} & 0 \\ Y_i & 0 & -R^{-1} \end{bmatrix} \leq 0 \\
&\begin{bmatrix} \gamma_2 & (E_i^r)^T(0) \\ E_i^r(0) & X_i \end{bmatrix} \geq 0
\end{aligned}
\tag{6.14}
$$

in which the terms ε_i^{j+} and ε_i^{j-} are defined as

$$
\varepsilon_i^{j+} = \varepsilon_i|_{\varepsilon_{ij}=+N_{\varepsilon_i}^R B_{\varepsilon_i}, \varepsilon_{ik}=0(k\neq j)}\ ,\ \varepsilon_i^{j-} = \varepsilon_i|_{\varepsilon_{ij}=-N_{\varepsilon_i}^R B_{\varepsilon_i}, \varepsilon_{ik}=0(k\neq j)} \tag{6.15}
$$

where ε_{ij} (j = 1,...,$\mathrm{N}_{\varepsilon_\mathrm{i}}$) are the uncertain (nonzero) elements of the matrix ε_i, and N_{ε_i} and $N_{\varepsilon_i}^R$ represent the number of nonzero elements and rows of the matrix ε_i, respectively.

Proof: *The proof is similar to that of Lemma 6.1. The objective is to satisfy the LMI conditions in (6.14). These LMI conditions cannot be directly verified since the matrix ε_i is unknown. However, the unknown matrix ε_i is bounded, that is $||\varepsilon_i|| < B_{\varepsilon_i}$ (*k = 1,...,$\mathrm{N}_{\varepsilon_\mathrm{i}}$*). Therefore, the summation of the absolute values of the uncertain (nonzero) elements on each row of the matrix ε_i is less than B_{ε_i}. This implies that the sum of the absolute values of the uncertain (nonzero) elements on all $N_{\varepsilon_i}^R$ rows of the matrix ε_i is less than $N_{\varepsilon_i}^R B_{\varepsilon_i}$, that is*

$$\sum_{j=1}^{\mathrm{N}_{\varepsilon_\mathrm{i}}} ||\varepsilon_{ij}|| < N_{\varepsilon_i}^R B_{\varepsilon_i} \tag{6.16}$$

The condition (6.16) *can be represented by a convex polygon region in the* N_{ε_i}*-dimensional space corresponding to* $\begin{bmatrix} \varepsilon_{i1} & \varepsilon_{i2} & \cdots & \varepsilon_{iN_{\varepsilon_i}} \end{bmatrix}^T$*. This convex region is surrounded and covered by the vertices*

$$\begin{bmatrix} +N_{\varepsilon_i}^R B_{\varepsilon_i} \\ 0 \\ \vdots \\ 0 \end{bmatrix}, \begin{bmatrix} -N_{\varepsilon_i}^R B_{\varepsilon_i} \\ 0 \\ \vdots \\ 0 \end{bmatrix}, \begin{bmatrix} 0 \\ +N_{\varepsilon_i}^R B_{\varepsilon_i} \\ \vdots \\ 0 \end{bmatrix}, \begin{bmatrix} 0 \\ -N_{\varepsilon_i}^R B_{\varepsilon_i} \\ \vdots \\ 0 \end{bmatrix} \tag{6.17}$$
$$, ..., \begin{bmatrix} 0 \\ 0 \\ \vdots \\ +N_{\varepsilon_i}^R B_{\varepsilon_i} \end{bmatrix}, \begin{bmatrix} 0 \\ 0 \\ \vdots \\ -N_{\varepsilon_i}^R B_{\varepsilon_i} \end{bmatrix}$$

Now, if the LMI conditions in (6.14) *hold for the vertices in* (6.17)*, then they hold for all values of the unknown matrix* ε_i*. Therefore, if there exists a matrix* Y_i *and a positive definite matrix* $X_i > 0$ *that satisfy the LMI conditions in* (6.14) *for* $\varepsilon_i \in \{\varepsilon_i^{j+}, \varepsilon_i^{j-}\}$*,* $j = 1, ..., N_{\varepsilon_i}$*, then* Y_i *and* X_i *satisfy the LMI conditions in* (6.14) *for the unknown matrix* ε_i*, and therefore the solution to the* H_∞ *optimal feedback matrix* K_i *is calculated according to* $K_i = Y_i X_i^{-1}$*.* ■

Now that the robust controllers are designed, in the following a constraint will be imposed on certain desired input vectors in order to ensure that the error specification is satisfied.

Theorem 6.3. *Assume that the error specification* (e_s) *of the formation mission is violated by the partially LL-recovered vehicle* $\#k$*, and that the FLFR module takes* $\omega_{ki} = 0$*,* $\forall i \neq k$ *according to Theorem 6.1 and implements the robust controller according to Theorem 6.2 for the partially LL-recovered vehicle* $\#k$*. In order to satisfy the error specification* (e_s)*, the FLFR module has to impose a constraint on the desired input vector* $U^d_{\mathscr{N}^{+[1,\infty]}(\{k\})}$*, which is defined as*

$$U^d_{\mathscr{N}^{+[1,\infty]}(\{k\})} \triangleq \tag{6.18}$$
$$\left(diag\left(Logic\left\{1 \in \mathscr{N}^{+[1,\infty]}(\{k\})\right\}, \cdots, Logic\left\{N \in \mathscr{N}^{+[1,\infty]}(\{k\})\right\}\right) \otimes I_{r\times r}\right) U^d$$

where

$$Logic\left\{i \in \mathscr{N}^{+[1,\infty]}(\{k\})\right\} \triangleq \begin{cases} 1 & i \in \mathscr{N}^{+[1,\infty]}(\{k\}) \\ 0 & i \notin \mathscr{N}^{+[1,\infty]}(\{k\}) \end{cases}$$

Proof: *Taking $\omega_{ki} = 0$, $\forall i \neq k$ as in Theorem 6.1, the dynamics of all the vehicles become independent from that of the partially LL-recovered vehicle #k, and hence the tracking error of vehicle #k does not propagate to the entire formation flight system. Taking*

$$\mathrm{T}_{\varepsilon_k} = \begin{bmatrix} 0_{r\times r} & \cdots & 0_{r\times r} & I_{r\times r} & 0_{r\times r} & \cdots & 0_{r\times r} \end{bmatrix}$$

where there are a total of N blocks, out of which the k^{th} block is nonzero and all other N-1 blocks are zero. Using the robust controller as in Theorem 6.2, the tracking error dynamics of the partially LL-recovered vehicle #k becomes

$$\dot{E}_k^r = (A + (\hat{B}_k + \Delta\hat{B}_k)K_k)E_k^r$$

$$+ \varepsilon_k \mathrm{T}_{\varepsilon_k}(I_{Nr\times Nr} - \hat{\Omega}_0)^{-1}(I_{Nr\times Nr} - \hat{\Omega}_1)U^d(t)$$

whose Laplace transform is given by

$$E_k^r(s) = \underbrace{(sI - A - (\hat{B}_k + \Delta\hat{B}_k)K_k)^{-1}}_{G_k(s)} \varepsilon_k T_{\varepsilon_k}(I_{Nr\times Nr} - \hat{\Omega}_0)^{-1}(I_{Nr\times Nr} - \hat{\Omega}_1)U^d_{\mathscr{N}^{+[1,\infty]}(\{k\})}(s)$$

where $G_k(s)$ is the transfer function matrix, and $U^d(s)$ is now replaced by $U^d_{\mathscr{N}^{+[1,\infty]}(\{k\})}(s)$. This is due to the term $T_{\varepsilon_k}(I_{Nr\times Nr} - \hat{\Omega}_0)^{-1}(I_{Nr\times Nr} - \hat{\Omega}_1)$ above, for which a similar argument as in Remark 6.3 (for equations (6.11) and (6.12)) can be made to show that the coefficients of U_i^d, $\forall i \in \mathscr{N}^{+[1,\infty]}(\{k\}) = \cup_{s=0}^{\infty}\mathscr{N}^s(\{k\})$ are nonzero and the coefficients of U_i^d, $\forall i \notin \mathscr{N}^{+[1,\infty]}(\{k\}) = \cup_{s=0}^{\infty}\mathscr{N}^s(\{k\})$ are zero. It is for this reason that the operator Logic$\{.\}$ is used in the definition of $U^d_{\mathscr{N}^{+[1,\infty]}(\{k\})}$ in equation (6.18). Taking

$$H_k \triangleq \sup_{\substack{t\in R^+ \\ ||\varepsilon_k|| < B_{\varepsilon_k}}} \left\| \int_{\tau=0}^{t} G_k(t-\tau)\varepsilon_k T_{\varepsilon_k}(I_{Nr\times Nr} - \hat{\Omega}_0)^{-1}(I_{Nr\times Nr} - \hat{\Omega}_1)d\tau \right\|$$

we get

$$||E_k^r(t)|| \leq H_k \sup_{t\in R^+} ||U^d_{\mathscr{N}^{+[1,\infty]}(\{k\})}(t)|| = B_{E_k^r} \tag{6.19}$$

Let us now assume that an external (environmental) disturbance D_{ext}, that is bounded by B_{ext} (i.e., $||D_{ext}|| < B_{ext}$), is applied to the formation flight system as indicated in (6.1). *Following along the similar steps above, equation* (6.19) *is now modified as follows*

$$||E_k^r(t)|| \leq B_{E_k^r} + T_{E_k^r} = B_{tot} \tag{6.20}$$

where

$$T_{E_k^r} \triangleq \sup_{\substack{t \in R^+ \\ ||\varepsilon_k|| < B_{\varepsilon_k}}} \left\| \int_{\tau=0}^{t} G(t-\tau) B_{ext} d\tau \right\|$$

Using the equation (6.5) *of Remark 6.1, the sufficient condition for the error specification to be satisfied is that*

$$B_{tot} < \frac{e_s}{\Omega_{\max} L_{\max}}$$

Replacing for $B_{E_k^r}$ and B_{tot} from equations (6.19) *and* (6.20), *respectively, we obtain*

$$\sup_{t \in R^+} ||U^d_{\mathscr{N}^{+[1,\infty]}(\{k\})}(t)|| < \frac{1}{H_k} \left(\frac{e_s}{\Omega_{\max} L_{\max}} - T_{E_k^r} \right) \tag{6.21}$$

which requires the FLFR module imposes a constraint on the desired input vector $U^d_{\mathscr{N}^{+[1,\infty]}(\{k\})}(t)$. This completes the proof of the theorem. ■

In this section, the FLFR module is developed for a single partially LL-recovered vehicle. In case that multiple vehicles are partially LL-recovered in the formation, the concept of a supporting neighbor is introduced and formulated in the next section.

6.5 FLFR Module Using Supporting Neighbor (SN) for Multiple Actuator Failures

Theorem 6.1 implies that if a vehicle $\#k$ is partially recovered ($\varepsilon_k \neq 0$) by the LLFR module, then it is disqualified by the FLFR module to be in the nearest neighbor set of other vehicles. Moreover, Theorem 6.3 implies that the FLFR module imposes constraints on all the vehicles in the s-order ($s < N$) neighbor set (as per Definition 2.6) of the partially LL-recovered vehicle $\#k$. This constraint is in terms of the desired input vectors as formulated in equation (6.21).

Consider the index set $\{i_1, i_2, ..., i_{N_F}\}$ of all the N_F partially LL-recovered vehicles $\#i_k$ ($i_k \in \{i_1, i_2, ..., i_{N_F}\}$). In order to localize the effects of actuator faults and prevent their corresponding errors from propagation to the entire formation, one can take $\omega_{i_k j} = 0$, $\forall i_k \in \{i_1, i_2, ..., i_{N_F}\}$ and $\forall j \notin \{i_1, i_2, ..., i_{N_F}\}$ (as per Theorem 6.1). On the other hand,

in order to minimize the number of constrained vehicles in the s-order neighbor set (as per Theorem 6.3), one can choose a unique non-faulty or fully LL-recovered vehicle $\#i_{SN}$ ($i_{SN} \notin \{i_1, i_2, ..., i_{N_F}\}$) as a supporting neighbor (SN), such that:

a) the supporting neighbor does not have any neighbor, that is $\mathcal{N}(\{i_{SN}\}) = \emptyset$, and

b) the partially LL-recovered vehicles $\#i_k$ ($i_k \in \{i_1, i_2, ..., i_{N_F}\}$) do not have any other neighbor than the supporting neighbor, that is $\mathcal{N}(\{i_k\}) = \{i_{SN}\}, \forall i_k \in \{i_1, i_2, ..., i_{N_F}\}$.

If the two conditions above are satisfied, then instead of N_F conditions (6.21) (corresponding to the N_F partially LL-recovered vehicles $\{i_1, i_2, ..., i_{N_F}\}$) one can satisfy the following single condition:

$$\sup_{t \in R^+} ||U^d_{\{i_1, i_2, ..., i_{N_F}, i_{SN}\}}(t)|| < \frac{1}{H_k} \left(\frac{e_s}{\Omega_{\max} L_{\max}} - T_{E_k^r} \right) \tag{6.22}$$

where

$$U^d_{\{i_1, i_2, ..., i_{N_F}, i_{SN}\}}(t) = \left[\begin{array}{cccc} (U^d_{i_1})^T & (U^d_{i_2})^T & \cdots & (U^d_{i_F})^T \quad (U^d_{i_{SN}})^T \end{array} \right]^T$$

Compared to the number of vehicles in the s-order ($s < N$) neighbor sets whose desired inputs are constrained by the N_F conditions (6.21), the number of vehicles in the s-order neighbor sets here reduces to one (corresponding to the one supporting neighbor $\#i_{SN}$) whose desired input is constrained by the single condition (6.22). The vehicle $\#i_{SN}$ is called a supporting neighbor since its desired input vector $U^d_{i_{SN}}$ needs to be adjusted (or constrained by equation (6.22)) in order to accommodate the performance deficiencies of the partially LL-recovered vehicles $\#i_k$ ($i_k \in \{i_1, i_2, ..., i_{N_F}\}$). However, the drawback of the above method is that one cannot design an arbitrary absolute measurement formation (AMF) digraph for the formation mission. In other words, by using the supporting neighbor technique one in fact constrains the flexibility in choosing the desired formation digraph.

6.6 Conclusions

In this chapter, a cooperative fault accommodation algorithm is proposed for multiple-vehicle formation flying missions embedded with absolute measurements. This framework provides two recovery modules, namely a low-level fault recovery (LLFR) module and a formation-level fault recovery (FLFR) module. In the LLFR module, a conventional recovery controller (RC) based on a given fault severity estimate is employed. In case that the LLFR controller cannot fully recover the faulty vehicle due to an imprecise fault estimate, the error bounds imposed by the mission specifications can be violated and

the supervisor identifies this violation and activates the FLFR module. This module is responsible for reconfiguring the weighted absolute measurement formation (WAMF) digraph, applying a robust controller, and imposing constraints on the desired input vectors of the partially LL-recovered vehicle and all the vehicles in its nearest neighbor set. Consequently, the formation mission specifications can still be guaranteed so that the fault is cooperatively recovered by our proposed scheme.

Chapter 7

Simulation Results

In this chapter, simulations are conducted for the satellite formation flight problem to confirm the validity of the analytical work that was developed in the previous chapters. The simulation results are presented in two main sections, namely the deep space (DS) and the planetary orbital environment (POE) formation missions. Our fault estimation method will cover all four types of actuator failures, namely float, lock-in-place (LIP), hard-over failure (HOF), and loss-of-effectiveness (LOE). But according to Remark 5.1, our fault accommodation method will be mainly focused on the loss-of-effectiveness (LOE) actuator failure (as per equation (2.5)).

7.1 Satellite Formation Mission in Deep Space (DS)

Consider the five-satellite formation in the xy-plane in deep space [6], whose relative measurement formation (RMF) digraph (as per Definition 2.3) is shown in Figure 7.1. The satellite dynamics can be approximated by double integrators [6], [7]. Since the dynamics of a satellite are decoupled along the three x, y and z axes, we only consider the x-axis dynamics here as all the results can be similarly extended to the other two axes. The x-axis dynamics of the i^{th} satellite, $i = 1, ..., 5$, including the external disturbances W_{x_i} and sensor measurement noise $V_{x_{ij}}$ are governed by

$$\begin{aligned} \dot{X}_{x_i} &= AX_{x_i} + B_{x_i}U_{x_i} + W_{x_i} \quad (i = 1, ..., N) \\ Y_{x_{ij}} &= X_{x_j} - X_{x_i} + V_{x_{ij}} \quad (j = 1, ..., N \ ; \ e_{ij} \in E_{RMF}) \end{aligned} \tag{7.1}$$

where

$$A = \begin{bmatrix} 0 & 1 \\ 0 & 0 \end{bmatrix} \ , \ B_{x_i} = \begin{bmatrix} 0 \\ \frac{b_{x_i}}{m_i} \end{bmatrix}$$

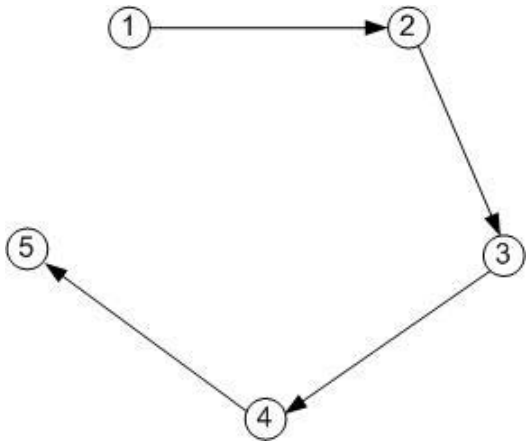

Figure 7.1: The RMF digraph of the five-satellite formation in deep space.

$X_{x_i} = (x_i, v_{x_i})^T \in R^2$ and $U_{x_i} = u_{x_i} \in R$ are the x-axis state vector (including position x_i and velocity v_{x_i}) and the control input vector (actuator force) of the satellite $\#i$ ($i \in \{1, ..., 5\}$), respectively, expressed in the local inertial frame. Moreover, $Y_{x_{ij}} = (y_{x_{ij}}, y_{v_{x_{ij}}})^T \in R^2$ is the output (measurement) vector of the relative position x_{ij} and velocity $v_{x_{ij}}$ between the two satellites $\#i$ and $\#j$ as follows

$$x_{ij} \triangleq x_j - x_i$$
$$v_{x_{ij}} \triangleq v_{x_j} - v_{x_i}$$

The subscripts "x_i" and "x_{ij}" above (as in X_{x_i} and $Y_{x_{ij}}$, respectively) represent the variables of the x-axis dynamics of the satellite $\#i$. The total mass of the satellite $\#i$ is denoted by m_i. The major environmental disturbance W_{x_i} in deep space is solar pressure [3]. It is calculated according to the formula $F_S = C_S I_S A_S / V_L$, where $C_S = 1.0$ is the solar radiation coefficient, I_S is the solar radiation intensity, A_S is the satellite cross-section area upon which solar radiation is forced, and $V_L = 3 \times 10^8$ is the speed of light. By taking $I_S = 3000(Watt/m^2)$ and $A_S = 1(m^2)$ the solar pressure becomes in the order of $10^{-5}(N)$. For simulations the sensor noise $V_{x_{ij}}$ is considered to be an additive zero-mean white Gaussian process with the variance of 10^{-4}.

The objective of the formation mission is a counter-clockwise rotation maneuver in the xy-plane with the frequency of $\omega = 0.1(rad/s)$, such that the satellites always maintain a polygon shape with the side lengths of $200(m)$ and with an error specification of $e_s = 0.010(m)$. The desired formation outputs are the relative distances among the neighboring satellites. In the following, we consider two scenarios presented in two subsections that correspond to float, lock-in-place, and hard-over actuator faults and loss-of-effectiveness actuator faults.

7.1.1 Float, Lock-in-Place, and Hard-Over Actuator Faults

In the case of float, lock-in-place, or hard-over actuator fault in satellite $\#i$ we have

$$b_{x_i} u_{x_i} = \pi_{x_i}$$

It should be pointed out that the faults that are considered here are of permanent type and correspond to actuators. From the estimation point of view, estimating either of the three actuator fault types namely float, lock-in-place or hard-over, is equivalent to estimating the one parameter π_{x_i}. Therefore, we consider a lock-in-place actuator fault in the following, and the results on float and hard-over actuator faults are not presented due to similarity with the results on lock-in-place actuator fault.

Assume that satellite #2 is subjected to a lock-in-place actuator fault, that is, $b_{x_2} u_{x_2} = \pi_{x_2} = 0.8$. Taking $X_{x_{ij}} \stackrel{\Delta}{=} X_{x_j} - X_{x_i} = (x_{ij}, v_{x_{ij}})^T$ and excluding the effects of external disturbances and sensor measurement noise, the relative dynamic equations of the formation become

$$\begin{aligned}
\dot{X}_{x_{12}} &= A X_{x_{12}} + \begin{bmatrix} 0 \\ \frac{\pi_{x_2}}{m_2} - \frac{b_{x_1} u_{x_1}}{m_1} \end{bmatrix} \\
\dot{X}_{x_{23}} &= A X_{x_{23}} + \begin{bmatrix} 0 \\ \frac{b_{x_3} u_{x_3}}{m_3} - \frac{\pi_{x_2}}{m_2} \end{bmatrix} \\
\dot{X}_{x_{34}} &= A X_{x_{34}} + \begin{bmatrix} 0 \\ \frac{b_{x_4} u_{x_4}}{m_4} - \frac{b_{x_3} u_{x_3}}{m_3} \end{bmatrix} \\
\dot{X}_{x_{45}} &= A X_{x_{45}} + \begin{bmatrix} 0 \\ \frac{b_{x_5} u_{x_5}}{m_5} - \frac{b_{x_4} u_{x_4}}{m_4} \end{bmatrix} \\
Y_{x_{ij}} &= X_{x_{ij}} \quad (i, j \in \{1, ..., 5\} \; ; \; e_{ij} \in E_{RMF})
\end{aligned} \tag{7.2}$$

Following the same steps that led to the linear system (2.11), the overall fault-augmented relative-dynamics state space model of the formation in equation (7.2) can be expressed in the form of a linear system whose state dependency (SD) digraph is depicted in Figure 7.2. According to this figure, the above linear system is structurally observable (using Proposition 3.1), and therefore sub-observers can be designed as shown next. We now design six sub-observers by using Procedure 3.1 as follows

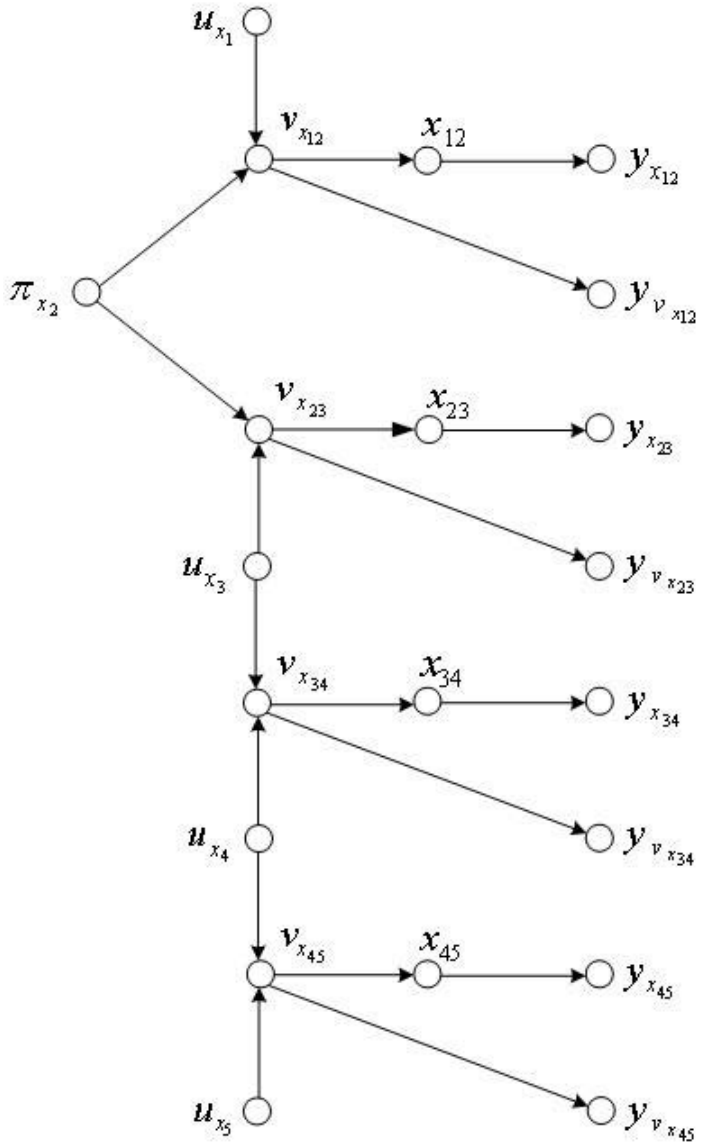

Figure 7.2: The state dependency (SD) digraph of the five-satellite formation in deep space due to a lock-in-place actuator fault.

$$
\begin{aligned}
(i) \quad & SO^{(1)}(R^{(1)}|I^{(1)}, O^{(1)}, D^{(1)}) \\
& R^{(1)} = \{\hat{x}_{12}^{(1)}, \hat{v}_{x12}^{(1)}, \hat{\pi}_{x_2}^{(1)}\}\ ,\ I^{(1)} = \{u_{x_1}\} \\
& O^{(1)} = \{y_{x_{12}}, y_{v_{x_{12}}}\}\ ,\ D^{(1)} = \{\} \\
(ii) \quad & SO^{(2)}(R^{(2)}|I^{(2)}, O^{(2)}, D^{(2)}) \\
& R^{(2)} = \{\hat{x}_{23}^{(2)}, \hat{v}_{x23}^{(2)}, \hat{\pi}_{x_2}^{(2)}\}\ ,\ I^{(2)} = \{u_{x_3}\} \\
& O^{(2)} = \{y_{x_{23}}, y_{v_{x_{23}}}\}\ ,\ D^{(2)} = \{\} \\
(iii) \quad & SO^{(3)}(R^{(3)}|I^{(3)}, O^{(3)}, D^{(3)}) \\
& R^{(3)} = \{\hat{x}_{34}^{(3)}, \hat{v}_{x34}^{(3)}\}\ ,\ I^{(3)} = \{u_{x_3}, u_{x_4}\} \\
& O^{(3)} = \{y_{x_{34}}, y_{v_{x_{34}}}\}\ ,\ D^{(3)} = \{\} \\
(iv) \quad & SO^{(4)}(R^{(4)}|I^{(4)}, O^{(4)}, D^{(4)}) \\
& R^{(4)} = \{\hat{x}_{45}^{(4)}, \hat{v}_{x45}^{(4)}\}\ ,\ I^{(4)} = \{u_{x_4}, u_{x_5}\} \\
& O^{(4)} = \{y_{x_{45}}, y_{v_{x_{45}}}\}\ ,\ D^{(4)} = \{\} \\
(v) \quad & SO^{(5)}(R^{(5)}|I^{(5)}, O^{(5)}, D^{(5)}) \\
& R^{(5)} = \{\hat{x}_{12}^{(5)}, \hat{v}_{x12}^{(5)}\}\ ,\ I^{(5)} = \{\} \\
& O^{(5)} = \{y_{x_{12}}, y_{v_{x_{12}}}\}\ ,\ D^{(5)} = \{\} \\
(vi) \quad & SO^{(6)}(R^{(6)}|I^{(6)}, O^{(6)}, D^{(6)}) \\
& R^{(6)} = \{\hat{x}_{23}^{(6)}, \hat{v}_{x23}^{(6)}\}\ ,\ I^{(6)} = \{\} \\
& O^{(6)} = \{y_{x_{23}}, y_{v_{x_{23}}}\}\ ,\ D^{(6)} = \{\}
\end{aligned}
$$

The directed graphs of the sub-observers are depicted in Figure 7.3, where the dashed edges represent the information that is required by the sub-observer to estimate the states in its range.

In order to estimate the severity of a fault in satellite #2, the estimation task starts at $T_1 = 0(sec)$ by using the initial set of sub-observers $Set_I^{so} = \{SO^{(1)}, SO^{(3)}, SO^{(4)}, SO^{(6)}\}$, where the sub-observer gains are selected by using Lemma 3.2 as follows

$$
K^{(1)} = \begin{bmatrix} -4.5000 & 0.5000 \\ -4.5375 & -16.0875 \\ 3.7125 & 14.1625 \end{bmatrix}\ ,\ K^{(3)} = K^{(4)} = \begin{bmatrix} -1.5 & -.5 \\ -.5 & -1.5 \end{bmatrix}
$$

and $SO^{(6)}$ represents direct measurements of the states x_{23} and $v_{x_{23}}$. Subsequently, at time $t \geq T_2 = 100(sec)$ satellite #1 is subjected to a process dynamics uncertainty/unreliability $\bar{W}_{x_1}$ that affects the estimation performance. This unreliability is due to an unexpected communication delay that occurs when satellite #1 sends its control signal $u_{x_1}(t)$ to the other satellites in its neighbor set $\mathcal{N}(\{1\})$ for filtering. In the following simulations this uncertainty is represented by $\bar{W}_{x_1}(t) = u_{x_1}(t-\tau) - u_{x_1}(t)$, where $\tau = 0.1(sec)$. In order to constrain and limit the effects of $\bar{W}_{x_2}$ on the local estimates and avoid its adverse effects on the estimates of all the states and parameters throughout the formation, by using the results from equations (3.15) and (3.16) at time T_2 the HL supervisor makes a decision

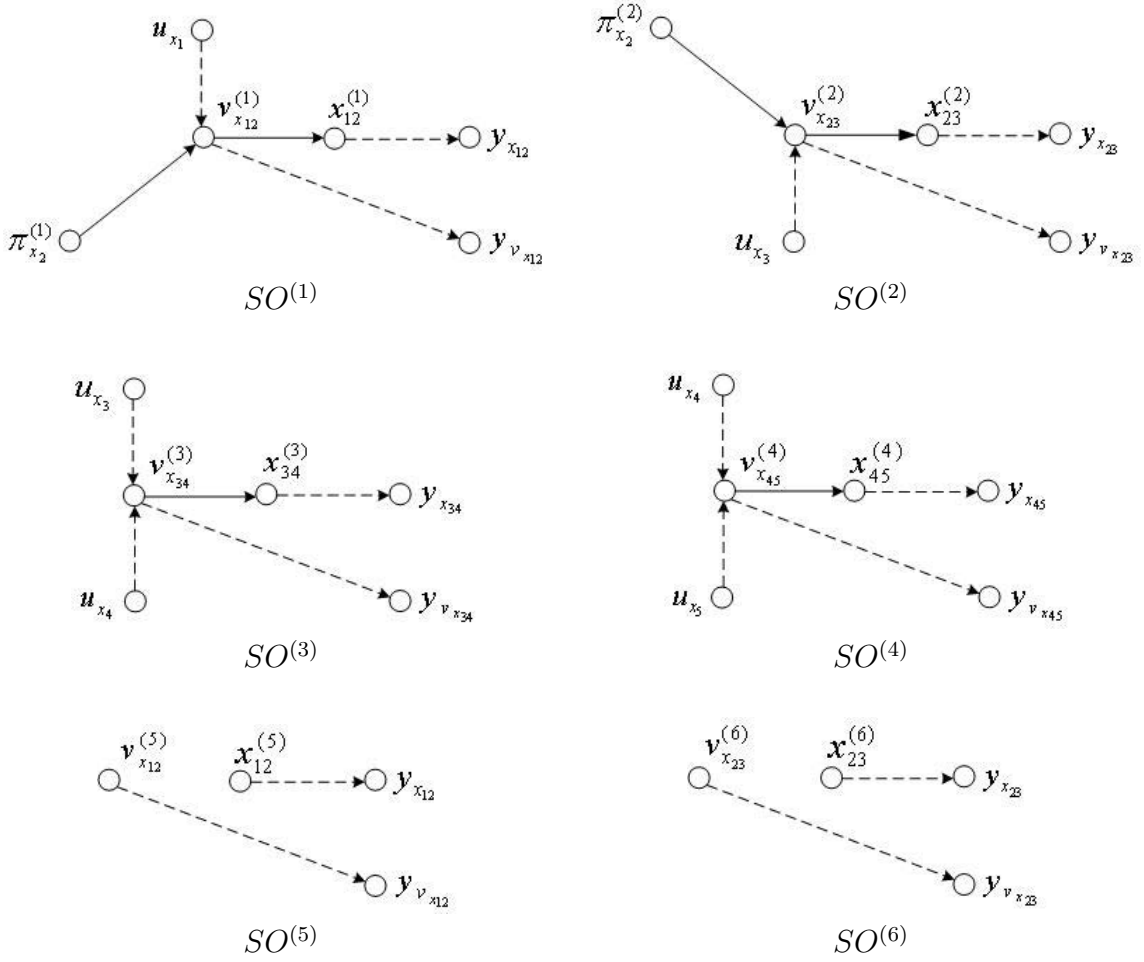

Figure 7.3: The directed graphs of the sub-observers corresponding to the linear model (7.2).

on switching from the initial set of sub-observers Set_I^{so} to the reconfigured set of sub-observers $Set_R^{so} = \{SO^{(2)}, SO^{(3)}, SO^{(4)}, SO^{(5)}\}$, where $K^{(2)} = K^{(1)}$ and $SO^{(5)}$ represents direct measurements of the states x_{12} and $v_{x_{12}}$.

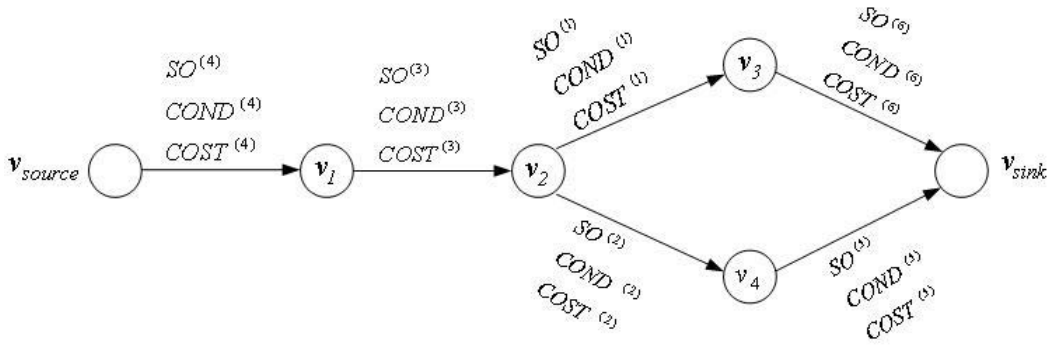

Figure 7.4: The E/WE digraph for the reconfigured set of sub-observers.

The estimation (E) digraph of the system is depicted in Figure 7.4. In this figure, the vertices are assigned as follows

$$\mathbf{v}_{source} = \begin{bmatrix} 0 \\ 0 \\ 0 \\ 0 \\ 0 \end{bmatrix}, \mathbf{v}_1 = \begin{bmatrix} 0 \\ 0 \\ 0 \\ 1 \\ 0 \end{bmatrix}, \mathbf{v}_2 = \begin{bmatrix} 0 \\ 0 \\ 1 \\ 1 \\ 0 \end{bmatrix}, \mathbf{v}_3 = \begin{bmatrix} 1 \\ 0 \\ 1 \\ 1 \\ 1 \end{bmatrix}, \mathbf{v}_4 = \begin{bmatrix} 0 \\ 1 \\ 1 \\ 1 \\ 1 \end{bmatrix}, \mathbf{v}_{sink} = \begin{bmatrix} 1 \\ 1 \\ 1 \\ 1 \\ 1 \end{bmatrix}$$

that correspond to the overall fault-augmented state $X = \begin{bmatrix} X_{x_{12}}^T & X_{x_{23}}^T & X_{x_{34}}^T & X_{x_{45}}^T & \pi_{x_2} \end{bmatrix}^T$. In case that there are no unreliabilities ($\bar{W}_{x_i} = 0$, $i = 1, ..., 5$), we have $COND^{(i)} = 0$, $i = 1, ..., 5$ and by using equations (3.15) and (3.16) the supervisor proposes the initial set of sub-observers $Set_I^{so} = \{SO^{(1)}, SO^{(3)}, SO^{(4)}, SO^{(6)}\}$. When the unreliability $\bar{W}_{x_1} \neq 0$ is imposed on the system, we have $COND^{(1)} = 1$ (or $COST^{(1)} \neq 0$), which requires the supervisor to propose the reconfigured set of sub-observers $Set_R^{so} = \{SO^{(2)}, SO^{(3)}, SO^{(4)}, SO^{(5)}\}$ by using equations (3.15) and (3.16).

In order to show the significance and effectiveness of our proposed cooperative estimation framework that switches from the initial set of sub-observers to the reconfigured set of sub-observers at time T_2, both the time intervals $T_{12} = [0\ 100](sec)$ and $T_{23} = [100\ 200](sec)$ are included in Figures 7.5 and 7.6. One can compare the T_{23}-interval of Figure 7.5 with that of Figure 7.6. The maximum norm of the estimation error for $\pi_{x_2}^{(1)}$, that is $max_{t \in T_{23}} |\hat{\pi}_{x_2}^{(1)}(t) - \pi_{x_2}^{(1)}(t)|$, by using the initial set of sub-observers Set_I^{so} (Figures 7.5) is calculated to be 0.05, while the maximum norm of the estimation error

for $\pi_{x_2}^{(2)}$ is shown to be less than 0.01 by using the reconfigured set of sub-observers Set_R^{so} (Figure 7.6). This clearly demonstrates that our proposed cooperative estimation scheme successfully makes the decision on switching from the initial set to the reconfigured set of sub-observers.

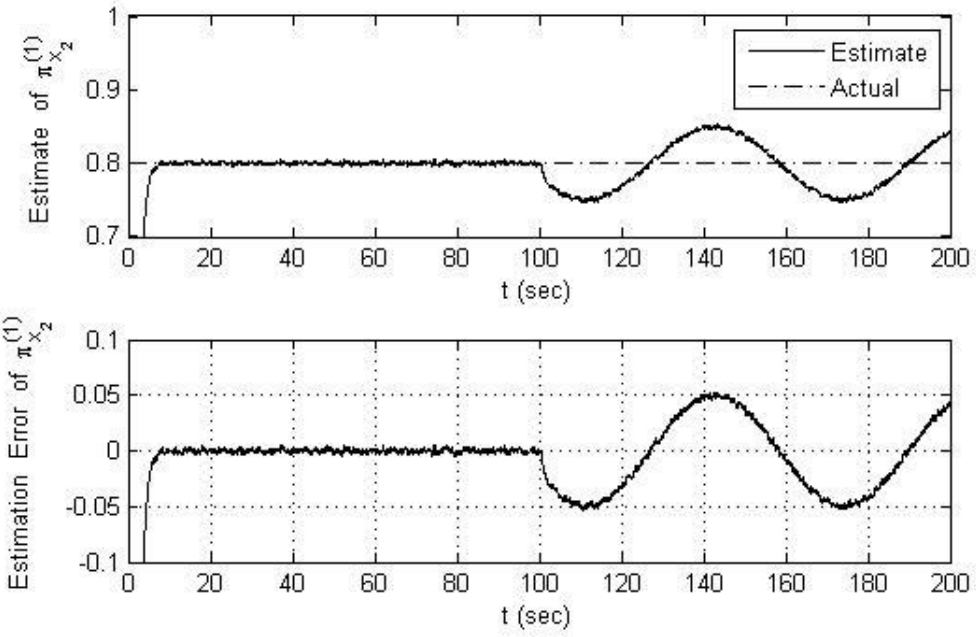

Figure 7.5: Actual, estimated, and the estimation error of the fault in satellite #2 by using the initial set of sub-observers.

7.1.2 Loss-of-Effectiveness (LOE) Actuator Faults

In the case of loss-of-effectiveness (LOE) actuator fault in satellite $\#i$ the x-axis actuator gain becomes

$$b_{x_i} = \bar{b}_{x_i} + \pi_{x_i}$$

where $\bar{b}_{x_i}$ and π_{x_i} represent the x-axis nominal (healthy) actuator gain and its corresponding loss-of-effectiveness (LOE) actuator fault signal, respectively. It should be pointed out again that the faults that are considered here are of permanent type. Taking $X_{x_{ij}} \triangleq X_{x_j} - X_{x_i} = (x_{ij}, v_{x_{ij}})^T$, $B_{x_{ij}} \triangleq (-B_{x_i}, B_{x_j})$ and $U_{x_{ij}} \triangleq [(U_{x_i})^T, (U_{x_j})^T]^T = (u_{x_i}, u_{x_j})^T$, the relative dynamic equation of the formation becomes

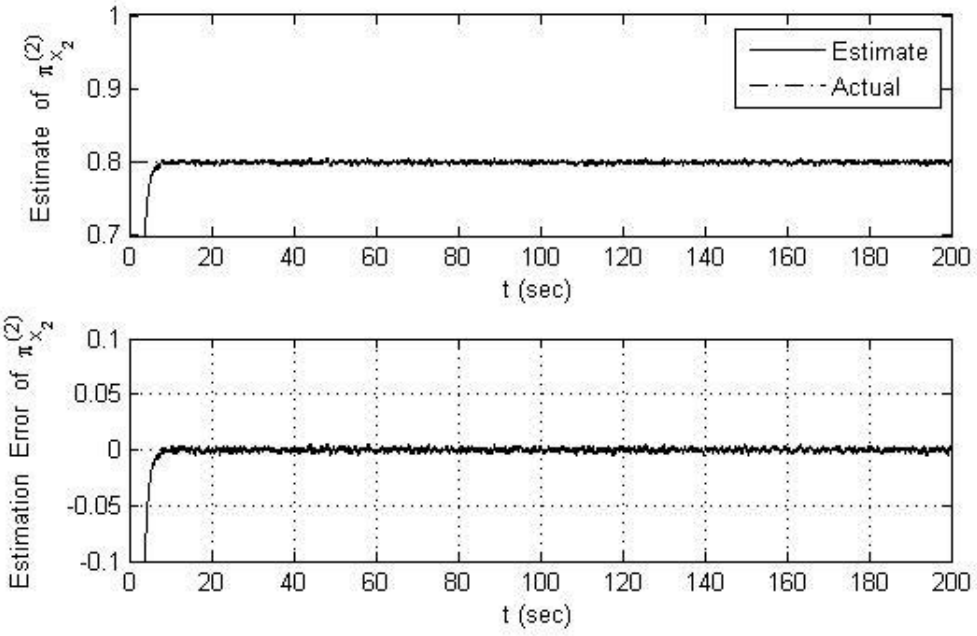

Figure 7.6: Actual, estimated, and the estimation error of the fault in satellite #2 by using the reconfigured set of sub-observers.

$$\begin{aligned} \dot{X}_{x_{ij}} &= AX_{x_{ij}} + B_{x_{ij}}U_{x_{ij}} \\ Y_{x_{ij}} &= X_{x_{ij}} \quad (e_{ij} \in E_{RMF}) \end{aligned} \tag{7.3}$$

Following the same steps that led to the bilinear system (2.10), the fault-augmented relative-dynamics state space model of the formation given in equation (7.3) can be expressed in the form of a bilinear system, whose state dependency (SD) digraph is depicted in Figure 7.7. According to this figure, the bilinear system is structurally observable (using Proposition 4.1), and therefore the sub-observers can be designed as shown subsequently.

Next, by using Procedure 4.1 we design 12 sub-observers $SO^{(k^{ij}_{ij})}$, $SO^{(k^{i}_{ij})}$, and $SO^{(k^{j}_{ij})}$ for $\{ij\} \in \{\{12\},\{23\},\{34\},\{45\}\}$ as follows

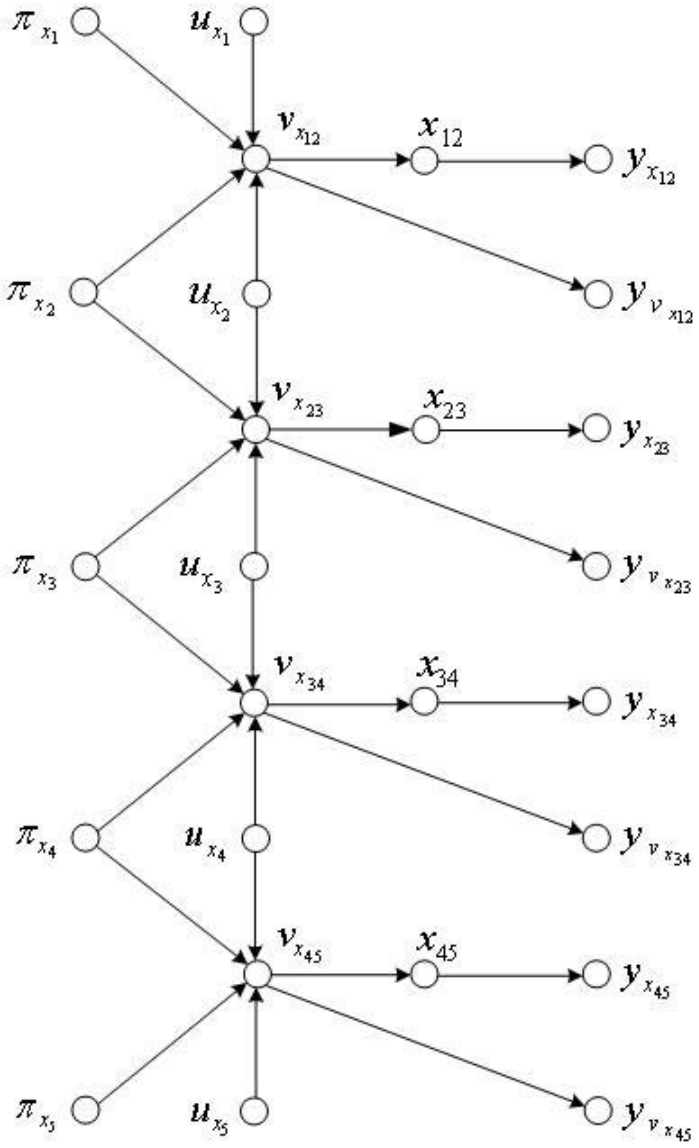

Figure 7.7: The state dependency (SD) digraph of the five-satellite formation in deep space due to loss-of-effectiveness actuator faults.

$$
\begin{aligned}
(i) \quad & SO^{(k_{ij}^{ij})}(R^{(k_{ij}^{ij})}|I^{(k_{ij}^{ij})}, O^{(k_{ij}^{ij})}, D^{(k_{ij}^{ij})}) \\
& R^{(k_{ij}^{ij})} = \{\hat{\pi}_{x_i}^{(k_{ij}^{ij})}, \hat{\pi}_{x_j}^{(k_{ij}^{ij})}\} \ , \ I^{(k_{ij}^{ij})} = \{u_{x_i}, u_{x_j}\} \\
& O^{(k_{ij}^{ij})} = \{y_{x_{ij}}, y_{v_{x_{ij}}}\} \ , \ D^{(k_{ij}^{ij})} = \{\} \\
(ii) \quad & SO^{(k_{ij}^{i})}(R^{(k_{ij}^{i})}|I^{(k_{ij}^{i})}, O^{(k_{ij}^{i})}, D^{(k_{ij}^{i})}) \\
& R^{(k_{ij}^{i})} = \{\hat{\pi}_{x_i}^{(k_{ij}^{i})}\} \ , \ I^{(k_{ij}^{i})} = \{u_{x_i}, u_{x_j}\} \\
& O^{(k_{ij}^{i})} = \{y_{x_{ij}}, y_{v_{x_{ij}}}\} \ , \ D^{(k_{ij}^{i})} = \{\hat{\pi}_{x_j}^{(k_{ij}^{i})}\} \\
(iii) \quad & SO^{(k_{ij}^{j})}(R^{(k_{ij}^{j})}|I^{(k_{ij}^{j})}, O^{(k_{ij}^{j})}, D^{(k_{ij}^{j})}) \\
& R^{(k_{ij}^{j})} = \{\hat{\pi}_{x_j}^{(k_{ij}^{j})}\} \ , \ I^{(k_{ij}^{j})} = \{u_{x_i}, u_{x_j}\} \\
& O^{(k_{ij}^{j})} = \{y_{x_{ij}}, y_{v_{x_{ij}}}\} \ , \ D^{(k_{ij}^{j})} = \{\hat{\pi}_{x_i}^{(k_{ij}^{j})}\}
\end{aligned}
$$

in which $\hat{x}_{ij}^{(k)}$ and $\hat{v}_{x_{ij}}^{(k)}$, $k \in \{k_{ij}^{ij}, k_{ij}^{i}, k_{ij}^{j}\}$ are eliminated from the range $R^{(k)}$ of the sub-observer $SO^{(k)}$ because these states are directly measured by the sensors $y_{x_{ij}}$ and $y_{v_{x_{ij}}}$. The directed graphs of the sub-observers are depicted in Figure 7.8, where the dashed edges represent the information that is required by the sub-observer to estimate the states in its range.

We consider the following three scenarios (A), (B), and (C). In scenario (A), all the satellites are fault free and the error specification $e_s = 0.010(m)$ is satisfied with a properly designed controller. In scenario (B), satellites #2, #3, and #4 are faulty and the HL supervisor activates the LLFR module. This module estimates the actuator faults by using cooperative estimators and incorporates the estimates in the LLFR controller to fully recover all the satellites. However, satellite #3 is partially recovered by the LLFR module due to a biased estimate of its fault, and consequently the error specification $e_s = 0.010(m)$ is violated. In scenario (C), the HL supervisor activates the FLFR module to cooperatively accommodate the partially LL-recovered satellite #3 so that the error specification can now be guaranteed. For sake of relative evaluation, the x-axis cumulative control effort is defined according to

$$E_{x_i}(t) = \int_{\tau=0}^{t} u_{x_i}^2(\tau)d\tau \quad (i = 1, ..., 5)$$

and is compared among the following three scenarios.

A. All the satellites are fault free: By using the centralized controller (5.10) with $\hat{b}_{x_i} = b_{x_i}$ $(i = 1, ..., 5)$ and setting the α_i parameters equal to one, i.e. $\alpha_i = 1$ $(i = 1, ..., 5)$, and by using Lemma 5.1 to calculate the centralized feedback gain

$$K = \begin{bmatrix} -2.9687 & -3.2813 \end{bmatrix}$$

the maximum tracking error that is obtained is quite acceptable (namely, $error = 0.005 < 0.010(m) = e_s$). Figure 7.9-(a) depicts the cumulative control effort that is expensed.

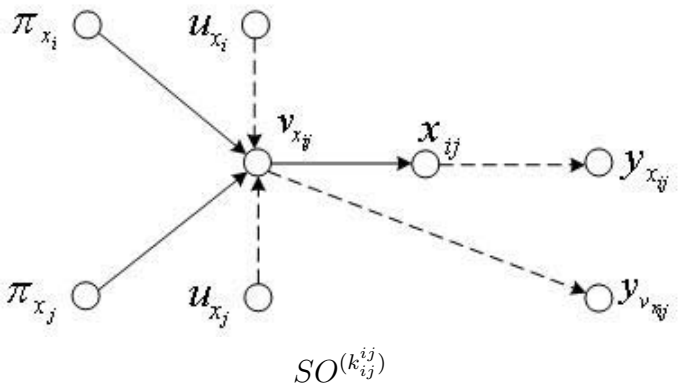

$SO^{(k_{ij}^{ij})}$

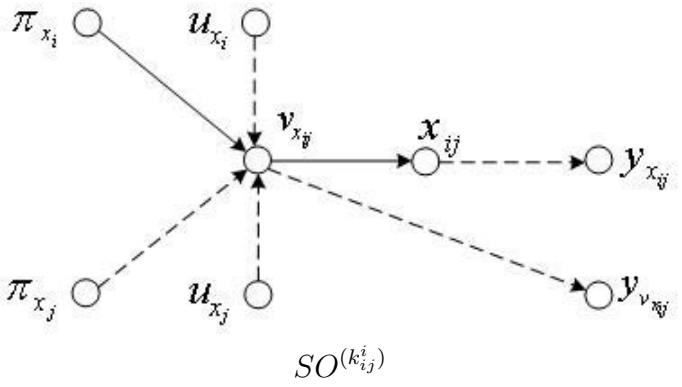

$SO^{(k_{ij}^{i})}$

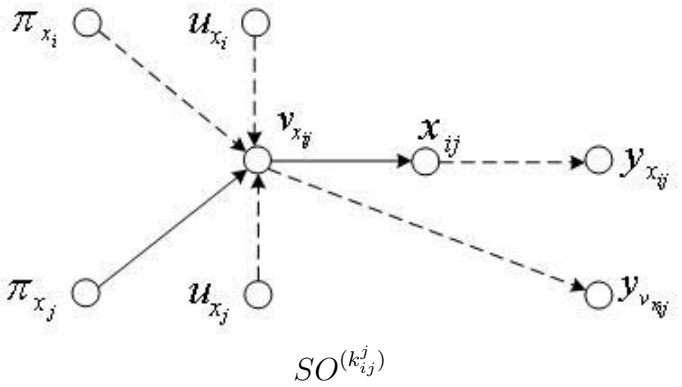

$SO^{(k_{ij}^{j})}$

Figure 7.8: The directed graphs of the sub-observers corresponding to the bilinear model (7.3).

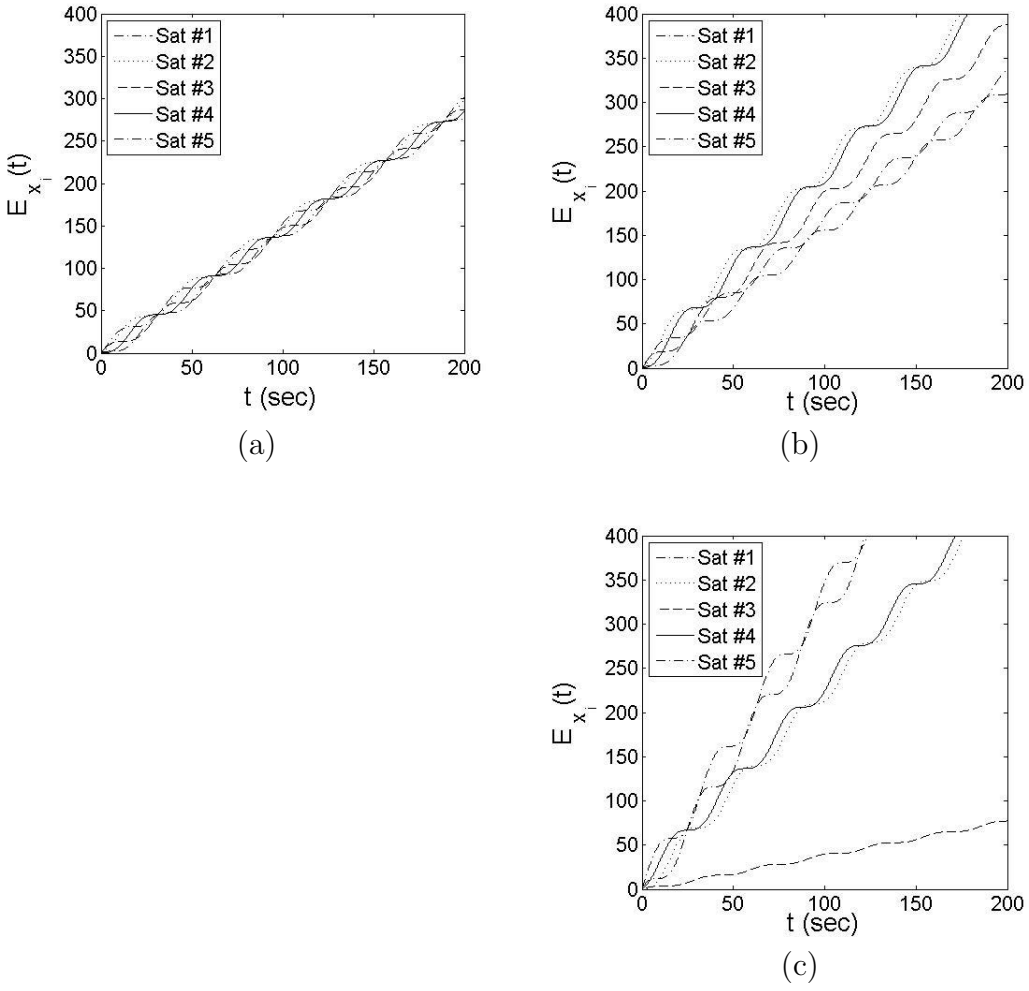

Figure 7.9: The x-axis cumulative centralized control effort for (a) all satellites are fault free, (b) faulty satellite #3 with the LLFR applied and $\alpha_3 = 1$, and (c) faulty satellite #3 with the HLFR applied and $\alpha_3 = 6.7$.

On the other hand one can use the decentralized controller (5.34) and Lemma 5.3 to calculate the decentralized feedback gains

$$\beta_{12}^1 = [2.8042 \;\; 1.7155] \;,\; \beta_{12}^2 = [0.3532 \;\; -0.8978]$$
$$\beta_{23}^2 = [0.5200 \;\; 3.3196] \;,\; \beta_{23}^3 = [-0.2470 \;\; -2.7707]$$
$$\beta_{34}^3 = [0.2470 \;\; 2.7707] \;,\; \beta_{34}^4 = [-0.5200 \;\; -3.3196]$$
$$\beta_{45}^4 = [-0.3532 \;\; 0.8978] \;,\; \beta_{45}^5 = [-2.8042 \;\; -1.7155]$$

and the parameter $\alpha = (\alpha_{12}, \alpha_{23}, \alpha_{34}, \alpha_{45})^T = (0.2, 0.4, 0.6, 0.8)^T \in R^4$ (with $||A_3^T(\alpha)|| = 0.6325$) chosen to minimize the energy of the input signal U_d in (5.34) by minimizing the cost function

$$f_{cost}(.) = \int_{t=0}^{\infty} U_d^T(t) U_d(t) dt$$

The resulting maximum tracking error is quite acceptable (namely, $error = 0.007 < 0.010(m) = e_s$). Figure 7.10-(a) depicts the cumulative control effort that is expensed.

B. Satellites #2, #3, and #4 are faulty and the fault in satellite #3 is partially recovered by the LLFR module: A 20% loss-of-effectiveness (LOE) fault is applied to the x-axis actuators of satellites #2, #3, and #4. In this case, the HL supervisor activates the LLFR module which performs cooperative fault estimation for the three faulty satellites.

At first the LLFR module successfully performs the estimation task by the initial set of sub-observers. Subsequently, at time $t \geq T_2 = 100(sec)$, satellite #3 is subjected to process dynamics unreliability $\bar{W}_{x_3}$ that affects the estimation performance. This unreliability is due to an unexpected communication delay that occurs when satellite #3 sends its control signal $u_{x_3}(t)$ to the other satellites in its neighbor set $\mathcal{N}(\{3\})$ for filtering. In the following simulations this uncertainty is represented by $\bar{W}_{x_3}(t) = u_{x_3}(t-\tau) - u_{x_3}(t)$, where $\tau = 0.1(sec)$. In order to constrain and limit the effects of $\bar{W}_{x_3}$ on the local estimates and avoid its adverse effects on the estimates of all the states and parameters throughout the formation, by using the results from equation (4.19) at time T_2 the HL supervisor makes a decision on switching from the initial set of sub-observers to the reconfigured set of sub-observers, as described in more detail below.

We consider the following sequential simulation steps:

1. In the time interval $T_{12} = [0, 100](sec)$, no unreliabilities are present in the system ($\bar{W}_{x_i} = 0,\; i = 1, ..., 5$). The weighted sub-observer dependency estimation

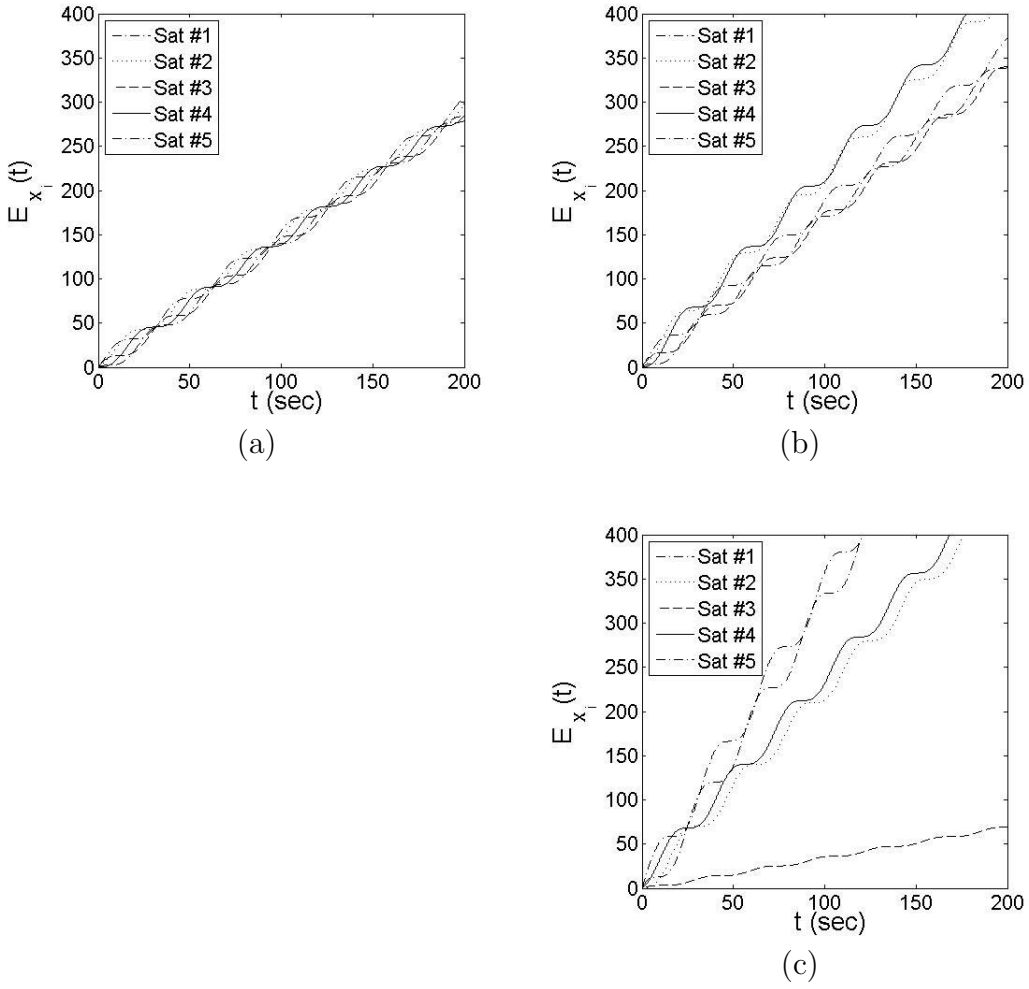

Figure 7.10: The x-axis cumulative decentralized control effort for (a) all satellites are fault free, (b) faulty satellite #3 with the LLFR applied and $||A_3^T|| = 0.6325$, and (c) faulty satellite #3 with the HLFR applied and $||A_3^T|| = 0.2530$.

(WSODE) digraph is shown in Figure 7.11, where the vertices are assigned as follows

$$\mathbf{v}_{source} = \begin{bmatrix} 0 \\ 0 \\ 0 \\ 0 \\ 0 \end{bmatrix}, \mathbf{v}_1 = \begin{bmatrix} 1 \\ 1 \\ 0 \\ 0 \\ 0 \end{bmatrix}, \mathbf{v}_2 = \begin{bmatrix} 1 \\ 1 \\ 1 \\ 0 \\ 0 \end{bmatrix}, \mathbf{v}_3 = \begin{bmatrix} 1 \\ 1 \\ 1 \\ 1 \\ 0 \end{bmatrix}, \mathbf{v}_4 = \begin{bmatrix} 0 \\ 1 \\ 1 \\ 0 \\ 0 \end{bmatrix}$$

$$\mathbf{v}_5 = \begin{bmatrix} 0 \\ 0 \\ 1 \\ 1 \\ 0 \end{bmatrix} \mathbf{v}_6 = \begin{bmatrix} 0 \\ 1 \\ 1 \\ 1 \\ 0 \end{bmatrix} \mathbf{v}_7 = \begin{bmatrix} 0 \\ 0 \\ 0 \\ 1 \\ 1 \end{bmatrix} \mathbf{v}_8 = \begin{bmatrix} 0 \\ 0 \\ 1 \\ 1 \\ 1 \end{bmatrix} \mathbf{v}_9 = \begin{bmatrix} 0 \\ 1 \\ 1 \\ 1 \\ 1 \end{bmatrix} \mathbf{v}_{sink} = \begin{bmatrix} 1 \\ 1 \\ 1 \\ 1 \\ 1 \end{bmatrix}$$

and the cumulative sub-observer costs are summarized in Table 7.1. For calculating the sub-observer costs, we take $C_R = 0$ (no recovery cost) and $C_E >> C_C$ (the estimation cost is weighted considerably more than the communication cost). For brevity, only the costs corresponding to the paths that pass through the vertices $\mathbf{v}_{source}$, $\mathbf{v}_1$, $\mathbf{v}_2$, $\mathbf{v}_3$, and $\mathbf{v}_{sink}$ are indicated in Table 7.1. It is concluded that the minimum cumulative sub-observer cost (as per equation (4.19)) corresponds to the initial set of sub-observers $Set_I^{so} = \{SO^{(k_{12}^{12})}, SO^{(k_{23}^{23})}, SO^{(k_{34}^{34})}, SO^{(k_{45}^{45})}\}$. This minimum cost is calculated to be 0. The corresponding sub-observer dependency (SOD) digraph is depicted in Figure 7.12, which is shown to be *acyclic* (as required by Theorem 3.1 for stability analysis).

2. At time $T_1 = 0(sec)$ the estimation process is started with the initial set of sub-observers $Set_I^{so} = \{SO^{(k_{12}^{12})}, SO^{(k_{23}^{23})}, SO^{(k_{34}^{34})}, SO^{(k_{45}^{45})}\}$, and the estimates for the fault signals in the time interval T_{12} are shown in Figures 7.13, 7.14, 7.15, 7.16, and 7.17. In order to show the effectiveness of our proposed fusion feedback (FF) algorithm, we take the constrained-state sub-observers (CSSOs) $SO^{(k_{12}^{12})}$ and $SO^{(k_{23}^{23})}$, whose common state is π_{x_2}, with the time constant $\tau = 20$ as in equation (4.29). The effectiveness of our proposed fusion feedback procedure (with $\ell = 10$ as in equation (4.38)) is depicted in Figure 7.18-(a) as compared with that in Figure 7.18-(b), in which there is no fusion feedback ($\ell = 1$). Figure 7.18-(a) shows that the constrained-state condition $\hat{\pi}_{x_2}^{(k_{12}^{12})} - \hat{\pi}_{x_2}^{(k_{23}^{23})} = 0$ on the common state π_{x_2} is satisfied by using the fusion feedback. Figure 7.19 shows the traces of the covariance matrices which remain bounded. This implies that the fusion feedback method does not interfere with the stability of the overall estimation algorithm. Moreover, the FF algorithm is ran for the values of $\ell = 1.5, 2, 2.5, ..., 6$. The maximum norm of the state constraint error in the time interval $[50\ 200](sec)$, that is $max_{t\in[50\ 200]}|\hat{\pi}_{x_2}^{(k_{12}^{12})}(t) - \hat{\pi}_{x_2}^{(k_{23}^{23})}(t)|$ versus ℓ is

depicted in Figure 7.20-(a), and the maximum covariance matrix traces of $SO^{(k_{12}^{12})}$ and $SO^{(k_{23}^{23})}$ versus ℓ are depicted in Figure 7.20-(b). These two figures indicate that by increasing the parameter ℓ, the maximum norm of the state constraint error becomes closer to zero by the FF algorithm, at the cost of increase in the two maximum covariance matrix traces.

3. In the time interval $T_{23} = [100, 200](sec)$, the unreliability $\bar{W}_{x_3} = u_{x_3}(t-\tau) - u_{x_3}(t)$, that was described earlier in this chapter, is imposed on the system. This situation is detected by the FDI module as per Assumption 3.1 during the time interval T_{23}. In this case, the weighted sub-observer dependency estimation (WSODE) digraph is shown in Figure 7.11 and the cumulative sub-observer costs are summarized in Table 7.1. According to this table, the cumulative cost of the initial set of sub-observer Set_I^{so} is calculated to be $3C_E$, which corresponds to the unreliable estimates of the three states π_{x_2}, π_{x_3}, and π_{x_4}. Since $C_E >> C_C$, by using the results from equation (4.19) the supervisor reconfigures the set of sub-observers such that the cumulative sub-observer cost (specially the estimation cost) is minimized. Therefore, the supervisor selects the reconfigured set of sub-observers $Set_R^{so} = \{SO^{(k_{12}^{12})}, SO^{(k_{23}^{3})}, SO^{(k_{45}^{45})}\}$, whose cumulative cost is $C_E + C_C cost_{c,2}^{(k_{23}^{3})}$. The corresponding sub-observer dependency (SOD) digraph is depicted in Figure 7.21, which is shown to be *acyclic* (as required by Theorem 3.1 for stability analysis).

4. At time $T_2 = 100(sec)$, the estimation process switches to the reconfigured set of sub-observers $Set_R^{so} = \{SO^{(k_{12}^{12})}, SO^{(k_{23}^{3})}, SO^{(k_{45}^{45})}\}$, and the estimates for the fault signals are shown in the time interval T_{23} in Figures 7.22, 7.23, 7.24, 7.25, and 7.26.

In order to demonstrate the significance and effectiveness of our proposed cooperative estimation framework that switches from the initial set of sub-observers Set_I^{so} to the reconfigured set of sub-observers Set_R^{so} at time T_2, both the time intervals $T_{12} = [0\ 100](sec)$ and $T_{23} = [100\ 200](sec)$ are included in Figures 7.13 - 7.17 and Figures 7.22 - 7.26. One can compare the T_{23}-interval estimation performance of the initial set of sub-observers in Figures 7.13 - 7.17 with that of reconfigured set of sub-observers in Figures 7.22 - 7.26, respectively. This comparison is summarized in Table 7.2. In this table, the means and variances of the fault signal estimation errors are provided for the initial and the reconfigured sets of sub-observers. It is clearly demonstrated that our proposed cooperative estimation scheme in the LLFR module successfully makes the decision on switching from the initial set to the reconfigured set of sub-observers.

Using the reconfigured set of sub-observers Set_R^{so}, the corresponding fault parameter in satellite #3 is estimated within a 10% relative error, that is $|\varepsilon_{x_3}|/b_{x_3} = |\hat{b}_{x_3} - b_{x_3}|/b_{x_3} \leq 0.10$. The estimates of the faults are ultimately used in the centralized LLFR controller. By using the centralized controller (5.10), the parameters α_i, and the centralized feedback

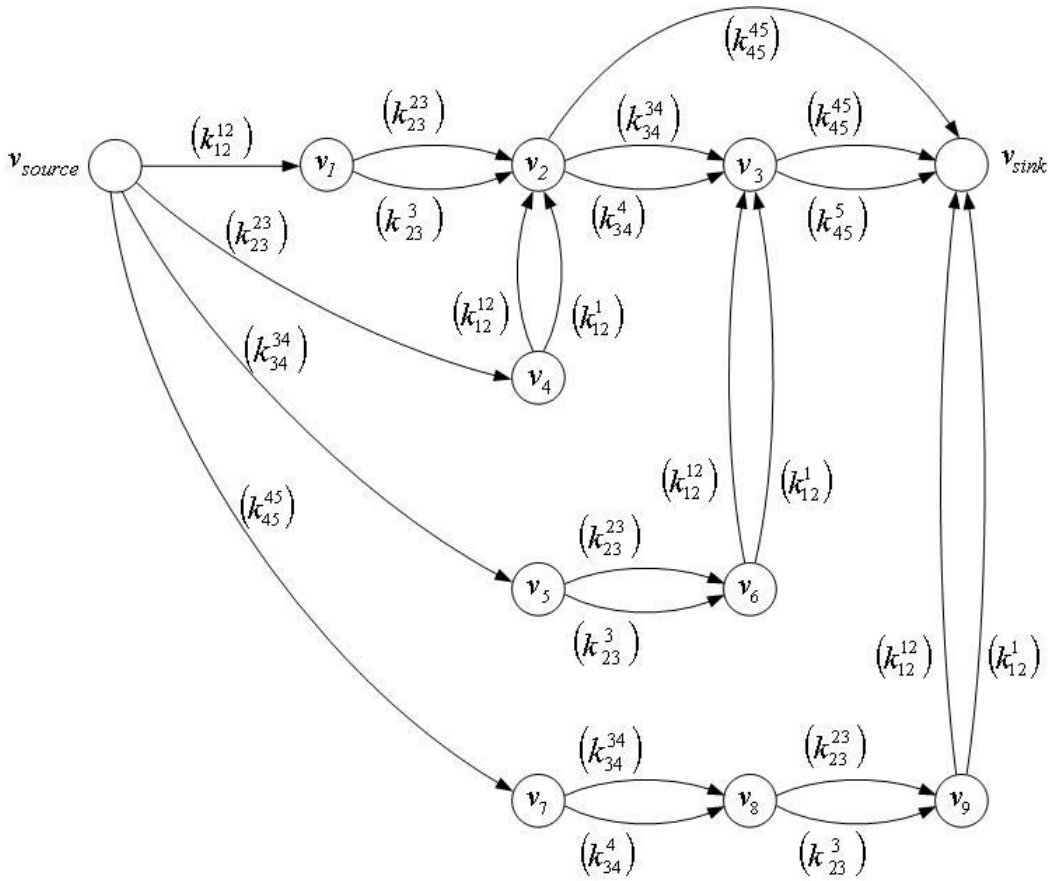

Figure 7.11: The WSODE digraph for the scenario (B) in which the sub-observer $SO^{(k)}$, $k \in \{k_{ij}^{ij}, k_{ij}^{i}, k_{ij}^{j}\}$ is denoted by "(k)" for simplicity. The costs (cumulative weights) are summarized in Table 7.1.

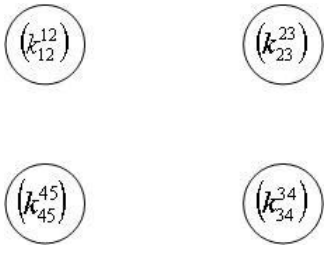

Figure 7.12: The *acyclic* SOD digraph for the initial set of sub-observers for the scenario (B). The sub-observer $SO^{(k)}$, $k \in \{k_{ij}^{ij}, k_{ij}^{i}, k_{ij}^{j}\}$ is denoted by "(k)" for simplicity. The digraph has no edges that means the SOs can work independently.

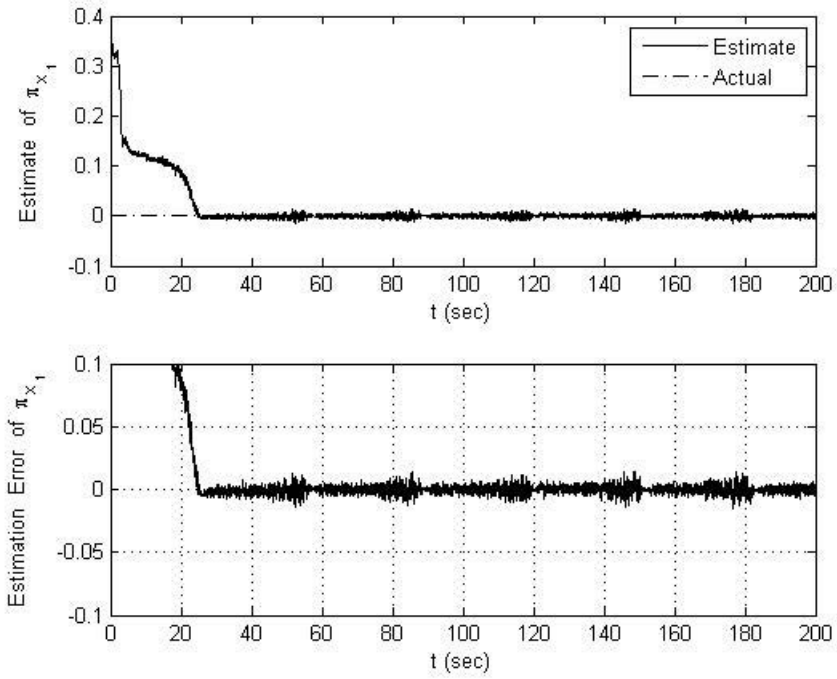

Figure 7.13: Actual, estimated, and the estimation error of the LOE fault in satellite #1 by using the initial set of sub-observers.

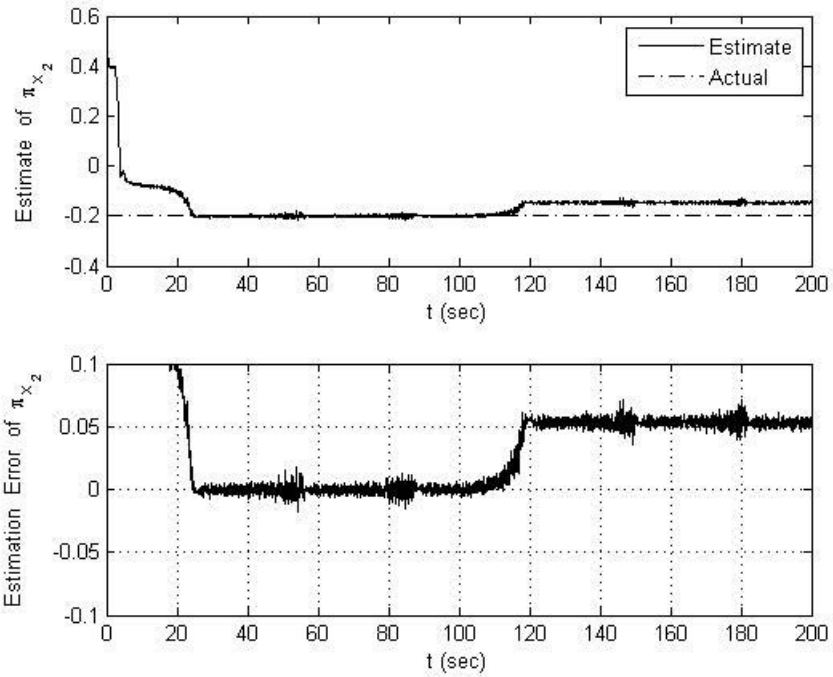

Figure 7.14: Actual, estimated, and the estimation error of the LOE fault in satellite #2 by using the initial set of sub-observers.

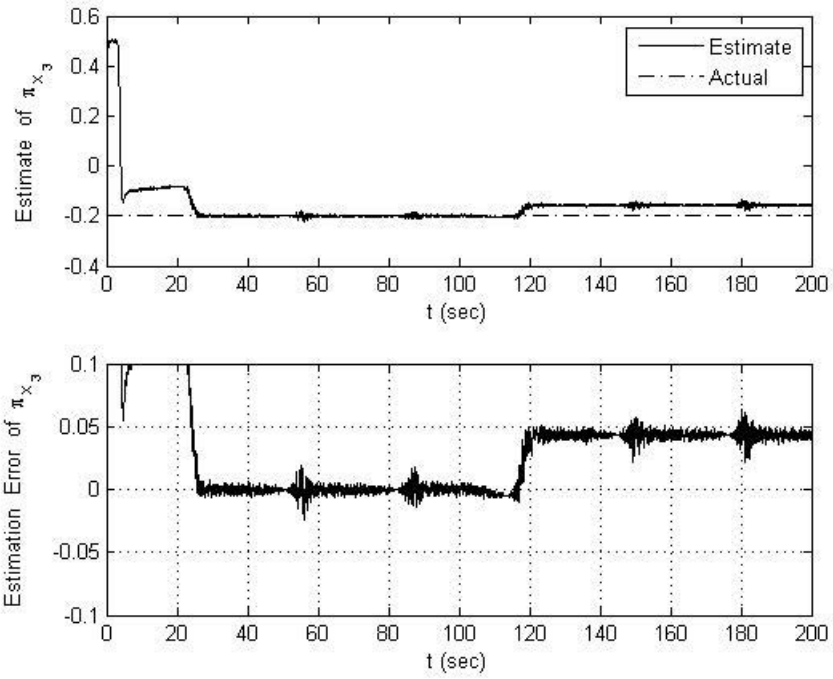

Figure 7.15: Actual, estimated, and the estimation error of the LOE fault in satellite #3 by using the initial set of sub-observers.

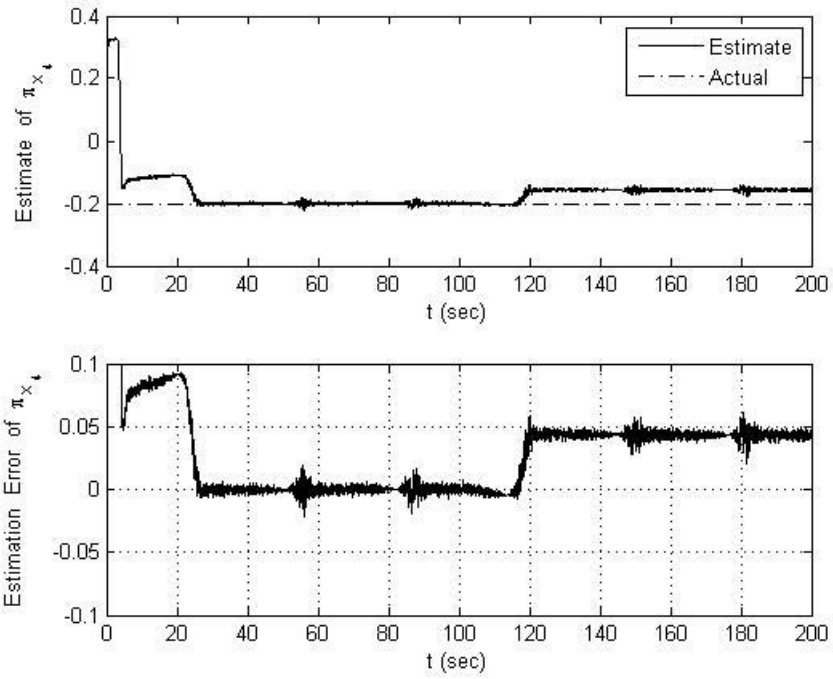

Figure 7.16: Actual, estimated, and the estimation error of the LOE fault in satellite #4 by using the initial set of sub-observers.

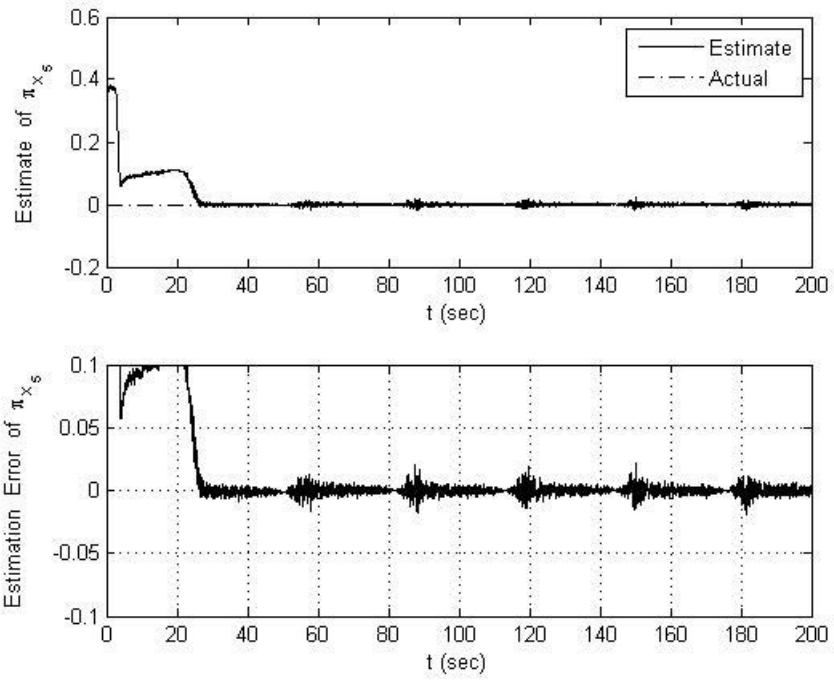

Figure 7.17: Actual, estimated, and the estimation error of the LOE fault in satellite #5 by using the initial set of sub-observers.

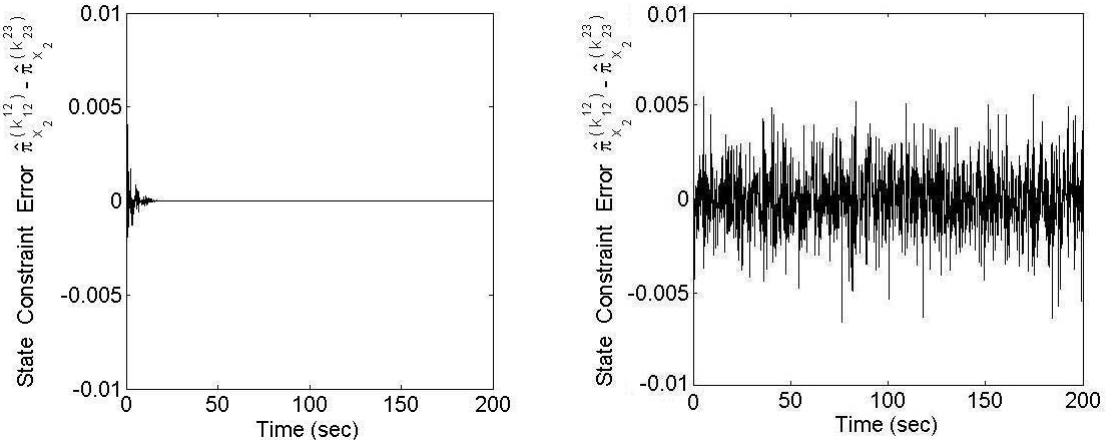

(a) (b)

Figure 7.18: The constraint error of the common state π_{x_2}, that is $\hat{\pi}_{x_2}^{(k_{12}^{12})} - \hat{\pi}_{x_2}^{(k_{23}^{23})}$, (a) with fusion feedback ($\ell = 10$) and (b) without fusion feedback ($\ell = 1$).

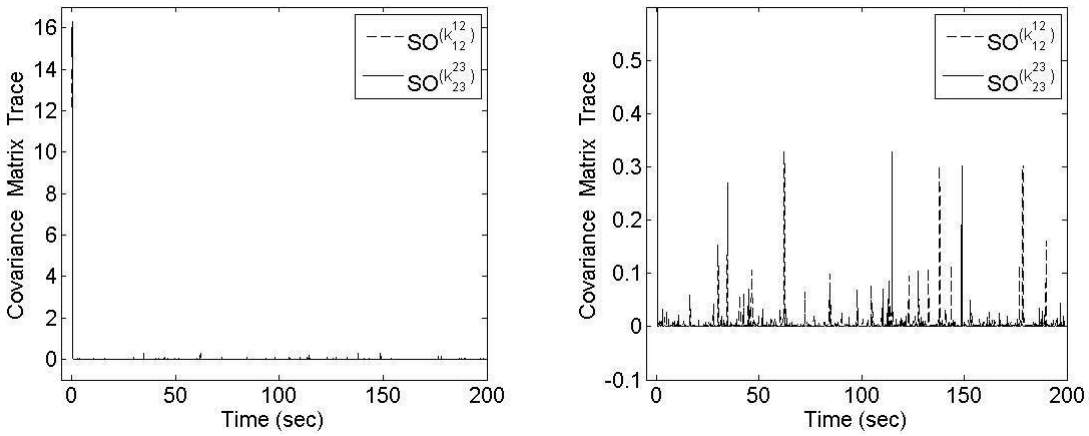

(a) (b)

Figure 7.19: Trace of the error covariance matrices for the two sub-observers $SO^{(k_{12}^{12})}$ and $SO^{(k_{23}^{23})}$ with (a) normal and (b) zoomed scale.

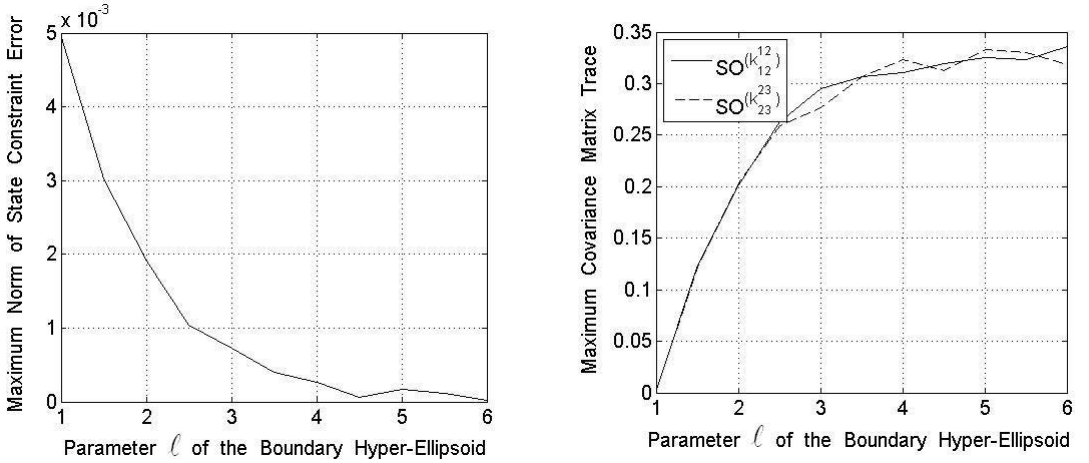

(a) (b)

Figure 7.20: (a) The maximum norm of the constraint error of the common state π_{x_2} in the time interval [50 200](sec), that is $max_{t\in[50\ 200]}|\hat{\pi}_{x_2}^{(k_{12}^{12})}(t) - \hat{\pi}_{x_2}^{(k_{23}^{23})}(t)|$, and (b) the maximum trace of the error covariance matrices for the two sub-observers $SO^{(k_{12}^{12})}$ and $SO^{(k_{23}^{23})}$ in the time interval [50 200](sec).

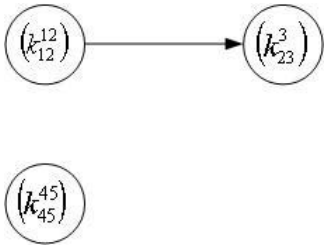

Figure 7.21: The *acyclic* SOD digraph for the reconfigured set of sub-observers. The sub-observer $SO^{(k)}$, $k \in \{k_{ij}^{ij}, k_{ij}^{i}, k_{ij}^{j}\}$ is denoted by "(k)" for simplicity. The sub-observers $SO^{(k_{12}^{12})}$ and $SO^{(k_{45}^{45})}$ can work independently, but $SO^{(k_{23}^{3})}$ depends on $SO^{(k_{12}^{12})}$.

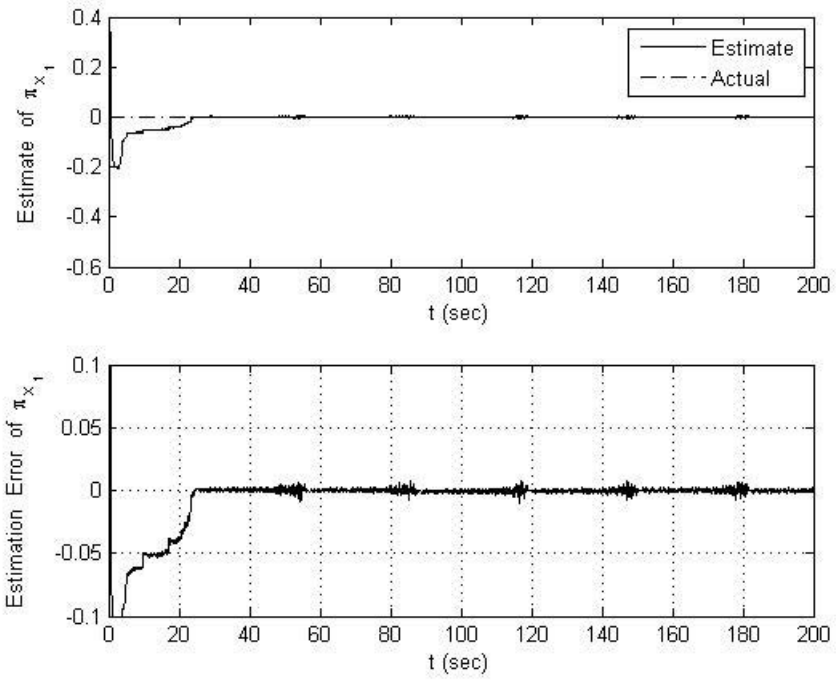

Figure 7.22: Actual, estimated, and the estimation error of the LOE fault in satellite #1 by using the reconfigured set of sub-observers.

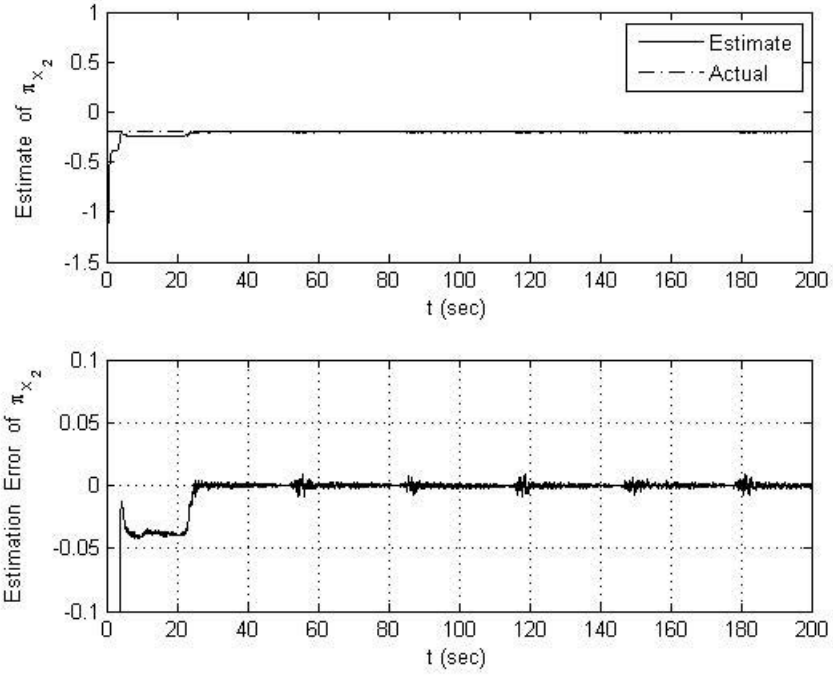

Figure 7.23: Actual, estimated, and the estimation error of the LOE fault in satellite #2 by using the reconfigured set of sub-observers.

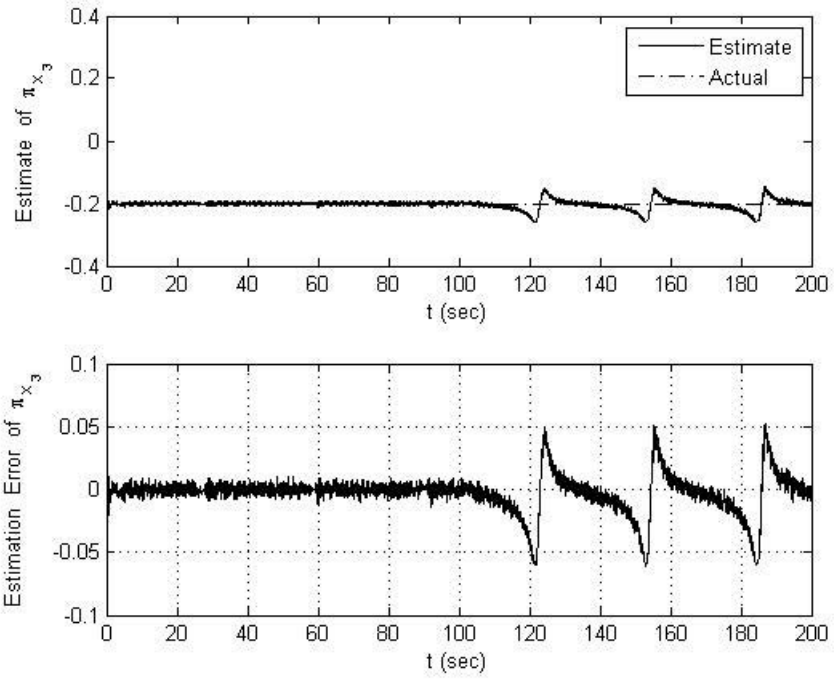

Figure 7.24: Actual, estimated, and the estimation error of the LOE fault in satellite #3 by using the reconfigured set of sub-observers.

Table 7.1: The cumulative sub-observer costs corresponding to the paths that pass through the vertices $\mathbf{v}_{source}$, $\mathbf{v}_1$, $\mathbf{v}_2$, $\mathbf{v}_3$, and $\mathbf{v}_{sink}$ as shown in Figure 7.11. Each cost has two components. The first component represents the estimation cost (the states whose estimates are unreliable are written in parentheses), and the second component represents the communication cost.

Sub-Observer Set	Cumulative Costs (Estimation/Communication)	
	$\bar{W}_{x_3} = 0$	$\bar{W}_{x_3} \neq 0$
$\{SO^{(k_{12}^{12})}, SO^{(k_{23}^{23})}, SO^{(k_{34}^{34})}, SO^{(k_{45}^{45})}\}$	$\begin{matrix}0\\0\end{matrix}$	$\begin{matrix}3\ (\pi_{x_2},\pi_{x_3},\pi_{x_4})\\0\end{matrix}$
$\{SO^{(k_{12}^{12})}, SO^{(k_{23}^{3})}, SO^{(k_{45}^{45})}\}$	$\begin{matrix}0\\cost_{c,2}^{(k_{23}^{3})}\end{matrix}$	$\begin{matrix}1\ (\pi_{x_3})\\cost_{c,2}^{(k_{23}^{3})}\end{matrix}$
$\{SO^{(k_{12}^{12})}, SO^{(k_{23}^{23})}, SO^{(k_{34}^{34})}, SO^{(k_{45}^{5})}\}$	$\begin{matrix}0\\cost_{c,4}^{(k_{45}^{5})}\end{matrix}$	$\begin{matrix}4\ (\pi_{x_2},\pi_{x_3},\pi_{x_4},\pi_{x_5})\\cost_{c,4}^{(k_{45}^{5})}\end{matrix}$
$\{SO^{(k_{12}^{12})}, SO^{(k_{23}^{23})}, SO^{(k_{34}^{4})}, SO^{(k_{45}^{45})}\}$	$\begin{matrix}0\\cost_{c,3}^{(k_{34}^{4})}\end{matrix}$	$\begin{matrix}3\ (\pi_{x_2},\pi_{x_3},\pi_{x_4})\\cost_{c,3}^{(k_{34}^{4})}\end{matrix}$
$\{SO^{(k_{12}^{12})}, SO^{(k_{23}^{23})}, SO^{(k_{34}^{4})}, SO^{(k_{45}^{5})}\}$	$\begin{matrix}0\\cost_{c,3}^{(k_{34}^{4})}+cost_{c,4}^{(k_{45}^{5})}\end{matrix}$	$\begin{matrix}4\ (\pi_{x_2},\pi_{x_3},\pi_{x_4},\pi_{x_5})\\cost_{c,3}^{(k_{34}^{4})}+cost_{c,4}^{(k_{45}^{5})}\end{matrix}$
$\{SO^{(k_{12}^{12})}, SO^{(k_{23}^{3})}, SO^{(k_{34}^{34})}, SO^{(k_{45}^{45})}\}$	$\begin{matrix}0\\cost_{c,2}^{(k_{23}^{3})}\end{matrix}$	$\begin{matrix}2\ (\pi_{x_3},\pi_{x_4})\\cost_{c,2}^{(k_{23}^{3})}\end{matrix}$
$\{SO^{(k_{12}^{12})}, SO^{(k_{23}^{3})}, SO^{(k_{34}^{34})}, SO^{(k_{45}^{5})}\}$	$\begin{matrix}0\\cost_{c,2}^{(k_{23}^{3})}+cost_{c,4}^{(k_{45}^{5})}\end{matrix}$	$\begin{matrix}4\ (\pi_{x_2},\pi_{x_3},\pi_{x_4},\pi_{x_5})\\cost_{c,2}^{(k_{23}^{3})}+cost_{c,4}^{(k_{45}^{5})}\end{matrix}$
$\{SO^{(k_{12}^{12})}, SO^{(k_{23}^{3})}, SO^{(k_{34}^{4})}, SO^{(k_{45}^{45})}\}$	$\begin{matrix}0\\cost_{c,2}^{(k_{23}^{3})}+cost_{c,3}^{(k_{34}^{4})}\end{matrix}$	$\begin{matrix}2\ (\pi_{x_3},\pi_{x_4})\\cost_{c,2}^{(k_{23}^{3})}+cost_{c,3}^{(k_{34}^{4})}\end{matrix}$
$\{SO^{(k_{12}^{12})}, SO^{(k_{23}^{3})}, SO^{(k_{34}^{4})}, SO^{(k_{45}^{5})}\}$	$\begin{matrix}0\\cost_{c,2}^{(k_{23}^{3})}+cost_{c,3}^{(k_{34}^{4})}+cost_{c,4}^{(k_{45}^{5})}\end{matrix}$	$\begin{matrix}3\ (\pi_{x_3},\pi_{x_4},\pi_{x_5})\\cost_{c,2}^{(k_{23}^{3})}+cost_{c,3}^{(k_{34}^{4})}+cost_{c,4}^{(k_{45}^{5})}\end{matrix}$
$\{SO^{(k_{12}^{12})}, SO^{(k_{34}^{34})}, SO^{(k_{45}^{45})}\}$	$\begin{matrix}0\\0\end{matrix}$	$\begin{matrix}2\ (\pi_{x_3},\pi_{x_4})\\0\end{matrix}$

gain K taken from part (A), the LLFR controller is activated. Figure 7.9-(b) depicts the cumulative control effort that is expensed. The maximum tracking error that is obtained is unacceptable due to the violation of the error specification e_s (namely, $error = 0.018(m) > 0.010(m) = e_s$). In other words, the faulty satellite #3 is partially recovered by the centralized LLFR controller.

On the other hand, the estimates of the faults can be used in the decentralized LLFR controller. By using the decentralized controller (5.34), the parameter vector α (with $||A_3^T(\alpha)|| = 0.6325$) and the decentralized feedback gains (β_{12}^1, β_{12}^2, β_{23}^2, β_{23}^3, β_{34}^3, β_{34}^4, β_{45}^4, and β_{45}^5) that are taken from part (A), and by using the estimates of the faults (including the biased estimates) in the LLFR controller, the results obtained are still an unacceptable increase in the maximum tracking error (namely, $error = 0.023(m) > 0.010(m) = e_s$). Therefore, the faulty satellite #3 is partially recovered by the decentralized LLFR controller. Figure 7.10-(b) depicts the cumulative control effort that is expensed.

In the case of a partially LL-recovered satellite #3, the decentralized controller distributes the effects of the local fault among all the tracking errors throughout the formation. However, the centralized controller constrains the local fault to the neighboring tracking errors and, hence, prevents the effects of the fault from spreading throughout the

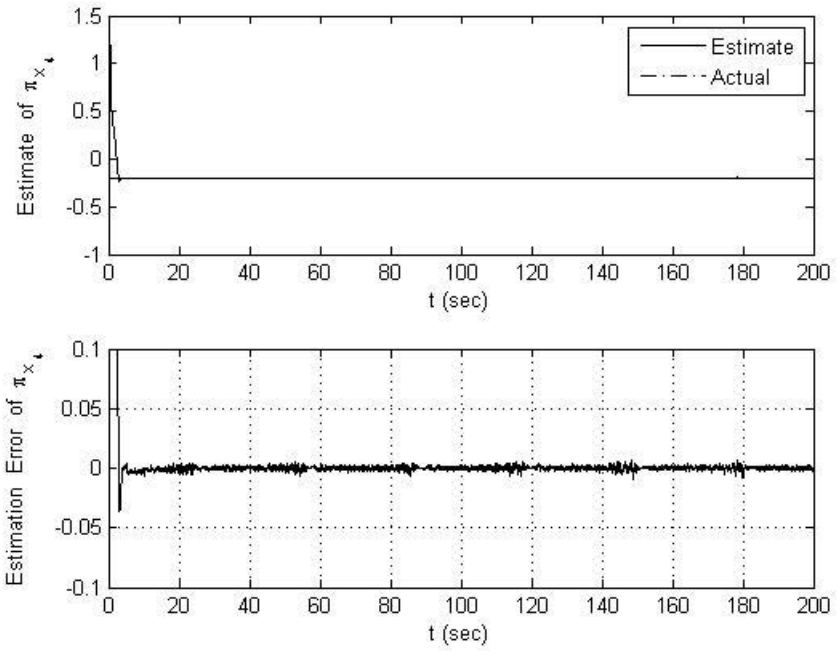

Figure 7.25: Actual, estimated, and the estimation error of the LOE fault in satellite #4 by using the reconfigured set of sub-observers.

formation. These effects are shown and compared in Table 7.3. The above advantage of the centralized controller is due to the fact that the associated error dynamics (5.15) has a reduced-order state vector that only includes the tracking errors e_{23} and e_{34}, which are local to the faulty satellite #3. On the other hand, corresponding to the decentralized controller, the error dynamics (5.39) has a full-order state vector that includes all the tracking errors e_{12}, e_{23}, e_{34}, and e_{45}. Therefore, there is a trade-off between selecting a centralized controller that requires a high level of communication resource among all the satellites, albeit resulting in a local manifestation of the fault, and the decentralized controller that requires a much reduced level of communication resource at the expense of leading to a global manifestation of the fault.

Since the fault estimate in satellite #3 is biased and inaccurate, satellite #3 is partially recovered by the LLFR module. Therefore, in part (C) below the supervisor activates the FLFR module in order to perform a cooperative fault accommodation among the five satellites in favor of the partially LL-recovered satellite #3.

C. The partially LL-recovered satellite #3 is cooperatively accommodated by the FLFR module: The centralized controller (5.10) is implemented by using the

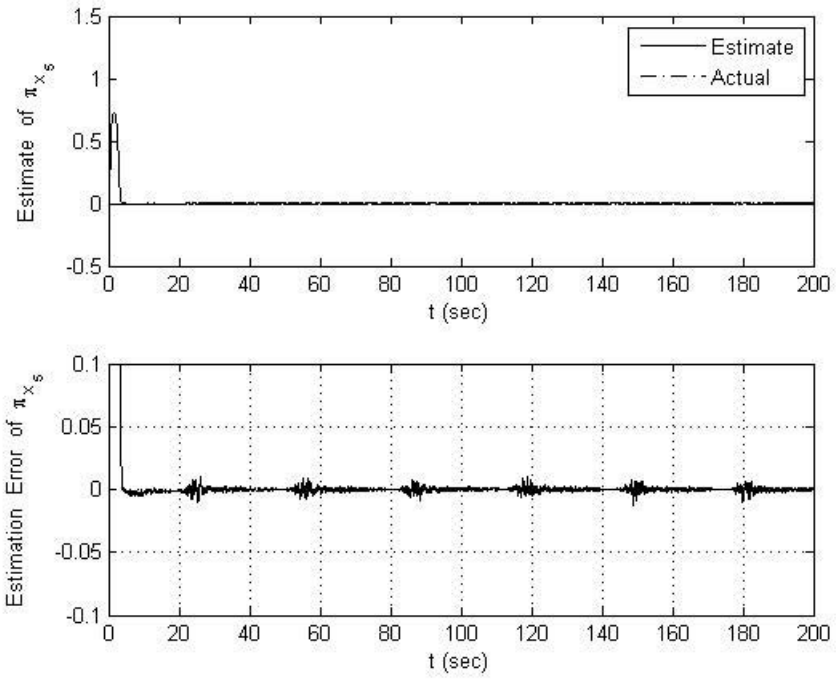

Figure 7.26: Actual, estimated, and the estimation error of the LOE fault in satellite #5 by using the reconfigured set of sub-observers.

Table 7.2: Comparison between the estimation performance of the initial set Set_I^{so} and reconfigured set Set_R^{so} of sub-observers for the cooperative estimation system in the time interval $T_{23} = [100, 200](sec)$.

Estimation Error Mean					
	π_{x_1}	π_{x_2}	π_{x_3}	π_{x_4}	π_{x_5}
Set_I^{so}	0.0006	0.0511	0.0452	0.0461	0.0005
Set_R^{so}	0.0004	0.0005	0.0158	0.0005	0.0004
Estimation Error Variance					
	π_{x_1}	π_{x_2}	π_{x_3}	π_{x_4}	π_{x_5}
Set_I^{so}	1.9×10^{-4}	1.1×10^{-2}	1.3×10^{-2}	1.8×10^{-2}	1.6×10^{-4}
Set_R^{so}	1.3×10^{-4}	1.7×10^{-4}	2.6×10^{-2}	1.5×10^{-4}	1.2×10^{-4}

Table 7.3: Performance comparison between the centralized and the decentralized controllers in terms of whether the local fault in satellite #3 affects the corresponding tracking errors ("Y"=yes) or not ("N"=no).

Controller	Effects of the local fault on the tracking errors									
	e_{12}	e_{23}	e_{24}	e_{25}	e_{13}	e_{14}	e_{15}	e_{34}	e_{35}	e_{45}
Centralized	N	Y	N	N	Y	N	N	Y	Y	N
Decentralized	Y	Y	Y	Y	Y	Y	Y	Y	Y	Y

parameters α_i taken from part (A) except for α_3 which corresponds to the partially LL-recovered satellite #3 and is taken within the interval $1 < \alpha_3 \leq 10$, and by using the centralized feedback gain K from part (A). Our proposed analytical method in Theorem 5.2 gives $\alpha_3 = 7.6$, which gives an acceptable maximum tracking error (namely, $error = 0.008(m) < 0.010(m) = e_s$). In this case, the cumulative control effort is shown in Figure 7.9-(c). Comparing Figure 7.9-(c) with Figure 7.9-(b), one can conclude that the more one increases the parameter α_3 in the FLFR process, the less satellite #3 will use control effort, and the more other satellites will use their control efforts to compensate for the deficiency of satellite #3. This is an interesting interpretation of the FLFR in favor of the partially LL-recovered satellite #3.

Alternatively, the decentralized controller (5.34) is next implemented by changing the parameter vector α according to Theorem 5.6 such that $||A_3^T(\alpha)||$ decreases from the initial value of 0.6325 that is used in scenarios (A) and (B), and in addition by using Theorem 5.5 the decentralized feedback gains are selected as

$$\beta_{12}^1 = [2.9345 \;\; 2.3452] \;,\; \beta_{12}^2 = [0.2678 \;\; -0.9986]$$
$$\beta_{23}^2 = [0.8678 \;\; 3.0980] \;,\; \beta_{23}^3 = [-0.4480 \;\; -2.3418]$$
$$\beta_{34}^3 = [0.6460 \;\; 2.0519] \;,\; \beta_{34}^4 = [-0.5591 \;\; -4.0048]$$
$$\beta_{45}^4 = [-0.6395 \;\; 0.9926] \;,\; \beta_{45}^5 = [-3.6295 \;\; -1.5503]$$

Our proposed analytical results from Theorem 5.6 yield $||A_3^T(\alpha)|| = 0.2530$, which results

in an acceptable maximum tracking error (namely, $error = 0.008(m) < 0.010(m) = e_s$). In this case, the cumulative control effort is depicted in Figure 7.10-(c). Comparing Figure 7.10-(c) with Figure 7.10-(b), one can conclude that the more $||A_3^T(\alpha)||$ is decreased by the FLFR process, the less satellite #3 will use its control effort, and the more other satellites will consume their control efforts to compensate for the deficiency of the satellite #3, as in the centralized control scheme.

In both centralized and decentralized controllers cases in the FLFR module, the specification e_s is ensured to be satisfied. For a different comparative evaluation between the centralized and the decentralized controllers performance in the three scenarios (A), (B) and (C), the total error norm which is defined according to $E_t^N = \sum_{e_{ij} \in E_{RMF}} |E_{x_{ij}}|$ is now utilized, where $E_{x_{ij}}$ denotes the x-axis tracking error between satellites $\#i$ and $\#j$. Figure 7.27 indicates and shows the total error norm for the three scenarios. According to this figure, the centralized controller imposes less total error norm on the formation system than the decentralized controller in all the three scenarios. This fact is compromised by a more stringent communication requirement for the centralized controller as compared to the decentralized controller.

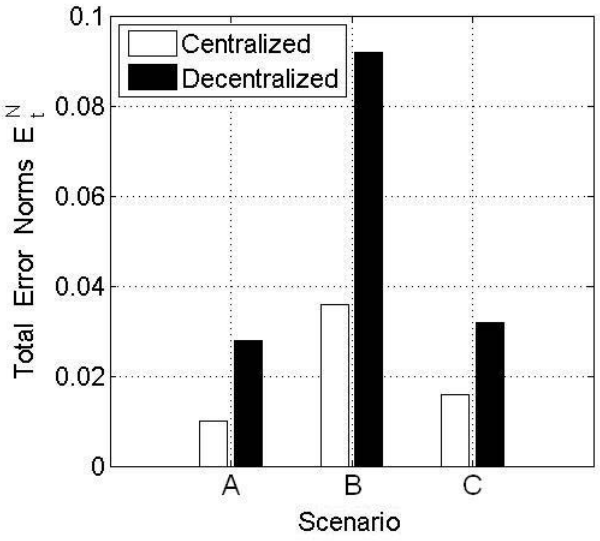

Figure 7.27: The total error norm.

In scenario (B) above, the unreliability $\bar{W}_{x_3}$ is characterized by a communication delay in the transmission of input data. Howerver, as explained earlier for equation (3.12), the unreliability $\bar{W}_{x_3}$ can also be due to the following sources, such as (a) dynamic model of the augmented faults, (b) communication delay in transmission of output date, and (c) communication delay in transmission of state estimates. The results corresponding to all these sources are not presented explicitly due to their similarity with the results

in scenario (B) above. In the following, we briefly present the results for the case of unreliability due to the dynamic model of the augmented fault.

Consider a 20% loss-of-effectiveness (LOE) fault in the x-axis actuators of the satellites #2, #3, and #4 as described in scenario (B) above. At first the LLFR module successfully performs the estimation task by the initial set of sub-observers Set_I^{so}. Subsequently, at time $t \geq T_2 = 100(sec)$, instead of the unreliability $\bar{W}_{x_3}$ characterized by a communication delay in the transmission of input data in scenario (B) above, satellite #3 is now subjected to the process dynamic unreliability $\bar{W}_{x_3} = 0.1\sin(0.2t)$. This unreliability describes the dynamic model of the fault parameter in satellite #3 by $\pi_{x_3} = -0.2 + 0.1\sin(0.2t)$ or equivalently $\dot{\pi}_{x_3} = 0.1\sin(0.2t)$ (as per equation (2.6)). In order to constrain and limit the effects of $\bar{W}_{x_3}$ on the local estimates and avoid its adverse effects on the estimates of all the states and parameters throughout the formation, by using the results from equation (4.19) at time T_2 the HL supervisor makes a decision to switch from the initial set of sub-observers Set_I^{so} to the reconfigured set of sub-observers Set_R^{so}. Table 7.4 summarizes the comparison between the T_{23}-interval estimation performance of the initial set of sub-observers Set_I^{so} and that of the reconfigured set of sub-observers Set_R^{so}. As can be seen from this table, the means and variances of the fault signal estimation errors are improved with Set_R^{so} as compared with Set_I^{so}. This again verifies the effectiveness of our proposed cooperative estimation scheme.

Table 7.4: Comparison between the estimation performance of the initial set Set_I^{so} and reconfigured set Set_R^{so} of sub-observers for the cooperative estimation system in the time interval $T_{23} = [100, 200](sec)$ for the case of dynamic fault model.

Estimation Error Mean					
	π_{x_1}	π_{x_2}	π_{x_3}	π_{x_4}	π_{x_5}
Set_I^{so}	0.0009	0.0673	0.0946	0.0387	0.0007
Set_R^{so}	0.0005	0.0006	0.0113	0.0004	0.0005
Estimation Error Variance					
	π_{x_1}	π_{x_2}	π_{x_3}	π_{x_4}	π_{x_5}
Set_I^{so}	3.6×10^{-4}	2.3×10^{-2}	4.2×10^{-2}	3.6×10^{-2}	2.8×10^{-4}
Set_R^{so}	3.4×10^{-4}	4.8×10^{-4}	3.8×10^{-2}	5.1×10^{-4}	2.5×10^{-4}

7.2 Satellite Formation Mission in Planetary Orbital Environment (POE)

Consider a five-satellite formation flight system in the planetary orbital environment (POE) [6], whose weighted absolute measurement formation (WAMF) digraph is shown in Figure 7.28-(a). Assuming that the distances among the satellites are much smaller

than the average orbit radius r_t, the orbital dynamics of satellites can be approximated by a linearized form that is known as the Hills equations [6]. For simplicity, we consider the special case of a circular orbit ($\dot{n} = 0$) with angular velocity $n = \sqrt{g_t/r_t}$, namely the Clohessy-Wiltshire (CW) equations of motion [6].

Taking $X_{x_i,y_i} = (x_i, v_{x_i}, y_i, v_{y_i})^T \in R^4$, $X_{z_i} = (z_i, v_{z_i})^T \in R^2$, $U_{x_i,y_i} = (u_{x_i}, u_{y_i})^T \in R^2$, $U_{z_i} = (u_{z_i}) \in R$, $Y_{x_i,y_i} = (y_{x_i}, y_{v_{x_i}}, y_{y_i}, y_{v_{y_i}})^T \in R^4$, $Y_{z_i} = (y_{z_i}, y_{v_{z_i}})^T \in R^2$, and including the effects of external disturbances W_{x_i,y_i} and W_{z_i} and sensor measurement noises V_{x_i,y_i} and V_{z_i}, the equations of motion for the satellite $\#i$, $i = 1, ..., 5$ is now governed by

$$\begin{aligned} &xy\text{-axes dynamics:} \quad \begin{cases} \dot{X}_{x_i,y_i} = A_{x,y} X_{x_i,y_i} + B_{x_i,y_i} U_{x_i,y_i} + W_{x_i,y_i} \\ Y_{x_i,y_i} = X_{x_i,y_i} + V_{x_i,y_i} \end{cases} \\ &z\text{-axis dynamics:} \quad \begin{cases} \dot{X}_{z_i} = A_z X_{z_i} + B_{z_i} U_{z_i} + W_{z_i} \\ Y_{z_i} = X_{z_i} + V_{z_i} \end{cases} \end{aligned} \tag{7.4}$$

where

$$A_{x,y} = \begin{bmatrix} 0 & 1 & 0 & 0 \\ 3n^2 & 0 & 0 & 2n \\ 0 & 0 & 0 & 1 \\ 0 & -2n & 0 & 0 \end{bmatrix} \quad , \quad B_{x_i,y_i} = \begin{bmatrix} 0 & 0 \\ \frac{b_{x_i}}{m_i} & 0 \\ 0 & 0 \\ 0 & \frac{b_{y_i}}{m_i} \end{bmatrix}$$

$$A_z = \begin{bmatrix} 0 & 1 \\ -n^2 & 0 \end{bmatrix} \quad , \quad B_{z_i} = \begin{bmatrix} 0 \\ \frac{b_{z_i}}{m_i} \end{bmatrix}$$

$(x_i, y_i, z_i)^T \in R^3$ and $(v_{x_i}, v_{y_i}, v_{z_i})^T \in R^3$ are the three-dimensional position and velocity coordinates in the local inertial frame, respectively, $(u_{x_i}, u_{y_i}, u_{z_i})^T \in R^3$ is the input vector, and $(y_{x_i}, y_{y_i}, y_{z_i})^T \in R^3$ and $(y_{v_{x_i}}, y_{v_{y_i}}, y_{v_{z_i}})^T \in R^3$ are the measurements of the position and velocity vectors, respectively. The actuators are modeled by the gains b_{x_i}, b_{y_i}, and b_{z_i}, and the total mass of the satellite $\#i$ is represented by m_i. The major environmental disturbances in the POE are atmospheric drag and J_2 perturbations [3], whose comparative importances are indicated in Figure 1.4.

The initial formation is positioned in the xy-plane at $2000(Km)$ altitude, where J_2 is the major disturbance of order 10^{-3} as shown in Figure 1.4. The objective is a counter-clockwise rotation maneuver in the xy-plane with the maximum frequency of $\omega_0 = 0.1(rad/s)$, such that the satellites always maintain a polygon shape with the side

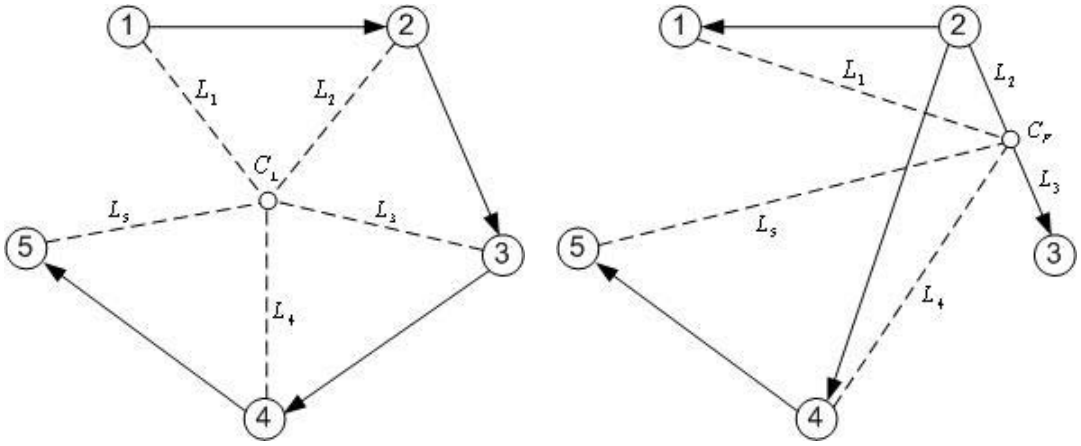

Figure 7.28: The WAMF digraphs used by (a) the LLFR and (b) the FLFR modules, in which the dashed lines represent the distances from the rotation centers C_L and C_F, respectively.

lengths of $L = 200(m)$, while the tracking error specification that is selected as $e_s = 0.010(m)$ is guaranteed. Since the xy-axes dynamics of the satellite is decoupled from its z-axis dynamics, in the following we only consider the xy-axes dynamics as given by equation (7.4).

7.2.1 Single Partially Low-Level (LL) Recovered Satellite

In this subsection, we consider the same three scenarios (A), (B), and (C) that were considered in the previous section. The results on actuator fault estimation by using the LLFR module are not presented here due to their similarity with the results in the previous section. The results on actuator fault accommodation by the FLFR module are presented for the three scenarios as detailed below.

A. All the satellites are fault free: We start with the WAMF digraph (as per Definition 2.7) which is shown in Figure 7.28-(a) with the adjacency matrix Ω as given by

$$\Omega = \begin{bmatrix} 0 & 0 & 0 & 0 & 0 \\ 1 & 0 & 0 & 0 & 0 \\ 0 & 1 & 0 & 0 & 0 \\ 0 & 0 & 1 & 0 & 0 \\ 0 & 0 & 0 & 1 & 0 \end{bmatrix} \tag{7.5}$$

The desired trajectories are designed based on the rotation center C_L (as shown in Figure 7.28-(a)) and equation (7.4), which yield $L_i = 0.5L/\sin(\pi/5)$, $i = 1, ..., 5$ and the desired xy-axes input vectors are given as follows:

$$\begin{bmatrix} u_{x_i}^d \\ u_{y_i}^d \end{bmatrix} = L_i \begin{bmatrix} b_{x_i}^{-1} & 0 \\ 0 & b_{y_i}^{-1} \end{bmatrix} \begin{bmatrix} (-\omega_0^2 - 2n\omega_0 - 3n^2)\cos(\omega_0 t + \phi_i) \\ (-\omega_0^2 - 2n\omega_0)\sin(\omega_0 t + \phi_i) \end{bmatrix} \tag{7.6}$$

where ϕ_i and L_i represent the desired trajectory phase of satellite $\#i$ and its distance from the rotation center, respectively. The information exchange requirement is determined according to Remark 6.2. The feedback matrices K_i, $i = 1, ..., 5$ are designed by using Lemma 6.1 as follows

$$K_i = \begin{bmatrix} -2.9987 & -3.2813 & 0.5417 & 0.7028 \\ -0.5417 & -0.7028 & -2.9687 & -3.2813 \end{bmatrix} \tag{7.7}$$

The maximum tracking error is found to be $error = 0.005(m) < 0.010 = e_s$ that is acceptable and within the overall mission specifications. The cumulative control effort is depicted in Figure 7.29-(a).

B. Satellites #2, #3, and #4 are faulty and the fault in satellite #3 is partially recovered by the LLFR controller: A 20% loss-of-effectiveness fault is applied to the x-axis actuators of the satellites #2, #3, and #4. Similar to the discussion in the previous section the HL supervisor activates the LLFR module. This module fully recovers the faulty satellites except for the satellite #3, whose fault is estimated within a 10% relative error tolerance, that is $|\varepsilon_{x_3}|/b_{x_3} = |\hat{b}_{x_3} - b_{x_3}|/b_{x_3} \leq 0.10$. The LLFR module implements the same WAMF diagraph as shown in Figure 7.28-(a), the same adjacency matrix as given by equation (7.5) and the same desired trajectories (and the desired xy-axes input vectors as given by equation (7.6)) as those designed based on the rotation center C_L in the previous scenario (A). Similar to scenario (A), the LLFR controller gain (7.7) is designed by invoking Lemma 6.1. The information exchange requirement is determined according to Remark 6.3. The cumulative control effort is depicted in Figure 7.29-(b). Due to the inaccurate estimate of the faulty parameter, the maximum tracking error that can be achieved by the LLFR module is found to be $error = 0.02(m) > 0.01 = e_s$, which corresponds to the faulty satellite #3 and is clearly unacceptable and does not meet the overall mission specifications. Therefore, satellite #3 is partially recovered by the LLFR controller at the low-level (LL), and hence the supervisor activates the FLFR module.

C. The partially LL-recovered satellite #3 is accommodated by the FLFR module: According to Theorem 6.1, the FLFR module reconfigures the formation structure and implements the new WAMF digraph as shown in Figure 7.28-(b) with the new adjacency matrix Ω as given by

$$\Omega = \begin{bmatrix} 0 & 1 & 0 & 0 & 0 \\ 0 & 0 & 0 & 0 & 0 \\ 0 & 1 & 0 & 0 & 0 \\ 0 & 1 & 0 & 0 & 0 \\ 0 & 0 & 0 & 1 & 0 \end{bmatrix} \tag{7.8}$$

The FLFR module activates a robust controller for the partially LL-recovered satellite #3 by using Theorem 6.2 which gives

$$K_3 = \begin{bmatrix} -3.2857 & -3.5824 & 0.8825 & 0.7295 \\ -0.6295 & -1.0386 & -2.7385 & -2.6201 \end{bmatrix} \tag{7.9}$$

Finally, in order to satisfy the error specification e_s, the FLFR module uses Theorem 6.3 to impose a constraint on the desired xy-axes input vectors (7.6) of the partially LL-recovered satellite #3 and its neighbor satellite #2. This constraint requires smaller distances L_i, $i = 1, 2$ from the new rotation center C_F as shown in Figure 7.28-(b) when compared to the original rotation center C_L that is shown in Figure 7.28-(a). The new rotation center C_F is chosen such that $L_1 = L_2 = L/2$ which satisfies the constraint that is imposed by Theorem 6.3 in the FLFR module. Therefore, the maximum tracking error that can be achieved by the FLFR module is found to be $error = 0.009(m) < 0.010 = e_s$, which is acceptable and satisfies the overall mission specifications. The cumulative control effort is depicted in Figure 7.29-(c).

7.2.2 Multiple Partially Low-Level (LL) Recovered Satellites

In this subsection, the satellites #2, #3, and #4 are subject to 20% loss-of-effectivenss actuator faults. The HL supervisor activates the LLFR module (the details are not presented here due to similarity to the discussions in the previous section). The result is that only satellite #4 is fully recovered by the LLFR module, and the fault parameters in the partially LL-recovered satellites #2 and #3 are estimated within 10% relative error tolerances, that is $|\varepsilon_{x_i}|/b_{x_i} = |\hat{b}_{x_i} - b_{x_i}|/b_{x_i} \leq 0.10$, $i = 2, 3$. The tolerances are caused by process dynamics unreliabilities $\bar{W}_{x_i} = u_{x_i}(t - \tau) - u_{x_i}(t)$ $(i = 2, 3)$, where $\tau = 0.1(sec)$, that affect the estimation performance. These unreliabilities are due to unexpected communication delays that occur when satellites #2 and #3 send their control signals $u_{x_i}(t)$, $i = 2, 3$ to the other satellites in their neighbor sets $\mathscr{N}(\{i\})$ for filtering.

In the LLFR module, the same WAMF digraph as shown in Figure 7.28 and the same adjacency matrix as given by equation (7.5) are utilized. The fault estimates are incorporated in the same controller gains K_i, $i = 1, ..., 5$ as given by equation (7.7), which is designed by using Lemma 6.1. By applying the LLFR controllers, the error specification is violated by the two satellites #2 and #3, that is $error = 0.02(m) > 0.01 = e_s$. The

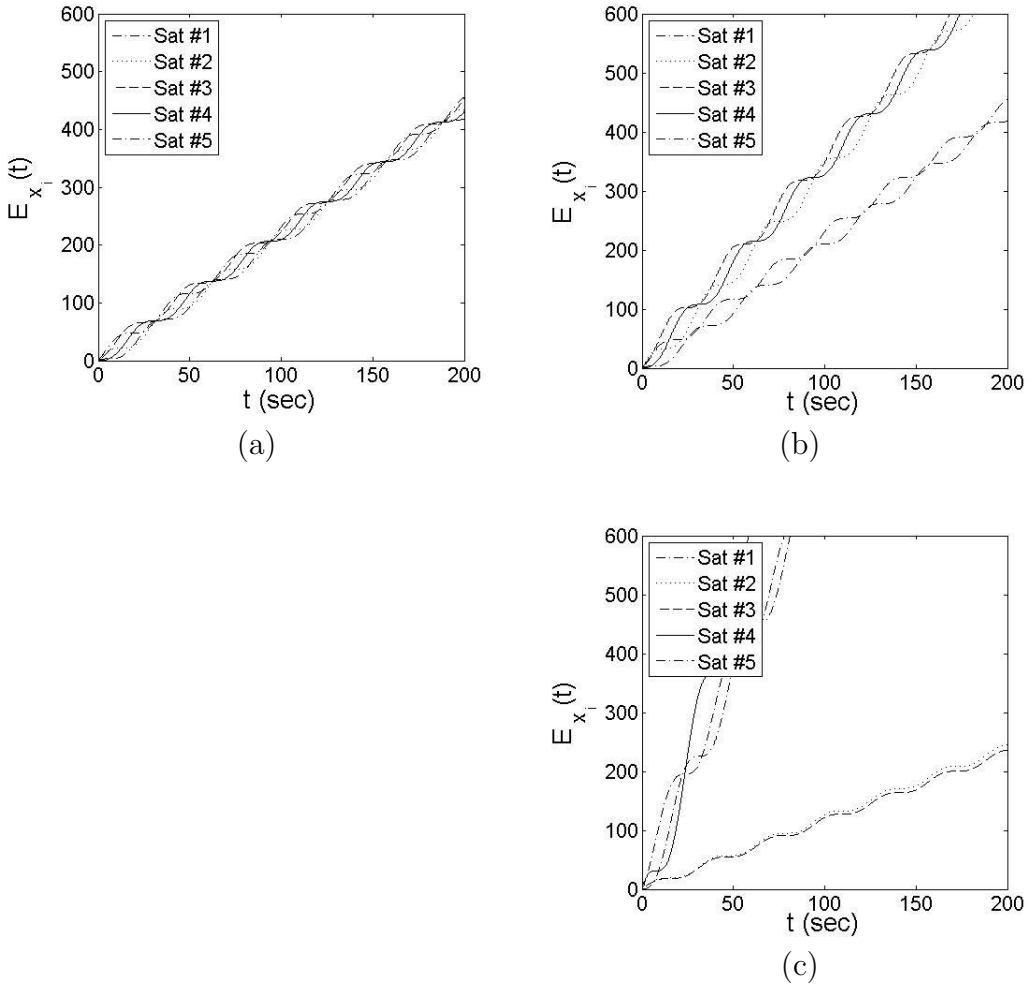

Figure 7.29: The x-axis cumulative control effort for (a) all satellites are fault free, (b) faulty satellite #3 with the LLFR applied, and (c) faulty satellite #3 with the HLFR applied.

cumulative control effort for the case of LLFR module is shown in Figure 7.31-(b). The HL supervisor activates the FLFR module to account for the performance degradations of the partially LL-recovered satellites.

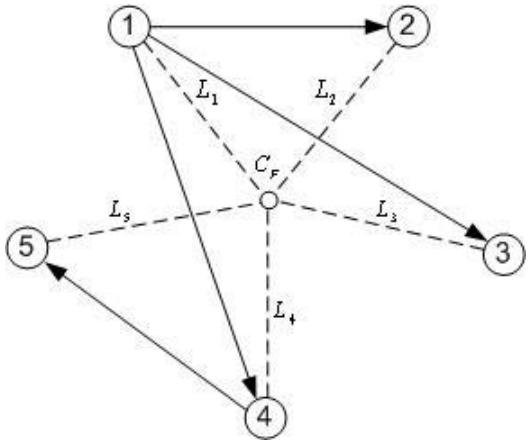

Figure 7.30: The WAMF digraph that is used by the FLFR module in which the dashed lines represent the distances from the rotation center C_F.

At the FLFR module, Theorem 6.1 is used to reconfigure the formation structure and implement the new WAMF digraph as shown in Figure 7.30 with the new adjacency matrix Ω as given by

$$\Omega = \begin{bmatrix} 0 & 0 & 0 & 0 & 0 \\ 1 & 0 & 0 & 0 & 0 \\ 1 & 0 & 0 & 0 & 0 \\ 1 & 0 & 0 & 0 & 0 \\ 0 & 0 & 0 & 1 & 0 \end{bmatrix} \tag{7.10}$$

Theorem 6.2 is now used to design the feedback gains K_2 and K_3 as given in equation (7.9) for the partially LL-recovered satellites. Finally, in order to satisfy the error specification e_s of the formation, Theorem 6.3 is used to impose constraints on the desired xy-axes input vectors (7.6) of the partially LL-recovered satellites #2 and #3 and their supporting neighbor (SN) satellite #1 (as shown in Figure 7.30). Considering equation (7.6), the FLFR module reduces the formation angular velocity of the rotation maneuver from $\omega_0 = 0.1(rad/s)$ to $\omega_0 = 0.078(rad/s)$. Therefore, the error specification of the formation mission is satisfied, that is $error = 0.009(m) < 0.010 = e_s$. The cumulative control effort for the case of the FLFR module is shown in Figure 7.31-(c).

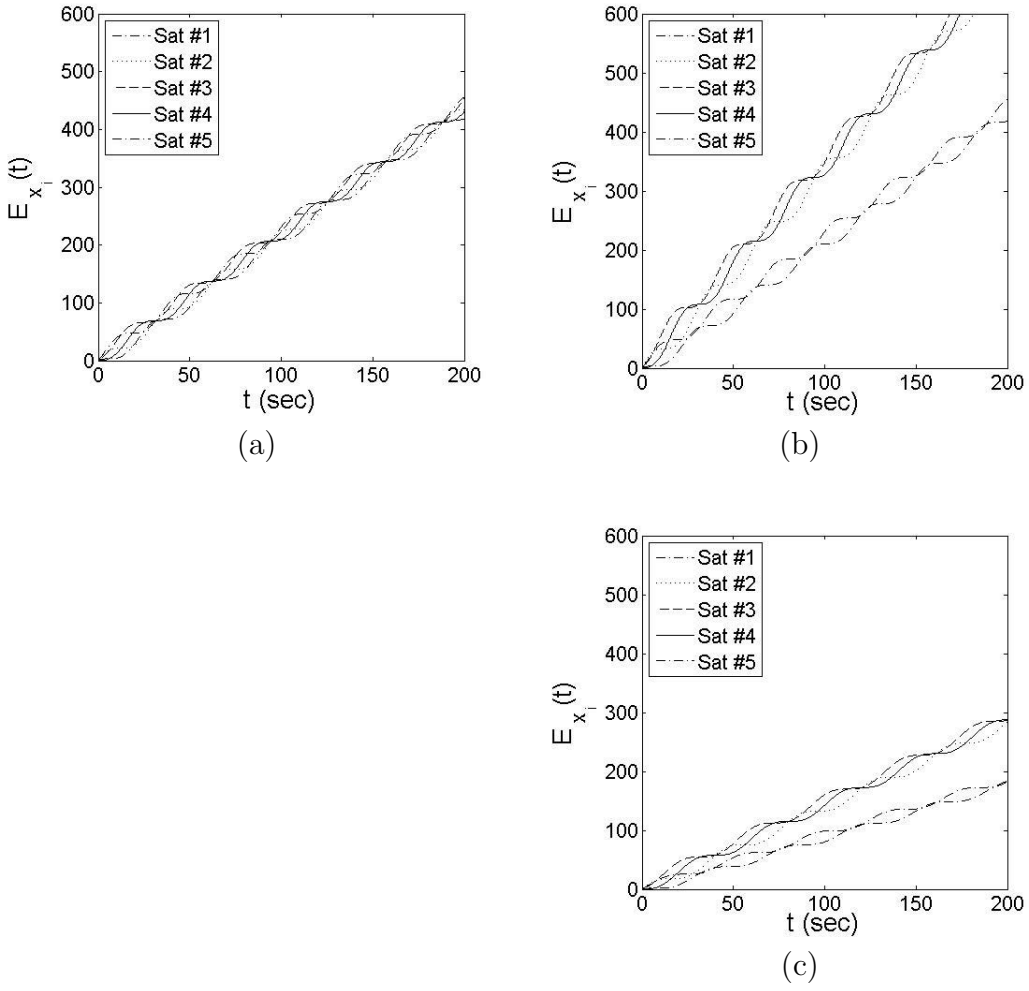

Figure 7.31: The x-axis cumulative control effort for (a) all satellites are fault free, (b) faulty satellites #2 and #3 with the LLFR applied, and (c) faulty satellites #2 and #3 with the HLFR applied.

7.3 Conclusions

In this chapter, the proposed cooperative fault estimation and accommodation framework is applied to the satellite formation flight missions in deep space (DS) and planetary orbital environment (POE). The lock-in-place and loss-of-effectiveness actuator faults are considered in both cases of single and multiple permanent faults. The cooperative fault estimation and accommodation tasks are performed based on the corresponding estimation and formation digraphs, respectively. It is shown that the proposed estimation and accommodation approaches can be integrated in order to constrain the effects of a fault on the local estimates and to compensate for the performance deficiency of a faulty satellite by imposing constraints on the desired input vectors. Simulation results do confirm the effectiveness of our analytical work.

Chapter 8

Conclusions and Future Work

In this chapter, the conclusions of this thesis are presented and a number of suggestions for future work are stated.

8.1 Conclusions

In this thesis, the problem of fault detection, isolation, and recovery (FDIR) in formation flight of unmanned vehicles is investigated. Towards this end, the FDIR problem is formulated into the problem of fault estimation and accommodation where a multi-level hierarchical and cooperative scheme is proposed and developed. It is shown that through the proposed framework we are able to improve and enhance the capabilities of the existing fault estimation and accommodation techniques as applied to formation flight of unmanned vehicles. The hierarchical architecture consists of three levels, namely a low-level (LL), a formation-level (FL), and a high-level (HL) fault estimation and accommodation modules.

The LL module corresponds to the vehicle and the system components in which conventional filtering methods are used to estimate the severity of a fault. Moreover, conventional linear control techniques are used to design low-level fault recovery (LLFR) controllers that are based on information from fault parameter estimates. When a fault is not properly estimated by the LL module, the performance of the LLFR controller becomes degradated, and hence the faulty vehicle will be considered as *partially LL-recovered*. In the high-level (HL) module, a performance monitoring (PM) scheme observes the behavior of all the vehicles in the formation and sends the information on degradation of the team performance to a HL supervisor. Once a degradation in the performance of the partially LL-recovered vehicle is detected, the HL module forwards the selected recovery solution to the FL module.

The HL supervisor observes the performance and behavior of the formation and

makes a decision on the selection of the most suitable distributed sub-observer reconfiguration and formation structure reconfiguration for the formation-level fault estimation (FLFE) and formation-level fault recovery (FLFR) modules, respectively. In the formation-level (FL) module, the interactions among the vehicles are taken into account and incorporated to estimate and accommodate faults in the vehicles more effectively. The FLFE module estimates the fault severities *cooperatively* by utilizing distributed estimation filters that are designated as *sub-observers* (SOs), whose cooperation and data fusion are managed and maintained by a HL supervisor. The FLFR module takes into account the performance degradations of a partially low-level recovered vehicle at the expense of a HL-driven formation structure reconfiguration which imposes certain criteria on the input signals of the other healthy vehicles.

Graph-based approaches and structural observability results are invoked to design the LL estimation filters or sub-observers. The decision-making criteria and guidelines for the HL supervisor are formulated as the problem of determining an optimal path on the proposed estimation (E), weighted estimation (WE), sub-observer dependency estimation (SODE), and weighted sub-observer dependency estimation (WSODE) digraphs.

In the low-level fault recovery (LLFR) module, the overall fault-augmented state space model is formulated as a linear time-invariant (LTI) system corresponding to the float, lock-in-place, and hard-over actuator failures. Consequently, conditions are derived that are based on the decentralized fixed mode (DFM) to examine feasibility of the cooperative sub-observers and guarantee stability of the overall estimation problem. Robust H_∞ linear filtering technique is also used to design the distributed and cooperative sub-observers.

On the other hand, corresponding to the case of loss-of-effectiveness actuator faults, the overall fault-augmented state space model is formulated as a bilinear system from the observability perspective and as a linear time-varying system from the filtering perspective. Therefore, the Kalman filtering (KF) technique is used to design the local sub-observers for our proposed cooperative estimation scheme. The ultimate boundedness of the estimation errors are analyzed by using Lyapunov theorey as well as the concept of an *acyclic* digraph within a graph-based framework. Whenever a state is commonly estimated by more than one sub-observer, a fusion feedback optimization problem is then formulated to fuse the common state estimates in order to modify the Kalman gains accordingly. The fault estimates are ultimately incorporated in the LLFR controllers in order to recover the formation performance subject to the actuator faults.

In order to evaluate the performance of the LLFR module, a HL performance monitoring (PM) module is introduced that identifies the *partially low-level (LL) recovered* vehicles that have violated the given desired *error specifications* of the formation mission.

Consequently, the PM module notifies the HL supervisor regarding the partially LL-recovered vehicles, and the HL supervisor makes a decision on activating the formation-level fault recovery (FLFR) module to accommodate the faulty vehicles.

The FLFR module compensates the performance degradation of a partially LL-recovered vehicle by imposing certain criteria on the input signals of the other healthy vehicles. When only the relative state measurements among the vehicles are available, the *centralized* and *decentralized* H_∞ control parameters are adjusted to accommodate the partially LL-recovered vehicle by enforcing the other healthy vehicles expending more control effort to compensate for the performance degradation of the faulty vehicle. In case of multiple actuator failures, a robust controller is designed to stabilize the nominal state space model of the formation system, and a constraint is imposed on the desired system inputs to satisfy the required error specification of the formation mission.

When only absolute state measurements of the formation vehicles are available, a general FLFR technique is developed that is based on theories from robust control and graph theory. Moreover, the notion of an *adjacency matrix* that is compatible with and can be implemented in both the centralized and decentralized approaches are utilized in this case. The FLFR module reconfigures the formation structure by adjusting the weights of the adjacency matrix of the so-called weighted absolute measurement formation (WAMF) digraph to prevent the error propagation effects of local faults. Subsequently, the FLFR module implements a robust H_∞ controller and imposes a constrain on the desired inputs. In order to accommodate the faults in the case of multiple partially LL-recovered vehicles, the notion of a *supporting neighbor (SN)* is introduced, whose desired input is adjusted (constrained) to take into account the performance deficiencies of all the partially LL-recovered vehicles.

For sake of illustration and to demonstrate the capabilities of the proposed solutions, in simulations the case of a five-satellite formation is considered both in deep space (DS) and in planetary orbital environment (POE). Three satellites are subjected to actuator faults, among which one satellite is subjected to uncertainties and unmodeled dynamics. These unreliabilities are represented by two scenarios, namely (a) an unexpected communication delay occurs when a satellite sends its control signal to the other satellites in its neighbor set for filtering, and (b) the fault is governed by a dynamic model instead of a constant parameter. In both of these unmodeled dynamics and unreliabilities it is shown that our proposed cooperative fault estimation technique does indeed constrain and limit the undesirable effects on the estimation process towards the formation mission. Moreover, our proposed cooperative fault accommodation technique compensates the performance degradation of a partially LL-recovered satellite by reconfiguring the formation structure and by imposing certain criteria on the input signals of the other healthy

satellites. Simulation results reported do indeed confirm the validity of our developed analytical work.

8.2 Future Work

In this thesis, the faults considered belong to the "permanent" category fault and conventional linear and bilinear dynamic models are employed for cooperative fault estimation. A permanent fault is not necessarily constant and can be time-varying, as opposed to an "intermittent" fault which is present for usually irregular intervals of time. Due to the nature of an intermittent fault, it can be argued that an effective approach for modeling these faults is through an event-based framework, e.g. through a discrete-event system (DES) model, or a finite state machine, e.g. through Markov models. In future, the situation of intermittent faults will also be investigated by using a hybrid model (e.g. interactive multiple model (IMM) or probabilistic hybrid automata (PHA)) that will represent a dynamic system of the formation flight of unmanned vehicles under different healthy and faulty scenarios. In order to estimate fault severities, our distributed and cooperative estimation technique will be extended to the more general case of a hybrid model. Conditions will be derived to guarantee stability of the overall estimation process while an optimal amount of information exchange among the sub-observers will be maintained. Moreover, our proposed cooperative fault accommodation strategy will be extended to the case of partially low-level (LL) recovered vehicles with intermittent faults. The intermittent faults will add nonlinearities to the linear model of the formation flight of unmanned systems. Lyapunov theory will be a proper candidate for design of the LLFR and FLFR controllers.

In this thesis, we considered the linear translational (orbital) dynamic model of unmanned vehicles, which are decoupled from the attitude dynamics and are subject to the measurement noise that are zero mean and white Guassian processes. For the case of nonlinear dynamic models with non-Gaussian noise, particle filtering (PF) (instead of Kalman filtering (KF)) approach will be implemented to improve and extend our proposed distributed and cooperative estimation techniques. This extended estimation framework will be used to estimate faults in case of coupled translational (orbital) and attitude dynamics of unmanned vehicles in formation flight systems. The simulations will be conducted on the 6 degrees-of-freedom (DOF) model of satellites. Moreover, Lyapunov-based controller design techniques will be used in our cooperative fault accommodation framework to extend and apply the results to the case of a partially low-level (LL) recovered satellite with nonlinear 6-DOF dynamic model.

In this thesis, the decision-making objective of the high-level (HL) "supervisor"

in the cooperative fault estimation part is modeled by the problem of determining optimal paths in the corresponding proposed estimation (E), weighted estimation (WE), sub-observer dependency estimation (SODE), and weighted sub-observer dependency estimation (WSODE) decision digraphs. Moreover, the HL performance monitoring (PM) module in the cooperative fault accommodation part is modeled by a simple limit-checker, which took the output measurements from all the sensors, compared them with the desired outputs, and determined whether the tracking errors are less than a certain error specification that is associated with the overall formation mission. In future, a discrete-event system (DES) will be investigated to play the role of a high-level (HL) supervisor in making decisions for both the cooperative fault estimation and accommodation parts. The DES supervisor will alleviate the need for using a large number of various look-up tables corresponding to the changes in the system parameters or the changes in the system failures. It turns out that this is a nontrivial exercise specially when the system dimension is too large as in the case of large-scale systems. The problem of finding the shortest path between two specified vertices of a weighted decision digraph is one of the well-known combinatorial optimization problems. Therefore, our future DES supervisory fault estimation and accommodation framework will be extended to the combinatorial optimization domain, and the combinatorial optimization techniques (e.g. Dijkstra algorithm) will be used to make an optimal decision by the high-level DES supervisor.

In this thesis, the sources of "model unreliabilities" are considered to be communication delays and fault parameter variations that are tackled by the low-level fault recovery (LLFR) module in the cooperative fault estimation module. The effects of model unreliabilities on the estimation performance are constrained by a HL supervisor that made decisions on reconfiguring the set of sub-observers to limit the resulting propagation of undesired errors throughout the formation system. In future, the case of model unreliabilities will be tackled by the formation-level fault recovery (FLFR) module in the cooperative fault accommodation part through designing a robust controller for the formation flight of unmanned vehicles. However, robustness of the FLFR controller to the model unreliabilities may cause conflicts with robustness of the controller to the uncertainties that are imposed by the partially LL-recovered vehicles. Therefore, a trade-off will be seeked that will compromise the roles of the LLFR and the FLFR modules in compensating for the model unreliabilities.

In the cooperative fault estimation part, we have assumed that there exists a fault detection and isolation (FDI) module, whose detailed study is beyond the scope of this thesis. However, in the FDI literature "estimation" techniques belong to one category of fault detection and isolation methods. Extending our proposed distributed and cooperative estimation scheme to also accomplish and be utilized to achieve the FDI task is a challenging problem. The solution to this problem requires further investigation by using

statistical analysis techniques, trend analysis tools, and hypothesis test methods on the estimation signals. Furthermore, it requires making proper assumptions, identifying the limitations, and verifying the cooperative or non-cooperative interactions between the (to-be-proposed) "estimation-based FDI" module and the (already-proposed) "fault severity estimation" module within our distributed and cooperative estimation framework. Addressing these issues rigorously do require and represent a major topic of research that is worth pursuing as future work.

In this thesis, the fault recovery controllers are designed without considering the actuator saturation constraints. In future, our proposed low-level fault recovery (LLFR) and formation-level fault recovery (FLFR) modules will be extended to the general case of formation flight systems subject to actuator saturation by using the Lyapunov-based control techniques.

Bibliography

[1] M. Aung, A. Ahmed, M. Wette, D. Scharf, J. Tien, G. Purcell, and M. Regehr. An overview of formation flying technology development for the terrestrial planet finder mission. *IEEE Aerospace Conference Proceedings*, 4:2667–2679, 2004.

[2] European Space Agency (ESA) publications: www.esa.int/esapub/br/br164/br164.pdf.

[3] C. D. Brown. *Elements of Spacecraft Design*. AIAA Education Series, 2002.

[4] R. W. Beard, J. Lawton, and F. Y. Hadaegh. A coordination architecture for spacecraft formation control. *IEEE Transactions on Control Systems Technology*, 9(6):777–790, 2001.

[5] W. Ren and R. W. Beard. A decentralized scheme for spacecraft formation flying via the virtual structure approach. *American Control Conference*, 2:1746–1751, 2003.

[6] D. P. Scharf, F. Y. Hadaegh, and S. R. Ploen. A survey of spacecraft formation flying guidance and control (part I): Guidance. *American Control Conference*, pages 1733–1739, 2003.

[7] D. P. Scharf, F. Y. Hadaegh, and S. R. Ploen. A survey of spacecraft formation flying guidance and control (part II): Control. *American Control Conference*, 4:2976–2985, 2004.

[8] V. Venkatasubramanian, R. Rengaswamy, K. Yin, and S. N. Kavuri. A review of process fault detection and diagnosis part I: Quantitative model-based methods. *Elsevier Journal of Computers and Chemical Engineering*, 27(3):293–311, 2003.

[9] V. Venkatasubramanian, R. Rengaswamy, and S. N. Kavuri. A review of process fault detection and diagnosis part II: Qualitative models and search strategies. *Elsevier Journal of Computers and Chemical Engineering*, 27(3):313–326, 2003.

[10] V. Venkatasubramanian, R. Rengaswamy, S. N. Kavuri, and K. Yin. A review of process fault detection and diagnosis part III: Process history based methods. *Elsevier Journal of Computers and Chemical Engineering*, 27(3):327–346, 2003.

[11] P. M. Frank and X. Ding. Survey of robust residual generation and evaluation methods in observer-based fault detection systems. *Journal of Process Control*, 7(6):403–424, 1997.

[12] E. A. Garcla and P.M. Frank. Deterministic nonlinear observer-based approaches to fault diagnosis: A survey. *Journal of Control Engineering Practice*, 5(5):663–670, 1997.

[13] P. M. Frank. On-line fault detection in uncertain nonlinear systems using diagnostic observers: a survey. *International Journal of Systems Science*, 25(12):2129–2154, 1994.

[14] P. M. Frank. Fault diagnosis in dynamic systems using analytical and knowledge-based redundancy - a survey and some new results. *Automatica*, 26(3):459–474, 1990.

[15] R. Isermann. Process fauls detection based on modelling and estimation methods - survey. *Automatica*, 20:387–404, 1984.

[16] J. S. H. Tsai, M. H. Lin, C. H. Zheng, S. M. Guo, and L. S. Shieh. Actuator fault detection and performance recovery with kalman filter-based adaptive observer. *International Journal of General Systems*, 36(4):375–398, 2007.

[17] T. Jiang, K. Khorasani, and S. Tafazoli. Parameter estimation-based fault detection, isolation and recovery for nonlinear satellite models. *IEEE Transaction on Control Systems Technology*, 16(4):799–808, July 2008.

[18] M. M. Tousi, A. G. Aghdam, and K. Khorasani. A hybrid fault diagnosis and recovery for a team of unmanned vehicles. *IEEE International Conference on System of Systems Engineering*, June 2008.

[19] J. N. Parra Bernal. A model-based fault recovery for the attitude control subsystems of a satellite using magnetic torquers. *Master Thesis, Department of Electrical and Computer Engineering, Concordia University, Montreal, Quebec*, August 2008.

[20] C. J. Digenis. The EO-1 mission and the advanced land imager. *Lincoln Laboratory Journal*, 15(2):161–164, 2005.

[21] O. Montenbruck and E. Gill. *CloudSat-CALIPSO Launch*. NASA Press Kit, 2005.

[22] I. Shames, B. Fidan, and B. D. O. Anderson. Close target reconnaissance using autonomous UAV formations. 47^{th} *IEEE Conference on Decision and Control*, pages 1729 –1734, 2008.

[23] D. van der Walle, B. Fidan, A. Sutton, C. Yu, and B. D. O. Anderson. Non-hierarchical UAV formation control for surveillance tasks. *American Control Conference*, pages 777–782, 2008.

[24] O. Burdakov, P. Doherty, K. Holmberg, J. Kvarnstrom, and P.-M. Olsson. Positioning unmanned aerial vehicles as communication relays for surveillance tasks. *Robotics: Science and Systems*, 2009.

[25] G. Kantor, S. Singh, R. Peterson, D. Rus, A. Das, V. Kumar, G. Pereira, and J. Spletzer. Distributed search and rescue with robot and sensor teams. *Springer Tracts in Advanced Robotics*, 24:529–538, 2006.

[26] R. M. Murray. Recent research in cooperative control of multivehicle systems. *J. Dyn. Sys., Meas., Control*, 129(5):571–583, 2007.

[27] S. Martnez. UAV cooperative decision and control: Challenges and practical approaches (shima, t. and rasmussen, s.; 2008) [bookshelf]. *IEEE Control Systems Magazine*, 30(2):104–107, 2010.

[28] T. Dierks and S. Jagannathan. Output feedback control of a quadrotor UAV using neural networks. *IEEE Transactions on Neural Networks*, 21(1):50–66, 2010.

[29] N. E. Kahveci, P. A. Ioannou, and M. D. Mirmirani. Adaptive LQ control with anti-windup augmentation to optimize UAV performance in autonomous soaring applications. *IEEE Transactions on Control Systems Technology*, 16(4):691–707, 2008.

[30] Y. Kang and J. K. Hedrick. Linear tracking for a fixed-wing UAV using nonlinear model predictive control. *IEEE Transactions on Control Systems Technology*, 17(5):1202–1210, 2009.

[31] J. R. Azinheira and A. Moutinho. Hover control of an UAV with backstepping design including input saturations. *IEEE Transactions on Control Systems Technology*, 16(3):517–526, 2008.

[32] T. Dierks and S. Jagannathan. Neural network control of quadrotor UAV formations. *American Control Conference*, pages 2990–2996, 2009.

[33] B. Yun, B. M. Chen, K. Y. Lum, and T. H. Lee. A leader-follower formation flight control scheme for UAV helicopters. *IEEE International Conference on Automation and Logistics (ICAL)*, pages 39–44, 2008.

[34] S. Kim and Y. Kim. Three dimensional optimum controller for multiple UAV formation flight using behavior-based decentralized approach. *International Conference on Control, Automation and Systems (ICCAS)*, pages 1387–1392, 2007.

[35] N. H. M. Linorman and H. H. T. Liu. Formation UAV flight control using virtual structure and motion synchronization. *American Control Conference*, pages 1782–1787, 2008.

[36] J. Choi and Y. Kim. Fuel efficient three dimensional controller for leader-follower UAV formation flight. *International Conference on Control, Automation and Systems (ICCAS)*, pages 806–811, 2007.

[37] Y. Zhong, F. Ting, F. Qiongjian, and L. Delin. UAV formation flight based on vision sensor. 27^{th} *Chinese Control Conference (CCC)*, pages 592–597, 2008.

[38] P. Rui. Multi-UAV formation maneuvering control based on Q-learning fuzzy controller. 2^{nd} *International Conference on Advanced Computer Control (ICACC)*, pages 252–257, 2010.

[39] L. Marsh, D. Gossink, S. P. Drake, and G. Calbert. UAV team formation for emitter geolocation. *Information, Decision and Control (IDC)*, pages 176–181, 2007.

[40] P. B. Sujit, J. M. George, and R. W. Beard. Multiple UAV coalition formation. *American Control Conference*, pages 2010–2015, 2008.

[41] X. Wang, V. Yadav, and S. N. Balakrishnan. Cooperative UAV formation flying with obstacle/collision avoidance. *IEEE Transactions on Control Systems Technology*, 15(4):672–679, 2007.

[42] H. Min, F. Sun, and F. Niu. Decentralized UAV formation tracking flight control using gyroscopic force. *IEEE International Conference on Computational Intelligence for Measurement Systems and Applications (CIMSA)*, pages 91–96, 2009.

[43] P. Wang and F. Hadaegh. Minimum-fuel formation reconfiguration of multiple free-flying spacecraft. *J. Asfro. Sci.*, 47(1,2):77–102, 1999.

[44] R. Beard and F. Hadaegh. Constellation templates: An approach to autonomous formation flying. *World Automation Congress*, Anchorage, Alaska, 1998.

[45] R. Beard and F. Hadaegh. Finite thrust control far satellite formation flying with state constraints. *American Control Conference*, 6:4383–4387, 1999.

[46] R. Beard and F. Hadaegh. Fuel optimization for unconstrained rotations of spacecraft formations. *J. Astro. Sci.*, 47(3):259–273, 1999.

[47] O. Montenbruck and E. Gill. *Satellite Orbits: Models, Methods, and Applications*. Springer-Verlag, 2000.

[48] D. A. Vallado. *Fundamentals of Astrodynamics and Applications*. Microcosm Press and Kluwer Academic Publishers, 2001.

[49] P. C. Hughes. *Spacecraft Attitude Dynamics*. John Wiley & Sons Inc., 1986.

[50] M. J. Sidi. *Spacecraft Dynamics & Control: A Practical Engineering Approach*. ambridge University Press, 2002.

[51] L. King, G. Parker, S. Deshmukh, and J. H. Chong. A study of interspacecraft coulomb forces and implications for formation flying. *AIAA Guid., Nav., & Contr. Conf.*, 2002.

[52] E. Wnuk and J. Golebiewska. Geopotential and luni-solar perturbations in the satellite constellation and formation flying dynamics. *AAS/AIAA Spaceflight Mech. Mtg.*, 2003.

[53] R. Sedwick, D. Miller, and E. Kong. Mitigation of differential perturbations in formation flying satellite clusters. *J. Astro. Sci.*, 47(3,4):309–331, 1999.

[54] S. Schweighart and R. Sedwick. A perturbative analysis of geopotential disturbances for satellite cluster formation flying. *IEEE Proceedings on Aerospace Conference*, 2:1001–1019, 2001.

[55] A. Sparks. Satellite formationkeeping control in the presence of gravity perturbations. *American Control Conference*, 2:844–848, 2000.

[56] J. P. How and M. Tillerson. Analysis of the impact of sensor noise on formation flying control. *American Control Conference*, 5:3986–3991, 2001.

[57] R. Beard, T. McLain, and F. Hadaegh. Fuel optimization for constrained rotation of spacecraft formations. *J. Guid., Contr. & Dyn.*, 23(2):339–346, 2001.

[58] M. Vasile and F. Zazzera. Direct multiphase optimisatian of multi-objective trajectory design problem. *AAS/AIAA Spaceflight Mech. Mtg.*, pages 1301–1319, 2002.

[59] R. W. Beard, J. Lawton, and F. Y. Hadaegh. A feedback architecture for formation control. *American Control Conference*, 6:4087–4091, 2000.

[60] R. Isermann. Model-based fault-detection and diagnosis - status and applications. *Elsevier Annual Reviews in Control*, 29(1):71–85, 2005.

[61] M. A. Massoumnia. A geometric approach to the synthesis of failure detection filters. *IEEE Transactions on Automatic Control*, 31(9):839–846, 1986.

[62] B. J. Patton. Robustness in model-based fault diagnosis: The 1995 situation. *International Federation of Automatic Control*, 21:103–123, 1997.

[63] N. Meskin and K. Khorasani. Fault detection and isolation of actuator faults in spacecraft formation flight. *Conference on Decision and Control*, pages 1159–1164, December 2006.

[64] N. Meskin and K. Khorasani. Fault detection and isolation in a redundant reaction wheels configuration of a satellite. *International Conference on Systems, Man and Cybernetics*, pages 3153–3158, October 2007.

[65] M. Basseville and I. V. Nikiforov. *Detection of abrupt changes - theory and application*. Information and System Sciences Series, Prentice Hall, 1993.

[66] C. T. Chang and J. I. Hwang. Simplification techniques for EKF computations in fault diagnosis - suboptimal gains. *Journal of Chemical Engineering Science*, 53(22):3853–3862, 1998.

[67] F. Caliskan and C. M. Hajiyev. EKF based surface fault detection and reconfiguration in aircraft control systems. *American Control Conference*, 2:1220–1224, 2000.

[68] N. Tudoroiu and K. Khorasani. Fault detection and diagnosis for reaction wheels of satellite's attitude control system using a bank of kalman filters. *IEEE Conference on Control Applications*, pages 1287–1292, 2005.

[69] J. Gertler. Analytical redundancy methods in fault detection and isolation. *Proceedings of IFAC/IAMCS symposium on safe process*, 1:9–21, 1991.

[70] J. Gertler and D. Singer. A new structural framework for parity equation-based failure detection and isolation. *Automatica*, 26(2):381–388, 1990.

[71] A. Barua, P. Sinha, K. Khorasani, and S. Tafazoli. A novel fault-tree approach for identifying potential causes of satellite reaction wheel failure. *Conference on Control Applications*, pages 1467–1472, August 2005.

[72] H. Vedam and V. Venkatasubramanian. Signed digraph based multiple fault diagnosis. *Computers & chemical engineering*, 21:S655–S660, 1997.

[73] N. H. Ulerich and G. J. Powers. On-line hazard aversion and fault diagnosis in chemical processes: the digraph + fault-tree method. *IEEE Transactions on Reliability*, 37(2):171–177, 1988.

[74] W. M. Caminhas, H. Tavares, and F. Gomide. A neurofuzzy approach for fault diagnosis in dynamic systems. *Proceedings of the Fifth IEEE International Conference on Fuzzy Systems*, 3:2032–2037, 1996.

[75] A. Guiotto and A. Martelli. SMARTFDIR: use of artificial intelligence in the implementation of a satellite FDIR. *Proceedings of DASIA*, June 2003.

[76] M. A. Swartwou. A systematic formulation of spacecraft health management decisions. *IEEE Proceedings Aerospace Conference*, 7:3393–3405, Mar 2001.

[77] Z. Gaoa and S. X. Ding. Actuator fault robust estimation and fault-tolerant control for a class of nonlinear descriptor systems. *Automatica*, 43:912 – 920, 2007.

[78] G. Tao, S. Chen, and S. M. Joshi. An adaptive control scheme for systems with unknown actuator failures. *Automatica*, 38:1027–1034, 2002.

[79] M. Basseville. On-board component fault detection and isolation using statistical local approach. *Automatica*, 34(11):1391–1415, 1998.

[80] Q. Zhang, M. Basseville, and A. Benveniste. Fault detection and isolation in nonlinear dynamic systems: a combined input-output and local approach. *Automatica*, 34(11):1359–1373, 1998.

[81] W. Chen and M. Saif. Actuator fault isolation and estimation for uncertain nonlinear systems. *IEEE International conference on Systems, Man and Cybernetics*, 3:2560–2565, October 2005.

[82] B. Jiang, M. Staroswiecki, and V. Cocquempot. Fault estimation in nonlinear uncertain systems using robust sliding-mode observers. *IEE Proceedings of Control Theory Applications*, 151(1):29–37, January 2004.

[83] X. G. Yan and C. Edwards. Robust decentralized actuator fault detection and estimation for large-scale systems using a sliding mode observer. *International Journal of Control*, 81(4):591–606, 2008.

[84] W. Chen and M. Saif. An iterative learning observer for fault detection and accommodation in nonlinear time-delay systems. *International Journal of Robust and Nonlinear control*, 16:1–19, 2006.

[85] W. Chen and M. Saif. Observer-based fault diagnosis of satellite systems subject to time-varying thruster faults. *ASME*, 129:352–356, May 2007.

[86] N. E. Wu, Y. Zhang, and K. Zhou. Detection, estimation, and accommodation of loss of control effectiveness. *International Journal of Adaptive Control and Signal Processing*, 14:775–795, 2000.

[87] L. Ni and C. R. Fuller. Control reconfiguration based on hierarchical fault detection and identification for unmanned underwater vehicles. *Journal of Vibration and Control*, 9:735–748, 2003.

[88] Y. Zhang, F. Wang, T. Hesketh, D. J. Clements, and R. Eaton. Fault accommodation for nonlinear systems using fuzzy adaptive sliding control. *International Journal of Systems Science*, 36(4):215–220, March 2005.

[89] M. M. Polycarpou. Fault accommodation of a class of multivariable nonlinear dynamical systems using a learning approach. *IEEE Transaction on Automatic Control*, 46(5), May 2001.

[90] K. S. Narendra and J. Balakrishnan. Adaptive control using multiple models. *IEEE Transaction on Automatic Control*, 42(2):171–187, February 1997.

[91] Y. Bar-Shalom, X.-R. Li, and T. Kirubarajan. *Estimation with Applications to Tracking and Navigation*. John Wiley & Sons Inc., 2001.

[92] Z. Gao, T. Breikin, and H. Wang. High-gain estimator and fault-tolerant design with application to a gas turbine dynamic system. *IEEE Transactions on Control Systems Technology*, 15(4):740–753, 2007.

[93] P. Ferguson and J. How. Decentralized estimation algorithms for formation flying spacecraft. *AIAA Guidance, Navigation and Control Conference*, AIAA paper number: 2003-5442, 2003.

[94] R. S. Smith and F. Y. Hadaegh. Distributed estimation, communication and control for deep space formations. *Control Theory & Applications, IET*, 1(2):445–451, March 2007.

[95] J. S. Smith and F. Y. Hadaegh. Closed-loop dynamics of cooperative vehicle formations with parallel estimators and communication. *IEEE Transaction on Automatic Control*, 52(8), August 2007.

[96] R. S. Smith and F. Y. Hadaegh. A distributed parallel estimation architecture for cooperative vehicle formation control. *IEEE American Control Conference*, pages 4219–4224, 2006.

[97] V. Saligrama and D. Castanon. Reliable distributed estimation with intermittent communications. *IEEE Conference on Decision and Control*, pages 6763–6768, December 2006.

[98] T. Chung, V. Gupta, J. Burdick, and R. Murray. On a decentralized active sensing strategy using mobile sensor platforms in a network. *IEEE Conference on Decision and Control*, pages 1914–1919, December 2004.

[99] T. Berg and H. Durrant-Whyte. Model distribution in decentralized multi-sensor date fusion. *Technical Report, University of Oxford*, 1990.

[100] A. Mutambara. *Decentralized estimation and control for multisensory systems*. CRC Press, Boca Raton, FL, 1998.

[101] U. A. Khan and J. M. F. Moura. Distributed kalman filters in sensor networks: bipartite fusion graphs. *IEEE Workshop on Statistical Signal Processing*, pages 700–704, 2007.

[102] U. A. Khan and J. M. F. Moura. Distributing the kalman filter for large-scale systems. *IEEE Transaction on Signal Processing*, 56(10, Part 1):4919–4935, October 2008.

[103] B. Jiang and F. N. Chowdhury. Fault estimation and accommodation for linear MIMO discrete-time systems. *IEEE Transactions on Control Systems Technology*, 13(3):493–499, 2005.

[104] D. M. Bevly and B. Parkinson. Cascaded kalman filters for accurate estimation of multiple biases, dead-reckoning navigation, and full state feedback control of ground vehicles. *IEEE Transactions on Control Systems Technology*, 15(2):199–208, 2007.

[105] W. Ren, R. W. Beard, and E. M. Atkins. A survey of consensus problems in multi-agent coordination. *IEEE American Control Conference*, 3:1859–1864, 2005.

[106] W. Ren, R. W. Beard, and D. B. Kingston. Multi-agent kalman consensus with relative uncertainty. *IEEE American Control Conference*, 3:1865– 1870, 2005.

[107] M. Alighanbari and J. P. How. An unbiased kalman consensus algorithm. *IEEE American Control Conference*, pages 3519–3524, 2006.

[108] R. Olfati-Saber and J. S. Shamma. Consensus filters for sensor networks and distributed sensor fusion. *IEEE Conference on Decision and Control*, pages 6698–6703, 2005.

[109] R. Olfati-Saber. Distributed kalman filtering for sensor networks. *IEEE Conference on Decision and Control*, pages 5492–5498, 2007.

[110] R. Olfati-Saber. Distributed kalman filter with embedded consensus filters. *IEEE Conference on Decision and Control*, pages 8179– 8184, 2005.

[111] M. Staroswiecki, G. Hoblos1, and A. Aitouche. Sensor network design for fault tolerant estimation. *International Journal of Adaptive Control and Signal Processing*, 18:55–72, 2004.

[112] M. Staroswiecki. A structural view of fault-tolerant estimation. *Journal of Systems and Control Engineering*, 221(16):905–914, 2007.

[113] J. Ritt. Differential algebra. *American Mathematical Society*, 1950.

[114] L. Ljung and T. Glad. On global identifiability for arbitrary model parametrizations. *Automatica*, 30(2):265–276, 1994, [Available Online:http://www.sciencedirect.com/science/article/B6V21-47X24RTGJ/2/c3c994c959b16b42eb98800b76af1442.

[115] S. Grenaille, D. Henry, and A. Zolghadri. Fault diagnosis in satellites using H-inf estimators. *IEEE International Conference on Systems, Man and Cybernetics*, 6:5195–5200, 2004.

[116] D. Liberzon. *Switching in Systems and Control*. Birkhauser, Boston, MA, 2003.

[117] S. M. Azizi, M. M. Tousi, and K. Khorasani. A multi-agent methodology for distributed and cooperative supervisory estimation subject to unreliable information. *IET Control Theory and Applications*, 2010, in press.

[118] S. M. Azizi and K. Khorasani. A sub-optimal distributed kalman filter with fusion feedback for acyclic systems. 48^{th} *IEEE Conference on Decision and Control*, pages 5151 – 5157, 2009.

[119] S. M. Azizi, M. M. Tousi, and K. Khorasani. A distributed and cooperative supervisory estimation of multi-agent systems - part I: Framework. *Canadian Conference on Electrical and Computer Engineering (CCECE)*, pages 1028 – 1033, 2009.

[120] M. M. Tousi, S. M. Azizi, and K. Khorasani. A distributed and cooperative supervisory estimation of multi-agent systems - part II: Verification and case study. *Canadian Conference on Electrical and Computer Engineering (CCECE)*, pages 1022 – 1027, 2009.

[121] S. M. Azizi and K. Khorasani. A distributed kalman filter for actuator fault estimation of deep-space formation flying satellites. *IEEE International Systems Conference (ISC)*, page 354 359, 2009.

[122] S. M. Azizi and K. Khorasani. A hybrid and switching framework for cooperative actuator fault estimation of formation flying satellites in deep space. *Asian Control Conference (ASCC)*, pages 1126 – 1131, 2009.

[123] S. M. Azizi, M. M. Tousi, and K. Khorasani. A distributed and cooperative supervisory estimation of multi-agent nonlinear systems. *Asian Control Conference (ASCC)*, pages 384 – 389, 2009.

[124] S. M. Azizi and K. Khorasani. A hierarchical architecture for cooperative actuator fault estimation and accommodation of formation flying satellites in deep space. *under second revision in IEEE Transactions on Aerospace and Electronic systems (TAES)*.

[125] S. M. Azizi and K. Khorasani. Cooperative actuator fault accommodation of formation flying vehicles with absolute measurements. *To appear in IEEE Conference on Decision and Control (CDC)*, 2010.

[126] S. M. Azizi and K. Khorasani. A hierarchical architecture for cooperative fault accommodation of formation flying satellites in deep space. *IEEE American Control Conference (ACC)*, page 4178 4183, 2009.

[127] S. M. Azizi and K. Khorasani. Cooperative fault accommodation in formation flying satellites. *IEEE International Conference on Control Applications (CCA)*, page 1127 1132, 2008.

[128] S. M. Azizi and K. Khorasani. A decentralized cooperative actuator fault accommodation of formation flying satellites in deep space. *IEEE International Systems Conference (ISC)*, page 230 235, 2009.

[129] J. Bang-Jensen and G. Gutin. *Digraphs: theory, algorithms, and applications*. Springer-Verlang, 2007.

[130] N. Deo. *Graph Theory with Applications to Engineering and Computer Science*. Prentice-Hall, Englewood cliffs, N.J., 1974.

[131] B. D. O. Anderson, B. Fidan, C. Yu, and D. Walle. *UAV Formation Control: Theory and Application*. Springer Berlin, Heidelberg, 2008.

[132] W. Ren, K. L. Moore, and Y. Q. Chen. High-order and model reference consensus algorithms in cooperative control of multivehicle systems. *Journal of Dynamic Systems, Measurement, and Control*, 129(5):678–688, 2007.

[133] E. J. Davison and T. N. Chang. Decentralized stabilization and pole assignment for general proper systems. *IEEE Trans. Automat. Contr.*, AC-35(6):652–664, 1990.

[134] S. P. Boyd, L. E. Ghaoui, E. Feron, and V. Balakrishnan. *Linear matrix Inequalities in Systems and Control Theory*. SIAM, 1994.

[135] S. Boyd and L. Vandenberghe. *Convex Optimization*. Lecture Notes for EE290N: Convex Optimization and Applications, University of California at Berkeley, Fall 1999.

[136] K. Zhou and P. P. Khargonekar. An algebraic riccati equation approach to H_∞ optimization. *Systems and Control Letters*, 11:85–91, 1988.

[137] J. D. Boskovic, S. E. Bergstrom, and R. K. Mehra. Retrofit reconfigurable flight control in the presence of control effector damage. *American Control Conference*, 4:2652–2657, 2005.

[138] Z. Chen. Bayesian filtering: from kalman filters to particle filters, and beyond. *Adaptive System Laboratory, McMaster University, Hamilton, ON, Canada, [Online: http://www.dsi.unifi.it/users/chisci/idfric/Nonlinear_ filtering_Chen.pdf]*.

[139] S. Haykin [editor]. *Kalman Filtering and Neural Networks, Adaptive and Learning Systems for Signal Processing, Communications and Control*. John Wiley & Sons, INC., New York, 2001.

[140] C. T. Lin. Structural controllability. *IEEE Transaction on Automatic Control*, 19(3):201–208, February 1974.

[141] C. Commault, J.-M. Dion, O. Sename, and R. Motyeian. Observer-based fault detection and isolation for structured systems. *IEEE Transaction on Automatic Control*, 47(12):2074–2079, December 2002.

[142] C. Commault, J.-M. Dion, and D. H. Trinh. Observability recovering by additional sensor implementation in linear structured systems. *IEEE Conference on Decision and Control and European Control Conference*, pages 7193–7197, 2005.

[143] C.-T. Chen. *Linear System Theory and Design*. Saunders College Publishing, Philadelphia, PA, USA, 1984.

[144] S. Wu, Y. Bi, X. Zeng, and L. Han. Assigning appropriate weights for the linear combination data fusion method in information retrieval. *Information Processing and Management*, 45:413–426, 2009.

[145] B. T. Bartell, G. W. Cottrell, and R. K. Belew. Automatic combination of multiple ranked retrieval systems. *Proceedings of ACM SIGIR'94*, pages 173–184, 1994.

[146] C. C. Vogt and G. W. Cottrell. Fusion via a linear combination of scores. *Information Retrieval*, 1(3):151–173, 1999.

[147] S. Wu and F. Crestani. Data fusion with estimated weights. *Proceedings of the 2002 ACM CIKM international conference on information and knowledge management*, pages 648–651, 2002.

[148] S. Wu and S. McClean. Improving high accuracy retrieval by eliminating the uneven correlation effect in data fusion. *Journal of American Society for Information Science and Technology*, 57(14):1962–1973, 2006.

[149] T. Boukhobza and F. Hamelina. Observability analysis for structured bilinear systems: A graph-theoretic approach. *Automatica*, 43(11):1968–1974, November 2007.

[150] T. Boukhobza. Generic uniform observability analysis for bilinear systems. *Automatica*, 44(12):3133–3138, December 2008.

[151] O. M. Grasselli and A. Isidori. Deterministic state reconstruction and reachability of bilinear processes. *Proceedings of IEEE Joint Automatic Control Conference*, pages 1423–1427, 1977.

[152] D. Lillis, F. Toolan, R. Collier, and J. Dunnion. Probfuse: a probabilistic approach to data fusion. *Proceedings of the 29th annual international ACM SIGIR conference*, pages 139–146, 2006.

[153] D. P. Scharf, F. Y. Hadaegh, and S. R. Ploen. A general stability condition for the leader/follower formation flying control architecture. website: http://trs-new.jpl.nasa.gov/dspace/bitstream/2014/38214/1/03-3467.pdf.

[154] M. Staroswiecki. A structural view of fault-tolerant estimation. *Journal of Systems and Control Engineering*, 221(16):905–914, 2007.

[155] D. L. Hall and J. Llinas. An introduction to multisensor data fusion. *Proceedings of the IEEE*, 85(1):6–23, 1997.

[156] N. Mesking and K. Khorasani. Actuator fault detection and isolation for a network of unmanned vehicles. *IEEE Transactions on Automatic Control*, 54(4):835–840, 2009.

[157] W. Wonham. *Supervisory Control of Discrete-Event Systems*. Systems Control Group, Edward S. Rogers Sr. Dept. of Electrical and Computer Engineering, University of Toronto, Canada; available at http://www.control.utoronto.ca/DES, 2009.

[158] Williamson. Observation of bilinear systems with application to biological control. *Automatica*, 13(3):243–254, 1977.

[159] H. K. Khalil. *Nonlinear Systems*. Third Edition, Prentice Hall, 2002.

[160] L. Lennart. *ystem Identification: Theory for the User, 2nd edition*. Prentice-Hall, Upper Saddle River, NJ, 1999.

[161] B. Robert and P. Hwang. *Introduction to Random Signals and Applied Kalman Filtering, 3rd edition*. Wiley, New York, NY, 1996.